Advances in Mathematical Physics

Theoretical and Computational Advances in Nonlinear Dynamical Systems

Lead Guest Editor: Zhi-Yuan Sun
Guest Editors: Panoyotis G. Kevrekidis, Xin Yu, and Kaliyaperumal Nakkeeran

Theoretical and Computational Advances in Nonlinear Dynamical Systems

Advances in Mathematical Physics

Theoretical and Computational Advances in Nonlinear Dynamical Systems

Lead Guest Editor: Zhi-Yuan Sun
Guest Editors: Panoyotis G. Kevrekidis, Xin Yu, and Kaliyaperumal Nakkeeran

Editorial Board

Contents

Hindawi
Advances in Mathematical Physics
Volume 2017, Article ID 3925964, 3 pages
https://doi.org/10.1155/2017/3925964

Editorial

Theoretical and Computational Advances in Nonlinear Dynamical Systems

Zhi-Yuan Sun,[1] Panayotis G. Kevrekidis,[2] Xin Yu,[3] and K. Nakkeeran[4]

[1]*Department of Physics, Technion-Israel Institute of Technology, 320000 Haifa, Israel*
[2]*Department of Mathematics and Statistics, University of Massachusetts, Amherst, MA 01003, USA*
[3]*School of Aeronautic Science and Engineering, Beihang University, Beijing 100191, China*
[4]*School of Engineering, University of Aberdeen, Aberdeen AB24 3UE, UK*

Correspondence should be addressed to Zhi-Yuan Sun; sunzhiyuan137@aliyun.com

Received 4 May 2017; Accepted 4 May 2017; Published 4 June 2017

1. Introduction

The theory of dynamical systems is a paradigm for studying various scientific phenomena, ranging from complex atomic lattices to planetary motion, from water waves to weather systems, from chemical reaction to biological behaviors, and many more. Relevant applications have widely arisen in multidisciplinary fields including mathematics, physics, chemistry, biology, and even economics and sociology. Due to the rapid development of theoretical and computational techniques in recent years, the role of nonlinearity in dynamical systems has attracted increasing interest and has been intensely investigated. Typical research areas include spatial and temporal evolution of nonlinear systems, pattern formation and their interactions, localized solutions and stability analysis, and many others. At the same time, the mathematical tools, for both of the symbolic and numerical aspects, have been developed in dealing with the nonlinear dynamical systems qualitatively and quantitatively. On the other hand, complexity of the nonlinear dynamical systems can be further portrayed when chaotic and stochastic behaviors are revealed. Interplay between nonlinearity and randomness is also a highlight topic which can be simulated and studied by modern computational resources.

Focusing on the *nonlinearity* of dynamical systems, this special issue has received more than 30 submissions, 12 papers of which have been accepted after strict review process. These papers cover works from theoretical analysis to applications in chaotic systems, fluid dynamics, solid mechanics, and stochastic and economical systems. Mathematical methods to analyze and obtain exact solutions for types of nonlinear dynamical systems have been included in our issue as well. A brief summary will be presented in the following sections. We expect these articles, including their substantial bibliographic resources, to be of great interest to the scholars in the relevant scientific and engineering communities.

2. Chaotic Systems and Networks

In their article "A Chaotic System with an Infinite Number of Equilibrium Points: Dynamics, Horseshoe, and Synchronization," the coauthors V.-T. Pham et al. introduce a new chaotic system which has hidden chaotic attractors with an infinite number of equilibrium points. They study dynamical properties of such a system via equilibrium analysis, bifurcation diagrams, and maximal Lyapunov exponents. The findings of topological horseshoes for this system are presented as well. The authors also investigate the possibility of synchronizing two new chaotic systems with infinite equilibria by using adaptive control.

In their article "Adaptive Modified Function Projective Lag Synchronization of Memristor-Based Five-Order Chaotic Circuit Systems," the coauthors Q. Li and S. Liu investigate the modified function projective lag synchronization of the memristor-based five-order chaotic circuit system with unknown bounded disturbances. They use the linear matrix inequality approach and Lyapunov stability theorem to establish an adaptive control law, which makes

two different chaotic states asymptotically synchronized up to a desired scaling function matrix. The simulation is performed to show the correctness and effectiveness of their control method.

In his/her article "Asymptotic Stability and Asymptotic Synchronization of Memristive Regulatory-Type Networks," the author J.-E Zhang investigates nonlinear dynamics of memristive networks. The author studies global asymptotic stability and global asymptotic synchronization for memristive regulatory-type networks, based on the M-matrix theory and Lyapunov stability theory. Simulations are also performed to support the theoretical results.

3. Fluid and Atmosphere Dynamics

In their article "Numerical Simulations of the Square Lid Driven Cavity Flow of Bingham Fluids Using Nonconforming Finite Elements Coupled with a Direct Solver," the coauthors R. Mahmood et al. perform numerical simulations in a single and double lid driven square cavity to study the flow of a Bingham viscoplastic fluid. Their implementations are done via finite element methods in the framework of a monolithic approach, and the results are obtained for Bingham numbers in the range of 0–500. They find that the number of iterations for Newton's method increases at large values of Bingham number due to enhanced nonlinearity.

In their article "Application of Adjoint Data Assimilation Method to Atmospheric Aerosol Transport Problems," the coauthors Minjie Xu et al. employ the adjoint assimilation method with the characteristic finite difference scheme to solve the atmospheric aerosol transport problem. Effectiveness of the method is shown in computing a Gaussian hump, and a better agreement with the ideal initial distribution is derived by using their adjoint method. In addition, a real case of $PM_{2.5}$ concentration distribution in China during the APEC 2014 is simulated and analyzed in this work.

4. Solid Mechanics

In their article "The Spreading Residue Harmonic Balance Method for Strongly Nonlinear Vibrations of a Restrained Cantilever Beam," the coauthors Y. H. Qian et al. study a fifth-order nonlinear problem that describes the strongly nonlinear vibration of an elastically restrained beam with a lumped mass. They employ the spreading residue harmonic balance method to derive approximate analytical solutions for such a system. Illustrative examples are provided to verify the accuracy of their method, and their solutions are compared with the ones obtained by using other typical methods, as well as some exact solutions.

In their article "Closed-Form Exact Solutions for the Unforced Quintic Nonlinear Oscillator," the coauthors A. Beléndez et al. obtain closed-form exact solutions for the periodic motion of a one-dimensional, undamped, quintic oscillator. They consider all possible combinations of positive and negative coefficients of the linear and quintic terms, which provides four different cases but only three different pairs of periodic solutions. Some particular cases are discussed with variation of the parameters, and the period is presented to be a function of the initial amplitude. The authors also consider oscillatory motions around the nonzero equilibrium point.

5. Stochastic System

In their article "Turing Bifurcation and Pattern Formation of Stochastic Reaction-Diffusion System," the coauthors Q. Zheng et al. study spontaneous pattern formation induced by noise. They present a method to solve a stochastic reaction-diffusion system and show how the Turing bifurcation and Hopf bifurcation arise through linear stability analysis of the local equilibrium. They also develop the amplitude equation with a pair of wave vectors by using the Taylor series expansion, multiscaling, and expansion in powers of small parameters. In addition, the authors point out that their analytical results agree with numerical simulations.

6. Mathematical Aspects

In their article "The General Solution of Differential Equations with Caputo-Hadamard Fractional Derivatives and Noninstantaneous Impulses," the coauthors X. Zhang et al. study a Caputo-Hadamard fractional differential equation with noninstantaneous impulses. They obtain an equivalent integral equation with some undetermined constants, which indicates the existence of general solution for this impulsive system. An example is also given to illustrate their results.

In their article "The Convergence Ball and Error Analysis of the Relaxed Secant Method," the coauthors R. Lin et al. propose a relaxed secant method. A radius estimate of the convergence ball of such a method is obtained for the nonlinear systems with Lipschitz continuous divided differences of the first order. The error estimate is also established with the matched convergence order. The authors discuss the relation between the radius and the speed of convergence with parameters and present some numerical examples.

In their article "Error Estimates on Hybridizable Discontinuous Galerkin Methods for Parabolic Equations with Nonlinear Coefficients," the coauthors M. Moon et al. perform error estimations of the hybridizable discontinuous Galerkin method for parabolic equations with nonlinear coefficients. They give the bounds for their estimates when the nonlinear coefficients obey the Lipschitz condition. The authors also prove that the errors for their estimations are bounded.

7. Economical System

In their article "Computation of the Stability and Complexity about Triopoly Price Game Model with Delay Decision," the coauthors Y. Wang et al. develop a price game model based on the entropy theory and chaos theory. They consider the three enterprises bounded rationality and use the cost function under the resource constraints. With variation of the delay parameters, bifurcation, stability, and chaos of the system are discussed, and the change of entropy is considered when the system is far away from its equilibrium. They also show that chaos of the system can be controlled effectively.

Acknowledgments

We would like to express our sincere thanks to all the authors and reviewers for their contributions to this special issue.

Zhi-Yuan Sun
Panayotis G. Kevrekidis
Xin Yu
K. Nakkeeran

Hindawi
Advances in Mathematical Physics
Volume 2017, Article ID 9736818, 11 pages
https://doi.org/10.1155/2017/9736818

Research Article

Error Estimates on Hybridizable Discontinuous Galerkin Methods for Parabolic Equations with Nonlinear Coefficients

Minam Moon,[1] Hyung Kyu Jun,[1] and Tay Suh[2]

[1]*Department of Mathematics, Korea Military Academy, Hwarangro 564, Seoul 01805, Republic of Korea*
[2]*Department of Mathematics, Korea University, Anamro 145, Seoul 02841, Republic of Korea*

Correspondence should be addressed to Hyung Kyu Jun; hkjun0327@kma.ac.kr

Received 11 November 2016; Revised 24 March 2017; Accepted 11 April 2017; Published 3 May 2017

Academic Editor: Kaliyaperumal Nakkeeran

HDG method has been widely used as an effective numerical technique to obtain physically relevant solutions for PDE. In a practical setting, PDE comes with nonlinear coefficients. Hence, it is inevitable to consider how to obtain an approximate solution for PDE with nonlinear coefficients. Research on using HDG method for PDE with nonlinear coefficients has been conducted along with results obtained from computer simulations. However, error analysis on HDG method for such settings has been limited. In this research, we give error estimations of the hybridizable discontinuous Galerkin (HDG) method for parabolic equations with nonlinear coefficients. We first review the classical HDG method and define notions that will be used throughout the paper. Then, we will give bounds for our estimates when nonlinear coefficients obey "Lipschitz" condition. We will then prove our main result that the errors for our estimations are bounded.

1. Introduction

In this paper, we obtain uniform-in-time convergence error estimates for the semidiscretization by hybridizable discontinuous Galerkin (HDG) methods for the parabolic equation with nonlinear coefficient.

$$u_t - \nabla \cdot (\kappa(u) \nabla u) = f, \quad \text{in } \Omega \times (0, T], \tag{1a}$$

$$u(x, t) = 0, \quad \text{on } \partial\Omega \times (0, T], \tag{1b}$$

$$u(x, 0) = u_0, \quad \text{on } \Omega. \tag{1c}$$

Here, $\kappa(u) \geq \kappa_0 > 0$ is a nonlinear coefficient, Ω is a bounded polyhedral domain in $\mathbb{R}^n$, $n = 2, 3$, and T is final time.

Parabolic equation (or sometimes denoted as "heat equation") describes the distribution of heat in a certain region over time with given boundary conditions. Hence, physically, u can be interpreted as a time-dependent function that describes the temperature at a given location. Despite the importance, both practical and purely theoretical, of finding exact solutions for parabolic equations, it is very difficult to obtain closed-form solutions for the parabolic equation with nonlinear coefficients. Details regarding parabolic equations and the way of applying numerical approximations in various contexts can be found in diverse sources such as [1–3] or [4].

As said earlier, parabolic equations are particularly interesting as the equations inherently contain physical meanings, that is, information regarding heat transfer. And in many contexts, in order to explain naturally observable phenomenon, parabolic equations with linear coefficients are insufficient: we inevitably face those equations with nonlinear coefficients. One of the most fundamental difficulties of dealing with parabolic equations (or any PDE) with nonlinear coefficients is that finding an exact solution is extremely difficult, if impossible (whereas existence of the solution can be easily shown when we require certain conditions on coefficients). Thus, we tend to focus on finding numerical approximations.

Various methods have been developed to find approximate solutions for given parabolic equations having nonlinear coefficients (or more generally, any PDE). Some examples of popular methods include but are not limited to finite

volume method [5], finite difference method [6], continuous Galerkin (CG) method [7], discontinuous Galerkin (DG) method [3, 7–9], HDG method [10, 11] (the method that we will mainly focus on), and mixed methods [12, 13]. Among the listed methods, DG has been studied the most.

Since Douglas Jr. et al. [14, 15] and Arnold [16] first introduced DG method for parabolic equations (and, at the same time, elliptic equations), it has been classically used to give physically meaningful approximate solutions [17], primarily because the method is notably advantageous over the continuous Galerkin (CG) method in many contexts. First, DG can be used in a much broader context as it can be used on general meshes. Furthermore, degrees of polynomials can be arbitrary. Also, DG can produce highly accurate discretization for convection-diffusion equations. It can also be applied to solve problems with unambiguous boundary conditions. Since DG can provide approximate solutions with high accuracy and it can be used on general meshes, the method has been widely used to solve nonlinear problems. Detailed explanations on DG methods can be found in [18].

However, there are some disadvantages on using DG method, and this inevitably gave a rise to HDG method, which tends to alleviate disadvantageous facets of DG. As [19] shows, HDG method, when compared to DG analyses (see [18, 20] and/or [21], e.g.), DG method produces larger globally coupled degrees of freedom than CG when the mesh size is invariant, since the degree of freedom is not shared by the boundary elements. In short, DG method is computationally ineffective when it is compared to CG method [18], and this shortcoming is the very reason the standard hybridizable discontinuous Galerkin (HDG) method was first introduced in [17] and developed. In HDG setting, the degrees of freedom associated with the numerical trances of the field variables solely matter in algebraic system. Degrees of freedom are substantially reduced as the numerical traces are only defined on the interelement boundaries. Consequentially, HDG method is very efficient [19].

As we are dealing with numerical approximations, one may ask how accurate our approximations are, and this question is what we would like to answer in this study. Previously, optimal convergence order for convection-diffusion equations was studied in L^2 norm of $k+1$ polynomials of degree k (see [19, 22]). Then, the choices of stabilization parameter were presented in numerical values and analyzed [23]. Then, based on optimal convergence and superconvergence of HDG methods, local postprocessing was developed in [24] for linear convection-diffusion equations and in [25] for nonlinear case to increase the convergence order of numerical solutions. Despite the importance of solving parabolic equations and the substantial number of researches on applying various techniques to give approximate solutions that tend to hint that, at least for now, HDG method seems to be the best tools we have in our pocket, error analysis has not been conducted yet. To have a sense on how accurate the approximate solution is, we obtained through HDG a method which is indispensable, primarily because we need to check whether the result obtained from the method is meaningful or not. We limit ourselves to parabolic equations with nonlinear coefficients and conduct error estimation to investigate how accurate our approximation is.

In this paper, we will conduct an error analysis within HDG frame. We will use HDG projections of exact solution, satisfying certain properties. Then, by computing the magnitude of the norm of the difference between the projected solution and the approximate solution, we compute how far HDG approximations can deviate from the exact solution. The main idea is to derive HDG error equations (that will be introduced in the third section), and, by using the error equations, we will derive several identities that will give an upper bound for the error.

The paper is organized in the following way: after this introduction, we will give some introduction on HDG method, and along with that, we will define notions regarding HDG method that will be used throughout the paper. Then, in Section 3, we will give a priori estimation while assuming certain bounds for the nonlinear coefficient. We will then give error estimations for the proposed HDG method.

2. Preliminaries

2.1. Notations and Norms. Let $\mathcal{T}_h$ be a conforming, shape-regular simplicial triangulation of our domain Ω [26]. For any element $K \in \mathcal{T}_h$, ∂K is defined to be the set of edges of K when $\dim(K) = 2$. When $\dim(K) = 3$, it is defined as the set of the faces of K and is denoted by F. Let $\partial\mathcal{T}_h := \cup_{K\in\mathcal{T}_h}\partial K$. Now, let ϵ_h denote the set of all edges/faces of the triangulation $\mathcal{T}_h$. ϵ_h^0 is the set of all interior faces of the triangulation. Now, for any element $K \in \mathcal{T}_h$, h_K is the diameter of K, and define $h := \max_{K\in\mathcal{T}_h} h_K$. Call this number the mesh size.

Throughout the paper, we will use the standard notations for Sobolev spaces and their norms on the domain Ω and the boundary. For example, $\|v\|_{s,\Omega}, |v|_{s,\Omega}, \|v\|_{s,\partial\Omega}, |v|_{s,\partial\Omega}, s > 0$, denote the Sobolev norms and seminorms on Ω and its boundary $\partial\Omega$. For an integer s, the Sobolev spaces are Hilbert spaces and the norms are defined by the L^2 norms on their weak derivatives up to the order s. When s is not an integer, the spaces are defined by the interpolation [27].

Furthermore, we use $\|\cdot\|_D$ to denote the $L^2(D)$-norm for any D. If $D = \Omega$, we simply write $\|\cdot\|$. We denote the norm and seminorm on any Sobolev space X by $\|\cdot\|_X$ and $|\cdot|_X$, respectively. We also denote $\|\cdot\|_{X(0,T;Y(\Omega))}$ by $\|\cdot\|_{X(Y)}$. For example,

$$\|f\|_{L^2(L^2)} := \left(\int_0^T \|f\|_{L^2}\, dt\right)^{1/2} \tag{2}$$

Set

$$\|w\|_{\tau,D}^2 := \int_{\partial D} \tau w^2 ds. \tag{3}$$

When $D = \Omega$, we replace $\|\cdot\|_{\tau,\Omega}$ by $\|\cdot\|_\tau$.

2.2. The HDG Method. We consider the following mixed form for the semidiscretization by hybridizable discontinuous Galerkin methods (HDG) of problems (1a), (1b), and (1c).

$$\alpha(u)\,\mathbf{q} + \nabla u = 0 \quad \text{in } \Omega \times (0,T], \tag{4a}$$

$$u_t + \nabla \cdot \mathbf{q} = f \quad \text{in } \Omega \times (0,T], \tag{4b}$$

$$u = 0 \quad \text{on } \partial\Omega \times (0,T], \tag{4c}$$

$$u(t=0) = u_0 \quad \text{on } \Omega, \tag{4d}$$

where $\alpha(u) = \kappa(u)^{-1}$.

For each time t on the interval $[0,T]$, the method yields a scalar approximation $u_h(t)$ to $u(t)$, a vector approximation $\mathbf{q}_h(t)$ to $\mathbf{q}(t)$, and a scalar approximation $\widehat{u}_h(t)$ to the trace of $u(t)$ on element boundaries, in spaces of the form

$$W_h := \left\{ w \in L^2(\Omega) : w|_K \in W(K),\ \forall K \in \mathcal{T}_h \right\}, \tag{5a}$$

$$\mathbf{V}_h := \left\{ \mathbf{v} \in \mathbf{L}^2(\Omega) : \mathbf{v}|_K \in \mathbf{V}(K),\ \forall K \in \mathcal{T}_h \right\}, \tag{5b}$$

$$M_h := \left\{ \mu \in L^2(\mathcal{E}_h) : \mu|_F \in M(F),\ \forall F \in \mathcal{E}_h \right\}, \tag{5c}$$

respectively, where

$$\begin{aligned} W(K) &= \mathcal{P}_k(K), \\ \mathbf{V}(K) &= \boldsymbol{\mathcal{P}}_k(K), \\ M(F) &= \mathcal{P}_k(F). \end{aligned} \tag{6}$$

Here, $\boldsymbol{\mathcal{P}}_k(K) := [\mathcal{P}_k(K)]^n$ and $\mathcal{P}_k(K)$ is the space of polynomial of total degree at most k.

With the spaces, HDG method provides approximations $(u_h, \mathbf{q}_h, \widehat{u}_h) \in W_h \times \mathbf{V}_h \times M_h$, determined by the following five restrictions:

For any $(w, \mathbf{v}, \mu) \in W_h \times \mathbf{V}_h \times M_h$, we require

$$(\alpha(u_h)\,\mathbf{q}_h, \mathbf{v})_{\mathcal{T}_h} - (u_h, \nabla \cdot \mathbf{v})_{\mathcal{T}_h} + \langle \widehat{u}_h, \mathbf{v} \cdot \mathbf{n} \rangle_{\partial\mathcal{T}_h} = 0, \tag{7a}$$

$$\begin{aligned} &(\partial_t u_h, w)_{\mathcal{T}_h} - (\mathbf{q}_h, \nabla w)_{\mathcal{T}_h} + \langle \widehat{\mathbf{q}}_h \cdot \mathbf{n}, w \rangle_{\partial\mathcal{T}_h} \\ &\quad = (f, w)_{\mathcal{T}_h}, \end{aligned} \tag{7b}$$

$$\langle \widehat{u}_h, \mu \rangle_{\partial\Omega} = 0, \tag{7c}$$

$$\langle \widehat{\mathbf{q}}_h \cdot \mathbf{n}, \mu \rangle_{\partial\mathcal{T}_h \setminus \partial\Omega} = 0, \tag{7d}$$

$$u_h(0) = Pu_0, \tag{7e}$$

with a numerical trace for the flux defined

$$\widehat{\mathbf{q}}_h \cdot \mathbf{n} = \mathbf{q}_h \cdot \mathbf{n} + \tau(u_h - \widehat{u}_h) \quad \text{on } \partial\mathcal{T}_h \tag{7f}$$

for some nonnegative stabilization parameter τ defined on $\partial\mathcal{T}_h$, which we assume to be piecewise constant on $\partial\mathcal{T}_h$. Here, Pu_0 is an L^2 projection of u_0 onto $\mathcal{P}_k$.

Now, for vector-valued functions $\mathbf{u}, \mathbf{v} \in (L^2(D))^k$, define $(\mathbf{u}, \mathbf{v})_D := \int_D \mathbf{u} \cdot \mathbf{v}$. For scalar-valued functions $u, v \in L^2(D)$, define $(u, v)_D := \int_D uv$, when the domain D is a subset of $\mathbb{R}^k$. If ∂D is in $\mathbb{R}^{k-1}$, define $\langle u, v \rangle_{\partial D} := \int_{\partial D} uv ds$. Then, we introduce the following notations:

$$\begin{aligned} (u, v)_{\mathcal{T}_h} &= \sum_{K \in \mathcal{T}_h} (u, v)_K, \\ \langle u, v \rangle_{\partial\mathcal{T}_h} &= \sum_{\partial K \in \partial\mathcal{T}_h} \langle u, v \rangle_{\partial K}. \end{aligned} \tag{8}$$

2.3. The Projection. The projection Π_h into $\mathbf{V}_h \times W_h$, which was first introduced in [11], is defined as follows.

Given $(\mathbf{q}, u) \in \mathbf{H}_{\text{div}}(\mathcal{T}_h) \times H^1(\mathcal{T}_h)$, the function $\Pi_h(\mathbf{q}, u) = (\boldsymbol{\Pi}_V \mathbf{q}, \Pi_W u)$ on an arbitrary simplex $K \in \mathcal{T}_h$ is the element of $\mathbf{V}_h \times W_h$ which solves

$$(\boldsymbol{\Pi}_V \mathbf{q}, \mathbf{v})_K = (\mathbf{q}, \mathbf{v})_K, \quad \forall \mathbf{v} \in \boldsymbol{\mathcal{P}}_{k-1}(K) \tag{9a}$$

$$(\Pi_W u, w)_K = (u, w)_K, \quad \forall w \in \mathcal{P}_{k-1}(K), \tag{9b}$$

$$\begin{aligned} \langle \boldsymbol{\Pi}_V \mathbf{q} \cdot \mathbf{n} + \tau \Pi_W u, \mu \rangle_F &= \langle \mathbf{q} \cdot \mathbf{n} + \tau u, \mu \rangle_F, \\ &\forall \mu \in \mathcal{P}_k(F), \end{aligned} \tag{9c}$$

for all faces F of the simplex T. Also, P_M denotes the L^2 orthogonal projection onto M_h.

Lemma 1. *If the local spaces $(W(K), \mathbf{V}(K)) = (\mathcal{P}_k(K), \boldsymbol{\mathcal{P}}_k(K))$ for $k \geq 0$ and τ are nonnegative, then the systems (9a), (9b), and (9c) are uniquely solvable for $\boldsymbol{\Pi}_V \mathbf{q}$ and $\Pi_W u$. Furthermore, there is a constant C independent of the choice of K and τ such that, for all $1 \leq s \leq k+1$,*

$$\begin{aligned} \left\| \mathbf{q} - \boldsymbol{\Pi}_V \mathbf{q} \right\|_K &\leq Ch^s \left(\|\mathbf{q}\|_{s,K} + \tau \|u\|_{s,K} \right), \\ \left\| u - \Pi_W u \right\|_K &\leq Ch^s \left(\|u\|_{s,K} + \tau^{-1} \|\nabla \cdot \mathbf{q}\|_{s,K} \right). \end{aligned} \tag{10}$$

Proof. See [11]. □

The existence and the uniqueness (which depend on the Lipschitz condition that will be presented in the next section and the choices of the approximation spaces and the stabilization parameter τ) on the solution for the system of equations (7a) to (7f) can be found in [28, 29].

We will later use the above lemma to figure out the convergence orders between our estimated solution and the exact solution.

3. A Priori Estimate

Let us first give an assumption on $\alpha(u)$. Remember that $\alpha(u) = \kappa(u)^{-1}$. Hence, we are giving restrictions to our nonlinear coefficient.

Assumption 2. α is chosen in such a way that there exist positive constants C_1, C_2, C_3 and C_4 such that, for all $u \in \mathbb{R}$, we have the following inequalities:

$$\begin{aligned} 0 < C_1 \leq \alpha(u) \leq C_2 < \infty, \\ -\infty < C_3 \leq \alpha'(u) \leq C_4 < \infty. \end{aligned} \tag{11}$$

We further assume that both $\alpha(u)$ and $\alpha'(u)$ are Lipschitz continuous.

With this condition on the nonlinear coefficient, we have the following result:

Lemma 3. *If Assumption 2 holds, then one has*

$$\begin{aligned}\left\|u_h\right\|_{L^\infty(L^2)} &\le C\left(\left\|\Pi_W u_0\right\| + \left\|f\right\|_{L^2(L^2)}\right),\\ \left\|\mathbf{q}_h\right\|_{L^2(L^2)} &\le C\left(\left\|\Pi_W u_0\right\| + \left\|f\right\|_{L^2(L^2)}\right),\end{aligned} \tag{12}$$

where C is a constant that does not depend on mesh size h.

Proof. Take $\mathbf{v} = \mathbf{q}_h$ in (7a), $w = u_h$ in (7b), $\mu = -\widehat{\mathbf{q}}_h \cdot \mathbf{n}$ in (7c), and $\mu = -\widehat{u}_h$ in (7d). Adding the resulting four equations, we get

$$\left(\alpha\left(u_h\right)\mathbf{q}_h, \mathbf{q}_h\right)_{\mathcal{T}_h} + \frac{1}{2}\frac{d}{dt}\left\|u_h\right\|^2 + \Theta_h = \left(f, u_h\right)_{\mathcal{T}_h}, \tag{13}$$

where

$$\begin{aligned}\Theta_h = &-\left(u_h, \nabla\cdot\mathbf{q}_h\right)_{\mathcal{T}_h} + \left\langle\widehat{u}_h, \mathbf{q}_h\cdot\mathbf{n}\right\rangle_{\partial\mathcal{T}_h} - \left(\mathbf{q}_h, \nabla u_h\right)_{\mathcal{T}_h}\\ &+ \left\langle\widehat{\mathbf{q}}_h\cdot\mathbf{n}, u_h\right\rangle_{\partial\mathcal{T}_h} - \left\langle\widehat{\mathbf{q}}_h\cdot\mathbf{n}, \widehat{u}_h\right\rangle_{\partial\mathcal{T}_h}.\end{aligned} \tag{14}$$

Using integration by parts and the definition of $\widehat{\mathbf{q}}_h\cdot\mathbf{n}$, (7f), we get

$$\Theta_h = \left\langle\widehat{\mathbf{q}}_h\cdot\mathbf{n} - \mathbf{q}_h\cdot\mathbf{n}, u_h - \widehat{u}_h\right\rangle_{\partial\mathcal{T}_h} = \left\|u_h - \widehat{u}_h\right\|_\tau^2. \tag{15}$$

Now use Cauchy-Schwarz and Young's inequality and observe that

$$\left|\left(f, u_h\right)_{\mathcal{T}_h}\right| \le \frac{1}{2}\left(\left\|f\right\|^2 + \left\|u_h\right\|^2\right). \tag{16}$$

Integrating with respect to time over the interval $(0, t)$ and using $u_h(0) = \Pi_W u_0$ along with the above results, we get the following inequality:

$$\begin{aligned}&\left\|u_h(t)\right\|^2 + 2C_1\int_0^t\left\|\mathbf{q}_h\right\|^2 + 2\int_0^t\left\|u_h - \widehat{u}_h\right\|_\tau^2\\ &\le \left\|\Pi_W u_0\right\|^2 + \int_0^t\left\|f\right\|^2 + \int_0^t\left\|u_h\right\|^2.\end{aligned} \tag{17}$$

Using Gronwall's lemma, we get

$$\begin{aligned}&\left\|u_h(t)\right\|^2 \le \left\|\Pi_W u_0\right\|^2 + \left\|f\right\|^2_{L^2(L^2)}, \quad \forall t\in(0,T],\\ &\int_0^t\left\|\mathbf{q}_h\right\|^2 \le C\left\|\Pi_W u_0\right\|^2 + C\left\|f\right\|^2_{L^2(L^2)}, \quad \forall t\in(0,T].\end{aligned} \tag{18}$$

This completes the proof. □

4. Error Estimations

Let us now derive error estimates for the proposed method.

4.1. Error Equations. For the remaining sections, we define

$$\begin{aligned}\mathbf{e}_q &:= \mathbf{\Pi}_V\mathbf{q} - \mathbf{q}_h,\\ e_u &:= \Pi_W u - u_h,\\ e_{\widehat{u}} &:= P_M u - \widehat{u}_h,\\ \boldsymbol{\delta}_q &:= \mathbf{q} - \mathbf{\Pi}_V\mathbf{q},\\ \delta_u &:= u - \Pi_W u.\end{aligned} \tag{19}$$

Remark 4. Note that, by triangle inequality,

$$\left\|u_h - u\right\| \le \left\|u - \Pi_W u\right\| + \left\|\Pi_W u - u_h\right\|. \tag{20}$$

The first term (i.e., $\|u-\Pi_W u\|$) that appears in RHS is bounded by Lemma 1. Hence, we only need to find an upper bound for $\Pi_W u - u_h =: e_u$. Similarly, we only need to bound $\mathbf{e}_q$ to give an upper bound for $\|\mathbf{q}_h - \mathbf{q}\|$.

Lemma 5. *One has*

$$\begin{aligned}&\left(\alpha\left(u_h\right)\mathbf{e}_q, \mathbf{v}\right)_{\mathcal{T}_h} - \left(e_u, \nabla\cdot\mathbf{v}\right)_{\mathcal{T}_h} + \left\langle e_{\widehat{u}}, \mathbf{v}\cdot\mathbf{n}\right\rangle_{\partial\mathcal{T}_h}\\ &\quad= -\left(\alpha\left(u_h\right)\boldsymbol{\delta}_q, \mathbf{v}\right)_{\mathcal{T}_h} + \left(\left(\alpha\left(u_h\right) - \alpha\left(u\right)\right)\mathbf{q}, \mathbf{v}\right)_{\mathcal{T}_h},\end{aligned} \tag{21a}$$

$$\begin{aligned}&\left(\partial_t e_u, w\right)_{\mathcal{T}_h} - \left(\mathbf{e}_q, \nabla w\right)_{\mathcal{T}_h} + \left\langle\mathbf{e}_{\widehat{q}}\cdot\mathbf{n}, w\right\rangle_{\partial\mathcal{T}_h}\\ &\quad= -\left(\partial_t\delta_u, w\right)_{\mathcal{T}_h},\end{aligned} \tag{21b}$$

$$\left\langle e_{\widehat{u}}, \mu\right\rangle_{\partial\Omega} = 0, \tag{21c}$$

$$\left\langle\mathbf{e}_{\widehat{q}}\cdot\mathbf{n}, \mu\right\rangle_{\partial\mathcal{T}_h\setminus\partial\Omega} = 0, \tag{21d}$$

$$e_u(0) = \Pi_W u_0 - P u_0, \tag{21e}$$

for all $(w, \mathbf{v}, \mu) \in W_h \times \mathbf{V}_h \times M_h$, where

$$\mathbf{e}_{\widehat{q}}\cdot\mathbf{n} = \mathbf{e}_q\cdot\mathbf{n} + \tau\left(e_u - e_{\widehat{u}}\right) \quad \text{on } \partial\mathcal{T}_h. \tag{21f}$$

Proof. For all $(w, \mathbf{v}, \mu) \in W_h \times \mathbf{V}_h \times M_h$, the exact solution $(u, \mathbf{q})$ obviously satisfies the following four equations:

$$\begin{aligned}&\left(\alpha\left(u\right)\mathbf{q}, \mathbf{v}\right)_{\mathcal{T}_h} - \left(u, \nabla\cdot\mathbf{v}\right)_{\mathcal{T}_h} + \left\langle u, \mathbf{v}\cdot\mathbf{n}\right\rangle_{\partial\mathcal{T}_h} = 0,\\ &\left(\partial_t u, w\right)_{\mathcal{T}_h} - \left(\mathbf{q}, \nabla w\right)_{\mathcal{T}_h} + \left\langle\mathbf{q}\cdot\mathbf{n}, w\right\rangle_{\partial\mathcal{T}_h} = \left(f, w\right)_{\mathcal{T}_h},\\ &\left\langle u, \mu\right\rangle_{\partial\Omega} = 0,\\ &\left\langle\mathbf{q}\cdot\mathbf{n}, \mu\right\rangle_{\partial\mathcal{T}_h\setminus\partial\Omega} = 0.\end{aligned} \tag{22}$$

Since P_M is the L^2 projection into M_h and satisfies the orthogonal property, we have

$$\left\langle\tau\left(P_M u - u\right), \mu\right\rangle_{\partial\mathcal{T}_h} = 0, \quad \forall\mu\in M_h. \tag{23}$$

By the properties of the projection $(\Pi_W, \mathbf{\Pi}_V, P_M)$, we have

$$\begin{aligned}
&\left(\alpha\left(u_h\right)\mathbf{\Pi}_V\mathbf{q},\mathbf{v}\right)_{\mathcal{T}_h}-\left(\Pi_W u,\nabla\cdot\mathbf{v}\right)_{\mathcal{T}_h}\\
&\quad+\left\langle P_M u,\mathbf{v}\cdot\mathbf{n}\right\rangle_{\partial\mathcal{T}_h}=\left(\alpha\left(u_h\right)\mathbf{\Pi}_V\mathbf{q},\mathbf{v}\right)_{\mathcal{T}_h}\\
&\quad-\left(\alpha\left(u\right)\mathbf{q},\mathbf{v}\right)_{\mathcal{T}_h},\\
&\left(\Pi_W\partial_t u,w\right)_{\mathcal{T}_h}-\left(\mathbf{\Pi}_V\mathbf{q},\nabla w\right)_{\mathcal{T}_h}\\
&\quad+\left\langle\mathbf{q}\cdot\mathbf{n}+\tau\left(\Pi_W u-P_M u\right),w\right\rangle_{\partial\mathcal{T}_h}=\left(f,w\right)_{\mathcal{T}_h}\\
&\quad-\left(\Pi_W\partial_t u-\partial_t u,w\right)_{\mathcal{T}_h},\\
&\left\langle P_M u,\mu\right\rangle_{\partial\mathcal{T}_h}=0,
\end{aligned}\tag{24}$$

for all $(w,\mathbf{v},\mu)\in W_h\times\mathbf{V}_h\times M_h$. Subtracting the first three equations defining the HDG method (i.e., (7a)–(7c)), from the above equations in order, we obtain (21a)–(21c).

By the definition of $\mathbf{e}_{\widehat{q}}\cdot\mathbf{n}$, (21f) and the property of the projection, (9c), we get

$$\begin{aligned}
\left\langle\mathbf{e}_{\widehat{q}}\cdot\mathbf{n},\mu\right\rangle_{\partial\mathcal{T}_h\backslash\partial\Omega}&=\left\langle\mathbf{q}\cdot\mathbf{n},\mu\right\rangle_{\partial\mathcal{T}_h\backslash\partial\Omega}\\
&\quad-\left\langle\mathbf{q}_h\cdot\mathbf{n},\mu\right\rangle_{\partial\mathcal{T}_h\backslash\partial\Omega}.
\end{aligned}\tag{25}$$

Notice that both of the above terms are zero. Hence, (21d) follows.

This completes the proof. □

Remark 6. Note that, by definition, $\|e_u(0)=\Pi_W u_0-Pu_0\|\le\|\Pi_W u_0-u_0\|+\|Pu_0-u_0\|$. Using Lemma 1, as in Remark 4, the two terms in the right hand side both vanish when h is small enough. Hence, from now on, to ease the computation, we assume that $e_u(0)=0$; that is, although in reality, to take account for $e_u(0)$, we have two extra nonzero terms $\|\Pi_W u_0-u_0\|$ and $\|Pu_0-u_0\|$ in equalities that we would show, we will ignore the two terms from now on for simplicity.

4.2. Estimations for e_u in $L^\infty(L^2)$

Lemma 7. *For any $t\in(0,T]$, one has*

$$\begin{aligned}
&\frac{1}{2}\left\|e_u\left(t\right)\right\|^2+\int_0^t\left(\alpha\left(u_h\right)\mathbf{e}_q,\mathbf{e}_q\right)_{\mathcal{T}_h}+\int_0^t\left\|e_u-e_{\widehat{u}}\right\|_\tau^2\\
&\quad=\mathbb{S}_1+\mathbb{S}_2+\mathbb{S}_3,
\end{aligned}\tag{26}$$

where

$$\begin{aligned}
\mathbb{S}_1&=-\int_0^t\left(\alpha\left(u_h\right)\boldsymbol{\delta}_q,\mathbf{e}_q\right)_{\mathcal{T}_h},\\
\mathbb{S}_2&=\int_0^t\left(\left(\alpha\left(u_h\right)-\alpha\left(u\right)\right)\mathbf{q},\mathbf{e}_q\right)_{\mathcal{T}_h},\\
\mathbb{S}_3&=-\int_0^t\left(\partial_t\delta_u,e_u\right)_{\mathcal{T}_h}.
\end{aligned}\tag{27}$$

Proof. Take $\mathbf{v}=\mathbf{e}_q$ in (21a), $w=e_u$ in (21b), $\mu=-\mathbf{e}_{\widehat{q}}\cdot\mathbf{n}$ in (21c), and $\mu=-e_{\widehat{u}}$ in (21d). Add the four equations that we get. We then get

$$\begin{aligned}
&\left(\alpha\left(u_h\right)\mathbf{e}_q,\mathbf{e}_q\right)_{\mathcal{T}_h}+\frac{1}{2}\frac{d}{dt}\left\|e_u\right\|^2+\Theta_h\\
&\quad=-\left(\alpha\left(u_h\right)\boldsymbol{\delta}_q,\mathbf{e}_q\right)_{\mathcal{T}_h}+\left(\left(\alpha\left(u_h\right)-\alpha\left(u\right)\right)\mathbf{q},\mathbf{e}_q\right)_{\mathcal{T}_h}\\
&\quad-\left(\partial_t\delta_u,e_u\right)_{\mathcal{T}_h},
\end{aligned}\tag{28}$$

where

$$\begin{aligned}
\Theta_h&=-\left(e_u,\nabla\cdot\mathbf{e}_q\right)_{\mathcal{T}_h}+\left\langle e_{\widehat{u}},\mathbf{e}_q\cdot\mathbf{n}\right\rangle_{\partial\mathcal{T}_h}-\left(\mathbf{e}_q,\nabla e_u\right)_{\mathcal{T}_h}\\
&\quad+\left\langle\mathbf{e}_{\widehat{q}}\cdot\mathbf{n},e_u\right\rangle_{\partial\mathcal{T}_h}-\left\langle e_{\widehat{u}},\mathbf{e}_{\widehat{q}}\cdot\mathbf{n}\right\rangle_{\partial\mathcal{T}_h}.
\end{aligned}\tag{29}$$

Using integration by parts and the definition of $\mathbf{e}_{\widehat{q}}\cdot\mathbf{n}$, (21f), we have

$$\Theta_h=\left\langle\mathbf{e}_{\widehat{q}}\cdot\mathbf{n}-\mathbf{e}_q\cdot\mathbf{n},e_u-e_{\widehat{u}}\right\rangle_{\partial\mathcal{T}_h}=\left\|e_u-e_{\widehat{u}}\right\|_\tau^2.\tag{30}$$

The identity we wanted to prove follows after integrating in time over the interval $(0,t)$ and using the fact that $e_u(0)=0$ by (21e). □

Theorem 8. *If Assumption 2 is satisfied and $f\in H^1(L^2)$, one has*

$$\begin{aligned}
&\left\|e_u\right\|_{L^\infty(L^2)}\\
&\quad\le C\left(\left\|\mathbf{q}-\mathbf{\Pi}_V\mathbf{q}_h\right\|_{L^2(L^2)}+\left\|u-\Pi_W u\right\|_{H^1(L^2)}\right),
\end{aligned}\tag{31}$$

where C is independent of mesh size h.

Proof of Theorem 8. Consider $\mathbb{S}_i$'s we defined in the previous lemma. Applying Cauchy-Schwarz and Young's inequalities to the equation that defines $\mathbb{S}_1$, we get the following inequality:

$$\begin{aligned}
\left|\mathbb{S}_1\right|&\le\int_0^t\left|\left(\alpha\left(u_h\right)\boldsymbol{\delta}_q,\mathbf{e}_q\right)_{\mathcal{T}_h}\right|\le C_2\int_0^t\left|\left(\boldsymbol{\delta}_q,\mathbf{e}_q\right)_{\mathcal{T}_h}\right|\\
&\le C\left\|\boldsymbol{\delta}_q\right\|_{L^2(L^2)}^2+\epsilon\int_0^t\left\|\mathbf{e}_q\right\|^2,
\end{aligned}\tag{32}$$

since $0<C_1\le\alpha(u)\le C_2<\infty,\ \forall u\in\mathbb{R}$.

Similarly, we get the following inequality for $\mathbb{S}_3$.

$$\left|\mathbb{S}_3\right|\le\int_0^t\left|\left(\partial_t\delta_u,e_u\right)_{\mathcal{T}_h}\right|\le C\left\|\partial_t\delta_u\right\|_{L^2(L^2)}^2+\epsilon\int_0^t\left\|e_u\right\|^2.\tag{33}$$

Since α is Lipschitz continuous and $\mathbf{q}\in\mathbf{H}_{\mathrm{div}}$, we have

$$\begin{aligned}
\left|\mathbb{S}_2\right|&\le\int_0^t\left|\left(\left(\alpha\left(u_h\right)-\alpha\left(u\right)\right)\mathbf{q},\mathbf{e}_q\right)_{\mathcal{T}_h}\right|\\
&\le C\int_0^t\left\|u_h-u\right\|\left\|\mathbf{e}_q\right\|\\
&\le C\int_0^t\left\|e_u+\delta_u\right\|^2+\epsilon\int_0^t\left\|\mathbf{e}_q\right\|^2\\
&\le C\left\|\delta_u\right\|_{L^2(L^2)}+C\int_0^t\left\|e_u\right\|^2+\epsilon\int_0^t\left\|\mathbf{e}_q\right\|^2.
\end{aligned}\tag{34}$$

Since α is bounded below by C_1, we get

$$C_1 \int_0^t \left\|\mathbf{e}_q\right\|^2 \leq \int_0^t \left(\alpha\left(u_h\right)\mathbf{e}_q, \mathbf{e}_q\right)_{\mathcal{T}_h}. \tag{35}$$

Therefore, we have

$$\begin{aligned}\left\|e_u(t)\right\|^2 &+ \left(C_1 - 2\epsilon\right)\int_0^t \left\|\mathbf{e}_q\right\|^2 + 2\int_0^t \left\|e_u - e_{\widehat{u}}\right\|_\tau^2 \\ &\leq C\left\|\boldsymbol{\delta}_q\right\|_{L^2(L^2)}^2 + C\left\|\delta_u\right\|_{L^2(L^2)}^2 + C\left\|\partial_t\delta_u\right\|_{L^2(L^2)}^2 \\ &\quad + \left(C+\epsilon\right)\int_0^t \left\|e_u\right\|^2.\end{aligned} \tag{36}$$

Take $\epsilon < C_1/2$ and apply Gronwall's lemma. We have

$$\begin{aligned}\left\|e_u(t)\right\|^2 &\leq C\left\|\boldsymbol{\delta}_q\right\|_{L^2(L^2)}^2 + C\left\|\delta_u\right\|_{L^2(L^2)}^2 \\ &\quad + C\left\|\partial_t\delta_u\right\|_{L^2(L^2)}^2, \quad \forall t \in (0,T].\end{aligned} \tag{37}$$

Therefore,

$$\begin{aligned}\left\|e_u\right\|_{L^\infty(L^2)} &\leq C\left\|\boldsymbol{\delta}_q\right\|_{L^2(L^2)} + C\left\|\delta_u\right\|_{L^2(L^2)} \\ &\quad + C\left\|\partial_t\delta_u\right\|_{L^2(L^2)}.\end{aligned} \tag{38}$$

□

Corollary 9. *If Assumption 2 is satisfied and $f \in H^1(L^2)$, one has*

$$\left\|\mathbf{e}_q\right\| \leq C\left(\left\|\mathbf{q} - \boldsymbol{\Pi}_V\mathbf{q}_h\right\| + \left\|u - \Pi_W u\right\|_{H^1(L^2)}\right), \tag{39}$$

where C is independent of mesh size h.

Proof. We obtained bounds for $\mathbb{S}_i$'s from the proof of Theorem 8. Using Lemma 7, we obtain the desired upper bound. □

Remark 10. Note that the above result gives (together with triangle inequality) an upper bound for $\|u - u_h\|$. Depending on how we discretize the time interval $(0,T]$, the convergence order with respect to time is determined. Note that the convergence order of $\|u - \Pi_W u\|_K$ with respect to the given space was already determined by Lemma 1. Hence, we only need to sum (or integrate if our discretization was continuous) with respect to time to determine the convergence order.

4.3. Estimations for $\mathbf{e}_q$ in $L^\infty(L^2)$

Lemma 11. *If Assumption 2 is satisfied and $f \in H^1(L^2)$, one has*

$$\begin{aligned}&\left\|\partial_t\mathbf{e}_q\right\|_{L^2(L^2)} \\ &\quad \leq C\left(\left\|\mathbf{q} - \boldsymbol{\Pi}_V\mathbf{q}\right\|_{H^1(L^2)} + \left\|u - \Pi_W u\right\|_{H^2(L^2)}\right),\end{aligned} \tag{40}$$

where C is independent of a mesh size h.

Proof. We differentiate all of error equations (21a)–(21e), with respect to time, and obtain

$$\begin{aligned}&\left(\partial_t\left(\alpha\left(u_h\right)\mathbf{e}_q\right), \mathbf{v}\right)_{\mathcal{T}_h} - \left(\partial_t e_u, \nabla\cdot v\right)_{\mathcal{T}_h} \\ &\quad + \left\langle\partial_t e_{\widehat{u}}, \mathbf{v}\cdot\mathbf{n}\right\rangle_{\partial\mathcal{T}_h} = -\left(\partial_t\left(\alpha\left(u_h\right)\boldsymbol{\delta}_q\right), \mathbf{v}\right)_{\mathcal{T}_h} \\ &\quad + \left(\partial_t\left(\left(\alpha\left(u_h\right) - \alpha(u)\right)\mathbf{q}\right), \mathbf{v}\right)_{\mathcal{T}_h}, \\ &\left(\partial_{tt}e_u, w\right)_{\mathcal{T}_h} - \left(\partial_t\mathbf{e}_q, \nabla w\right)_{\mathcal{T}_h} \\ &\quad + \left\langle\partial_t\mathbf{e}_{\widehat{q}}\cdot\mathbf{n}, w\right\rangle_{\partial\mathcal{T}_h} = -\left(\partial_{tt}\delta_u, w\right)_{\mathcal{T}_h}, \\ &\left\langle\partial_t e_{\widehat{u}}, \mu\right\rangle_{\partial\Omega} = 0, \\ &\left\langle\partial_t\mathbf{e}_{\widehat{q}}\cdot\mathbf{n}, \mu\right\rangle_{\partial\mathcal{T}_h\setminus\partial\Omega} = 0,\end{aligned} \tag{41}$$

for all $(w, \mathbf{v}, \mu) \in W_h \times \mathbf{V}_h \times M_h$, where

$$\partial_t\mathbf{e}_{\widehat{q}}\cdot\mathbf{n} = \partial_t\mathbf{e}_q\cdot\mathbf{n} + \tau\left(\partial_t e_u - \partial_t e_{\widehat{u}}\right) \quad \text{on } \partial\mathcal{T}_h. \tag{42}$$

Take $\mathbf{v} = \partial_t\mathbf{e}_q$, $w = \partial_t e_u$, $\mu = -\partial_t\mathbf{e}_{\widehat{q}}\cdot\mathbf{n}$, and $\mu = -\partial_t e_{\widehat{u}}$ in the above four equations in that order. Adding the resulting four equations and following the steps of calculation as in the previous lemma, we get

$$\begin{aligned}&\int_0^t \left(\alpha\left(u_h\right)\partial_t\mathbf{e}_q, \partial_t\mathbf{e}_q\right)_{\mathcal{T}_h} + \frac{1}{2}\left\|\partial_t e_u(t)\right\|^2 \\ &\quad + \int_0^t \left\|\partial_t e_u - \partial_t e_{\widehat{u}}\right\|_\tau^2 = \mathbb{T}_1 + \mathbb{T}_2 + \mathbb{T}_3 + \mathbb{T}_4,\end{aligned} \tag{43}$$

where

$$\begin{aligned}\mathbb{T}_1 &= -\int_0^t \left(\partial_t\left(\alpha\left(u_h\right)\boldsymbol{\delta}_q\right), \partial_t\mathbf{e}_q\right)_{\mathcal{T}_h}, \\ \mathbb{T}_2 &= \int_0^t \left(\partial_t\left(\left(\alpha\left(u_h\right) - \alpha(u)\right)\mathbf{q}\right), \partial_t\mathbf{e}_q\right)_{\mathcal{T}_h}, \\ \mathbb{T}_3 &= -\int_0^t \left(\partial_{tt}\delta_u, \partial_t e_u\right)_{\mathcal{T}_h}, \\ \mathbb{T}_4 &= -\int_0^t \left(\alpha'\left(u_h\right)\partial_t u_h\mathbf{e}_q, \partial_t\mathbf{e}_q\right)_{\mathcal{T}_h}.\end{aligned} \tag{44}$$

Note first that Lemma 1 tells us that

$$\left\|\boldsymbol{\delta}_q\right\| \leq Ch^s\left(\|q\| + \tau\|u\|\right). \tag{45}$$

Thus, whenever we have suitably small h, we will be able to make $\|\boldsymbol{\delta}_q\|$ as small as we want. Keeping this in mind, using Cauchy-Schwarz' and Young's inequalities, we get

$$\begin{aligned}\left|\mathbb{T}_1\right| &= \left|-\int_0^t \left(\partial_t\left(\alpha\left(u_h\right)\boldsymbol{\delta}_q\right), \partial_t\mathbf{e}_q\right)_{\mathcal{T}_h}\right| \\ &= \left|\int_0^t \left(\alpha'\left(u_h\right)\partial_t u_h\boldsymbol{\delta}_q, \partial_t\mathbf{e}_q\right)_{\mathcal{T}_h}\right.\end{aligned}$$

$$+\int_0^t \left(\alpha\left(u_h\right)\partial_t\boldsymbol{\delta}_q,\partial_t\mathbf{e}_q\right)_{\mathcal{T}_h}\Big| \le C\int_0^t \left\|\partial_t u_h\right\|^2 + \epsilon\int_0^t \left\|\partial_t\mathbf{e}_q\right\|^2 + C\int_0^t \left\|\partial_t\boldsymbol{\delta}_q\right\|^2 + \epsilon\int_0^t \left\|\partial_t\mathbf{e}_q\right\|^2 \le C\int_0^t \left\|\partial_t u_h\right\|^2 + C\left\|\partial_t\boldsymbol{\delta}_q\right\|^2_{L^2(L^2)} + 2\epsilon\int_0^t \left\|\partial_t\mathbf{e}_q\right\|^2. \tag{46}$$

To estimate $\mathbb{T}_2$, observe that (use the Lipschitz assumption on α and the fact that $\partial_t u$ is bounded)

$$\begin{aligned}\left|\alpha'\left(u_h\right)\partial_t u_h - \alpha'\left(u\right)\partial_t u\right| &\le \left|\alpha'\left(u_h\right)\partial_t u_h - \alpha'\left(u_h\right)\partial_t u\right| + \left|\alpha'\left(u_h\right)\partial_t u - \alpha'\left(u\right)\partial_t u\right| \\ &\le \left|\alpha'\left(u_h\right)\right|\left\|\partial_t u_h - \partial_t u\right\| + \left\|\partial_t u\right\|\left|\alpha'\left(u\right) - \alpha'\left(u_h\right)\right| \\ &\le C_1\left\|\partial_t\left(u_h - u\right)\right\| + C_2\left\|u_h - u\right\| \\ &\le C_1\left(\left\|\partial_t e_u\right\| + \left\|\partial_t\delta_u\right\|\right) + C_2\left(\left\|e_u\right\| + \left\|\delta_u\right\|\right).\end{aligned} \tag{47}$$

We then get the following estimations for $\mathbb{T}_2$:

$$\begin{aligned}\left|\mathbb{T}_2\right| &= \left|\int_0^t \left(\partial_t\left\{\left(\alpha\left(u_h\right) - \alpha\left(u\right)\right)\mathbf{q}\right\},\partial_t\mathbf{e}_q\right)_{\mathcal{T}_h}\right| \\ &= \left|\int_0^t \left(\left(\alpha\left(u_h\right) - \alpha\left(u\right)\right)\partial_t\mathbf{q},\partial_t\mathbf{e}_q\right)_{\mathcal{T}_h} + \int_0^t \left(\left(\alpha'\left(u_h\right)\partial_t u_h - \alpha'\left(u\right)\partial_t u\right)\mathbf{q},\partial_t\mathbf{e}_q\right)_{\mathcal{T}_h}\right| \\ &\le C\int_0^T \left\|u_h - u\right\|\left\|\partial_t\mathbf{e}_q\right\| + C\int_0^t \left(\left\|\partial_t\left(u_h - u\right)\right\| + \left\|u_h - u\right\|\right)\left\|\partial_t\mathbf{e}_q\right\| \\ &\le C\int_0^T \left(\left\|e_u\right\| + \left\|\delta_u\right\|\right)\left\|\partial_t\mathbf{e}_q\right\| + C\int_0^t \left(\left\|\partial_t e_u\right\| + \left\|\partial_t\delta_u\right\|\right)\left\|\partial_t\mathbf{e}_q\right\| \le C\left\|e_u\right\|^2_{L^\infty(L^2)} \\ &\quad + C\left\|\delta_u\right\|^2_{L^2(L^2)} + C\left\|\partial_t\delta_u\right\|^2_{L^2(L^2)} + C\int_0^t \left\|\partial_t e_u\right\|^2 + 4\epsilon\int_0^t \left\|\partial_t\mathbf{e}_q\right\|^2.\end{aligned} \tag{48}$$

Apply Cauchy-Schwarz and Young's inequalities and get the following inequality for $\mathbb{T}_3$:

$$\left|\mathbb{T}_3\right| \le \int_0^t \left|\left(\partial_{tt}\delta_u,\partial_t e_u\right)_{\mathcal{T}_h}\right| \le C\left\|\partial_{tt}\delta_u\right\|^2_{L^2(L^2)} + \epsilon\int_0^t \left\|\partial_t e_u\right\|^2. \tag{49}$$

Now let us derive an inequality for $\mathbb{T}$. Remember that it is a well-known that when we have a finite dimensional vector space endowed with two norms $\|\cdot\|_1$ and $\|\cdot\|_2$ then the two norms are equivalent. That is, for any vector $\mathbf{v}$ in that vector space, there exists two constants C_1 and C_2, independent of the choice of $\mathbf{v}$, such that $C_1\|\mathbf{v}\|_1 \le \|\mathbf{v}\|_2 \le C_2\|\mathbf{v}\|_1$. Now, observe that

$$\begin{aligned}\left|\mathbb{T}_4\right| &= \left|-\int_0^t \left(\alpha'\left(u_h\right)\partial_t u_h\mathbf{e}_q,\partial_t\mathbf{e}_q\right)_{\mathcal{T}_h}\right| \\ &\le \left|-\int_0^t \left(\alpha'\left(u_h\right)\partial_t\left(u_h - u\right)\mathbf{e}_q,\partial_t\mathbf{e}_q\right)_{\mathcal{T}_h}\right| + \left|-\int_0^t \left(\alpha'\left(u\right)\partial_t u\mathbf{e}_q,\partial_t\mathbf{e}_q\right)_{\mathcal{T}_h}\right|.\end{aligned} \tag{50}$$

Note that (using Lipschitz condition for α and the fact that $\partial_t u$ is bounded) the second term

$$\left|-\int_0^t \left(\alpha'\left(u\right)\partial_t u\mathbf{e}_q,\partial_t\mathbf{e}_q\right)_{\mathcal{T}_h}\right| \le C\left\|\mathbf{e}_q\right\|^2_{L^2(L^2)} + \epsilon\int_0^t \left\|\partial_t\mathbf{e}_q\right\|^2. \tag{51}$$

For the first term,

$$\left|-\int_0^t \left(\alpha'\left(u_h\right)\partial_t\left(u_h - u\right)\mathbf{e}_q,\partial_t\mathbf{e}_q\right)_{\mathcal{T}_h}\right|, \tag{52}$$

observe that (using Hölder's inequality and the fact that all norms are equivalent in a finite dimensional vector space)

$$\begin{aligned}&\left|-\int_0^t \left(\alpha'\left(u_h\right)\partial_t\left(u_h - u\right)\mathbf{e}_q,\partial_t\mathbf{e}_q\right)_{\mathcal{T}_h}\right| \\ &\le C\int_0^t \left(\left\|\partial_t e_u\right\| + \left\|\partial_t\delta_u\right\|\right)\left(\left\|\mathbf{e}_q\right\|_{L^4}\left\|\partial_t\mathbf{e}_q\right\|_{L^4}\right) \\ &\le C\int_0^t \left(\left\|\partial_t e_u\right\| + \left\|\partial_t\delta_u\right\|\right)\left(\left\|\mathbf{e}_q\right\|_{L^2}\left\|\partial_t\mathbf{e}_q\right\|_{L^2}\right).\end{aligned} \tag{53}$$

Using Corollary 9, we can take (by decreasing the mesh size of h) $\|\mathbf{e}_q\|$ as small as we want. Proceeding (similarly to how we derived an inequality for $\mathbb{T}_1$), we get

$$\begin{aligned}\left|\mathbb{T}_4\right| &= \left|-\int_0^t \left(\alpha'\left(u_h\right)\partial_t u_h\mathbf{e}_q,\partial_t\mathbf{e}_q\right)_{\mathcal{T}_h}\right| \\ &\le C\left\|\mathbf{e}_q\right\|^2_{L^2(L^2)} + C\int_0^t \left\|\partial_t e_u\right\|^2_{L^2(L^2)} + 2\epsilon\int_0^t \left\|\partial_t\mathbf{e}_q\right\|^2_{L^2(L^2)} + C\left\|\partial_t\delta_u\right\|^2_{L^2(L^2)}.\end{aligned} \tag{54}$$

Applying the Gronwall's lemma, we have

$$\left\|\partial_t e_u\right\|^2_{L^\infty(L^2)} \le C\left\|e_u\right\|^2_{L^\infty(L^2)} + C\left\|\mathbf{e}_q\right\|^2_{L^2(L^2)} + C\left\|\boldsymbol{\delta}_q\right\|^2_{H^1(L^2)} + C\left\|\delta_u\right\|^2_{H^2(L^2)}. \tag{55}$$

Applying the error estimates of Theorem 8 and Corollary 9, we obtain

$$\left\|\partial_t \mathbf{e}_q\right\|^2_{L^2(L^2)} \le C\left\|\boldsymbol{\delta}_q\right\|^2_{H^1(L^2)} + C\left\|\delta_u\right\|^2_{H^2(L^2)}. \tag{56}$$

Therefore,

$$\begin{aligned}\left\|\partial_t \mathbf{e}_q\right\|_{L^2(L^2)} &\le C\left\|\mathbf{q} - \boldsymbol{\Pi}_V \mathbf{q}\right\|_{H^1(L^2)} \\ &\quad + C\left\|u - \Pi_W u\right\|_{H^2(L^2)},\end{aligned} \tag{57}$$

and we are done. □

Lemma 12. *For any $t \in (0, T]$, one has*

$$\begin{aligned}&\int_0^t \frac{d}{dt}\left(\alpha\left(u_h\right)\mathbf{e}_q, \mathbf{e}_q\right)_{\mathcal{T}_h} + \int_0^t \left\|\partial_t e_u\right\|^2 \\ &\quad + \frac{1}{2}\left\|e_u(t) - e_{\widehat{u}}(t)\right\|^2_\tau \\ &= \frac{1}{2}\left\|e_u(0) - e_{\widehat{u}}(0)\right\|^2_\tau + \mathbb{M}_1 + \mathbb{M}_2 + \mathbb{M}_3 + \mathbb{M}_4,\end{aligned} \tag{58}$$

where

$$\begin{aligned}\mathbb{M}_1 &= -\int_0^t \left(\partial_t\left(\alpha\left(u_h\right)\boldsymbol{\delta}_q\right), \mathbf{e}_q\right)_{\mathcal{T}_h}, \\ \mathbb{M}_2 &= \int_0^t \left(\partial_t\left\{\left(\alpha\left(u_h\right) - \alpha(u)\right)\mathbf{q}\right\}, \mathbf{e}_q\right)_{\mathcal{T}_h}, \\ \mathbb{M}_3 &= -\int_0^t \left(\partial_t \delta_u, \partial_t e_u\right)_{\mathcal{T}_h}, \\ \mathbb{M}_4 &= \int_0^t \left(\alpha\left(u_h\right)\mathbf{e}_q, \partial_t \mathbf{e}_q\right)_{\mathcal{T}_h}.\end{aligned} \tag{59}$$

Proof. We keep all the error equations except for (21a) and (21c); instead of the two, we use the equations obtained from differentiating the two equations with respect to time t. That is, we have the following equations:

$$\begin{aligned}&\left(\partial_t\left(\alpha\left(u_h\right)\mathbf{e}_q\right), \mathbf{v}\right)_{\mathcal{T}_h} - \left(\partial_t e_u, \nabla\cdot\mathbf{v}\right)_{\mathcal{T}_h} \\ &\quad + \left\langle \partial_t e_{\widehat{u}}, \mathbf{v}\cdot\mathbf{n}\right\rangle_{\partial\mathcal{T}_h} = -\left(\partial_t\left(\alpha\left(u_h\right)\boldsymbol{\delta}_q\right), \mathbf{v}\right)_{\mathcal{T}_h} \\ &\quad + \left(\partial_t\left\{\left(\alpha\left(u_h\right) - \alpha(u)\right)\mathbf{q}\right\}, \mathbf{v}\right)_{\mathcal{T}_h}, \\ &\left(\partial_t e_u, w\right)_{\mathcal{T}_h} - \left(\mathbf{e}_q, \nabla w\right)_{\mathcal{T}_h} \\ &\quad + \left\langle \mathbf{e}_{\widehat{q}}\cdot\mathbf{n}, w\right\rangle_{\partial\mathcal{T}_h} = -\left(\partial_t \delta_u, w\right)_{\mathcal{T}_h}, \\ &\left\langle \partial_t e_{\widehat{u}}, \mu\right\rangle_{\partial\Omega} = 0, \\ &\left\langle \mathbf{e}_{\widehat{q}}\cdot\mathbf{n}, \mu\right\rangle_{\partial\mathcal{T}_h\setminus\partial\Omega} = 0, \\ &e_u(0) = 0,\end{aligned} \tag{60}$$

for all $(w, \mathbf{v}, \mu) \in W_h \times \mathbf{V}_h \times M_h$, where $\mathbf{e}_{\widehat{q}}\cdot\mathbf{n} = \mathbf{e}_q\cdot\mathbf{n} + \tau(e_u - e_{\widehat{u}})$ on $\partial\mathcal{T}_h$.

Substitute $\mathbf{v} = \mathbf{e}_q$ to the first equation, $w = \partial_t e_u$ to the second one, $\mu = -\mathbf{e}_{\widehat{q}}\cdot\mathbf{n}$ to the third one, and $\mu = -\partial_t e_{\widehat{u}}$ to the fourth one. Adding the resulting four equations, we get

$$\begin{aligned}&\frac{d}{dt}\left(\alpha\left(u_h\right)\mathbf{e}_q, \mathbf{e}_q\right)_{\mathcal{T}_h} + \left\|\partial_t e_u\right\|^2 + \Xi_h \\ &\quad = \left(\partial_t\left(\alpha\left(u_h\right)\mathbf{e}_q\right), \mathbf{e}_q\right)_{\mathcal{T}_h} + \left(\alpha\left(u_h\right)\mathbf{e}_q, \partial_t \mathbf{e}_q\right)_{\mathcal{T}_h} \\ &\qquad + \left\|\partial_t e_u\right\|^2 + \Xi_h \\ &\quad = -\left(\partial_t\left(\alpha\left(u_h\right)\boldsymbol{\delta}_q\right), \mathbf{e}_q\right)_{\mathcal{T}_h} \\ &\qquad + \left(\partial_t\left\{\left(\alpha\left(u_h\right) - \alpha(u)\right)\mathbf{q}\right\}, \mathbf{e}_q\right)_{\mathcal{T}_h} \\ &\qquad - \left(\partial_t \delta_u, \partial_t e_u\right)_{\mathcal{T}_h} + \left(\alpha\left(u_h\right)\mathbf{e}_q, \partial_t \mathbf{e}_q\right)_{\mathcal{T}_h},\end{aligned} \tag{61}$$

where

$$\begin{aligned}\Xi_h &= \left\langle \mathbf{e}_{\widehat{q}}\cdot\mathbf{n} - \mathbf{e}_q\cdot\mathbf{n}, \partial_t\left(e_u - e_{\widehat{u}}\right)\right\rangle_{\partial\mathcal{T}_h} \\ &= \frac{1}{2}\frac{d}{dt}\left\|e_u - e_{\widehat{u}}\right\|^2_\tau.\end{aligned} \tag{62}$$

Integrating in time over the interval $(0, t)$, we can get the desired identity. □

Theorem 13. *If Assumption 2 holds, and $f \in H^1(L^2)$, one has*

$$\begin{aligned}\left\|\mathbf{e}_q\right\|_{L^\infty(L^2)} &\le C\left(\left(\left\|\mathbf{q} - \boldsymbol{\Pi}_V\mathbf{q}(0)\right\| + \left\|u_0 - \Pi_W u_0\right\|\right)\right. \\ &\quad \left. + \left\|\mathbf{q} - \boldsymbol{\Pi}_V\mathbf{q}\right\|_{H^1(L^2)} + \left\|u - \Pi_W u\right\|_{H^2(L^2)}\right),\end{aligned} \tag{63}$$

where C is independent of mesh size h.

Proof. To get the above estimate, we consider the identity obtained from the previous lemma. By Cauchy-Schwarz and Young's inequalities, we get the following inequality for $\mathbb{M}_1$:

$$\begin{aligned}\left|\mathbb{M}_1\right| &= \left|-\int_0^t \left(\partial_t\left(\alpha\left(u_h\right)\boldsymbol{\delta}_q\right), \mathbf{e}_q\right)_{\mathcal{T}_h}\right| \\ &= \left|\int_0^t \left(\left(\alpha'\left(u_h\right)\partial_t u_h \boldsymbol{\delta}_q\right), \mathbf{e}_q\right)_{\mathcal{T}_h}\right. \\ &\quad \left. + \int_0^t \left(\left(\alpha\left(u_h\right)\partial_t \boldsymbol{\delta}_q\right), \mathbf{e}_q\right)_{\mathcal{T}_h}\right| \le \epsilon\int_0^t \left\|\partial_t u_h\right\|^2 \\ &\quad + C\int_0^t \left\|\mathbf{e}_q\right\|^2 + C\int_0^t \left\|\partial_t \boldsymbol{\delta}_q\right\|^2 + \epsilon\int_0^t \left\|\mathbf{e}_q\right\|^2 \\ &\le \epsilon\int_0^t \left\|\partial_t u_h\right\|^2 + C\left\|\partial_t \boldsymbol{\delta}_q\right\|^2_{L^2(L^2)} + 2\epsilon\int_0^t \left\|\mathbf{e}_q\right\|^2.\end{aligned} \tag{64}$$

Note that

$$\begin{aligned}&\left|\alpha'\left(u_h\right)\partial_t u_h - \alpha'(u)\partial_t u\right| \\ &\quad \le C_1\left(\left\|\partial_t e_u\right\| + \left\|\partial_t \delta_u\right\|\right) + C_2\left(\left\|e_u\right\| + \left\|\delta_u\right\|\right).\end{aligned} \tag{65}$$

Hence,

$$
\begin{aligned}
|\mathbb{M}_2| &= \left| \int_0^t \left(\partial_t \left\{ \left(\alpha\left(u_h\right) - \alpha\left(u\right) \right) \mathbf{q} \right\}, \mathbf{e}_q \right)_{\mathcal{T}_h} \right| \\
&= \left| \int_0^t \left(\left(\alpha\left(u_h\right) - \alpha\left(u\right) \right) \partial_t \mathbf{q}, \mathbf{e}_q \right)_{\mathcal{T}_h} \right. \\
&\quad \left. + \int_0^t \left(\left(\alpha'\left(u_h\right) \partial_t u_h - \alpha'\left(u\right) \partial_t u \right) \mathbf{q}, \mathbf{e}_q \right)_{\mathcal{T}_h} \right| \\
&\leq C \int_0^T \left\| u_h - u \right\| \left\| \mathbf{e}_q \right\| \\
&\quad + C \int_0^t \left(\left\| \partial_t \left(u_h - u \right) \right\| + \left\| \left(u_h - u \right) \right\| \right) \left\| \mathbf{e}_q \right\| \\
&\leq C \int_0^T \left(\left\| e_u \right\| + \left\| \delta_u \right\| \right) \left\| \mathbf{e}_q \right\| \\
&\quad + C \int_0^t \left(\left\| \partial_t e_u \right\| + \left\| \partial_t \delta_u \right\| \right) \left\| \mathbf{e}_q \right\| \leq C \left\| e_u \right\|^2_{L^\infty(L^2)} \\
&\quad + C \left\| \delta_u \right\|^2_{L^2(L^2)} + C \left\| \partial_t \delta_u \right\|^2_{L^2(L^2)} + (3\epsilon + C) \int_0^t \left\| \mathbf{e}_q \right\|^2 \\
&\quad + \epsilon \int_0^t \left\| \partial_t e_u \right\|^2 .
\end{aligned} \tag{66}
$$

Applying Cauchy-Schwarz and Young's inequalities, we get

$$
\begin{aligned}
|\mathbb{M}_3| &\leq \int_0^t \left| \left(\partial_t \delta_u, \partial_t e_u \right)_{\mathcal{T}_h} \right| \\
&\leq C \left\| \partial_t \delta_u \right\|^2_{L^2(L^2)} + \epsilon \int_0^t \left\| \partial_t e_u \right\|^2 , \\
|\mathbb{M}_4| &= \left| - \int_0^t \left(\alpha\left(u_h\right) \mathbf{e}_q, \partial_t \mathbf{e}_q \right)_{\mathcal{T}_h} \right| \\
&\leq \left\| \partial_t \mathbf{e}_q \right\|^2_{L^2(L^2)} + \epsilon \int_0^t \left\| \mathbf{e}_q \right\|^2 .
\end{aligned} \tag{67}
$$

Applying the error estimations from Lemma 11 and Theorem 8, we have

$$
\begin{aligned}
&\left\| \mathbf{e}_q\left(t\right) \right\|^2 + \left(\frac{1}{C_1} - 2\epsilon \right) \int_0^t \left\| \partial_t e_u \right\|^2 \\
&\quad + \frac{1}{2C_1} \left\| e_u - e_{\widehat{u}}\left(t\right) \right\|^2_\tau \\
&\leq \left\| \mathbf{e}_q\left(0\right) \right\|^2 + \frac{1}{2C_1} \left\| e_u\left(0\right) - e_{\widehat{u}}\left(0\right) \right\|^2_\tau \\
&\quad + C \left(\left\| \boldsymbol{\delta}_q \right\|^2_{L^2(L^2)} + \left\| \partial_t \boldsymbol{\delta}_q \right\|^2_{L^2(L^2)} \right) \\
&\quad + C \left(\left\| \delta_u \right\|^2_{L^2(L^2)} + \left\| \partial_t \delta_u \right\|^2_{L^2(L^2)} + \left\| \partial_{tt} \delta_u \right\|^2_{L^2(L^2)} \right) \\
&\quad + (C + 6\epsilon) \int_0^t \left\| \mathbf{e}_q \right\|^2 .
\end{aligned} \tag{68}
$$

Take $\epsilon < 1/2C_1$ and use Gronwall's lemma. We obtain

$$
\begin{aligned}
&\left\| \mathbf{e}_q\left(t\right) \right\|^2 \\
&\leq C \left(\left\| \mathbf{e}_q\left(0\right) \right\|^2 + \frac{1}{2C_1} \left\| e_u\left(0\right) - e_{\widehat{u}}\left(0\right) \right\|^2_\tau \right) \\
&\quad + C \left(\left\| \boldsymbol{\delta}_q \right\|^2_{L^2(L^2)} + \left\| \partial_t \boldsymbol{\delta}_q \right\|^2_{L^2(L^2)} \right) \\
&\quad + C \left(\left\| \delta_u \right\|^2_{L^2(L^2)} + \left\| \partial_t \delta_u \right\|^2_{L^2(L^2)} + \left\| \partial_{tt} \delta_u \right\|^2_{L^2(L^2)} \right), \\
&\qquad \forall t \in (0, T] .
\end{aligned} \tag{69}
$$

Next, we note that if we differentiate Lemma 7 and evaluate the resulting equation at $t = 0$, we obtain

$$
\begin{aligned}
&\left\| \mathbf{e}_q\left(0\right) \right\|^2 + \frac{1}{2C_1} \left\| e_u - e_{\widehat{u}_h}\left(0\right) \right\|^2_\tau \\
&\leq \left| \left(\alpha\left(u_h\right) \boldsymbol{\delta}_q\left(0\right), \mathbf{e}_q\left(0\right) \right)_{\mathcal{T}_h} \right| \\
&\quad + \left| \left(\left(\alpha\left(u_h\left(0\right)\right) - \alpha\left(u\left(0\right)\right) \right) \mathbf{q}\left(0\right), \mathbf{e}_q\left(0\right) \right)_{\mathcal{T}_h} \right|, \\
&\leq C \left\| \boldsymbol{\delta}_q\left(0\right) \right\|^2 + C \left\| \delta_u\left(0\right) \right\|^2 + 2\epsilon \left\| \mathbf{e}_q\left(0\right) \right\|^2 ,
\end{aligned} \tag{70}
$$

since $e_u(0) = 0$. Therefore, we have the following inequality that bounds $\|\mathbf{e}_q\|_{L^\infty(L^2)}$:

$$
\begin{aligned}
&\left\| \mathbf{e}_q \right\|_{L^\infty(L^2)} \\
&\leq C \left(\left\| \boldsymbol{\delta}_q\left(0\right) \right\| + \left\| \delta_u\left(0\right) \right\| \right) \\
&\quad + C \left(\left\| \boldsymbol{\delta}_q \right\|_{L^2(L^2)} + \left\| \partial_t \boldsymbol{\delta}_q \right\|_{L^2(L^2)} \right) \\
&\quad + C \left(\left\| \delta_u \right\|_{L^2(L^2)} + \left\| \partial_t \delta_u \right\|_{L^2(L^2)} + \left\| \partial_{tt} \delta_u \right\|_{L^2(L^2)} \right) \\
&\leq C \left(\left\| \boldsymbol{\delta}_q\left(0\right) \right\| + \left\| \delta_u\left(0\right) \right\| \right) + C \left\| \boldsymbol{\delta}_q \right\|_{H^1(L^2)} \\
&\quad + C \left\| \delta_u \right\|_{H^2(L^2)} ,
\end{aligned} \tag{71}
$$

and the proof is complete. □

5. Conclusion

In this research, we have presented error estimates on HDG methods for parabolic equations having nonlinear coefficients. Under Lipschitz assumption, that is, Assumption 2, we have found upper bounds for errors $\mathbf{e}_q, e_u$. Using Lemma 1 and "integrate with respect to time t" (or, if time is discretized, summing), we can find how far our estimated solutions can deviate, in terms of a mesh size h from the actual solution. As HDG method is very practical and efficient when compared to classical DG methods such as [16, 18], or [30], the error estimation gives us how reliable our estimation is.

There are some possible generalizations of our result. First, we can replace Lipschitz assumption by more general conditions on which the existence of solutions for PDE can be guaranteed. Other further research topics include changing

the local spaces for the projection. Our main tool for the research was the projection. We projected the solutions to the space of polynomials, and we can possibly use L^2 projection instead.

In our future work, we plan to propose and develop the method by implementing it to the multiscale settings, which will give how the method can be applied to find an approximate solution with satisfying error bounds, without being too time-costly.

As aforementioned, parabolic problems with heterogeneous coefficients inherently are practically applicable in many situations such as porous media. We hope our method would further enrich related studies.

Conflicts of Interest

The authors declare that there are no conflicts of interest regarding the publication of this paper.

Acknowledgments

Minam Moon's work was supported by the Hwa-Rang Dae Research Institute in 2017.

References

[1] F. Gastaldi and A. Quarteroni, "On the coupling of hyperbolic and parabolic systems: Analytical and numerical approach," *Applied Numerical Mathematics*, vol. 6, pp. 3–31, 1989.

[2] P. D. Lax and A. N. Milgram, "Parabolic equations," in *Contributions to the theory of partial differential equations, Annals of Mathematics Studies*, vol. 33 of *Annals of Mathematics Studies*, pp. 167–190, Princeton University Press, Princeton, NJ, USA, 1954.

[3] B. Riviere and M. F. Wheeler, *A discontinuous Galerkin method applied to nonlinear parabolic equations*, Discontinuous Galerkin methods, Springer, Berlin, Germany, 2000.

[4] V. Thomee, *Galerkin finite element method for parabolic problems, Volume 25 of Springer Series in Computational Mathematics*, vol. 25, Springer-Verlag, Berlin, Germany, 2nd edition, 2006.

[5] G. D. Raithby and E. H. Chui, "Finite-volume method for predicting a radiant heat transfer in enclosures with participating media," *Journal of Heat Transfer*, vol. 112, no. 2, pp. 415–423, 1990.

[6] J. J. Benito, F. Urena, and L. Gavete, "Solving parabolic and hyperbolic equations by the generalized finite difference method," *Journal of Computational and Applied Mathematics*, vol. 209, no. 2, pp. 208–233, 2007.

[7] B. Cockburn, G. E. Karniadakis, and C.-W. Shu, "The development of discontinuous Galerkin methods," in *Discontinuous Galerkin Methods*, Springer, Berlin, Germany, 2000.

[8] J. Douglas Jr. and T. Dupont, "Galerkin methods for parabolic equations," *SIAM Journal on Numerical Analysis*, vol. 7, pp. 575–626, 1970.

[9] D. Schotzau and C. Schwab, "Time discretization of parabolic problems by the hp-version of the discontinuous Galerkin finite element method," *SIAM Journal on Numerical Analysis*, vol. 38, no. 3, pp. 837–875, 2000.

[10] B. Chabaud and B. Cockburn, "Uniform-in-time superconvergence of HDG methods for the heat equation," *Mathematics of Computation*, vol. 81, no. 277, pp. 107–129, 2012.

[11] B. Cockburn, J. Gopalakrishnan, and F.-J. Sayas, "A projection-based error analysis of HDG methods," *Mathematics of Computation*, vol. 79, no. 271, pp. 1351–1367, 2010.

[12] R. Eymard, D. Hilhorst, and M. Vohralik, "A combined finite volume nonconforming/mixed-hybrid finite element scheme for degenerate parabolic problems," *Numerische Mathematik*, vol. 105, no. 1, pp. 73–131, 2006.

[13] C. Johnson and V. Thomee, "Error estimates for some mixed finite element methods for parabolic type problems," *RAIRO-Analyse Numérique*, vol. 15, no. 1, pp. 41–78, 1981.

[14] J. Douglas Jr. and T. Dupont, *Lecture Notes in Physics*, vol. 58 of *chapter Interior penalty procedures for elliptic and parabolic Galerkin methods*, Springer-Verlag, Berlin, Germany, 1976.

[15] M. F. Wheeler, "An elliptic collocation-finite element method with interior penalties," *SIAM Journal on Numerical Analysis*, vol. 15, no. 1, pp. 152–161, 1978.

[16] D. N. Arnold, "An interior penalty finite element method with discontinuous elements," *SIAM Journal on Numerical Analysis*, vol. 19, no. 4, pp. 742–760, 1982.

[17] B. Cockburn, J. Gopalakrishnan, and R. Lazarov, "Unified hybridization of discontinuous GALerkin, mixed, and continuous GALerkin methods for second order elliptic problems," *SIAM Journal on Numerical Analysis*, vol. 47, no. 2, pp. 1319–1365, 2009.

[18] D. N. Arnold, F. Brezzi, B. Cockburn, and L. D. Marini, "Unified analysis of discontinuous Galerkin methods for elliptic problems," *SIAM Journal on Numerical Analysis*, vol. 39, no. 5, pp. 1749–1779, 2002.

[19] B. Cockburn, W. Qiu, and K. Shi, "Conditions for superconvergence of HDG methods for second-order elliptic problems," *Mathematics of Computation*, vol. 81, no. 279, pp. 1327–1353, 2012.

[20] B. Cockburn, B. Dong, and J. Guzman, "Superconvergent LDG-hybridizable Galerkin method for second-order elliptic problems," *Mathematics of Computation*, vol. 77, pp. 1887–1916, 2008.

[21] M. Dryja, "On discontinuous Galerkin methods for elliptic problems with discontinuous coefficients," *Computational Methods in Applied Mathematics*, vol. 3, no. 1, pp. 76–85, 2003.

[22] B. Cockburn, J. Guzmán, and H. Wang, "Superconvergent discontinuous Galerkin methods for second-order elliptic problems," *Mathematics of Computation*, vol. 78, no. 265, pp. 1–24, 2009.

[23] B. Cockburn, B. Dong, J. Guzmán, M. Restelli, and R. Sacco, "A hybridizable discontinuous Galerkin method for steady-state convection-diffusion-reaction problems," *SIAM Journal of Scientific Computing*, vol. 31, no. 5, pp. 3827–3846, 2009.

[24] N. C. Nguyen, J. Peraire, and B. Cockburn, "An implicit high-order hybridizable discontinuous Galerkin method for linear convection-diffusion equations," *Journal of Computational Physics*, vol. 228, no. 9, pp. 3232–3254, 2009.

[25] N. C. Nguyen, J. Peraire, and B. Cockburn, "An implicit high-order hybridizable discontinuous Galerkin method for nonlinear convection-diffusion equations," *Journal of Computational Physics*, vol. 228, no. 23, pp. 8841–8855, 2009.

[26] P. Ciarlet, *The Finite Element Method for Elliptic Problems*, North-Holland, Amsterdam, The Netherlands, 1978.

[27] P. Grisvard, *Elliptic Problems in Nonsmooth Domains*, Pitman, Boston, Mass, USA, 1985.

[28] H.-Z. Chen and H. Wang, "An optimalâorder error estimate on an H1âGalerkin mixed method for a nonlinear parabolic equation in porous medium flow," *Numerical Methods for Partial Differential Equations*, vol. 26, no. 1, pp. 188–205, 2010.

[29] R. Z. Dautov and E. M. Fedotov, "Abstract theory of hybridizable discontinuous Galerkin methods for second-order quasilinear elliptic problems," *Computational Mathematics and Mathematical Physics*, vol. 54, no. 3, pp. 474–490, 2014.

[30] C.-C. Chu, I. G. Graham, and T.-Y. Hou, "A new multiscale finite element method for high-contrast elliptic interface problems," *Mathematics of Computation*, vol. 79, no. 272, pp. 1915–1955, 2010.

Hindawi
Advances in Mathematical Physics
Volume 2017, Article ID 5214616, 8 pages
https://doi.org/10.1155/2017/5214616

Research Article

The Spreading Residue Harmonic Balance Method for Strongly Nonlinear Vibrations of a Restrained Cantilever Beam

Y. H. Qian,[1] J. L. Pan,[1] S. P. Chen,[2] and M. H. Yao[3]

[1]*College of Mathematics, Physics and Information Engineering, Zhejiang Normal University, Jinhua, Zhejiang 321004, China*
[2]*College of Mathematics, Xiamen University of Technology, Xiamen 361024, China*
[3]*College of Mechanical Engineering, Beijing University of Technology, Beijing 100124, China*

Correspondence should be addressed to Y. H. Qian; qyh2004@zjnu.cn

Received 2 October 2016; Revised 21 February 2017; Accepted 20 March 2017; Published 10 April 2017

Academic Editor: Zhi-Yuan Sun

The exact solutions of the nonlinear vibration systems are extremely complicated to be received, so it is crucial to analyze their approximate solutions. This paper employs the spreading residue harmonic balance method (SRHBM) to derive analytical approximate solutions for the fifth-order nonlinear problem, which corresponds to the strongly nonlinear vibration of an elastically restrained beam with a lumped mass. When the SRHBM is used, the residual terms are added to improve the accuracy of approximate solutions. Illustrative examples are provided along with verifying the accuracy of the present method and are compared with the HAM solutions, the EBM solutions, and exact solutions in tables. At the same time, the phase diagrams and time history curves are drawn by the mathematical software. Through analysis and discussion, the results obtained here demonstrate that the SRHBM is an effective and robust technique for nonlinear dynamical systems. In addition, the SRHBM can be widely applied to a variety of nonlinear dynamic systems.

1. Introduction

A lot of problems in physical, mechanical, and aeronautical technology and even in structural applications are essentially nonlinear. Majority of the nonlinear dynamical models are mainly composed of a group of differential equations and auxiliary conditions for modeling processes [1]. In general, it is difficult to obtain the exact solution for strongly nonlinear high dimensional dynamic systems. Hence, the analytical approximate solution of the nonlinear problem has become the research object of many scholars in recent years [2–28].

Generally speaking, the fifth-order Duffing type problem with the inertial and static nonlinear terms is sophisticated all the better [29]. Recently, some scholars have tried to study this kind of nonlinear problem. For instance, Telli and Kopmaz [30] and Lai and Lim [31] used the harmonic balance method to study the linear and nonlinear springs. S.-S. Chen and C.-K. Chen [32] dealt with this fifth-order nonlinear problem by applying the differential transformation approach. Subsequently, Ganji et al. [33] and Mehdipour et al. [34], respectively, brought in the homotopy perturbation method, amplitude-frequency formulation, and the energy balance method. They used these methods to solve this strongly nonlinear problem, and lower-order approximate solutions are yielded. Qian et al. [35] studied the nonlinear vibrations of cantilever beam by the HAM. Latterly, Guo et al. [36, 37] have presented the residue harmonic balance solution procedure to approximate the periodic behavior of different oscillation systems and they have obtained some more accurate results. Ju and Xue [38, 39] proposed the global residue harmonic balance method to study strongly nonlinear systems. Comparing the obtained solutions with the exact one, they discovered that the approximate results excellently agree with the exact one. Lee [40] used the multilevel residue harmonic balance method to solve a nonlinear panel coupled with extended cavity.

The principal intention of this paper is to investigate the utility of the spreading residue harmonic balance method (SRHBM) [36] for the fifth-order strongly nonlinear problem. The paper consists of the following several parts. Section 2 describes how the strongly nonlinear equation is educed from the governing equations of the cantilever beam model in

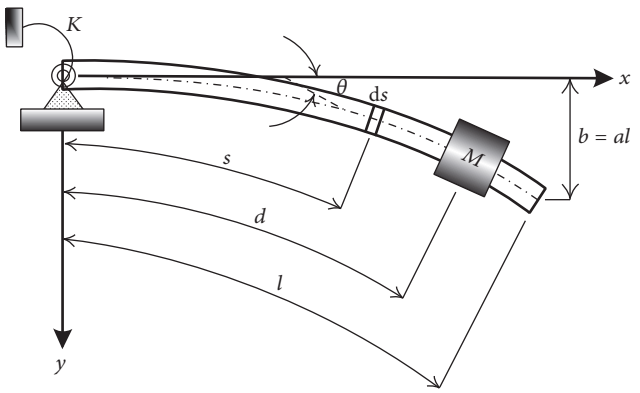

Figure 1: Geometry and coordinate system for a beam with a lumped mass.

a nutshell. In Section 3, the SRHBM is introduced and the solution process of different order solutions will be presented. The numerical examples of the SRHBM are rendered and compared with other solutions in Section 4. Finally, conclusion of the paper is drawn in Section 5.

2. Mathematical Formulation

An isotropic slender beam with uniform length l and mass m per unit length is considered, as shown in Figure 1 [25]. It is assumed that the beam thickness is much smaller than the beam length, so the effects of shear deformation and rotary inertia can be ignored. The angle of inclination is θ and the beam displacement is $a = b/l$. For the boundary condition constraints, one of the conditions is hinged at the bottom of a rotational spring with stiffness K, and the other condition is independent. Moreover, the intermediate lumped mass M is also connected in $s = d$ along the beam span. By the Euler-Lagrange differential equation, the fifth-order Duffing type temporal problem with strongly inertial and static nonlinearities is able to be derived as follows [25]:

$$\begin{aligned} &\ddot{x} + x + \varepsilon_1 x^2 \ddot{x} + \varepsilon_1 x \dot{x}^2 + \varepsilon_2 x^4 \ddot{x} + 2\varepsilon_2 x^3 \dot{x}^2 + \varepsilon_3 x^3 \\ &\quad + \varepsilon_4 x^5 = 0, \\ &x(0) = A, \\ &\dot{x}(0) = 0, \end{aligned} \tag{1}$$

where x is the dimensionless deflection at the tip of the beam, A is the maximum amplitude, the overdot indicates the derivative relative to t, and ε_1, ε_2, ε_3, and ε_4 are parameters. For the complete formulation of (1), readers are referred to [25] for details.

3. Solution Methodology

In the following, the spreading residue harmonic is used to solve (1). Firstly, by introducing a new variable $\tau = \omega t$ and substituting it into (1), we can get

$$\begin{aligned} &\omega^2 x'' + x + \varepsilon_1 \omega^2 x^2 x'' + \varepsilon_1 \omega^2 x x'^2 + \varepsilon_2 \omega^2 x^4 x'' \\ &\quad + 2\varepsilon_2 \omega^2 x^3 x'^2 + \varepsilon_3 x^3 + \varepsilon_4 x^5 = 0, \\ &x(0) = A, \\ &x'(0) = 0, \end{aligned} \tag{2}$$

where x' represents the first-order derivative with respect to τ and ω is the unknown angular frequency of (1).

Since we discuss the existence of a periodic solution, we usually choose the base functions

$$\{\cos[(2k-1)\tau] \mid k = 1, 2, 3, \ldots\}, \tag{3}$$

and we find the expression of the steady state solutions

$$\begin{aligned} x(\tau) &= x_0(\tau) + p x_1(\tau) + p^2 x_2(\tau) + \cdots, \\ \omega^2 &= \omega_0^2 + p\omega_1 + p^2 \omega_2 + \cdots, \end{aligned} \tag{4}$$

where p is an order parameter and ω_i $(i = 0, 1, 2, \ldots)$ are unknown.

Next, we mainly analyze the zeroth-order harmonic approximation, the first-order harmonic approximation, and the second-order harmonic approximation.

3.1. The Zeroth-Order Harmonic Approximation. To meet the initial conditions in (2), we can set the following initial guess solution of $x(\tau)$; that is,

$$x_0(\tau) = A\cos(\tau), \quad \tau = \omega_0 t. \tag{5}$$

Substituting (5) into (2), the equation is yielded:

$$\begin{aligned} R_0(\tau) &= \omega_0^2 x_0''(\tau) + x_0(\tau) + \varepsilon_1 \omega_0^2 x_0^2(\tau) x_0''(\tau) \\ &\quad + \varepsilon_1 \omega_0^2 x_0(\tau) x_0'^2(\tau) + \varepsilon_2 \omega_0^2 x_0^4(\tau) x_0''(\tau) \\ &\quad + 2\varepsilon_2 \omega_0^2 x_0^3(\tau) x_0'^2(\tau) + \varepsilon_3 x_0^3(\tau) + \varepsilon_4 x_0^5(\tau) = \left[A\left(1\right.\right. \\ &\quad \left. - \omega_0^2 + \frac{3}{4}A^2\varepsilon_3 - \frac{1}{2}\varepsilon_1 A^2 \omega_0^2 + \frac{5}{8}A^4\varepsilon_4 - \frac{3}{8}A^4\varepsilon_2\omega_0^2\right)\Big] \\ &\quad \cdot \cos(\tau) + \left[A^3\left(\frac{1}{4}\varepsilon_3 - \frac{1}{2}\varepsilon_1\omega_0^2 + \frac{5}{16}A^2\varepsilon_4\right.\right. \\ &\quad \left.\left. - \frac{7}{16}A^2\varepsilon_2\omega_0^2\right)\right]\cos(3\tau) + \left[\frac{1}{16}A^5\left(\varepsilon_4 - 3\varepsilon_2\omega_0^2\right)\right] \\ &\quad \cdot \cos(5\tau). \end{aligned} \tag{6}$$

$R_0(\tau)$ denotes the zeroth-order residual term. When $R_0(\tau) = 0$, $x_0(\tau)$ is the exact solution.

Based on the Galerkin procedure, the secular term $\cos(\tau)$ cannot appear on the right hand side of (6). Equating the term's coefficient to zero, we obtain a linear equation containing an unknown ω_0. Through solving that equation, we are able to work out the unknown frequency ω_0:

$$\omega_0 = \sqrt{\frac{8 + 6A^2\varepsilon_3 + 5A^4\varepsilon_4}{8 + 4A^2\varepsilon_1 + 3A^4\varepsilon_2^2}}. \tag{7}$$

In addition, the zeroth-order approximation solution can be obtained as follows:

$$x_0(\tau) = A\cos(\omega_0 t). \tag{8}$$

When the obtained zeroth-order solution is substituted into (6), the terms of $\cos(3\tau)$ and $\cos(5\tau)$ generally are not zero.

3.2. The First-Order Harmonic Approximations. Substituting (4) into (2), the coefficient of parameter p is put forward, and we can obtain

$$\begin{aligned}\phi_1(\tau) = {} & \omega_0^2\left[x_1'' \right.\\ & + \varepsilon_1\left(x_1 x_0'^2 + 2x_0 x_0' x_1' + 2x_0 x_1 x_0'' + x_0^2 x_1''\right)\\ & \left. + \varepsilon_2\left(6x_0^2 x_1 x_0'^2 + 4x_0^3 x_0' x_1' + 4x_0^3 x_1 x_0'' + x_0^4 x_1''\right)\right]\\ & + \omega_1\left[x_0'' + \varepsilon_1\left(x_0 x_0'^2 + x_0^2 x_0''\right)\right.\\ & \left. + \varepsilon_2\left(2x_0^3 x_0'^2 + x_0^4 x_0''\right)\right] + x_1 + 3\varepsilon_3 x_0^2 x_1 + 5\varepsilon_4 x_0^4 x_1.\end{aligned} \tag{9}$$

According to (3), we choose the following equation as the solution of the representation:

$$x_1(\tau) = a_{3,1}[\cos(\tau) - \cos(3\tau)], \tag{10}$$

where $a_{3,1}$ is the unknown.

Combining (10) with (9), we consider

$$R_1(\tau) = \phi_1(\tau) + R_0(\tau). \tag{11}$$

We can obtain

$$\begin{aligned}R_1(\tau) = {} & \left[a_{3,1}\left(1-\omega_0^2\right) - A\omega_1 + \frac{3}{2}A^2 a_{3,1}\varepsilon_3\right.\\ & \left. - \frac{1}{2}A^3\omega_1\varepsilon_1 + \frac{5}{16}A^4 a_{3,1}\left(5\varepsilon_4 + \varepsilon_2\omega_0^2\right) - \frac{3}{8}A^5\varepsilon_2\omega_1\right]\\ & \cdot\cos(\tau) + \left[\left(9a_{3,1}\omega_0^2 - a_{3,1}\right)\right.\\ & + A^2\left(\frac{7}{2}a_{3,1}\varepsilon_1\omega_0^2 - \frac{3}{4}a_{3,1}\varepsilon_3\right)\\ & + A^3\left(\frac{1}{4}\varepsilon_3 - \frac{1}{2}\varepsilon_1\left(\omega_0^2 + \omega_1\right)\right)\\ & + A^4\left(\frac{31}{16}a_{3,1}\omega_0^2\varepsilon_2 - \frac{5}{16}a_{3,1}\varepsilon_4\right)\\ & \left. + A^5\left(\frac{5}{16}\varepsilon_4 - \frac{7}{16}\varepsilon_2\left(\omega_0^2 + \omega_1\right)\right)\right]\cos(3\tau)\\ & + \left[A^2\left(\frac{9}{2}a_{3,1}\varepsilon_1\omega_0^2 - \frac{3}{4}a_{3,1}\varepsilon_3\right)\right.\\ & + A^4 a_{3,1}\left(\frac{61}{16}\varepsilon_2\omega_0^2 - \frac{15}{16}\varepsilon_4\right)\\ & \left. + A^5\left(\frac{1}{16}\varepsilon_4 - \frac{3}{16}\varepsilon_2\left(\omega_0^2 + \omega_1\right)\right)\right]\cos(5\tau)\\ & + \left[A^4 a_{3,1}\left(\frac{31}{16}\varepsilon_2\omega_0^2 - \frac{5}{16}\varepsilon_4\right)\right]\cos(7\tau).\end{aligned} \tag{12}$$

To increase the accuracy, (11) should be added in the zeroth-order residual term $R_0(\tau)$.

Based on the Galerkin procedure, (12) should not contain secular terms. Letting coefficients of $\cos(\tau)$ and $\cos(3\tau)$ be zeros, hence, we obtain a linear equation set containing two unknowns ω_1 and $a_{3,1}$. Through solving the equation set, we can get

$$\begin{aligned}\omega_1 = {} & \frac{A^2\left(16 + 24A^2\varepsilon_3 + 25A^4\varepsilon_4 + \left(5A^4\varepsilon_2 - 16\right)\omega_0^2\right)N}{M},\\ a_{3,1} = {} & \frac{2A^3\left(8 + 4A^2\varepsilon_1 + 3A^4\varepsilon_2\right)N}{M},\end{aligned} \tag{13}$$

where

$$\begin{aligned}M = {} & 256\left(1 - 9\omega_0^2\right) + A^8\varepsilon_2\left(205\varepsilon_4 - 151\varepsilon_2\omega_0^2\right)\\ & + 16A^6\left(15\varepsilon_2\varepsilon_3 + 15\varepsilon_1\varepsilon_4 - 34\varepsilon_1\varepsilon_2\omega_0^2\right)\\ & - 16A^4\left(-13\varepsilon_2 - 18\varepsilon_1\varepsilon_3 - 5\varepsilon_4\right.\\ & \left. + 4\left(7\varepsilon_1^2 + 23\varepsilon_2\right)\omega_0^2\right) + 64A^2\left(3\varepsilon_3 + \varepsilon_1\left(4 - 34\omega_0^2\right)\right),\\ N = {} & 4\varepsilon_3 - 8\varepsilon_1\omega_0^2 + A^2\left(5\varepsilon_4 - 7\varepsilon_2\omega_0^2\right).\end{aligned} \tag{14}$$

Therefore, the first-order harmonic approximation can be procured:

$$\begin{aligned}\omega_{(1)} = {} & \sqrt{\omega_0^2 + \omega_1},\\ x_{(1)}(\tau) = {} & x_{(0)}(\tau) + x_1(\tau)\\ = {} & \left(A + a_{3,1}\right)\cos(\tau) - a_{3,1}\cos(3\tau),\\ & \tau = \omega_{(1)} t.\end{aligned} \tag{15}$$

When the obtained first-order solution is substituted into (12), the terms of $\cos(5\tau)$ and $\cos(7\tau)$ commonly are not zero.

3.3. The Second-Order Harmonic Approximations. Substituting (4) to (2) and presenting the coefficient of parameter p^2 yield

$$\begin{aligned}\phi_2(\tau) = {} & \omega_0^2\left(6\varepsilon_2 x_0 x_1^2 x_0'^2 + \varepsilon_1 x_2 x_0'^2 + 6\varepsilon_2 x_2 x_0^2 x_0'^2\right.\\ & + 2\varepsilon_1 x_1 x_0' x_1' + 12\varepsilon_2 x_0^2 x_1 x_0' x_1' + \varepsilon_1 x_0 x_1'^2 + 2\varepsilon_2 x_0^3 x_1'^2\\ & + 2\varepsilon_1 x_0 x_0' x_2' + 4\varepsilon_2 x_0^3 x_0' x_2' + \varepsilon_1 x_1^2 x_0'' + 6\varepsilon_2 x_0^2 x_1^2 x_0''\\ & + 2\varepsilon_1 x_0 x_2 x_0'' + 4\varepsilon_2 x_0^3 x_2 x_0'' + 2\varepsilon_1 x_0 x_1 x_1''\\ & + 4\varepsilon_2 x_0^3 x_1 x_1'' + x_2'' + \varepsilon_1 x_0^2 x_2'' + \varepsilon_2 x_0^4 x_2''\left.\right)\\ & + \omega_1\left(\varepsilon_1 x_1 x_0'^2 + 6\varepsilon_2 x_0^2 x_1 x_0'^2 + 2\varepsilon_1 x_0 x_0' x_1'\right.\\ & \left. + 4\varepsilon_2 x_0^3 x_0' x_1' + 2\varepsilon_1 x_0 x_1 x_0'' + 4\varepsilon_2 x_0^3 x_1 x_0'' + x_1''\right.\end{aligned}$$

$$+\varepsilon_1 x_0^2 x_1'' + \varepsilon_2 x_0^4 x_1'') + \omega_2 (\varepsilon_1 x_0 x_0'^2 + 2\varepsilon_2 x_0^3 x_0'^2 + x_0'' + \varepsilon_1 x_0^2 x_0'' + \varepsilon_2 x_0^4 x_0'') + 3\varepsilon_3 x_0 x_1^2 + 10\varepsilon_4 x_0^3 x_1^2 + x_2 + 3\varepsilon_3 x_0^2 x_2 + 5\varepsilon_4 x_0^4 x_2. \tag{16}$$

Observing (16), we know it is linear with respect to ω_2 and $x_2(\tau)$. In accordance with the form of (3), we apply

$$x_2(\tau) = a_{3,2}[\cos(\tau) - \cos(3\tau)] + a_{5,2}[\cos(\tau) - \cos(5\tau)], \tag{17}$$

where $a_{3,2}$ and $a_{5,2}$ are unknowns.

Combining (17) with (16) and calculating the equation

$$R_2(\tau) = \phi_2(\tau) + R_1(\tau), \tag{18}$$

we can obtain

$$\begin{aligned} R_2(\tau) = {} & \left[A\left(\frac{9}{4}a_{3,1}^2\varepsilon_3 - \frac{7}{2}a_{3,1}^2\varepsilon_1\omega_0^2 - \omega_2\right) + A^2\left(\frac{3}{2}a_{3,2}\varepsilon_3 + \frac{9}{4}a_{5,2}\varepsilon_3 - \frac{3}{2}a_{5,2}\varepsilon_1\omega_0^2\right) + A^3\left(\frac{15}{4}a_{3,1}^2\varepsilon_4 - \frac{13}{4}a_{3,1}^2\varepsilon_2\omega_0^2 - \frac{1}{2}\varepsilon_1\omega_2\right) + \frac{1}{16}\right. \\ & \cdot A^4\left(25a_{3,2}\varepsilon_4 + 45a_{5,2}\varepsilon_4 + 5a_{3,2}\varepsilon_2\omega_0^2 - 15a_{5,2}\varepsilon_2\omega_0^2 + 5a_{3,1}\varepsilon_2\omega_1\right) - \frac{3}{8}A^5\varepsilon_2\omega_2 + \left(a_{3,2} + a_{5,2} - a_{3,2}\omega_0^2\right. \\ & \left.\left. - a_{5,2}\omega_0^2 - a_{3,1}\omega_1\right)\right]\cos(\tau) + \left[Aa_{3,1}^2\left(\frac{17}{2}\varepsilon_1\omega_0^2 - \frac{9}{4}\varepsilon_3\right) + A^2\left(\frac{7}{2}a_{3,2}\varepsilon_1\omega_0^2 - \frac{3}{4}a_{3,2}\varepsilon_3 + \varepsilon_1\left(3a_{5,2}\omega_0^2 + \frac{7}{2}a_{3,1}\omega_1\right)\right) - \frac{1}{2}\right. \\ & \cdot A^3\left(a_{3,1}^2\left(5\varepsilon_4 - 13\varepsilon_2\omega_0^2\right) + \varepsilon_1\omega_2\right) + \frac{1}{16}A^4\left(5a_{5,2}\varepsilon_4 - 5a_{3,2}\varepsilon_4 + 31a_{3,2}\varepsilon_2\omega_0^2 + 41a_{5,2}\varepsilon_2\omega_0^2 + 31a_{3,1}\varepsilon_2\omega_1\right) \\ & \left. - \frac{7}{16}A^5\varepsilon_2\omega_2 + \left(9a_{3,2}\omega_0^2 + 9a_{3,1}\omega_1 - a_{3,2}\right)\right]\cos(3\tau) + \left[Aa_{31}^2\left(\frac{7}{2}\varepsilon_1\omega_0^2 - \frac{3}{4}\varepsilon_3\right) + A^2\left(13a_{5,2}\varepsilon_1\omega_0^2 - \frac{3}{2}a_{5,2}\varepsilon_3 - \frac{3}{4}\left(a_{3,1} + a_{3,2}\right)\left(\varepsilon_3 - 6\varepsilon_1\omega_0^2\right)\right.\right. \\ & \left.\left. + \frac{9}{2}a_{3,1}\varepsilon_1\omega_1\right) + \frac{1}{2}A^3a_{3,1}^2\left(17\varepsilon_2\omega_0^2 - 5\varepsilon_4\right) + \frac{1}{16}\right. \\ & \left. \cdot A^4\left(147a_{5,2}\varepsilon_2\omega_0^2 - 25a_{5,2}\varepsilon_4 - \left(a_{3,1} + a_{3,2}\right)\left(15\varepsilon_4 - 61\varepsilon_2\omega_0^2\right) + 61a_{3,1}\varepsilon_2\omega_1\right) + \frac{1}{16}A^5\left(\varepsilon_4 - 3\varepsilon_2\left(\omega_0^2 + \omega_1 + \omega_2\right)\right) + \left(25a_{5,2}\omega_0^2 - a_{5,2}\right)\right]\cos(5\tau) \\ & + \left[A\left(\frac{3}{4}a_{3,1}^2\varepsilon_3 - \frac{17}{2}a_{3,1}^2\varepsilon_1\omega_0^2\right) - A^2a_{5,2}\left(\frac{3}{4}\varepsilon_3 - \frac{19}{2}\varepsilon_1\omega_0^2\right) + \frac{1}{8}A^3a_{3,1}^2\left(5\varepsilon_4 - 43\varepsilon_2\omega_0^2\right)\right. \\ & + A^4\left(-\frac{5}{16}a_{3,2}\varepsilon_4 - \frac{5}{4}a_{5,2}\varepsilon_4 + \frac{31}{16}a_{3,2}\varepsilon_2\omega_0^2 + \frac{39}{4}a_{5,2}\varepsilon_2\omega_0^2 - \frac{5}{16}a_{3,2}\varepsilon_4\right. \\ & \left.\left.\left. + \frac{1}{16}a_{3,1}\left(31\varepsilon_2\left(\omega_0^2 + \omega_1\right)\right)\right)\right]\cos(7\tau) + \left[\frac{1}{8}\cdot A^3a_{3,1}^2\left(5\varepsilon_4 - 51\varepsilon_2\omega_0^2\right) - \frac{5}{16}A^4a_{5,2}\left(\varepsilon_4 - 11\varepsilon_2\omega_0^2\right)\right]\cos(9\tau). \end{aligned} \tag{19}$$

With the purpose of increasing the accuracy, (18) should be put on the first-order residual term $R_1(\tau)$.

In order to prevent the right hand side of (19) from exhibiting the secular terms $\cos(\tau)$, $\cos(3\tau)$, and $\cos(5\tau)$, we make all their coefficients equal to zero. Then, we can get three linear equations containing three unknown parameters $a_{3,2}$, $a_{5,2}$, and ω_2. According to the three linear equations, we can solve the three unknowns. Thus, the *second*-order harmonic approximation is shown:

$$\begin{aligned} \omega_{(2)} &= \sqrt{\omega_0^2 + \omega_1 + \omega_2}, \\ x_{(2)}(\tau) &= x_{(0)}(\tau) + x_1(\tau) + x_2(\tau), \quad \tau = \omega_{(2)}t. \end{aligned} \tag{20}$$

In conclusion, we draw the kth-order harmonic approximation ($k = 2, 3, 4, \ldots$)

$$\begin{aligned} x_{(k)}(\tau) &= x_{(k-1)}(\tau) + x_k(\tau), \\ \omega_{(k)} &= \sqrt{\omega_{(k-1)}^2 + \omega_k} \quad k = 2, 3, 4, \ldots, \\ x_{(k-1)}(\tau) &= x_{(k-2)}(\tau) + x_{k-1}(\tau), \\ \omega_{(k-1)} &= \sqrt{\omega_{(k-2)}^2 + \omega_{k-1}}, \\ x_k(\tau) &= \sum_{i=1}^{k} a_{2i+1,k}[\cos(\tau) - \cos((2i+1)\tau)], \\ x_{(0)} &= A\cos(\tau), \ \omega_{(0)} = \omega_0, \ k = 2, 3, 4, \ldots. \end{aligned} \tag{21}$$

4. Results and Discussion

In order to make sure of the effectiveness of the current technique, we compare the results from the second-order spreading residue harmonic balance approach ω_{SRHB} with the

Table 1: Comparison of the SRHBM frequencies, EBM frequencies, HAM frequencies, and the exact frequencies for various parameters.

Mode	A	ε_1	ε_2	ε_3	ε_4	ω_{EBM}	ω_{HAM}	ω_{SRHB}	ω_{ex}
1	1.0	0.326845	0.129579	0.232598	0.087584	1.01235	1.01232	1.01004	1.01015
2	0.5	1.642033	0.913055	0.313561	0.204297	0.935046	0.938636	0.935072	0.93639
3	0.2	4.051486	1.665232	0.281418	0.149677	0.965613	0.966516	0.965843	0.96664
4	0.3	8.205578	3.145368	0.272313	0.133708	0.860678	0.871382	0.863939	0.86426

Table 2: Comparison of the SRHBM relative error, EBM relative error, and HAM relative error with the exact frequencies for various parameters.

Mode	A	ε_1	ε_2	ε_3	ε_4	$\frac{\lvert\omega_{\text{EBM}}-\omega_{\text{ex}}\rvert}{\omega_{\text{ex}}}\times 100\%$	$\frac{\lvert\omega_{\text{HAM}}-\omega_{\text{ex}}\rvert}{\omega_{\text{ex}}}\times 100\%$	$\frac{\lvert\omega_{\text{SRHB}}-\omega_{\text{ex}}\rvert}{\omega_{\text{ex}}}\times 100\%$
1	1.0	0.326845	0.129579	0.232598	0.087584	0.21789	0.21482	0.010889
2	0.5	1.642033	0.913055	0.313561	0.204297	0.14353	0.23986	0.140753
3	0.2	4.051486	1.665232	0.281418	0.149677	0.106244	0.01283	0.08245
4	0.3	8.205578	3.145368	0.272313	0.133708	0.414459	0.82406	0.037142

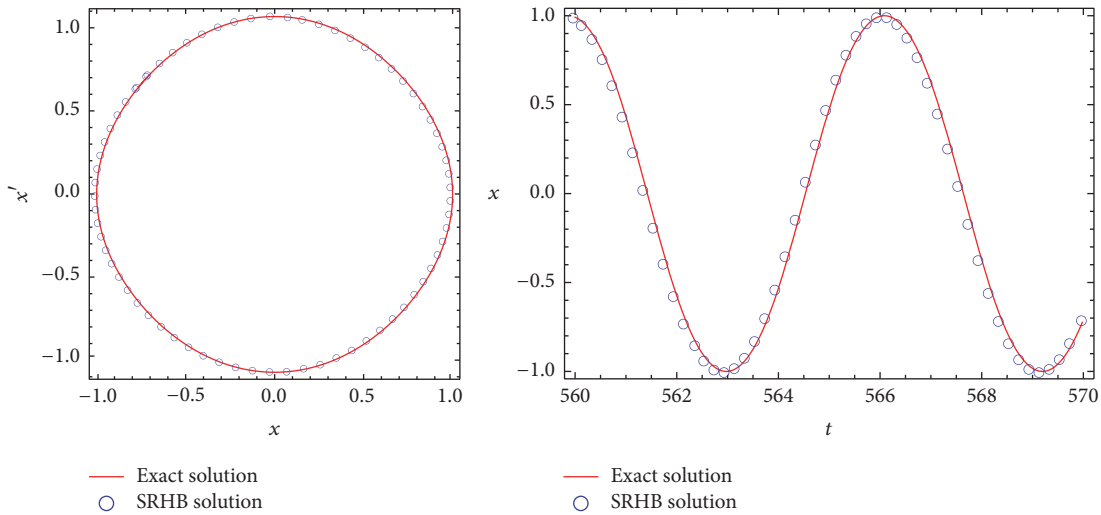

Figure 2: Comparison of the approximate and exact solutions of Mode 1.

energy balance method ω_{EBM} [34], the homotopy analysis method ω_{HAM} [35], and the exact solution ω_{ex} [33], which are presented in Table 1, for different parameters ε_i $(i = 1, 2, 3, 4)$ and amplitudes of vibration A, where the exact solution ω_{ex} is computed using the numerical technique. The relative errors of vibration frequency are tabulated in Table 2.

For Mode 1 in Table 2, we observe that the relative error between ω_{SRHB} and ω_{ex} is much less than the relative error between ω_{HAM} and ω_{ex}. The same goes for Mode 2 and Mode 4. However, the relative error between ω_{SRHB} and ω_{ex} for Mode 3 is more than the relative error between ω_{HAM} and ω_{ex}. Hence, we conclude that the accuracy of the second-order SRHBM solutions is improved in Mode 1, Mode 2, and Mode 4. Similarly, from Table 2, the SRHBM relative error is smaller than EBM relative error in Mode 1, Mode 2, Mode 3, and Mode 4. These results show that the approximate solutions obtained by the SRHBM are closer to the exact solutions.

To further demonstrate the accuracy of the spreading residue harmonic balance approach, the time history responses and the phase portrait are rendered for four different sets of parameters in Figures 2–5. From the phase portrait diagram, we obviously discover that the second-order residue harmonic balance solutions are very consistent with the exact solutions. From the phase portrait, we observe that the system is a periodic motion. Moreover, in the whole range, the presented approximate solutions converge to the exact solutions. Extraordinarily, we argue for t in $[560, 570]$.

5. Conclusions

In this paper, the spreading residue harmonic balance method is applied to discuss the strongly nonlinear vibration system. Particularly, we take a restrained cantilever beam as an example. The SRHBM does not need to add small parameters in the calculation process. Besides, this approach approximates the exact solution quickly and only the first- or second-order approximations. And by comparing its results with HAM and EBM for various parameters and amplitudes

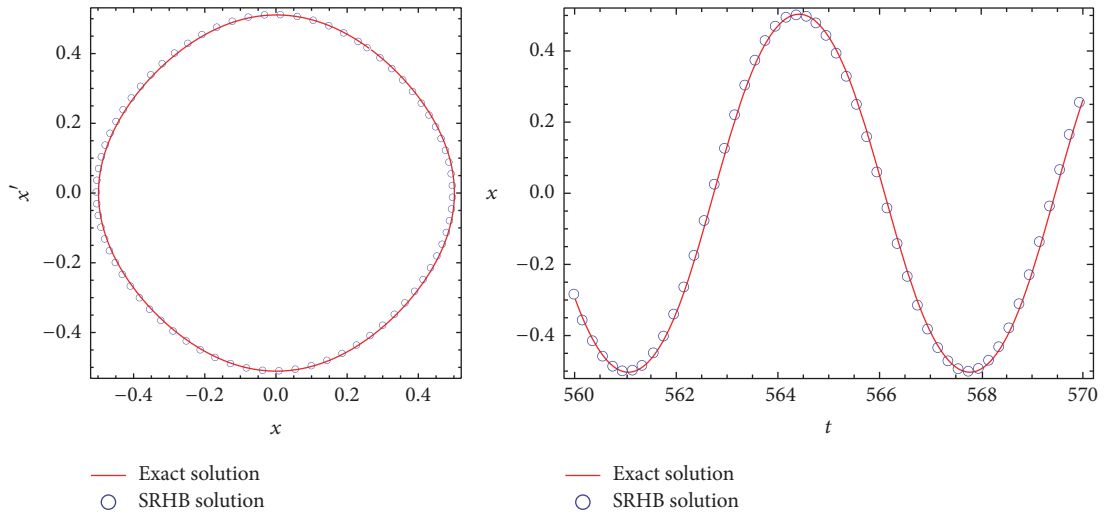

Figure 3: Comparison of the approximate and exact solutions of Mode 2.

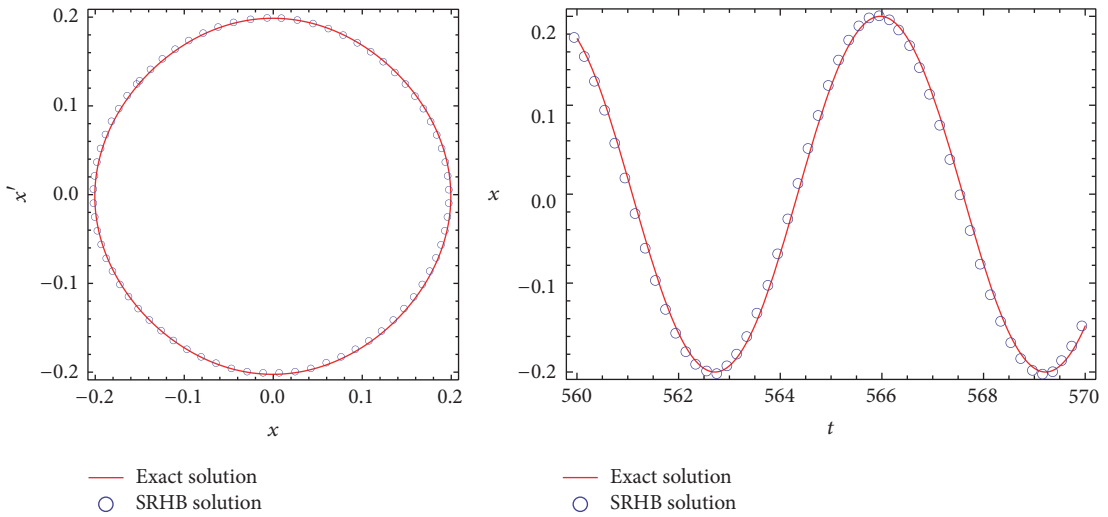

Figure 4: Comparison of the approximate and exact solutions of Mode 3.

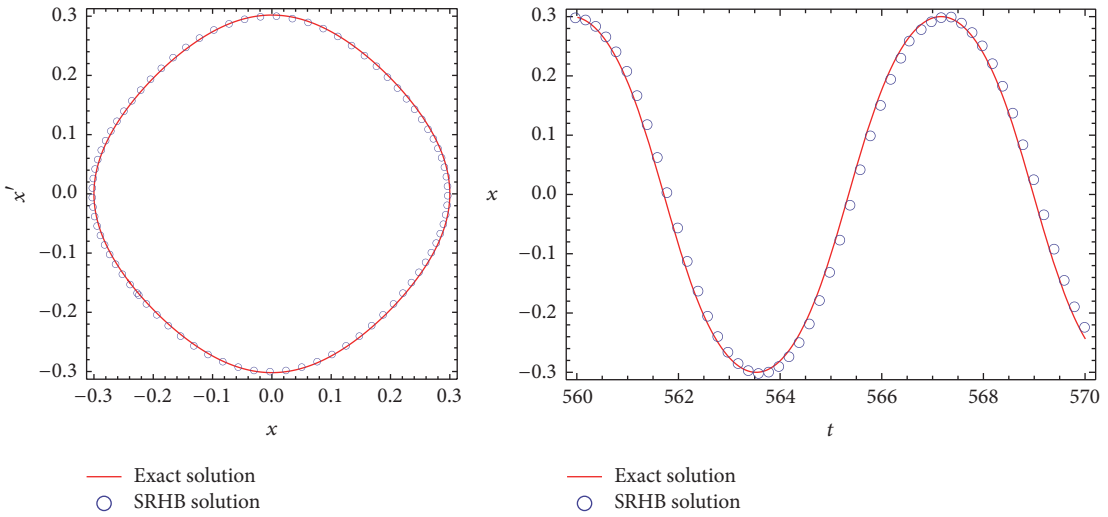

Figure 5: Comparison of the approximate and exact solutions of Mode 4.

of vibration, it reveals that SRHBM can be used to solve a nonlinear equation with high nonlinearities. According to the figures and tables, it is effective to explain that the presented approximations are more accurate. Therefore, we can conclude that the SRHBM is more available and effective. Ultimately, we consider that the SRHBM can be used to deal with more complex strongly nonlinear vibration problems.

Conflicts of Interest

The authors declare that there are no conflicts of interest regarding the publication of this paper.

Authors' Contributions

All the authors contributed equally and significantly to the writing of this paper. All the authors read and approved the final manuscript.

Acknowledgments

The authors gratefully acknowledge the support of the National Natural Science Foundation of China (NNSFC) through Grants nos. 11572288, 11302184, and 11372015.

References

[1] R. E. Mickens, *Mathematical Methods for the Natural and Engineering Sciences*, World Scientific, Singapore, 2004.

[2] O. Abdulaziz, N. F. M. Noor, and I. Hashim, "Homotopy analysis method for fully developed MHD micropolar fluid flow between vertical porous plates," *International Journal for Numerical Methods in Engineering*, vol. 78, no. 7, pp. 817–827, 2009.

[3] Y. M. Chen and J. K. Liu, "Homotopy analysis method for limit cycle flutter of airfoils," *Applied Mathematics and Computation*, vol. 203, no. 2, pp. 854–863, 2008.

[4] R. R. Pušenjak, "Extended Lindstedt-Poincare method for non-stationary resonances of dynamical systems with cubic nonlinearities," *Journal of Sound & Vibration*, vol. 314, no. 1-2, pp. 194–216, 2008.

[5] P. Amore and A. Aranda, "Improved Lindstedt-Poincaré method for the solution of nonlinear problems," *Journal of Sound and Vibration*, vol. 283, no. 3–5, pp. 1115–1136, 2005.

[6] M. Senator and C. N. Bapat, "A perturbation technique that works even when the nonlinearity is not small," *Journal of Sound and Vibration*, vol. 164, no. 1, pp. 1–27, 1993.

[7] Y. K. Cheung, S. H. Chen, and S. L. Lau, "A modified Lindstedt-Poincaré method for certain strongly nonlinear oscillators," *International Journal of Non-Linear Mechanics*, vol. 26, no. 3-4, pp. 367–378, 1991.

[8] Q.-Q. Hu, C. W. Lim, and L.-Q. Chen, "Nonlinear vibration of a cantilever with a Derjaguin-Müller-Toporov contact end," *International Journal of Structural Stability and Dynamics*, vol. 8, no. 1, pp. 25–40, 2008.

[9] K. Huseyin and R. Lin, "An intrinsic multiple-scale harmonic balance method for nonlinear vibration and bifurcation problems," *International Journal of Non-Linear Mechanics*, vol. 26, no. 5, pp. 727–740, 1991.

[10] L.-L. Ke, J. Yang, S. Kitipornchai, and Y. Xiang, "Flexural vibration and elastic buckling of a cracked timoshenko beam made of functionally graded materials," *Mechanics of Advanced Materials and Structures*, vol. 16, no. 6, pp. 488–502, 2009.

[11] S. K. Lai, C. W. Lim, B. S. Wu, C. Wang, Q. C. Zeng, and X. F. He, "Newton-harmonic balancing approach for accurate solutions to nonlinear cubic-quintic Duffing oscillators," *Applied Mathematical Modelling*, vol. 33, no. 2, pp. 852–866, 2009.

[12] S. J. Liao, "An approximate solution technique not depending on small parameters: a special example," *International Journal of Non-Linear Mechanics*, vol. 30, no. 3, pp. 371–380, 1995.

[13] S. Liao, *Beyond Perturbation: Introduction to the Homotopy Analysis Method*, vol. 2 of *CRC Series: Modern Mechanics and Mathematics*, Chapman & Hall/CRC, Boca Raton, Fla, USA, 2003.

[14] S. J. Liao, "Comparison between the homotopy analysis method and homotopy perturbation method," *Applied Mathematics and Computation*, vol. 169, no. 2, pp. 1186–1194, 2005.

[15] S. J. Liao, "An optimal homotopy-analysis approach for strongly nonlinear differential equations," *Communications in Nonlinear Science and Numerical Simulation*, vol. 15, no. 8, pp. 2003–2016, 2010.

[16] C. W. Lim, R. Xu, S. K. Lai, Y. M. Yu, and Q. Yang, "Nonlinear free vibration of an elastically-restrained beam with a point mass via the newton-harmonic balancing approach," *International Journal of Nonlinear Sciences and Numerical Simulation*, vol. 10, no. 5, pp. 661–674, 2009.

[17] T. Pirbodaghi, S. H. Hoseini, M. T. Ahmadian, and G. H. Farrahi, "Duffing equations with cubic and quintic nonlinearities," *Computers and Mathematics with Applications*, vol. 57, no. 3, pp. 500–506, 2009.

[18] F. F. Seelig, "Unrestricted harmonic balance II. Application to stiff ordinary differential equations in enzyme catalysis," *Journal of Mathematical Biology*, vol. 12, no. 2, pp. 187–198, 1981.

[19] J. L. Summers and M. D. Savage, "Two timescale harmonic balance. I. Application to autonomous one-dimensional nonlinear oscillators," *Philosophical Transactions of the Royal Society B: Biological Sciences*, vol. 340, no. 1659, pp. 473–501, 1992.

[20] R. A. Van Gorder and K. Vajravelu, "On the selection of auxiliary functions, operators, and convergence control parameters in the application of the Homotopy Analysis method to nonlinear differential equations: a general approach," *Communications in Nonlinear Science and Numerical Simulation*, vol. 14, no. 12, pp. 4078–4089, 2009.

[21] H. Wagner, "Large-amplitude free vibrations of a beam," *Journal of Applied Mechanics*, vol. 32, no. 4, pp. 887–892, 1965.

[22] C. Wang and I. Pop, "Analysis of the flow of a power-law fluid film on an unsteady stretching surface by means of homotopy analysis method," *Journal of Non-Newtonian Fluid Mechanics*, vol. 138, no. 2-3, pp. 161–172, 2006.

[23] B. Wu and P. Li, "A method for obtaining approximate analytic periods for a class of nonlinear oscillators," *Meccanica*, vol. 36, no. 2, pp. 167–176, 2001.

[24] K. Yabushita, M. Yamashita, and K. Tsuboi, "An analytic solution of projectile motion with the quadratic resistance law using the homotopy analysis method," *Journal of Physics. A. Mathematical and Theoretical*, vol. 40, no. 29, pp. 8403–8416, 2007.

[25] S. S. Ganji, D. D. Ganji, H. Babazadeh, and N. Sadoughi, "Application of amplitude-frequency formulation to nonlinear oscillation system of the motion of a rigid rod rocking back,"

Mathematical Methods in the Applied Sciences, vol. 33, no. 2, pp. 157–166, 2010.

[26] D. D. Ganji, H. B. Rokni, M. G. Sfahani, and S. S. Ganji, "Approximate traveling wave solutions for coupled Whitham-Broer-Kaup shallow water," *Advances in Engineering Software*, vol. 41, no. 7-8, pp. 956–961, 2010.

[27] S. S. Ganji, A. Barari, and D. D. Ganji, "Approximate analysis of two-massspring systems and buckling of a column," *Computers and Mathematics with Applications*, vol. 61, no. 4, pp. 1088–1095, 2011.

[28] S. S. Ganji, A. Barari, L. B. Ibsen, and G. Domairry, "Differential transform method for mathematical modeling of jamming transition problem in traffic congestion flow," *Central European Journal of Operations Research*, vol. 20, no. 1, pp. 87–100, 2012.

[29] M. N. Hamdan and N. H. Shabaneh, "On the large amplitude free vibrations of a restrained uniform beam carrying an intermediate lumped mass," *Journal of Sound and Vibration*, vol. 199, no. 5, pp. 711–736, 1997.

[30] S. Telli and O. Kopmaz, "Free vibrations of a mass grounded by linear and nonlinear springs in series," *Journal of Sound and Vibration*, vol. 289, no. 4-5, pp. 689–710, 2006.

[31] S. K. Lai and C. W. Lim, "Accurate approximate analytical solutions for nonlinear free vibration of systems with serial linear and nonlinear stiffness," *Journal of Sound and Vibration*, vol. 307, no. 3, pp. 720–736, 2007.

[32] S.-S. Chen and C.-K. Chen, "Application of the differential transformation method to the free vibrations of strongly nonlinear oscillators," *Nonlinear Analysis. Real World Applications*, vol. 10, no. 2, pp. 881–888, 2009.

[33] S. S. Ganji, D. D. Ganji, M. G. Sfahani, and S. Karimpour, "Application of AFF and HPM to the systems of strongly nonlinear oscillation," *Current Applied Physics*, vol. 10, no. 5, pp. 1317–1325, 2010.

[34] I. Mehdipour, D. D. Ganji, and M. Mozaffari, "Application of the energy balance method to nonlinear vibrating equations," *Current Applied Physics*, vol. 10, no. 1, pp. 104–112, 2010.

[35] Y. H. Qian, S. K. Lai, W. Zhang, and Y. Xiang, "Study on asymptotic analytical solutions using HAM for strongly nonlinear vibrations of a restrained cantilever beam with an intermediate lumped mass," *Numerical Algorithms*, vol. 58, no. 3, pp. 293–314, 2011.

[36] Z. Guo and W. Zhang, "The spreading residue harmonic balance study on the vibration frequencies of tapered beams," *Applied Mathematical Modelling*, vol. 40, no. 15, pp. 7195–7203, 2016.

[37] Z. Guo and X. Ma, "Residue harmonic balance solution procedure to nonlinear delay differential systems," *Applied Mathematics and Computation*, vol. 237, pp. 20–30, 2014.

[38] P. Ju and X. Xue, "Global residue harmonic balance method to periodic solutions of a class of strongly nonlinear oscillators," *Applied Mathematical Modelling*, vol. 38, no. 24, pp. 6144–6152, 2014.

[39] P. Ju and X. Xue, "Global residue harmonic balance method for large-amplitude oscillations of a nonlinear system," *Applied Mathematical Modelling*, vol. 39, no. 2, pp. 449–454, 2015.

[40] Y. Y. Lee, "Free vibration analysis of a nonlinear panel coupled with extended cavity using the multi-level residue harmonic balance method," *Thin-Walled Structures*, vol. 98, pp. 332–336, 2016.

Hindawi
Advances in Mathematical Physics
Volume 2017, Article ID 2717352, 10 pages
https://doi.org/10.1155/2017/2717352

Research Article

Computation of the Stability and Complexity about Triopoly Price Game Model with Delay Decision

Yuling Wang,[1] Shubing Guo,[2] and Shide Duan[1]

[1]*School of Economics, South-Central University for Nationalities, Wuhan, China*
[2]*College of Management and Economics, Tianjin University, Tianjin 300072, China*

Correspondence should be addressed to Shubing Guo; sbguo20160831@126.com

Received 1 January 2017; Accepted 21 February 2017; Published 10 April 2017

Academic Editor: Kaliyaperumal Nakkeeran

We develop the price game model based on the entropy theory and chaos theory, considering the three enterprises are bounded rationality and using the cost function under the resource constraints; that is, the yield increase will bring increased costs. The enterprises of new model adopt the delay decision with the delay parameters τ_1 and τ_2, respectively. According to the change of delay parameters τ_1 and τ_2, the bifurcation, stability, and chaos of the system are discussed, and the change of entropy when the system is far away from equilibrium is considered. Prices and profits are found to lose stability and the evolution of the system tends to the equilibrium state of maximum entropy. And it has a big fluctuation with the increase of τ_1 and τ_2. In the end, the chaos is controlled effectively. The entropy of the system decreases, and the interior reverts to order. The results of this study are of great significance for avoiding the chaos when the enterprises make price decisions.

1. Introduction

The oligopoly is a universal market state between perfect competition and complete monopoly. Game theory, entropy theory, and nonlinear dynamics provide new impetus for oligopoly theory. There are a lot of oligopolies in the market, such as China Mobile, China Unicom, and China Telecom, forming a complex system with increasing entropy. These oligopoly enterprises constantly carry on the price game in order to maximize the benefits. Many scholars have studied the content of oligopoly game from different perspectives, such as entropy theory, chaos, and game theory. Zhang et al. [1] built a Bertrand repeated game model with linear demand function and studied its system complexity. Xu and Ma [2] investigated the dynamic model of a Bertrand game with delay in insurance market. They discussed the existence of the Nash equilibrium point of the game and researched the stability of the system. Sun and Ma [3] considered a two-player quantum game in the presence of a thermal decoherence modeled with the method of a rigorous Davies. It shows how the energy dissipation and pure decoherence make changes on the payoffs of the players in the game. Dajka et al. [4] studied the complex dynamics of a nonlinear model on the basis of Bertrand game in Chinese cold rolled steel market. Fanti et al. [5] analyzed the dynamics of a Bertrand duopoly with products which become divided. The results showed that an increase in either the degree of substitutability or complementarity between products of different varieties was the reason of complexity in a competition game. Xiangyu and Xiaoyong [6] used the information theory and entropy theory to build the models to measure the entropy of the four market structures which are perfect competition, monopolistic competition, oligopoly, and complete monopoly and compare the entropy of the four market structures. Naimzada and Tramontana [7] considered a Cournot–Bertrand duopoly model based on linear demand and cost functions with product differentiation. Li and Ma [8] considered the R&D input competition model in oligopoly market on the basis of that the players are heterogeneous, bounded rational, and adaptive adjustment. Fan et al. [9] investigated two types of players and concluded the output duopoly game with heterogeneous players. They studied the influence of players' different behavior on the dynamics of game. Yali [10] built a duopoly game model and investigated its stability with bounded rationality strategy and state delay. Gao et al. [11] discussed equilibrium stability of a nonlinear Cournot

duopoly game, where one player can evaluate its opponent's output in the future in light of straightforward extrapolative foresight. Peng et al. [12] analyzed a dynamic of triopoly Bertrand repeated model with the zero marginal cost. Bischi and Naimzada [13] concluded the dynamical characteristics of bounded rationality duopoly game. Ma and Tu [14] carried out the corresponding extension of the complex dynamics to macroeconomic model with time delays considering the macroeconomic model of money supply. Ma and Wang [15] considered a closed-loop supply chain with product recovery, which is composed of one manufacturer and one retailer. The situation may lead to complicated dynamic phenomena such as bifurcation and chaos. That is to say, the entropy of the system is increasing too. Hale [16] investigated existence and the local stable region of the Nash equilibrium point. Ma and Si [17] studied a continuous Bertrand duopoly game model with two-stage delay. Ma and Bangura [18] studied financial and economic system when the three parameters were changed.

By combining them, it is found that most of the studies are based on the discrete system, and the attention to the research of continuous system is not much, with lack of analysis from the in-system state and entropy theory, considering the delayed decision is less. Therefore, the model of [19] is improved based on the entropy theory and chaos theory, considering the three companies are bounded rationality and using a new cost function, and its chaotic characteristics and system entropy changes were analyzed. In the course of the study, the special case of $\tau_1 = \tau_2 = \tau$ is overcome, $\tau_1 \neq \tau_2$, and $\tau_1 > 0$, $\tau_2 > 0$ are discussed. The improved model is more fit to the reality, and the research results are of guiding significance to the enterprise price decision.

This paper is organized as follows: in Section 2, based on [19], a triopoly price game model with delay is improved. In Section 3, the stability of system and the existence of Hopf bifurcation are analyzed. In Section 4, numerical simulation is used to find out the influence of delay on the stability of price and profit by virtue of time series, the attractor, bifurcation diagram, Lyapunov exponent, 3D surface chat, and initial value sensitivity, as well as the contacts between dynamic state and the situation of entropy change in the system. In Section 5, the effective control of chaos is achieved by control method of the state variables feedback and parameter variation in the system. Finally, we have some conclusions in the last section.

2. The Model

The triopoly dynamic game model is developed in [19] which makes adaptive decision, bounded rational decision, and delayed bounded rational decision, respectively. The stability of the system and the existence of Hopf bifurcation are studied in this paper. The model is described as follows:

$$\begin{aligned}
\dot{p}_1(t) &= \nu_1 p_1 \left[\frac{\left(a + d_1 w p_2(t) + d_1(1-w) p_2(t-\tau) + f_1 p_3(t) + b_1 c_1\right)}{(2b_1)} - p_1(t-\tau) \right], \\
\dot{p}_2(t) &= \nu_2 p_2 \left[a - 2b_2 w p_2(t) - 2b_2(1-w) p_2(t-\tau) + d_2 p_3(t) + f_2 p_1(t) + b_2 c_2 \right], \\
\dot{p}_3(t) &= \nu_3 p_3 \left[a - 2b_3 p_3(t) + d_3 p_1(t) + f_3 w p_2(t) + f_3(1-w) p_2(t-\tau) + b_3 c_3 \right],
\end{aligned} \tag{1}$$

where $a, b_i, d_i, f_i > 0$, $i = 1, 2, 3$, a represents the largest market demand for products, b_i is elastic demand, d_i, f_i represents the substitution rate between the two companies, respectively, p_i, q_i denote the price and output of the product, respectively, $0 < w < 1$ represents the weight of the current price, and $1 - w$ represents the weight of price of $t - \tau$ time. The cost function with linear form is $C_i(q_i) = c_i q_i$, $i = 1, 2, 3$, and c_i is marginal profit. In (1), the first enterprise adopts the adaptive pricing strategy with delay, where τ_1 denotes the delay parameter; the other two enterprises employ the finite rational pricing strategy. In addition, the second enterprise used the postponement strategy, where τ_2 stands for the delay parameter. The linear cost function under the condition of sufficient resources was used. Then $\tau_1 = \tau_2 = \tau$ was discussed.

Because price information is asymmetry, we consider three companies are bounded rationality based on model [19] and build the price game model with enterprises 1 and 2 with delay parameters τ_1 and τ_2, respectively. The cost function will obviously increase under limited resources; that is, $C_i(q_i) = c_{i0} + c_i q_i^2$ $i = 1, 2, 3$, where c_{i0} is the fixed cost. We further have the improved model with price game:

$$\begin{aligned}
\dot{p}_1(t) &= \nu_1 p_1 \left[\left(1 + 2b_1 c_1\right) a - \left(2b_1 + 2b_1^2 c_1\right) p_1(t-\tau_1) \right. \\
&\quad \left. + \left(d_1 + 2b_1 c_1 d_1\right) p_2(t-\tau_2) + \left(f_1 + 2b_1 c_1 f_1\right) p_3(t) \right], \\
\dot{p}_2(t) &= \nu_2 p_2 \left[\left(1 + 2b_2 c_2\right) a - \left(2b_2 + 2b_2^2 c_2\right) p_2(t-\tau_2) \right. \\
&\quad \left. + \left(d_2 + 2b_2 c_2 d_2\right) p_3(t) + \left(f_2 + 2b_2 c_2 f_2\right) p_1(t-\tau_1) \right], \\
\dot{p}_3(t) &= \nu_3 p_3 \left[\left(1 + 2b_3 c_3\right) a - \left(2b_3 + 2b_3^2 c_3\right) p_3(t) \right. \\
&\quad + \left(d_3 + 2b_3 c_3 d_3\right) p_1(t-\tau_1) \\
&\quad \left. + \left(f_3 + 2b_3 c_3 f_3\right) p_2(t-\tau_2) \right].
\end{aligned} \tag{2}$$

3. Local Stability at Equilibrium Points

In a competitive market, the equilibrium points must be nonnegative. Considering generality, we assume that $E_*(p_1^*, p_2^*, p_3^*)$ is a Nash equilibrium point of model (2), where

$$p_1^* > 0,$$
$$p_2^* > 0, \tag{3}$$
$$p_3^* > 0.$$

We study the existence of Hopf bifurcation of the system at $E_*(p_1^*, p_2^*, p_3^*)$. Let $h_1(t) = p_1(t) - p_1^*$, $h_2(t) = p_2(t) - p_2^*$, and $h_3(t) = p_3(t) - p_3^*$, with $p_1(t)$, $p_2(t)$, and $p_3(t)$ instead of $h_1(t)$, $h_2(t)$, and $h_3(t)$, respectively, when $h = 0$. We have the linear form of the system through Jacobian matrix as follows:

$$\begin{aligned}
\dot{p}_1(t) &= -\nu_1 p_1^* \left(2b_1 + 2b_1^2 c_1\right) p_1(t-\tau_1) \\
&\quad + \nu_1 p_1^* \left(d_1 + 2b_1 c_1 d_1\right) p_2(t-\tau_2) \\
&\quad + \nu_1 p_1^* \left(f_1 + 2b_1 c_1 f_1\right) p_3(t), \\
\dot{p}_2(t) &= -\nu_2 p_2^* \left(2b_2 + 2b_2^2 c_2\right) p_2(t-\tau_2) \\
&\quad + \nu_2 p_2^* \left(d_2 + 2b_2 c_2 d_2\right) p_3(t) \\
&\quad + \nu_2 p_2^* \left(f_2 + 2b_2 c_2 f_2\right) p_1(t-\tau_1), \\
\dot{p}_3(t) &= -\nu_3 p_3^* \left(2b_3 + 2b_3^2 c_3\right) p_3(t) \\
&\quad + \nu_3 p_3^* \left(d_3 + 2b_3 c_3 d_3\right) p_1(t-\tau_1) \\
&\quad + \nu_3 p_3^* \left(f_3 + 2b_3 c_3 f_3\right) p_2(t-\tau_2).
\end{aligned} \tag{4}$$

The determinant of (4) is

$$\left|\lambda E - J(E_*)\right| = 0, \tag{5}$$

where

$$J(E_*) = \begin{vmatrix} J_{11} & J_{12} & J_{13} \\ J_{21} & J_{22} & J_{23} \\ J_{31} & J_{32} & J_{33} \end{vmatrix},$$

$$\begin{aligned}
J_{11} &= -\nu_1 p_1^* \left(2b_1 + 2b_1^2 c_1\right), \\
J_{12} &= \nu_1 p_1^* \left(d_1 + 2b_1 c_1 d_1\right), \\
J_{13} &= \nu_1 p_1^* \left(f_1 + 2b_1 c_1 f_1\right), \\
J_{21} &= \nu_2 p_2^* \left(f_2 + 2b_2 c_2 f_2\right), \\
J_{22} &= -\nu_2 p_2^* \left(2b_2 + 2b_2^2 c_2\right), \\
J_{23} &= \nu_2 p_2^* \left(d_2 + 2b_2 c_2 d_2\right), \\
J_{31} &= \nu_3 p_3^* \left(d_3 + 2b_3 c_3 d_3\right), \\
J_{32} &= \nu_3 p_3^* \left(f_3 + 2b_3 c_3 f_3\right), \\
J_{33} &= -\nu_3 p_3^* \left(2b_3 + 2b_3^2 c_3\right).
\end{aligned} \tag{6}$$

Therefore the characteristic equation for system (4) is

$$\begin{aligned}
&\lambda^3 + k_1\lambda^2 + \left(k_2\lambda^2 + k_3\lambda\right) e^{-\lambda\tau_1} + \left(k_4\lambda^2 + k_5\lambda\right) e^{-\lambda\tau_2} \\
&\quad + \left(k_6\lambda + k_7\right) e^{-\lambda\tau_1} e^{-\lambda\tau_2} = 0,
\end{aligned} \tag{7}$$

where

$$\begin{aligned}
k_1 &= 2b_3 p_3^* \nu_3 + 2b_3^2 c_3 p_3^* \nu_3, \\
k_2 &= 2b_1 p_1^* \nu_1 + 2b_1^2 c_1 p_1^* \nu_1, \\
k_3 &= 4b_1 b_3 p_1^* p_3^* \nu_1 \nu_3 - d_3 f_1 p_1^* p_3^* \nu_1 \nu_3 \\
&\quad + 4b_1^2 b_3 c_1 p_1^* p_3^* \nu_1 \nu_3 + 4b_1 b_3^2 c_3 p_1^* p_3^* \nu_1 \nu_3 + \cdots \\
&\quad - 2b_3 c_3 d_3 f_1 p_1^* p_3^* \nu_1 \nu_3, \\
k_4 &= 2b_2 p_2^* \nu_2 + 2b_2^2 c_2 p_2^* \nu_2, \\
k_5 &= 4b_2 b_3 p_2^* p_3^* \nu_2 \nu_3 - d_2 f_3 p_2^* p_3^* \nu_2 \nu_3 \\
&\quad + 4b_2^2 b_3 c_2 p_2^* p_3^* \nu_2 \nu_3 + 4b_2 b_3^2 c_3 p_2^* p_3^* \nu_2 \nu_3 + \cdots \\
&\quad - 2b_3 c_3 d_2 f_3 p_2^* p_3^* \nu_2 \nu_3, \\
k_6 &= 4b_1 b_2 p_1^* p_2^* \nu_1 \nu_2 + 4b_1^2 b_2 c_1 p_1^* p_2^* \nu_1 \nu_2 \\
&\quad + 4b_1 b_2^2 c_2 p_1^* p_2^* \nu_1 \nu_2 + \cdots \\
&\quad - 4b_1 b_2 c_1 c_2 d_1^2 f_2 p_1^* p_2^* \nu_1 \nu_2, \\
k_7 &= 8b_1 b_2 b_3 p_1^* p_2^* p_3^* \nu_1 \nu_2 \nu_3 - 2b_1 d_2 f_3 p_1^* p_2^* p_3^* \nu_1 \nu_2 \nu_3 \\
&\quad + \cdots - 8b_1 b_2 b_3 c_1 c_2 c_3 d_1^2 d_2 d_3 p_1^* p_2^* p_3^* \nu_1 \nu_2 \nu_3.
\end{aligned} \tag{8}$$

We discuss the effects of τ_1, τ_2 on the stability of system (4) when $\tau_1 \neq \tau_2$, $\tau_1 > 0$, $\tau_2 > 0$.

At this point, the characteristic equation of system (4) is

$$\begin{aligned}
&\lambda^3 + k_1\lambda^2 + \left(k_2\lambda^2 + k_3\lambda\right) e^{-\lambda\tau_1} + \left(k_4\lambda^2 + k_5\lambda\right) e^{-\lambda\tau_2} \\
&\quad + \left(k_6\lambda + k_7\right) e^{-\lambda(\tau_1+\tau_2)} = 0.
\end{aligned} \tag{9}$$

We consider (2) with τ_2 in its stable range, regarding τ_1 as a parameter. Taking into account the generality, we discuss system (2) under the case mentioned in [14], and $\tau_2 \in [0, \tau_{20})$. τ_{20} is defined as in [14]. Therefore we have

$$\begin{aligned}
\tau_{2k}^{(j)} &= \frac{1}{\omega_{2k}} \arccos\left\{\frac{(D - AC)\omega_{2k}^4 + (AE - BD)\omega_{2k}^2}{C^2\omega_{2k}^4 + (D^2 - 2CE)\omega_{2k}^2 + E^2}\right\} \\
&\quad + \frac{2j\pi}{\omega_{2k}}, \quad k = 1, 2, 3, 4, 5, \quad j = 0, 1, 2, \ldots
\end{aligned} \tag{10}$$

$$\tau_{20} = \min\left\{\tau_{2k}^{(0)}\right\}, \quad k \in \{1, 2, 3, 4, 5\}, \omega_{20} = \omega_{2k_0},$$

where ω_{2k}, $i = 1, 2, 3, \ldots, k$, are the positive roots of

$$H_1\omega_2^{10} + H_2\omega_2^8 + H_3\omega_2^6 + H_4\omega_2^4 + H_5\omega_2^2 + H_6 = 0, \tag{11}$$

where

$$\begin{aligned}
H_1 &= C^2, \\
H_2 &= D^2 - 2CE - 2BC^2 + A^2C^2 - C^4, \\
H_3 &= 4BCE + E^2 + A^2D^2 + B^2C^2 + 2D^2B - 2A^2CE \\
&\quad + 4C^3E - 2C^2D^2,
\end{aligned}$$

$$
\begin{aligned}
H_4 &= A^2E^2 - 2E^2B - 2B^2CE + B^2D^2 - 6C^2E^2 - D^4 \\
&\quad - 4CED^2, \\
H_5 &= B^2E^2 - 2D^2E^2 + 4CE^3, \\
H_6 &= -E^4, \\
A &= k_1 + k_2, \\
B &= k_3, \\
C &= k_4, \\
D &= k_5 + k_6, \\
E &= k_7.
\end{aligned} \tag{12}
$$

Let $\lambda = i\omega_1$ $(\omega_1 > 0)$ be a root of (9). Then

$$
\begin{aligned}
&A_4 \sin\omega_1\tau_1 + B_4 \cos\omega_1\tau_1 = \omega_1^3, \\
&C_4 \sin\omega_1\tau_1 + D_4 \cos\omega_1\tau_1 \\
&\quad = k_1\omega_1^2 + k_4\omega_1^2 \cos\omega_1\tau_2 - k_5\omega_1 \sin\omega_1\tau_2,
\end{aligned} \tag{13}
$$

where

$$
\begin{aligned}
A_4 &= k_2\omega_1^2 - k_6\omega_1 \sin\omega_1\tau_2 - k_7 \cos\omega_1\tau_2, \\
B_4 &= k_3\omega_1 + k_6\omega_1 \cos\omega_1\tau_2 - k_7 \sin\omega_1\tau_2, \\
C_4 &= k_3\omega_1 + k_6\omega_1 \cos\omega_1\tau_2 - k_7 \sin\omega_1\tau_2, \\
D_4 &= k_6\omega_1 \sin\omega_1\tau_2 - k_2\omega_1^2 + k_7 \cos\omega_1\tau_2.
\end{aligned} \tag{14}
$$

For (13), we can obtain that

$$
\begin{aligned}
\sin\omega_1\tau_1 &= \frac{N_1\omega_1^4 + N_2\omega_1^3 + N_3\omega_1^2 + N_4\omega_1}{N_{10}\omega_1^4 + N_{11}\omega_1^3 + N_{12}\omega_1^2 + N_{13}\omega_1 + N_{14}}, \\
\cos\omega_1\tau_1 &= \frac{N_5\omega_1^5 + N_6\omega_1^4 + N_7\omega_1^3 + N_8\omega_1^2 + N_9\omega_1}{N_{10}\omega_1^4 + N_{11}\omega_1^3 + N_{12}\omega_1^2 + N_{13}\omega_1 + N_{14}}, \\
N_1 &= k_6 \cos\omega_1\tau_2 - k_2k_4 \cos\omega_1\tau_2 - k_1k_2 + k_3, \\
N_2 &= k_4k_6 \cos\omega_1\tau_2 \sin\omega_1\tau_2 + k_1k_6 \sin\omega_1\tau_2 \\
&\quad - k_7 \sin\omega_1\tau_2 + k_2k_5 \sin\omega_1\tau_2, \\
N_3 &= k_4k_7 \cos^2\omega_1\tau_2 + k_1k_7 \cos\omega_1\tau_2 \\
&\quad - k_5k_6 \sin^2\omega_1\tau_2, \\
N_4 &= k_5k_7 \cos\omega_1\tau_2 \sin\omega_1\tau_2, \\
N_5 &= k_2, \\
N_6 &= -k_6 \sin\omega_1\tau_2, \\
N_7 &= k_1k_3 + k_1k_6 \cos\omega_1\tau_2 + k_3k_4 \cos\omega_1\tau_2 \\
&\quad + k_4k_6 \cos^2\omega_1\tau_2 - k_7 \cos\omega_1\tau_2, \\
N_8 &= k_1k_7 \sin\omega_1\tau_2 - k_4k_7 \cos\omega_1\tau_2 \sin\omega_1\tau_2 \\
&\quad + k_5k_6 \sin\omega_1\tau_2 \cos\omega_1\tau_2 \\
&\quad + k_3k_5 \sin\omega_1\tau_2, \\
N_9 &= k_5k_7 \sin^2\omega_1\tau_2, \\
N_{10} &= k_2^2, \\
N_{11} &= -2k_2k_6 \sin\omega_1\tau_2, \\
N_{12} &= k_3^2 + 2k_3k_6 \cos\omega_1\tau_2 + k_6^2 - 2k_2k_7 \cos\omega_1\tau_2, \\
N_{13} &= -2k_3k_7 \sin\omega_1\tau_2, \\
N_{14} &= k_7^2.
\end{aligned} \tag{15}
$$

For (15), we obtain the following equation:

$$
\begin{aligned}
&M_{10}\omega_1^{10} + M_9\omega_1^9 + M_8\omega_1^8 + M_7\omega_1^7 + M_6\omega_1^6 + M_5\omega_1^5 \\
&\quad + M_4\omega_1^4 + M_3\omega_1^3 + M_2\omega_1^2 + M_1\omega_1 + M_0 = 0, \\
&M_{10} = N_5^2, \\
&M_9 = N_1^2N_6^2 + 2N_5N_7 - N_{10}^2, \\
&M_8 = 2N_5N_6, \\
&M_7 = 2N_1N_2 + 2N_5N_8 + 2N_6N_7 - 2N_{10}N_{11}, \\
&M_6 = N_2^2 + 2N_1N_3 + N_7^2 + 2N_6N_8 + 2N_5N_9 - N_{11}^2 \\
&\quad - 2N_{10}N_{12}, \\
&M_5 = 2N_1N_4 + 2N_2N_3 + 2N_7N_8 + 2N_6N_9 \\
&\quad - 2N_{10}N_{13} - 2N_{11}N_{12}, \\
&M_4 = N_3^2 + 2N_2N_4 + N_8^2 + 2N_7N_9 - N_{12}^2 - 2N_{11}N_{13} \\
&\quad - 2N_{10}N_{14}, \\
&M_3 = 2N_3N_4 + 2N_8N_9 - 2N_{12}N_{13} - 2N_{11}N_{14}, \\
&M_2 = N_4^2 + N_9^2 - N_{13}^2 - 2N_{12}N_{14}, \\
&M_1 = -2N_{13}N_{14}, \\
&M_0 = -N_{14}^2.
\end{aligned} \tag{16}
$$

Suppose that $(H1)$: (16) has finite positive roots. We define the roots of (16) as $\omega_{11}, \omega_{12}, \omega_{13}, \ldots, \omega_{1k}$. For every fixed ω_{1i} $(i = 1, 2, 3, \ldots, k)$, there exists a sequence $\tau_{1i}^{(j)} \mid j = 0, 1, 2, \ldots$ which satisfies (16). It is

$$
\begin{aligned}
\tau_{1i}^{(j)} &= \frac{1}{\omega_{1i}} \\
&\quad \cdot \arccos\left\{\frac{N_5\omega_{1i}^5 + N_6\omega_{1i}^4 + N_7\omega_{1i}^3 + N_8\omega_{1i}^2 + N_9\omega_{1i}}{N_{10}\omega_{1i}^4 + N_{11}\omega_{1i}^3 + N_{12}\omega_{1i}^2 + N_{13}\omega_{1i} + N_{14}}\right\} \\
&\quad + \frac{2j\pi}{\omega_{1i}}, \quad i = 1, 2, 3, \ldots, k, \quad j = 0, 1, 2, \ldots.
\end{aligned} \tag{17}
$$

Let

$$\tau_{10} = \min\left\{\tau_{1i}^{(j)} \mid i = 1, 2, 3, \ldots, k,\ j = 0, 1, 2, \ldots\right\},$$
$$\omega_{10} = \omega_{1i_0}. \tag{18}$$

When $\tau_1 = \tau_{10}$, (9) has a pair of purely imaginary roots $\pm i\omega_{10}$ for $\tau_2 \in [0, \tau_{20})$. In the following, we take the derivative of λ with respect to τ_1 in (9) for the transversality condition of Hopf bifurcation, and we have

$$\left[\frac{d\lambda}{d\tau_1}\right]^{-1} = \frac{-3\lambda^2 - 2k_1\lambda - (2k_2\lambda + k_3)e^{-\lambda\tau_1} - (2k_4 + k_5)e^{-\lambda\tau_2} - k_6e^{-(\tau_1+\tau_2)}}{(k_2\lambda^3 + k_3\lambda^2)e^{-\lambda\tau_1} + (k_4\lambda^3 + k_5\lambda^2)e^{-\lambda\tau_2} + (k_6\lambda + k_7\lambda)e^{-\lambda(\tau_1+\tau_2)}} - \frac{\tau_1}{\lambda}. \tag{19}$$

Then we further have

$$\left[\frac{d\lambda(\tau_{10})}{d\tau_1}\right]^{-1}_{\lambda=i\omega_{10}} = \frac{S_1S_3 + S_2S_4}{S_3^2 + S_4^2}, \tag{20}$$

where

$$\begin{aligned}
S_1 &= 3\omega_{10}^2 - 2k_2\omega_{10}\sin\omega_{10}\tau_{10} + k_3\cos\omega_{10}\tau_{10} \\
&\quad - 2k_4\omega_{10}\sin\omega_{10}\tau_2 - k_5\cos\omega_{10}\tau_2 \\
&\quad - k_6\cos(\omega_{10}\tau_{10} - \omega_{10}\tau_2), \\
S_2 &= k_5\sin\omega_{10}\tau_2 - 2k_1\omega_{10} - 2k_2\omega_{10}\cos\omega_{10}\tau_{10} \\
&\quad - k_3\sin\omega_{10}\tau_{10} - 2k_4\omega_{10}\cos\omega_{10}\tau_2 \\
&\quad - k_6\sin(\omega_{10}\tau_{10} + \omega_{10}\tau_2), \\
S_3 &= -k_2\omega_{10}^3\sin\omega_{10}\tau_{10} - k_3\omega_{10}^2\cos\omega_{10}\tau_{10} \\
&\quad - k_4\omega_{10}^3\sin\omega_{10}\tau_2 - k_5\omega_{10}^2\cos\omega_{10}\tau_2 \\
&\quad + (k_6 + k_7)\omega_{10}\sin(\omega_{10}\tau_{10} + \omega_{10}\tau_2), \\
S_4 &= -k_2\omega_{10}^3\cos\omega_{10}\tau_{10} + k_3\omega_{10}^2\sin\omega_{10}\tau_{10} \\
&\quad - k_4\omega_{10}^3\cos\omega_{10}\tau_2 + k_5\omega_{10}^2\sin\omega_{10}\tau_2 \\
&\quad + (k_6 + k_7)\omega_{10}\cos(\omega_{10}\tau_{10} + \omega_{10}\tau_2).
\end{aligned} \tag{21}$$

Obviously, if $(H2)$: $S_1S_3 + S_2S_4 \neq 0$, based on the above discussions and by the general Hopf bifurcation theorem in [15], we can obtain the results as follows.

If $H(1)$-$H(2)$ hold, when $\tau_2 \in [0, \tau_{20})$, then the Nash equilibrium point $E_*(p_1^*, p_2^*, p_3^*)$ of system (2) is asymptotically stable for $\tau_1 \in [0, \tau_{10})$ and it is unstable as $\tau_1 > \tau_{10}$. System (2) will be under Hopf bifurcation at $E_*(p_1^*, p_2^*, p_3^*)$ when $\tau_1 = \tau_{10}$.

4. Numerical Simulations

The impacts of delay on the stability of system (2) are analyzed by a series of tools in this section. It supports the theoretical research in Section 3 by time series, bifurcation, Lyapunov exponents, attractor, and initial value sensitivity.

The parameters of system (2) are taken to be $a = 5$, $b_1 = 3.2$, $b_2 = 3.5$, $b_3 = 3.8$, $d_1 = 0.3$, $d_2 = 0.4$, $d_3 = 0.5$, $f_1 = 0.35$, $f_2 = 0.45$, and $f_3 = 0.55$; the marginal costs of three dairy product companies are $c_1 = 0.003$, $c_2 = 0.006$, and $c_3 = 0.009$; the initial prices of their products are $p_1(0) = 0.4$, $p_2(0) = 0.5$, and $p_3(0) = 0.6$; the speeds of price adjustment are $\nu_1 = \nu_2 = \nu_3 = 0.5$; the fixed cost of the enterprise is $c_{10} = 1$, $c_{20} = 1.5$, and $c_{30} = 2$. Considering the following system, it is easy to calculate the Nash equilibrium point of system (2) which is $E_*(0.8723, 0.8329, 0.8012)$.

$$\begin{aligned}
\dot{p}_1(t) &= 0.20\,(5.0960 - 6.4614p_1(t - \tau_1) \\
&\quad + 0.3058p_2(t - \tau_2) + 0.3567p_3(t)), \\
\dot{p}_2(t) &= 0.25\,(5.2100 - 7.1470p_2(t - \tau_2) \\
&\quad + 0.4168p_3(t) + 0.4689p_1(t - \tau_1)), \\
\dot{p}_3(t) &= 0.30\,(5.3420 - 7.8599p_3(t) \\
&\quad + 0.5342p_1(t - \tau_1) + 0.5876p_2(t - \tau_2)).
\end{aligned} \tag{22}$$

From (10) and (11), we can get $\omega_{20} = 3.612$, $\tau_{20} = 0.508$. In order to facilitate the calculation, let $\tau_2 = 0.45 \in [0, \tau_{20})$. On the basis of (18), we have $\tau_{10} = 0.547$, $S_1S_3 + S_2S_4 = 512.74 \neq 0$, so $(H1)$-$(H2)$ hold. From the conclusion of the third section, we know that the Nash equilibrium point E_* is asymptotically stable when $\tau_1 \in [0, \tau_{10})$ and unstable when $\tau_1 > \tau_{10}$. As $\tau_1 = \tau_{10}$, Hopf bifurcation will occur.

4.1. The Influence of τ_1 on the Stability of System (22). Figures 1(a) and 2(a) show that system (22) is stable when $\tau_1 = 0.530 < \tau_{10} = 0.547$. When $\tau_1 = 0.560 > \tau_{10} = 0.547$, the system is unstable. This phenomenon can be found in Figures 1(b) and 2(b). The numerical simulation is consistent with the theoretical analysis.

Figure 3 describes the process of system (22) from stable into chaos. From Figure 3(a), we can find that the system has bifurcation, and τ_1 has the greatest impact on p_1 and has less influence on p_2. The change trend of the Lyapunov exponent in Figure 3(b) verifies the conclusion of Figure 3(a) p_3. We clearly find the bifurcation of system (22) when $\tau_1 = 0.547$ in Figure 3(b). Therefore, for enterprises in the price decision, it is necessary to ensure that $\tau_1 < 0.547$ when $\tau_2 = 0.45$.

4.2. The Influence of τ_1 on Initial Value Sensitivity. If we take the initial value of p_1 is 0.4 and 0.401, respectively, the value of p_1 will change after iterations. When $\tau_1 = 0.530 < \tau_{10} = 0.547$, after 61 iterations, the difference of p_1 is 6.144 times of the initial difference 0.001. It can be described by Figure 4(a).

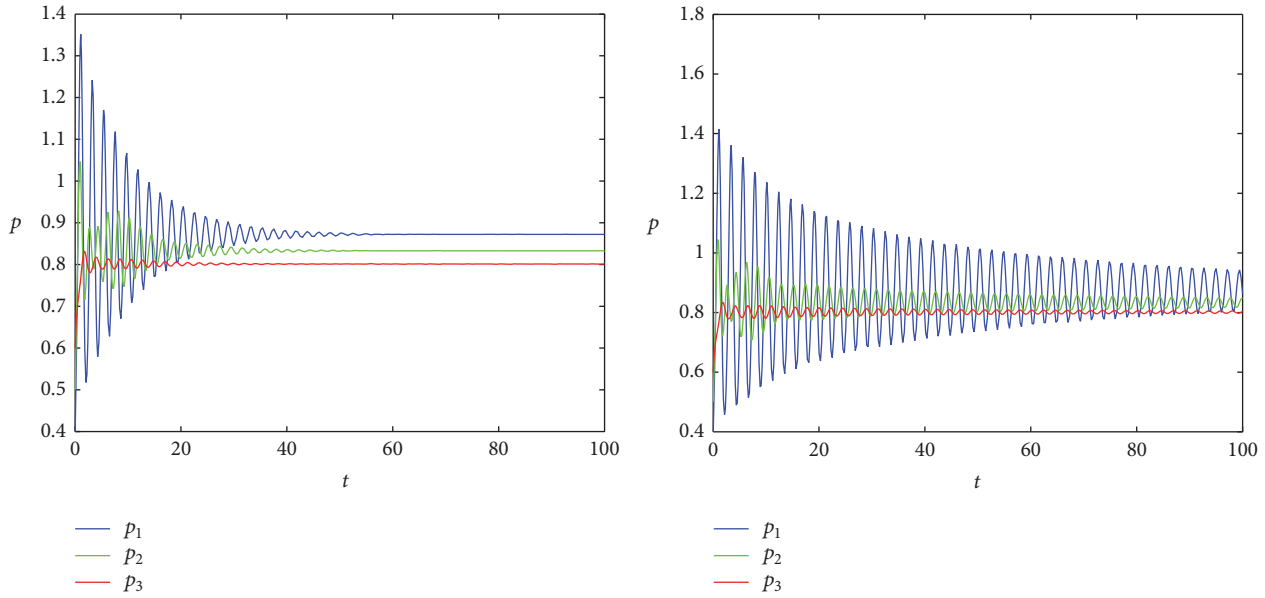

(a) $\tau_1 = 0.530 < \tau_{10} = 0.547$ (b) $\tau_1 = 0.560 > \tau_{10} = 0.547$

FIGURE 1: The time series of system (22) when $\tau_2 = 0.45$.

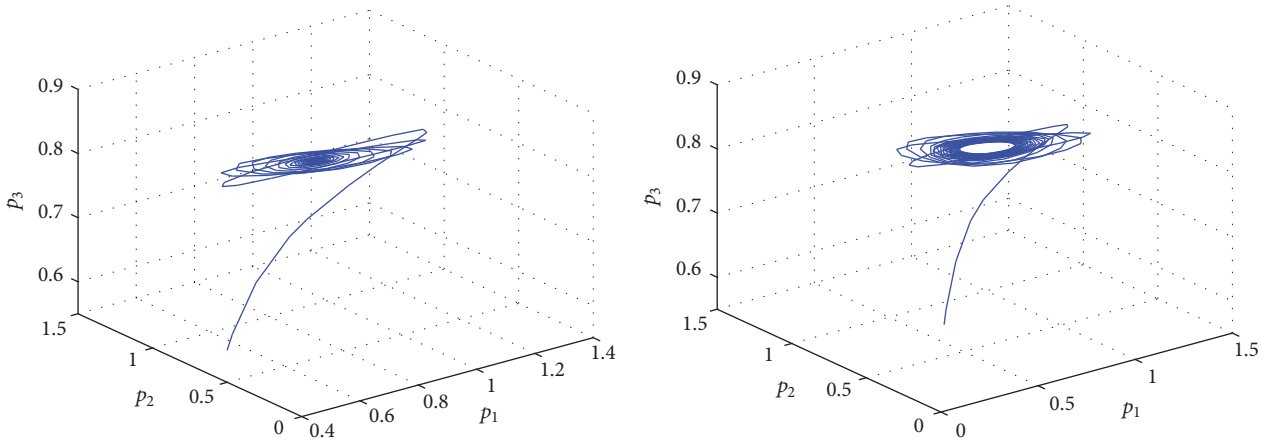

(a) $\tau_1 = 0.530 < \tau_{10} = 0.547$ (b) $\tau_1 = 0.560 > \tau_{10} = 0.547$

FIGURE 2: The attractor of system (22) when $\tau_2 = 0.45$.

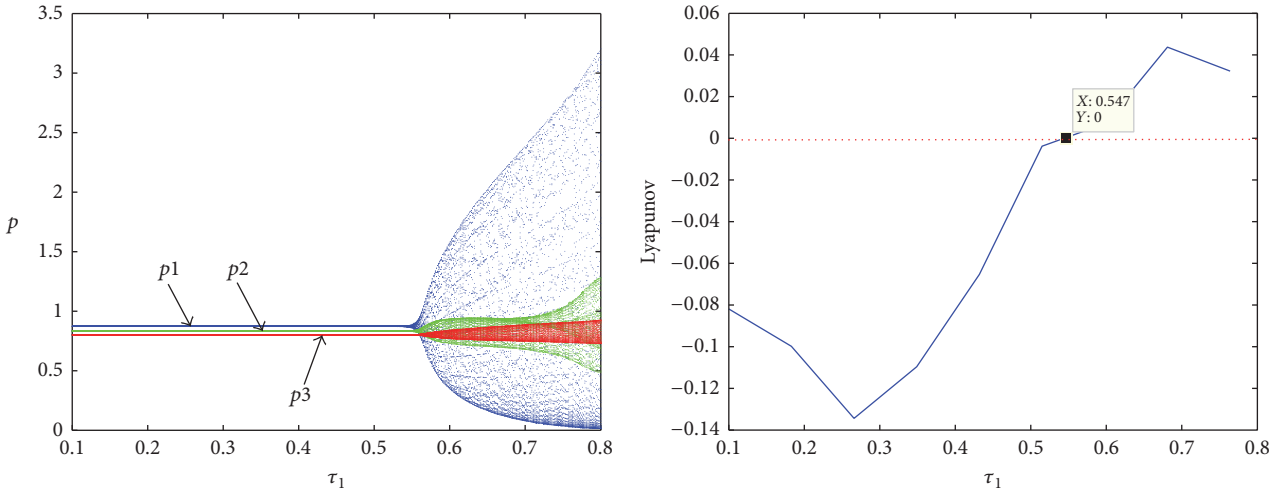

(a) Price bifurcation (b) The biggest Lyapunov exponent

FIGURE 3: The influence of τ_1 on system (22) when $\tau_2 = 0.45$.

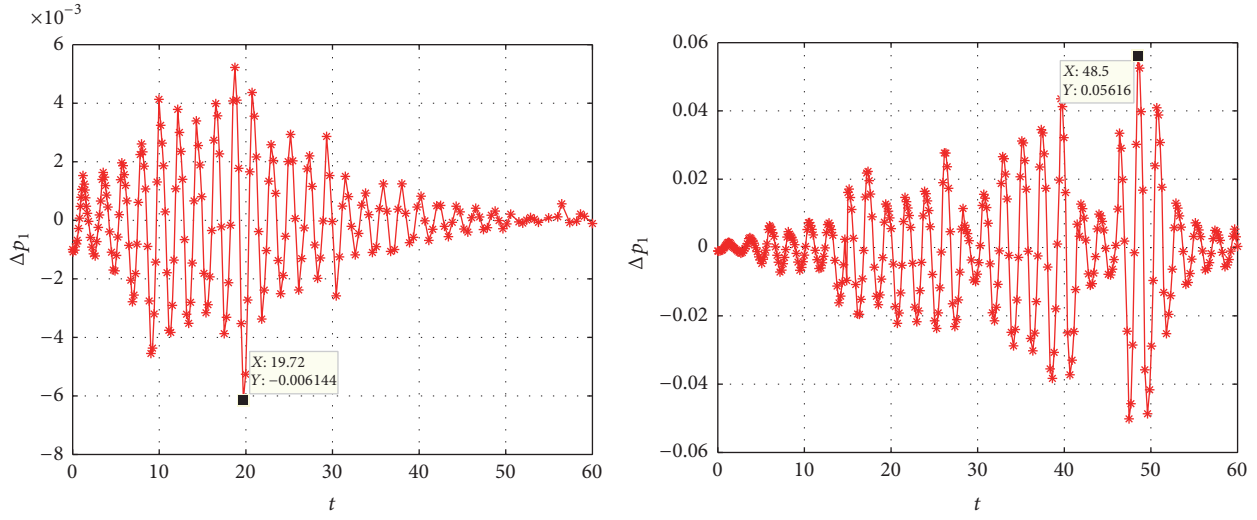

(a) $\tau_1 = 0.530 < \tau_{10} = 0.547$ (b) $\tau_1 = 0.560 > \tau_{10} = 0.547$

FIGURE 4: The sensitivity of p_1 to initial value $(0.4, 0.401)$ when $\tau_2 = 0.45$.

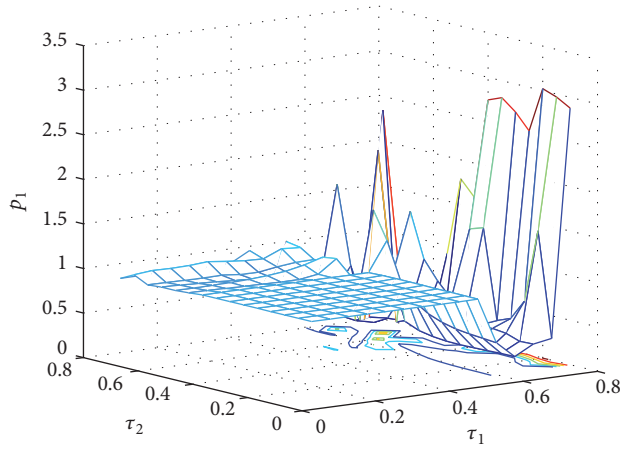

FIGURE 5: The influence of τ_1 and τ_2 on price.

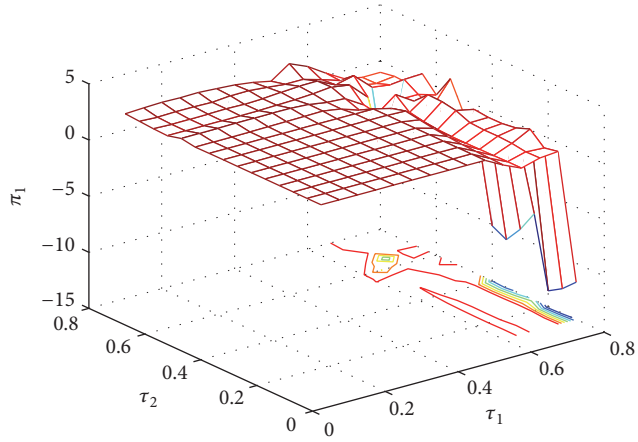

FIGURE 6: The influence of τ_1 and τ_2 on profit.

In Figure 4(b), when $\tau_1 = 0.560 > \tau_{10} = 0.547$, after 61 iterations, the difference of p_1 is 56.16 times of the initial difference 0.001. At this point, the value of p_1 has strong dependence on the initial value. Therefore, we know that system (22) is already in chaos. So we can infer that price decisions-making will have many unpredictable, tiny price adjustments which will have a greater price deviation.

4.3. The Influence of τ_1 and τ_2 on Stability of Price. We take τ_1 and τ_2 as parameters to study the effects of τ_1 and τ_2 on the price stability. With the increase of τ_1 and τ_2, the price changed from stable to unstable in Figure 5. When τ_1 is greater than 0.52, the price will experience fluctuations; when τ_2 is more than 0.5, the price will lose stability. When price is stable, the price will be stable at 0.8723. When price is chaotic, the highest price is 2.967 for $\tau_1 = 0.8$, $\tau_2 = 0.15$; the lowest price is 0.01871 for $\tau_1 = 0.75$, $\tau_2 = 0.75$. Therefore, enterprises should ensure that τ_1 and τ_2 are in a reasonable range when the price is set.

4.4. The Influence of τ_1 and τ_2 on Stability of Profit. We can see from Figure 6, when $\tau_1 > 0.52$, the profit will be unstable; when $\tau_2 > 0.5$, the profit will fluctuate. As profit is in stable condition, the profit is stable at 1.367. When the profit is in an unstable state, the maximum profit is 1.367; the lowest profit is −13.6 for $\tau_1 = 0.8$, $\tau_2 = 0.2$. Through the analysis we can know that with the increase of τ_1 and τ_2, profit will decline but not higher than the stable value. Therefore, enterprises must maintain a reasonable value of τ_1 and τ_2; otherwise there will be a loss.

5. Chaos Control

From the above analysis, we realize that the price and profit are in a state of chaos, which can lead to the fluctuation of

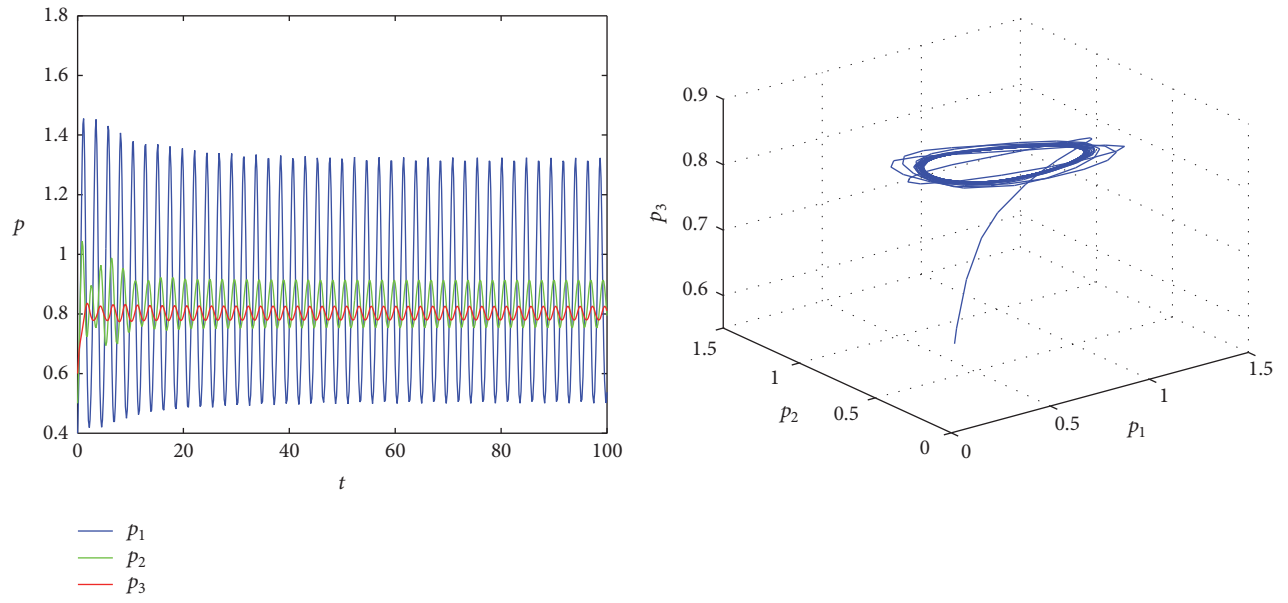

(a) Time series (b) Attractor

Figure 7: The time series and attractor $\tau_1 = 0.58$, $\tau_2 = 0.45$.

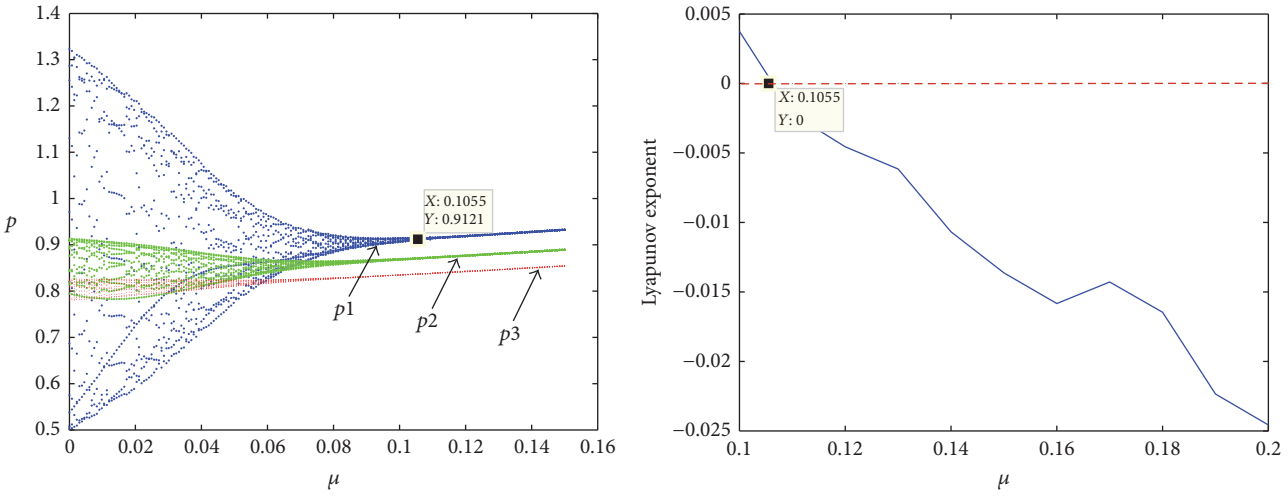

(a) Bifurcation (b) Lyapunov exponents

Figure 8: The influence of μ on the system when $\tau_1 = 0.58$, $\tau_2 = 0.45$.

the price and the profit. Therefore, we should take measures to prevent the system from entering a chaotic state or make it recover to a stable state. Below we take the method of the state variables feedback and parameter variation to control the system. Let $\tau_1 = 0.58$ and $\tau_2 = 0.45$; we can find that the system is chaotic from Figure 5. The time series and attractor of system (2) when $\tau_1 = 0.58$, $\tau_2 = 0.45$ are shown in Figure 7.

Adding control variable μ in system (22), then system (22) becomes

$$\begin{aligned}
\dot{p}_1(t) &= (1-\mu)\,0.20\,(5.0960 - 6.4614 p_1(t-\tau_1) \\
&\quad + 0.3058 p_2(t-\tau_2) + 0.3567 p_3(t)) + \mu p_1(t), \\
\dot{p}_2(t) &= (1-\mu)\,0.25\,(5.2100 - 7.1470 p_2(t-\tau_2) \\
&\quad + 0.4168 p_3(t) + 0.4689 p_1(t-\tau_1)) + \mu p_2(t), \\
\dot{p}_3(t) &= (1-\mu)\,0.30\,(5.3420 - 7.8599 p_3(t) \\
&\quad + 0.5342 p_1(t-\tau_1) + 0.5876 p_2(t-\tau_2)) + \mu p_3(t).
\end{aligned} \tag{23}$$

The effect of μ on system (23) is shown in Figure 8. We can get that when $\mu = 0.1055$, system (23) has bifurcation phenomenon. That is to say, when $\mu < 0.1055$, system (23) is chaotic, and when $\mu > 0.1055$, system (23) is stable. With the

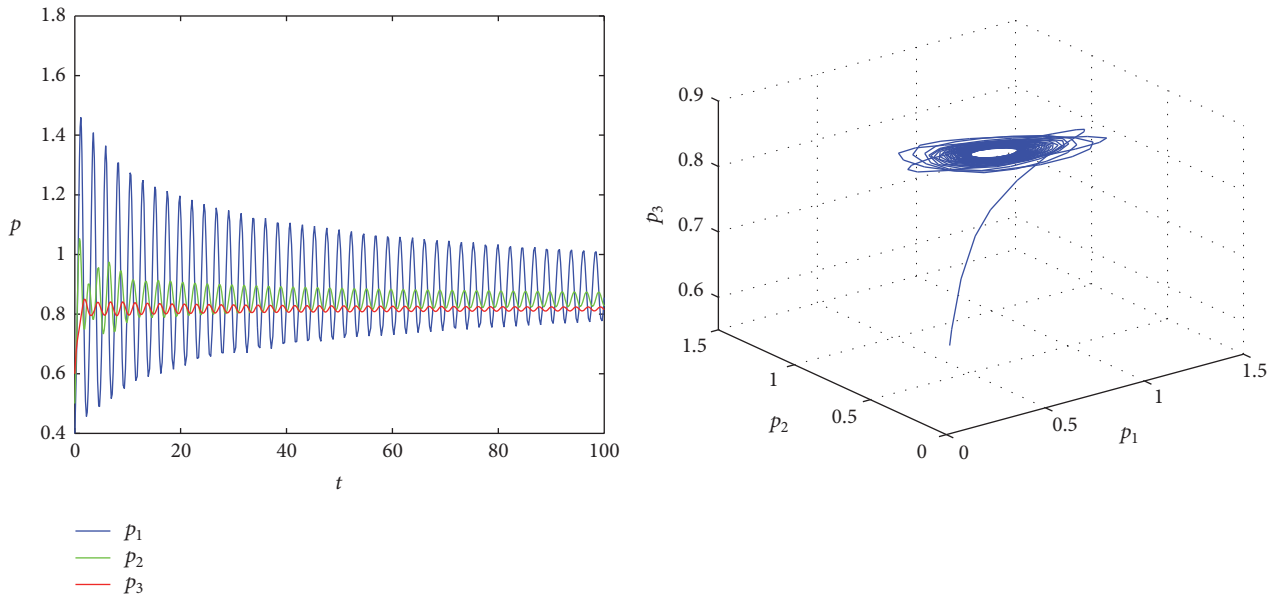

(a) Time series (b) Attractor

FIGURE 9: The time series and attractor when $\mu = 0.05 < 0.1055$.

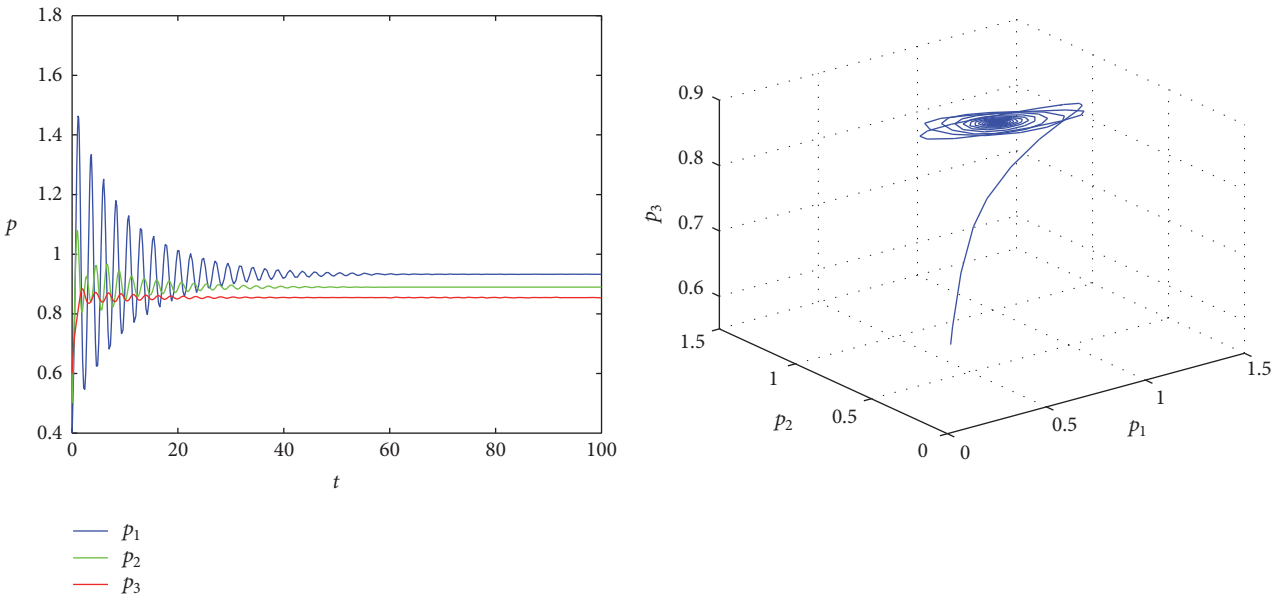

(a) Time series (b) Attractor

FIGURE 10: The time series and attractor when $\mu = 0.15 > 0.1055$.

increase of μ, the system changes from chaotic state to stable state.

Let $\mu = 0.05 < 0.1055$; we can find that system (23) is chaotic from Figure 8. The time series and attractor of system (23) are shown in Figure 9.

Let $\mu = 0.15 > 0.1055$; we can see that system (23) is stable from Figure 8. The time series and attractor of system (23) are shown in Figure 10. Compared with Figures 9 and 10, chaos is controlled. The bigger the value of μ is, the more obvious the control effect is.

6. Conclusions

The model of [19] was improved considering three enterprises are bounded rationality and using the cost function under the resource constraints. At the same time, delay strategy was used by the first and second enterprises. Firstly, when τ_2 is fixed, the influence of τ_1 on the stability of the system is considered. Secondly, the effects of τ_1, τ_2 on the stability of price and profit were studied. The research shows that the value of τ_1 and τ_2 must be ensured in a reasonable range,

and the price and profit are stable; otherwise there will be violent fluctuations. Finally, measures are taken to control chaos of system (2) successfully. The results of the paper play an important guiding value for the enterprise to carry on the price decision.

Conflicts of Interest

The authors declare no conflicts of interest.

Acknowledgments

The paper is supported by "The Fundamental Research Funds for the Central Universities," South-Central University for Nationalities (CSY13011). The authors extend their gratitude to Fengshan Si, Yuhua Xu, and Junjie Li for their help in model building and computing.

References

[1] J. Zhang, D. Zhou, and Y. Wang, "Complex dynamics analysis for a Bertrand duopoly model with bounded rationality," in *Proceedings of the International Conference on Management Science and Engineering (ICMSE '09)*, Moscow, Russia, September 2009.

[2] W. Xu and J. Ma, "Study on the dynamic model of a duopoly game with delay in insurance market," *WSEAS Transactions on Mathematics*, vol. 11, no. 7, pp. 615–624, 2012.

[3] Z. Sun and J. Ma, "Complexity of triopoly price game in Chinese cold rolled steel market," *Nonlinear Dynamics. An International Journal of Nonlinear Dynamics and Chaos in Engineering Systems*, vol. 67, no. 3, pp. 2001–2008, 2012.

[4] J. Dajka, M. Łobejko, and J. Sładkowski, "Payoffs and coherence of a quantum two-player game in a thermal environment," *Entropy*, vol. 17, no. 12, pp. 7736–7751, 2015.

[5] L. Fanti, L. Gori, C. Mammana, and E. Michetti, "The dynamics of a Bertrand duopoly with differentiated products: synchronization, intermittency and global dynamics," *Chaos, Solitons & Fractals*, vol. 52, pp. 73–86, 2013.

[6] Z. Xiangyu and Q. Xiaoyong, "A research on measure model of market structure entropy under the condition of competition and monopoly," *Journal of Industrial Technological Economics*, vol. 2, article 011, 2013.

[7] A. K. Naimzada and F. Tramontana, "Dynamic properties of a Cournot-Bertrand duopoly game with differentiated products," *Economic Modelling*, vol. 29, no. 4, pp. 1436–1439, 2012.

[8] T. Li and J. Ma, "The complex dynamics of R&D competition models of three oligarchs with heterogeneous players," *Nonlinear Dynamics*, vol. 74, no. 1-2, pp. 45–54, 2013.

[9] Y. Fan, T. Xie, and J. Du, "Complex dynamics of duopoly game with heterogeneous players: a further analysis of the output model," *Applied Mathematics and Computation*, vol. 218, no. 15, pp. 7829–7838, 2012.

[10] L. U. Yali, "Dynamics of a delayed Duopoly game with increasing marginal costs and bounded rationality strategy," *Procedia Engineering*, vol. 15, pp. 4392–4396, 2011.

[11] X. Gao, W. Zhong, and S. Mei, "Equilibrium stability of a nonlinear heterogeneous duopoly game with extrapolative foresight," *Mathematics and Computers in Simulation*, vol. 82, no. 11, pp. 2069–2078, 2012.

[12] J. Peng, Z. Miao, and F. Peng, "Study on a 3-dimensional game model with delayed bounded rationality," *Applied Mathematics and Computation*, vol. 218, no. 5, pp. 1568–1576, 2011.

[13] G. I. Bischi and A. Naimzada, "Global analysis of a dynamic duopoly game with bounded rationality," in *Advances in Dynamic Games and Applications (Kanagawa, 1996)*, vol. 5, pp. 361–385, Birkhauser Boston, Boston, Mass, USA, 2000.

[14] J. Ma and H. Tu, "Analysis of the stability and Hopf bifurcation of money supply delay in complex macroeconomic models," *Nonlinear Dynamics*, vol. 76, no. 1, pp. 497–508, 2014.

[15] J. Ma and H. Wang, "Complexity analysis of dynamic noncooperative game models for closed-loop supply chain with product recovery," *Applied Mathematical Modelling*, vol. 38, no. 23, pp. 5562–5572, 2014.

[16] J. Hale, *Theory of Functional Differential Equations*, Springer, New York, NY, USA, 2nd edition, 1977.

[17] J. Ma and F. Si, "Complex dynamics of a continuous Bertrand duopoly game model with two-stage delay," *Entropy. An International and Interdisciplinary Journal of Entropy and Information Studies*, vol. 18, no. 7, 2016.

[18] J. Ma and H. I. Bangura, "Complexity analysis research of financial and economic system under the condition of three parameters' change circumstances," *Nonlinear Dynamics*, vol. 70, no. 4, pp. 2313–2326, 2012.

[19] J. Ma, Y. Wang, and W. Xu, "Research on the triopoly dynamic game model based on different rationalities and its chaos control," *WSEAS Transactions on Mathematics*, vol. 13, pp. 983–991, 2014.

Hindawi
Advances in Mathematical Physics
Volume 2017, Article ID 5865403, 14 pages
https://doi.org/10.1155/2017/5865403

Research Article

Application of Adjoint Data Assimilation Method to Atmospheric Aerosol Transport Problems

Minjie Xu,[1] Kai Fu,[2] and Xianqing Lv[1]

[1] *Physical Oceanography Laboratory, Ocean University of China, Qingdao 266100, China*
[2] *School of Mathematical Science, Ocean University of China, Qingdao 266100, China*

Correspondence should be addressed to Kai Fu; kfu@ouc.edu.cn

Received 17 November 2016; Revised 28 February 2017; Accepted 8 March 2017; Published 30 March 2017

Academic Editor: Zhi-Yuan Sun

We propose combining the adjoint assimilation method with characteristic finite difference scheme (CFD) to solve the aerosol transport problems, which can predict the distribution of atmospheric aerosols efficiently by using large time steps. Firstly, the characteristic finite difference scheme (CFD) is tested to compute the Gaussian hump using large time step sizes and is compared with the first-order upwind scheme (US1) using small time steps; the US1 method gets E_2 error of 0.2887 using $\Delta t = 1/450$, while CFD method gets a much smaller E_2 of 0.2280 using a much larger time step $\Delta t = 1/45$. Then, the initial distribution of $PM_{2.5}$ concentration is inverted by the adjoint assimilation method with CFD and US1. The adjoint assimilation method with CFD gets better accuracy than adjoint assimilation method with US1 while adjoint assimilation method with CFD costs much less computational time. Further, a real case of $PM_{2.5}$ concentration distribution in China during the APEC 2014 is simulated by using adjoint assimilation method with CFD. The simulation results are in good agreement with the observed values. The adjoint assimilation method with CFD can solve large scale aerosol transport problem efficiently.

1. Introduction

Atmospheric aerosols are solid and liquid particles suspended in the air with the aerodynamic diameters between 0.001 μm and 100 μm. Aerosol particles that enter the atmosphere directly in the form of particles are called primary particles (primary aerosols), and those generated by gas in the atmosphere are called secondary particles (secondary aerosols). Atmospheric aerosol particles include smoke, haze, dust, pollen, and suspended microorganisms, which not only have an impact on environment, but also are a great concern for human health, as small particles can be inhaled into human body and cause disorders of the respiratory system, endocrine system, immune system, and so on [1–3]. Therefore, it is very important to get the prediction of the temporal and spatial distribution of atmospheric aerosols by numerical simulation.

Recently, there were many works on the developments of numerical models of atmospheric aerosols. Grell et al. [4] built the WRF/Chem model to simulate the distribution of pollutants in the northeastern United States; Tie et al. [5] used WRF/Chem model in the characterizations of chemical oxidants in Mexico City; Freitas et al. [6] developed the CATT-BRAMS model and studied the amount of $PM_{2.5}$ in the surface of the southwest Amazon Basin; Han et al. [7] used RAMS-CMAQ to predict the temporal and spatial distribution of nitrate wet deposition in East Asian region; Hudischewskyj and Seigneur [8] used Lagrangian plume models to study aerosols problem; Fu and Liang [9] developed the conservative characteristic finite difference method to predict the distribution of atmospheric aerosols.

The spatial and temporal variations of atmospheric aerosols are affected by several physical and chemical processes, like convection, diffusion, deposition, and so on, which make the prediction of the spatial and temporal distribution of atmospheric aerosols difficult. Meanwhile, parameters in model such as the initial condition play an important role in getting good predictions, but they are hard to be decided. Many studies had demonstrated that the

adjoint assimilation method is a good way to optimize the uncertain parameters using the observation data [10, 11].

The adjoint assimilation method is the combination of optimal control theory and variation principle. In this method, the atmospheric mathematical model is used as constraint condition, and the parameters of model are adjusted by assimilating observational data which can make the simulations of the model be in good agreement with the observations. Panofsky [12] proposed the data assimilation method in 1949 and obtained the objective analysis with two-dimensional global polynomial interpolation method; Constantinescu et al. [13] used chemical data assimilation techniques for improving chemical initial and boundary conditions to quantify the uncertainties of the air quality forecasts; Yumimoto and Uno [14] used data assimilation to inverse modeling of CO emissions; Koo et al. [15] used inverse modeling to predict PM_{10} in East Asia; Elbern et al. [16] applied 4D-variational data assimilation with an adjoint air quality model to chemical transport model; Wang et al. [17] applied adjoint assimilation method in a Marine Ecosystem Dynamical Model.

Due to the stability constraint of tradition methods such as upwind schemes [18, 19], numerical simulations of atmospheric aerosol transport problem need to be carried out by using very small time step sizes, which causes very high computational cost. Douglas Jr. and Russell [20] proposed characteristic method to solve convection-diffusion equations, which has high order accuracy and enables using large time steps; Pironneau and Tabata [21] studied the stability and convergence of the Galerkin-characteristic schemes; Rui and Tabata [22] studied the characteristic finite element scheme for convection-diffusion problems. In this paper, we propose the adjoint assimilation method with characteristic finite difference scheme (CFD) to predict the distribution of atmospheric aerosols. Numerical tests of the moving of a Gaussian hump show that CFD method can get more accurate solutions than the US1 method. Then numerical experiments of the adjoint method with ideal initial condition are carried out, which show the initial distribution of $PM_{2.5}$ concentration computed by the adjoint assimilation method with CFD is more accurate than that of adjoint assimilation method with US1, and adjoint assimilation method with CFD uses much less time. Finally, we simulate a realistic $PM_{2.5}$ aerosol transport problem during APEC 2014. The result shows that the adjoint assimilation method with CFD can obtain very good results even using very large time steps.

The paper is organized as follows. Section 2 presents the adjoint assimilation method. In Section 3, numerical experiments are taken and the results are analyzed. Finally, conclusions are given in Section 4.

2. Model and Method

Taking the studied atmospheric aerosol model as a constrain condition, the adjoint assimilation method can optimize the parameters of model by assimilating observation data and make the simulated results close to the observations. The basic idea of the adjoint assimilation method [23] is as follows. Firstly, we define a model by the governing equations and its parameters such as initial conditions. Then by optimizing the parameters, we minimize the cost function which measures the data misfit between the numerical solution of model and the observed data. In this paper, the adjoint assimilation method includes the atmospheric aerosol transport model, the adjoint model, and assimilation processes. The atmospheric aerosol transport model is used to predict the distribution of atmospheric aerosols and the adjoint model is used to get the gradient of the cost function on the initial condition. In assimilation processes, we can optimize the initial condition of model. Then we can use the atmospheric aerosol transport model with the initial condition to predict the distribution of atmospheric aerosols.

2.1. The Atmospheric Aerosol Transport Model. Generally speaking, the spatial and temporal variations of atmospheric aerosols are affected by several physical and chemical processes [24, 25], such as convection, diffusion, deposition, chemical reaction, and emissions, which make the prediction of the spatial and temporal distribution of atmospheric aerosols very difficult. In this paper, taking the physical and chemical processes as source term without considering the specific details, we consider the following atmospheric aerosol transport model:

$$\frac{\partial C}{\partial t} + u\frac{\partial C}{\partial x} + v\frac{\partial C}{\partial y} - \frac{\partial}{\partial x}\left(A_H\frac{\partial C}{\partial x}\right) - \frac{\partial}{\partial y}\left(A_H\frac{\partial C}{\partial y}\right) = S, \tag{1}$$

$$C\left(t^0, x, y\right) = C^0\left(x, y\right), \tag{2}$$

where t is time and x, y are components of the Cartesian coordinate system; C is the mass concentration of atmospheric aerosol; (u, v) is the horizontal wind velocity; A_H is the horizontal diffusivity coefficient; S is the source term; $C^0(x, y)$ is the given initial condition. Constant boundary conditions are used at the inflow boundary Γ^{IN}, and nongradient boundary conditions are used at the outflow boundary Γ^{OUT}:

$$\begin{aligned} \frac{\partial C}{\partial t} &= 0, \quad \text{on } \Gamma^{\mathrm{IN}}, \\ \frac{\partial C}{\partial n} &= 0, \quad \text{on } \Gamma^{\mathrm{OUT}}. \end{aligned} \tag{3}$$

Let Δx and Δy be the space step of x- and y-directions and Δt the time step. Let $C_{i,j}^n$ denote the atmospheric aerosol concentration at $(i\Delta x, j\Delta y)$ at $t^n = n\Delta t$.

Governing equation (1) can be solved by several numerical schemes, such as the first-order upwind difference scheme, which is usually adopted in the adjoint assimilation method for its simplicity [26–28] and is given as follows:

$$\frac{C_{i,j}^{n+1} - C_{i,j}^n}{\Delta t} + u_{i,j}^n\frac{C_{u\mathrm{up}}^n - C_{u\mathrm{dn}}^n}{\Delta x_j} + v_{i,j}^n\frac{C_{v\mathrm{up}}^n - C_{v\mathrm{dn}}^n}{\Delta y} = \frac{1}{\Delta x_j}\left(A_H\left(\frac{C_{i+1,j}^n - C_{i,j}^n}{\Delta x_j}\right)\right.$$

$$
\begin{aligned}
&- A_H\left(\frac{C^n_{i,j} - C^n_{i-1,j}}{\Delta x_j}\right)\Bigg)\\
&+ \frac{1}{\Delta y}\left(A_H\left(\frac{C^n_{i,j+1} - C^n_{i,j}}{\Delta y}\right)\right.\\
&\left.- A_H\left(\frac{C^n_{i,j} - C^n_{i,j-1}}{\Delta y}\right)\right) + S^n_{i,j},
\end{aligned}
\tag{4}
$$

where the upwind scheme is used in the advection term:

$$
\begin{aligned}
C^n_{u\mathrm{up}} &= C^n_{i,j},\\
C^n_{u\mathrm{dn}} &= C^n_{i-1,j}\\
&\qquad \text{if } u^n_{i,j} > 0,\\
C^n_{u\mathrm{up}} &= C^n_{i+1,j},\\
C^n_{u\mathrm{dn}} &= C^n_{i,j}\\
&\qquad \text{if } u^n_{i,j} < 0,\\
C^n_{v\mathrm{up}} &= C^n_{i,j},\\
C^n_{v\mathrm{dn}} &= C^n_{i,j-1}\\
&\qquad \text{if } v^n_{i,j} > 0,\\
C^n_{v\mathrm{up}} &= C^n_{i,j+1},\\
C^n_{v\mathrm{dn}} &= C^n_{i,j}\\
&\qquad \text{if } v^n_{i,j} < 0.
\end{aligned}
\tag{5}
$$

The stabilization condition of scheme (4) is

$$
\begin{aligned}
&\max\left\{\left(A_H + \frac{u^n_{i,j}\Delta x_j}{2}\right)\frac{\Delta t}{\left(\Delta x_j\right)^2}, \left(A_H + \frac{v^n_{i,j}\Delta y}{2}\right)\right.\\
&\left.\cdot\frac{\Delta t}{\left(\Delta y\right)^2}\right\} \le \frac{1}{2}.
\end{aligned}
\tag{6}
$$

Due to stabilization condition (6), very small time step has to be used in the computation, which causes long simulation time. Therefore, we propose using the adjoint assimilation method with characteristic finite difference scheme. As the variation of atmospheric aerosol mass concentration is small along the characteristic curve, then, by computing (1) along the characteristic direction, this method can get more accurate solutions even using large time step size.

As shown in Figure 1, let $C^n_{i,j}$ be the aerosol concentration at $\vec{x} = (i\Delta x, j\Delta y)$ at $t^n = n\Delta t$. We assume that the atmospheric aerosol mass concentration at each grid point at $t = t^n$ is known, and we want to know the atmospheric aerosol mass concentration at $t = t^{n+1}$. Let the characteristic direction be denoted by τ, and let $X(\tau; \vec{x}, t^{n+1})$ be the characteristic curve [29]:

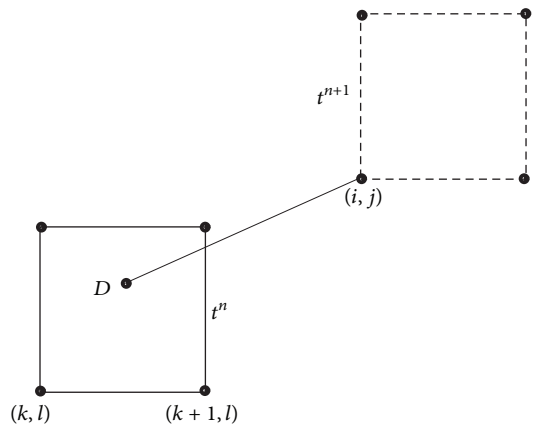

Figure 1: The process of constructing characteristic finite difference schemes.

$$
\frac{dX\left(\tau; \vec{x}, t^{n+1}\right)}{d\tau} = U\left(X\left(\tau; \vec{x}, t^{n+1}\right), \tau\right), \tag{7}
$$

$$
X\left(t^{n+1}; \vec{x}, t^{n+1}\right) = \vec{x}. \tag{8}
$$

Denote the intersection point of $X(\tau; \vec{x}, t^{n+1})$ with the time level t^n by $\vec{x}^*$ (point D in Figure 1). We solve $\vec{x}^*$ from (7)-(8) by

$$
\vec{x}^* = X\left(t^n; \vec{x}, t^{n+1}\right) = \vec{x} - U\left(\vec{x}, t^{n+1}\right)\Delta t. \tag{9}
$$

The atmospheric aerosol concentration $\overline{C}^n_{i,j}$ at $\vec{x}^*$ can be determined by the interpolation of the concentrations at the points $C^n_{k,l}$, $C^n_{k+1,l}$, $C^n_{k,l+1}$, $C^n_{k+1,l+1}$ surrounding $\vec{x}^*$. Then the characteristic finite difference scheme is given as

$$
\begin{aligned}
\frac{C^{n+1}_{i,j} - \overline{C}^n_{i,j}}{\Delta t} &= \frac{1}{\Delta x_j}\left(A_H\left(\frac{C^{n+1}_{i+1,j} - C^{n+1}_{i,j}}{\Delta x_j}\right)\right.\\
&\left.- A_H\left(\frac{C^{n+1}_{i,j} - C^{n+1}_{i-1,j}}{\Delta x_j}\right)\right)\\
&+ \frac{1}{\Delta y}\left(A_H\left(\frac{C^{n+1}_{i,j+1} - C^{n+1}_{i,j}}{\Delta y}\right)\right.\\
&\left.- A_H\left(\frac{C^{n+1}_{i,j} - C^{n+1}_{i,j-1}}{\Delta y}\right)\right) + S^n_{i,j},
\end{aligned}
\tag{10}
$$

where

$$
\begin{aligned}
&\overline{C}^n_{i,j} = a_{00}C^n_{k,l} + a_{01}C^n_{k,l+1} + a_{10}C^n_{k+1,l} + a_{11}C^n_{k+1,l+1},\\
&\left(x_k < \overline{x}_i < x_{k+1},\ y_l < \overline{y}_j < y_{l+1}\right),
\end{aligned}
$$

$$a_{00} = \frac{x_{k+1} - \overline{x}_i}{\Delta x} \frac{y_{l+1} - \overline{y}_j}{\Delta y},$$

$$a_{01} = \frac{x_{k+1} - \overline{x}_i}{\Delta x} \frac{\overline{y}_j - y_l}{\Delta y},$$

$$a_{10} = \frac{\overline{x}_i - x_k}{\Delta x} \frac{y_{l+1} - \overline{y}_j}{\Delta y},$$

$$a_{11} = \frac{\overline{x}_i - x_k}{\Delta x} \frac{\overline{y}_j - y_l}{\Delta y}. \tag{11}$$

Then the atmospheric aerosol transport problem can be solved by scheme (10) in N time steps.

2.2. The Adjoint Model. The adjoint method, which is derived by using the Lagrange multiplier method and the adjoint operator in functional analysis, plays an important role in the estimation of model parameters, such as initial condition. Nguyen et al. [30] used the adjoint method to estimate the state and parameter in 1D hyperbolic PDEs; Zhao and Lu [31] estimated the parameter in ecosystem model.

We define the cost function as

$$J(C) = \frac{1}{2} \int_\Omega \left(C - C'\right)^T K_C \left(C - C'\right) d\Omega, \tag{12}$$

where C is the solution of atmospheric aerosol transport problem; C' is the observed data of atmospheric aerosol; T denotes matrix transposition; Ω denotes model domain; K_C is the weighting matrix of C' and is defined as

$$K_C = \begin{cases} 1, & \text{if the observations are available,} \\ 0, & \text{otherwise.} \end{cases} \tag{13}$$

The problem is then transformed into an unconstrained minimization problem. Define the Lagrange function as

$$\begin{aligned} L\left(\lambda, C, C'\right) &= J(C) + \langle \lambda, F(C,S) \rangle = J(C) \\ &+ \int_\Omega \lambda \left\{ \frac{\partial C}{\partial t} + u\frac{\partial C}{\partial x} + v\frac{\partial C}{\partial y} - \frac{\partial}{\partial x}\left(A_H \frac{\partial C}{\partial x}\right) \right. \\ &\left. - \frac{\partial}{\partial y}\left(A_H \frac{\partial C}{\partial y}\right) - S \right\} d\Omega, \end{aligned} \tag{14}$$

where λ is the Lagrangian multiplier, which is a function of t, C, S. To get the minimum of the cost function, based on Lagrange multiplier theory, we make the first-order derivatives of Lagrange function be zero, as follows:

$$\frac{\partial L}{\partial \lambda} = 0, \tag{15}$$

$$\frac{\partial L}{\partial C} = 0, \tag{16}$$

$$\frac{\partial L}{\partial S} = 0. \tag{17}$$

In fact, (15) is (1), and the adjoint equation can be derived from (16).

Firstly, we simplify $\partial L/\partial C$ by subsection integration

$$\begin{aligned} \frac{\partial L}{\partial C} &= -\int_\Omega \left\{ \frac{\partial \lambda}{\partial t} + \frac{\partial (u\lambda)}{\partial x} + \frac{\partial (v\lambda)}{\partial y} + \frac{\partial}{\partial x}\left(A_H \frac{\partial \lambda}{\partial x}\right) \right. \\ &\left. + \frac{\partial}{\partial y}\left(A_H \frac{\partial \lambda}{\partial y}\right) \right\} d\Omega \\ &+ \int_\Omega \left\{ K_C \left(C - C'\right) \right\} d\Omega. \end{aligned} \tag{18}$$

Then the adjoint equation becomes

$$\begin{aligned} &\frac{\partial \lambda}{\partial t} + \frac{\partial (u\lambda)}{\partial x} + \frac{\partial (v\lambda)}{\partial y} + \frac{\partial}{\partial x}\left(A_H \frac{\partial \lambda}{\partial x}\right) \\ &\quad + \frac{\partial}{\partial y}\left(A_H \frac{\partial \lambda}{\partial y}\right) = K_C \left(C - C'\right). \end{aligned} \tag{19}$$

For the solution of adjoint equation (19), the first-order upwind scheme is given similar to (4) as

$$\begin{aligned} \frac{\lambda_{i,j}^n - \lambda_{i,j}^{n+1}}{\Delta t} &= u_{i,j}^{n+1} \frac{\lambda_{u\mathrm{up}}^{n+1} - \lambda_{u\mathrm{dn}}^{n+1}}{\Delta x_j} + v_{i,j}^{n+1} \frac{\lambda_{v\mathrm{up}}^{n+1} - \lambda_{v\mathrm{dn}}^{n+1}}{\Delta y} \\ &+ \frac{1}{\Delta x_j}\left(A_H \left(\frac{\lambda_{i+1,j}^{n+1} - \lambda_{i,j}^{n+1}}{\Delta x_j} \right) \right. \\ &\left. - A_H \left(\frac{\lambda_{i,j}^{n+1} - \lambda_{i-1,j}^{n+1}}{\Delta x_j} \right) \right) \\ &+ \frac{1}{\Delta y}\left(A_H \left(\frac{\lambda_{i,j+1}^{n+1} - \lambda_{i,j}^{n+1}}{\Delta y} \right) \right. \\ &\left. - A_H \left(\frac{\lambda_{i,j}^{n+1} - \lambda_{i,j-1}^{n+1}}{\Delta y} \right) \right) - K_C \left(C_{i,j}^{n+1} - C'^{n+1}_{i,j} \right), \end{aligned} \tag{20}$$

where

$$\begin{aligned} \lambda_{u\mathrm{up}}^{n+1} &= \lambda_{i,j}^{n+1}, \\ \lambda_{u\mathrm{dn}}^{n+1} &= \lambda_{i-1,j}^{n+1}, \\ &\qquad \text{if } u_{i,j}^{n+1} < 0, \\ \lambda_{u\mathrm{up}}^{n+1} &= \lambda_{i+1,j}^{n+1}, \\ \lambda_{u\mathrm{dn}}^{n+1} &= \lambda_{i,j}^{n+1}, \\ &\qquad \text{if } u_{i,j}^{n+1} > 0, \end{aligned}$$

$$\begin{aligned}
&\lambda_{v\mathrm{up}}^{n+1} = \lambda_{i,j}^{n+1},\\
&\lambda_{v\mathrm{dn}}^{n+1} = \lambda_{i,j-1}^{n+1},\\
&\qquad\qquad \text{if } v_{i,j}^{n+1} < 0,\\
&\lambda_{v\mathrm{up}}^{n+1} = \lambda_{i,j+1}^{n+1},\\
&\lambda_{v\mathrm{dn}}^{n+1} = \lambda_{i,j}^{n+1},\\
&\qquad\qquad \text{if } v_{i,j}^{n+1} > 0.
\end{aligned} \tag{21}$$

We propose the characteristic finite difference schemes for (19)

$$\begin{aligned}
\frac{\lambda_{i,j}^{n} - \overline{\lambda}_{i,j}^{n+1}}{\Delta t} &= \frac{1}{\Delta x_j}\left(A_H\left(\frac{\lambda_{i+1,j}^{n} - \lambda_{i,j}^{n}}{\Delta x_j}\right)\right.\\
&\left. - A_H\left(\frac{\lambda_{i,j}^{n} - \lambda_{i-1,j}^{n}}{\Delta x_j}\right)\right)\\
&+ \frac{1}{\Delta y}\left(A_H\left(\frac{\lambda_{i,j+1}^{n} - \lambda_{i,j}^{n}}{\Delta y}\right)\right.\\
&\left. - A_H\left(\frac{\lambda_{i,j}^{n} - \lambda_{i,j-1}^{n}}{\Delta y}\right)\right) - K_C\left(C_{i,j}^{n+1} - C'^{n+1}_{i,j}\right),
\end{aligned} \tag{22}$$

where

$$\begin{aligned}
\overline{\lambda}_{i,j}^{n+1} &= a_{00}\lambda_{k,l}^{n+1} + a_{01}\lambda_{k,l+1}^{n+1} + a_{10}\lambda_{k+1,l}^{n+1} + a_{11}\lambda_{k+1,l+1}^{n+1},\\
&\left(x_k < \overline{x}_i < x_{k+1},\ y_l < \overline{y}_j < y_{l+1}\right),\\
a_{00} &= \frac{x_{k+1} - \overline{x}_i}{\Delta x}\frac{y_{l+1} - \overline{y}_j}{\Delta y},\\
a_{01} &= \frac{x_{k+1} - \overline{x}_i}{\Delta x}\frac{\overline{y}_j - y_l}{\Delta y},\\
a_{10} &= \frac{\overline{x}_i - x_k}{\Delta x}\frac{y_{l+1} - \overline{y}_j}{\Delta y},\\
a_{11} &= \frac{\overline{x}_i - x_k}{\Delta x}\frac{\overline{y}_j - y_l}{\Delta y}.
\end{aligned} \tag{23}$$

Based on (14), we get the gradient of the cost function on the initial conditions of the aerosol mass concentration $C_{i,j}^{0}$:

$$\begin{aligned}
\frac{\partial J}{\partial C^0} = \left[\frac{\partial \lambda}{\partial t} + \frac{\partial (u\lambda)}{\partial x} + \frac{\partial (v\lambda)}{\partial y} + \frac{\partial}{\partial x}\left(A_H\frac{\partial \lambda}{\partial x}\right)\right.\\
\left. + \frac{\partial}{\partial y}\left(A_H\frac{\partial \lambda}{\partial y}\right)\right]^0.
\end{aligned} \tag{24}$$

Then the optimization of the initial condition can be obtained by the steepest descent method. The relationship between C^0 and gradient is as follows:

$$C^0{}_{\mathrm{new}} = C^0{}_{\mathrm{old}} - \alpha\frac{\partial J}{\partial C^0}, \tag{25}$$

where α is the step size of steepest descent method.

With the initial condition obtained in the adjoint method, we can get more accurate simulation results by the aerosol transport model.

3. Numerical Simulation

3.1. Numerical Experiment of Aerosol Transport Model. In this section, we first consider a transport of a Gaussian hump. The characteristic finite difference scheme (CFD) and the first-order upwind scheme (US1) are used to solve atmospheric aerosols model (1), and the results of two schemes are compared.

The initial condition is given as

$$\begin{aligned}
c(x, y, 0) = \exp\left(-\frac{(x - x_0)^2 + (y - y_0)^2}{2\sigma_0^2}\right),\\
(x, y) \in \Omega,
\end{aligned} \tag{26}$$

where the initial center is $(x_0, y_0) = (-0.4, 0)$ and $2\sigma_0^2 = 0.02$. The horizontal diffusivity coefficient is $A_H = 0.001$, the spatial domain is $\Omega = [-1, 1] \times [-1, 1]$, and $t \in (0, T] = (0, \pi/4]$. The velocity is $(u, v) = (-4y, 4x)$.

The exact solution of the problem with the given initial condition is

$$c(x, y, t) = \exp\left(-\frac{(\widetilde{x} - x_0)^2 + (\widetilde{y} - y_0)^2}{2{\sigma_0}^2 + 4A_H}\right), \tag{27}$$

where

$$\begin{aligned}
\widetilde{x} &= x\cos(4t) + y\sin(4t),\\
\widetilde{y} &= -x\sin(4t) + y\cos(4t).
\end{aligned} \tag{28}$$

Let $C^n(x, y)$ denote the approximate solution. The errors L_∞ and L_2 are defined as follows:

$$\begin{aligned}
E_\infty^n &= \max_{i,j}\left\{\left|c\left(x_i, y_j, t^n\right) - C^n\left(x_i, y_j\right)\right|\right\},\\
E_2^n &= \sqrt{\sum_{i,j}\Delta x\Delta y\left(c\left(x_i, y_j, t^n\right) - C^n\left(x_i, y_j\right)\right)^2}.
\end{aligned} \tag{29}$$

We choose different time grids $N_t = 45, 50, 55, 60, 75$ and small space step of $\Delta x = \Delta y = h = 1/200$ to compute the errors and ratios in time of the characteristic finite difference scheme (CFD) and the first-order upwind scheme (US1). The results are shown in Table 1. We can find the ratio in time of CFD method is first order, but US1 method can not get stable results using these large time step sizes. Therefore, due to the limit of stability (6), we choose different time grids

Table 1: Errors and ratios in time of the characteristic finite difference scheme (CFD) and the first-order upwind scheme (US1) using small space step of $h = 1/200$.

	N_t	45	50	55	60	75
US1	E_∞	1.5720e + 51	3.2108e + 56	4.0470e + 61	3.5640e + 66	2.2081e + 80
	Ratio	—	−1.1605e + 2	−1.2322e + 2	−1.3085e + 2	−1.4232e + 2
	E_2	3.4389e + 49	5.9727e + 54	8.1163e + 59	7.2351e + 64	5.2907e + 78
	Ratio	—	−1.1451e + 2	−1.2401e + 2	−1.3099e + 2	−1.4306e + 2
CFD	E_∞	2.1983e − 1	1.9882e − 1	1.8218e − 1	1.6750e − 1	1.3652e − 1
	Ratio	—	0.9535	0.9169	0.9660	0.9163
	E_2	4.0790e − 2	3.7005e − 2	3.3867e − 2	3.1225e − 2	2.5355e − 2
	Ratio	—	0.9243	0.9297	0.9336	0.9331

Table 2: Errors and ratios in time of the characteristic finite difference scheme (CFD) and the first-order upwind scheme (US1) using different time steps and space step of $h = 1/90, 1/100, 1/110, 1/120, 1/150$.

(a)

	N_t	450	500	550	600	750
US1	E_∞	2.8873e − 1	2.6926e − 1	2.5213e − 1	2.3696e − 1	2.0070e − 1
	Ratio	—	0.6624	0.6899	0.7131	0.7443
	E_2	4.3042e − 2	3.9833e − 2	3.7073e − 2	3.4672e − 2	2.9038e − 2
	Ratio	—	0.7352	0.7535	0.7694	0.7947

(b)

	N_t	45	50	55	60	75
CFD	E_∞	2.2796e − 1	2.0689e − 1	1.8933e − 1	1.7449e − 1	1.4119e − 1
	Ratio	—	0.9204	0.9306	0.9386	0.9488
	E_2	4.1029e − 2	3.7005e − 2	3.3867e − 2	3.1225e − 2	2.5355e − 2
	Ratio	—	0.9019	0.9125	0.9214	0.9333

Table 3: Errors and ratios in space of the characteristic finite difference scheme (CFD) and the first-order upwind scheme (US1) using small time step of $N_t = 400$.

	h	1/40	1/50	1/60	1/70	1/80
US1	E_∞	4.7095e − 1	4.2104e − 1	3.7863e − 1	3.4243e − 1	3.1126e − 1
	Ratio	—	0.5020	0.5823	0.6520	0.7147
	E_2	7.5471e − 2	6.5945e − 2	5.8315e − 2	5.2054e − 2	4.6817e − 2
	Ratio	—	0.6047	0.6744	0.7368	0.7940
CFD	E_∞	4.6345e − 1	4.1301e − 1	3.7034e − 1	3.3406e − 1	3.0294e − 1
	Ratio	—	0.5353	0.5907	0.6303	0.6546
	E_2	7.4605e − 2	6.5022e − 2	5.7361e − 2	5.1086e − 2	4.5847e − 2
	Ratio	—	0.6161	0.6876	0.7516	0.8102

$N_t = 450, 500, 550, 600, 750$ and the same space steps of $h = 1/90, 1/100, 1/110, 1/120, 1/150$ which are proportional to time steps. The experimental results are shown in Figure 2. Comparing to the maximum value 0.8649 of the exact solution, the US1 gets only 0.6680 when $\Delta t = T/750$, while CFD method gets a better result of 0.8134 using a much larger Δt of $T/75$. The errors and ratios are shown in Table 2. We can find the ratios of US1 method and CFD method are both first order, while CFD method converges faster than US1 method and gets better results. Even the CFD method uses large time steps; the errors with different Δt are much smaller than those of the first-order upwind scheme (US1). For example, when $N_t = 450$, E_∞ and E_2 of US1 are 2.8873×10^{-1} and 4.3042×10^{-2}, respectively; when $N_t = 45$, E_∞ and E_2 of CFD are 2.2796×10^{-1} and 4.1029×10^{-2}, respectively.

Then we choose different space grids $\Delta x = \Delta y = h = 1/40, 1/50, 1/60, 1/70, 1/80$ and small time step of $N_t = 400$ to compute the errors and ratios in space of the characteristic finite difference scheme (CFD) and the first-order upwind scheme (US1). As exhibited in Table 3, both US1

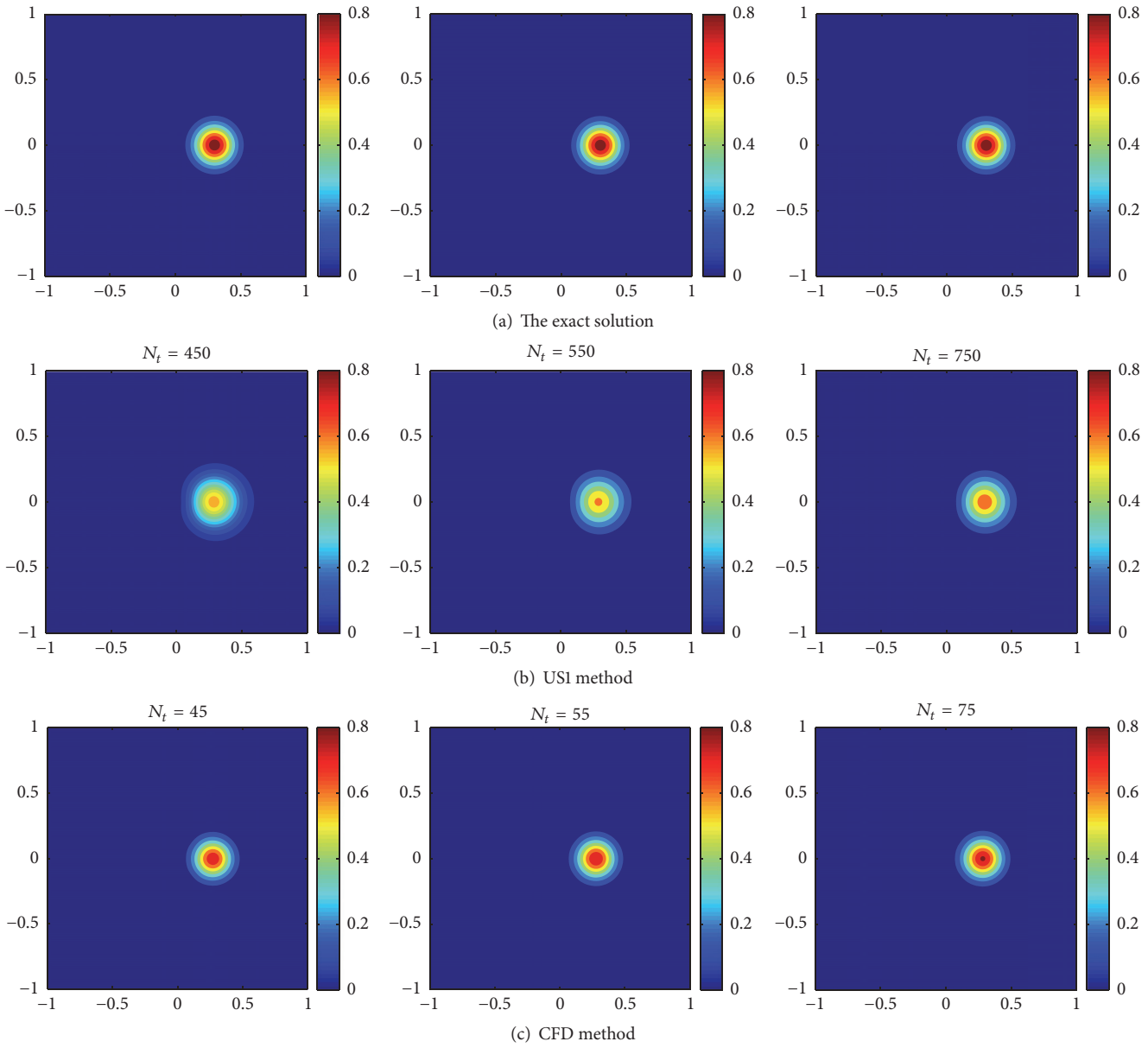

FIGURE 2: The results of (b) the US1 method and (c) the CFD method at $T = \pi/4$ using different time steps and proportional space steps comparing with (a) the exact solution.

method and CFD method get first-order accuracy in space, while the convergence rate of US1 method is less than CFD method. Besides, the errors with different h are smaller than those of the first-order upwind scheme (US1). For example, when $h = 1/60$, E_∞ and E_2 of US1 are 3.7864×10^{-1} and 5.8315×10^{-2}, respectively. While E_∞ and E_2 of CFD are 3.7034×10^{-1} and 5.7361×10^{-2}, respectively.

The results clearly show that the characteristic finite difference scheme (CFD) can get better solutions of the atmospheric model (1) than the first-order upwind scheme while greatly saving the computational time by using large time step size.

3.2. Numerical Experiment of the Adjoint Model. In this subsection, we consider getting initial field of $PM_{2.5}$ aerosol mass concentration of atmospheric transport model (1) by using the adjoint method. Initial conditions have important effects on the simulation results of the aerosol transport model. However, in most cases, instead of getting initial distribution of all the simulated mesh grids, we can only get observations for a few locations, which leads to big error of the final results. Therefore, we use the adjoint method to obtain reasonable initial fields that can get good simulation results.

In this experiment, we first give an ideal initial distribution of $PM_{2.5}$ aerosol mass concentration and solve

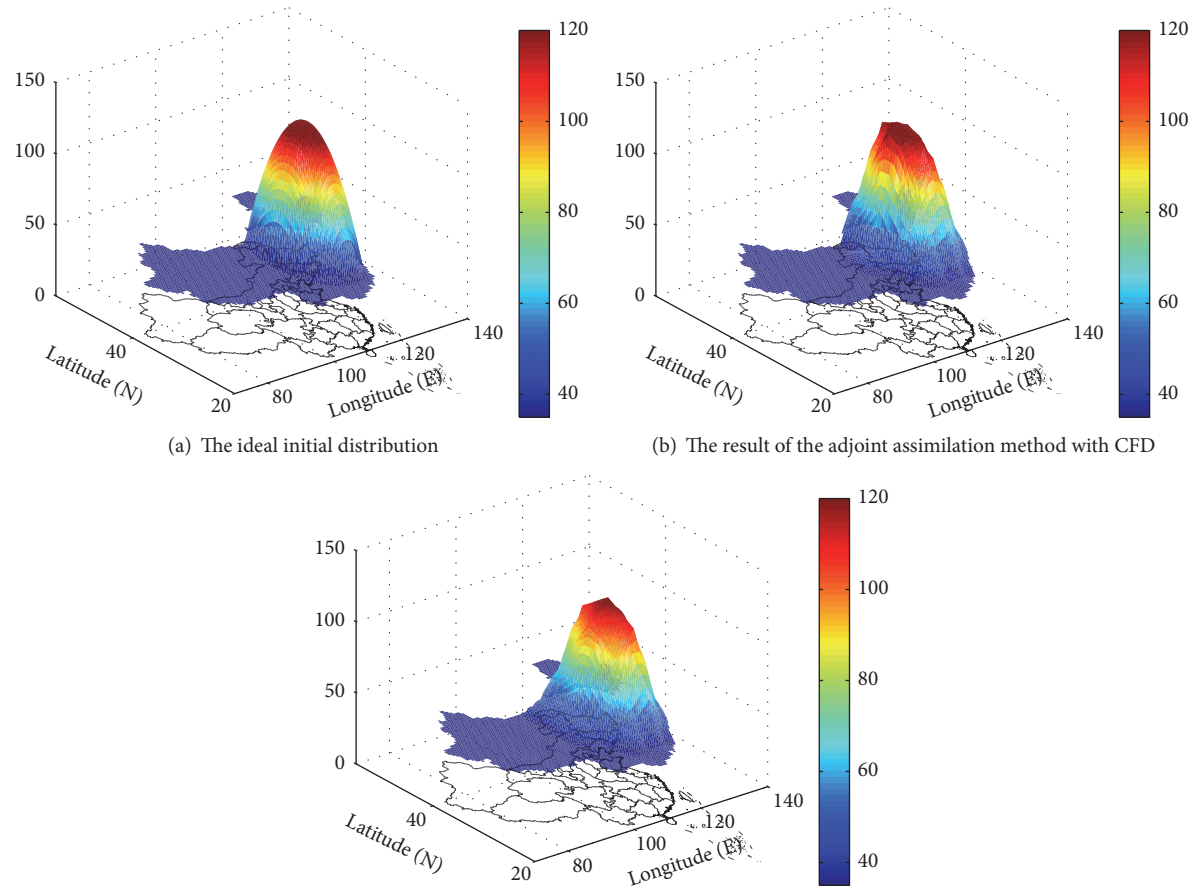

(a) The ideal initial distribution

(b) The result of the adjoint assimilation method with CFD

(c) The result of the adjoint assimilation method with US1

FIGURE 3: The 3D images of the results inverted by the adjoint assimilation method with different schemes.

aerosol transport model (1). Taking the solution as the observation, the experiments are carried out in the following steps.

Step 1. Give a priori distribution of initial condition, solve the aerosol transport model with this initial condition, and get simulated results.

Step 2. Solve cost function (12) using the simulated results and the observation. If the solution decreases to a very small value or the number of iterations exceeds the given iterative steps, then stop; otherwise, continue to run Step 3.

Step 3. Calculate the gradient of the cost function by the adjoint model and adjust initial field with the gradient. Then, new initial value is obtained and run Step 1.

The simulation domain is 70°E~140°E, 20°N~55°N with $0.5^\circ \times 0.5^\circ$ spatial resolution that covers China mainland, and the simulation time is 7 days. The simulation time steps of the US1 method and the CFD method are 600 s and 7200 s, respectively. The horizontal diffusion coefficient is $A_H = 100\,\mathrm{m}^2/\mathrm{s}$.

Since the $PM_{2.5}$ pollution is more serious in the north of China than other areas [32, 33], in EX 1 the mass concentration of $PM_{2.5}$ is given as follows:

$$C(i,j) = \begin{cases} -\left[(\mathrm{lon}(i) - 113.6)^2 + (\mathrm{lat}(j) - 34.7)^2\right] + 130, & \text{if } -\left[(\mathrm{lon}(i) - 113.6)^2 + (\mathrm{lat}(j) - 34.7)^2\right] + 130 > 35, \\ 35, & \text{if } -\left[(\mathrm{lon}(i) - 113.6)^2 + (\mathrm{lat}(j) - 34.7)^2\right] + 130 \le 35. \end{cases} \tag{30}$$

First-order upwind scheme (20) and CFD scheme (22) are used to solve adjoint model (19). And we can compute the initial distribution of $PM_{2.5}$ by the adjoint assimilation method. The results of experiment are shown in Figures 3 and 4. Comparing to the results of adjoint assimilation method with US1, the adjoint assimilation method with CFD gets better agreements with the ideal initial distribution even using large time steps.

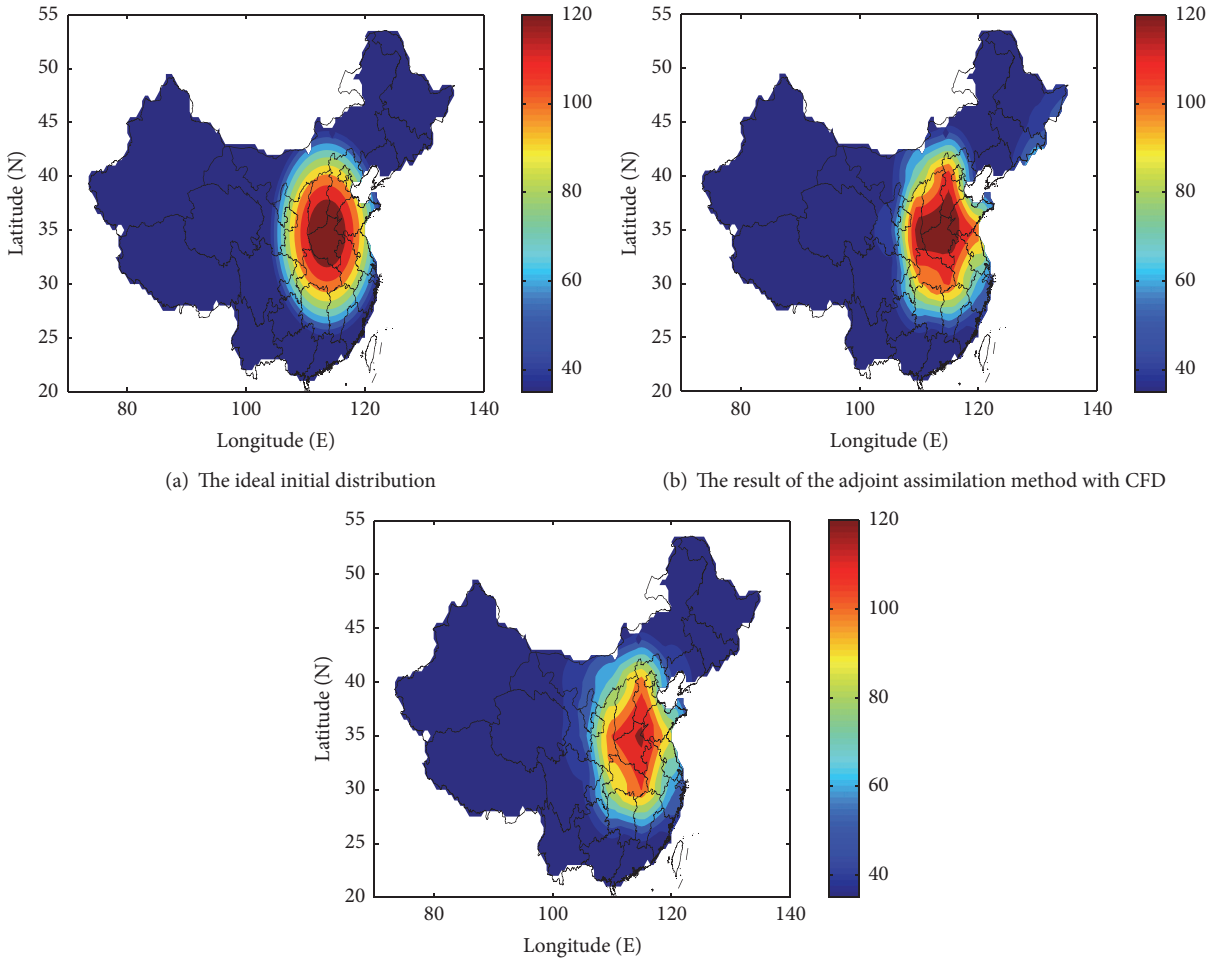

(a) The ideal initial distribution

(b) The result of the adjoint assimilation method with CFD

(c) The result of the adjoint assimilation method with US1

FIGURE 4: The 2D images of the results inverted by the adjoint assimilation method with different schemes.

TABLE 4: J_{50}/J_1, errors, and run time inverted by the adjoint assimilation method with different schemes.

	Method	$\frac{J_{50}}{J_1}$	MAE (μg/m^3)		E_∞ (μg/m^3)	E_2 (μg/m^3)	Time (s)
			Before assimilation	After assimilation			
EX1	CFD	4.1174$e-3$	33.8274	3.6432	2.9095	0.5355	64.86
	US1	5.8143$e-3$	33.8274	5.3705	11.1768	0.6618	257.11
EX2	CFD	2.8311$e-3$	57.7805	3.6802	8.8527	0.4689	53.63
	US1	2.9662$e-3$	57.7805	6.5276	10.8295	0.7204	253.06

The errors and running time are shown in Table 4. J_{50} is the final value of cost function and J_1 is the initial value of cost function. We find the adjoint assimilation method with US1 gets J_{50}/J_1 of 4.1174×10^{-3}, mean absolute error (MAE) reducing to 3.6432 μg/m^3, E_∞ of 2.9095 μg/m^3, and E_2 of 0.5355 μg/m^3 using computational time of 257.11 s, while the adjoint assimilation method with CFD gets better results with J_{50}/J_1 of 5.8143×10^{-3}, mean absolute error (MAE) reducing to 5.3705 μg/m^3, E_∞ of 11.1768 μg/m^3, and E_2 of 0.6618 μg/m^3 using a much less computational time of 64.86 s.

We then carry out an experiment with another ideal mass concentration of $PM_{2.5}$ of folding line distribution:

$$C(i,j) = \begin{cases} [(\text{lon}(i) - 70.0) \times 3] - 25, & 90 < \text{lon}(i) < 117, \\ 114.5 - [(\text{lon}(i) - 116.5) \times 5], & 117 \le \text{lon}(i) \le 132, \\ 35.0, & \text{others}. \end{cases} \quad (31)$$

The results of experiment are shown in Figure 5. Similarly, we can see that even using large time steps, the inverted initial

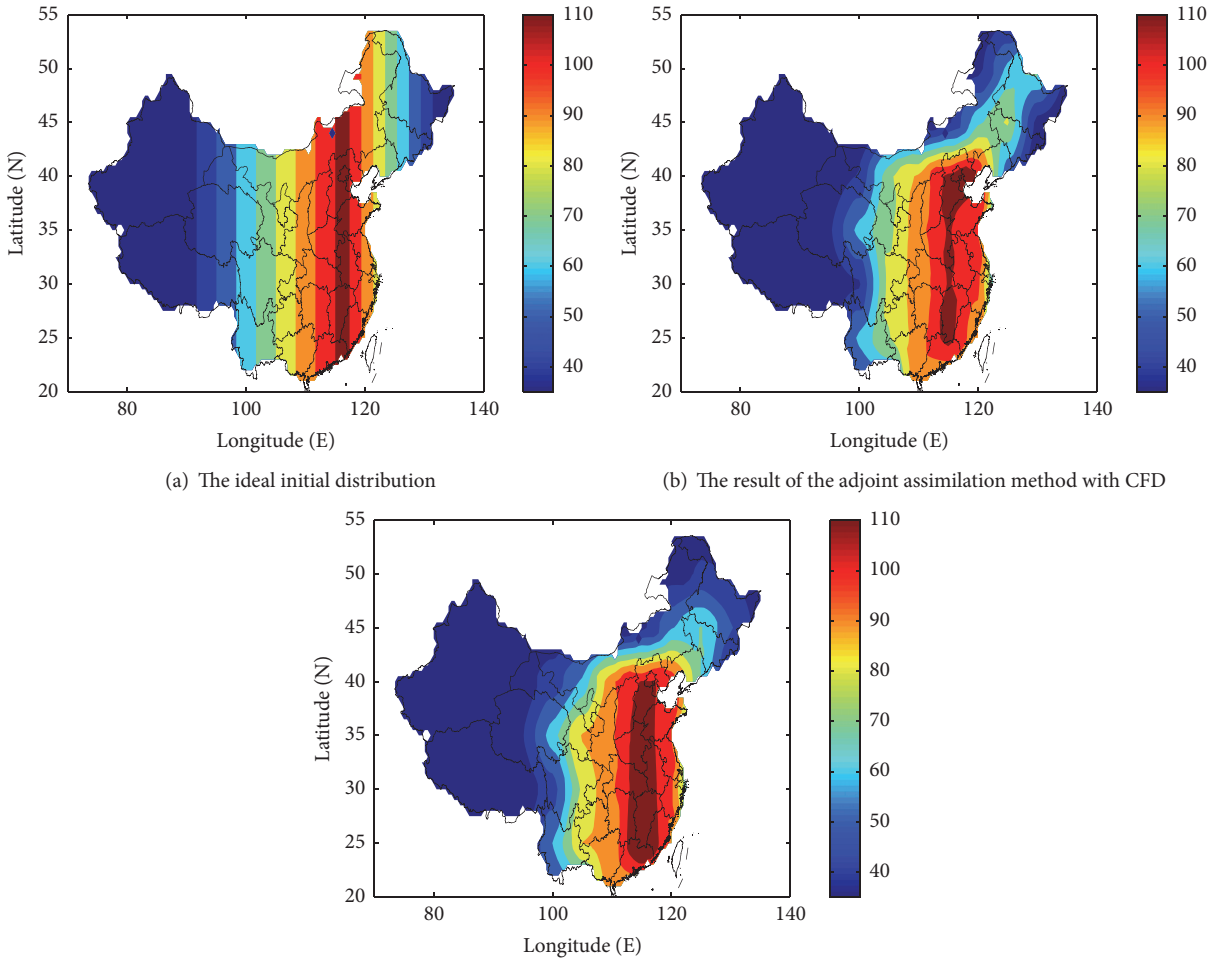

(a) The ideal initial distribution

(b) The result of the adjoint assimilation method with CFD

(c) The result of the adjoint assimilation method with US1

FIGURE 5: The 2D images of the results inverted by the adjoint assimilation method with different schemes.

distribution of the adjoint assimilation method with CFD is more accurate than the adjoint assimilation method with US1 comparing to the ideal initial distribution.

Table 4 shows the errors and running time. We find the adjoint assimilation method with US1 gets J_{50}/J_1 of 2.8311×10^{-3}, mean absolute error (MAE) reducing to $3.6802\,\mu g/m^3$, E_∞ of $8.8527\,\mu g/m^3$, and E_2 of $0.4689\,\mu g/m^3$ using 600 s time step, while the adjoint assimilation method with CFD gets smaller J_{50}/J_1 of 2.9662×10^{-3}, mean absolute error (MAE) reducing to $6.5276\,\mu g/m^3$, E_∞ of $10.8295\,\mu g/m^3$, and E_2 of $0.7204\,\mu g/m^3$ using a much larger time step of 7200 s.

Running the adjoint assimilation method with US1 costs the computational time of 253.06 s, while it costs only 53.63 s using CFD.

The experiments show that the adjoint assimilation method with CFD can invert ideal initial distribution of aerosol concentration very well using large time steps.

3.3. Practical Experiments. In this part, a real case of the $PM_{2.5}$ concentration during APEC 2014 in China is carried out by our adjoint assimilation method. We compare the results of adjoint assimilation method with CFD using large time steps with the results of US1 method using small time steps. We take the experiment for the period from November 5 to November 11, 2014. The studied area (70°E~140°E, 20°N~55°N) covers China and is divided into 140×70 grid cells with the horizontal resolution of $0.5° \times 0.5°$. The temporal resolutions of adjoint assimilation method with US1 and adjoint assimilation method with CFD are 600 s and 7200 s, respectively. We obtain the distribution of $PM_{2.5}$ aerosol mass concentration in November from of the historical database of the air quality (https://wat.epmap.org/). Besides, we obtain wind data in November from the National Centers for Environmental Prediction (NCEP). The background wind is determined by the interpolation of these wind data. The horizontal diffusion coefficient is taken as $A_H = 100\,m^2/s$. When iteration times are over 300, the computing stops.

By the adjoint method, we get the initial distribution of $PM_{2.5}$ aerosol mass concentration in Nov. 5. The spatial distribution of inverted $PM_{2.5}$ concentration in Nov. 5 is shown in Figure 6. Comparing to the observation of $PM_{2.5}$ in Nov. 5 in Figure 6(a), the initial distribution of $PM_{2.5}$ concentration inverted by the adjoint assimilation method with the characteristic finite difference scheme (CFD) using

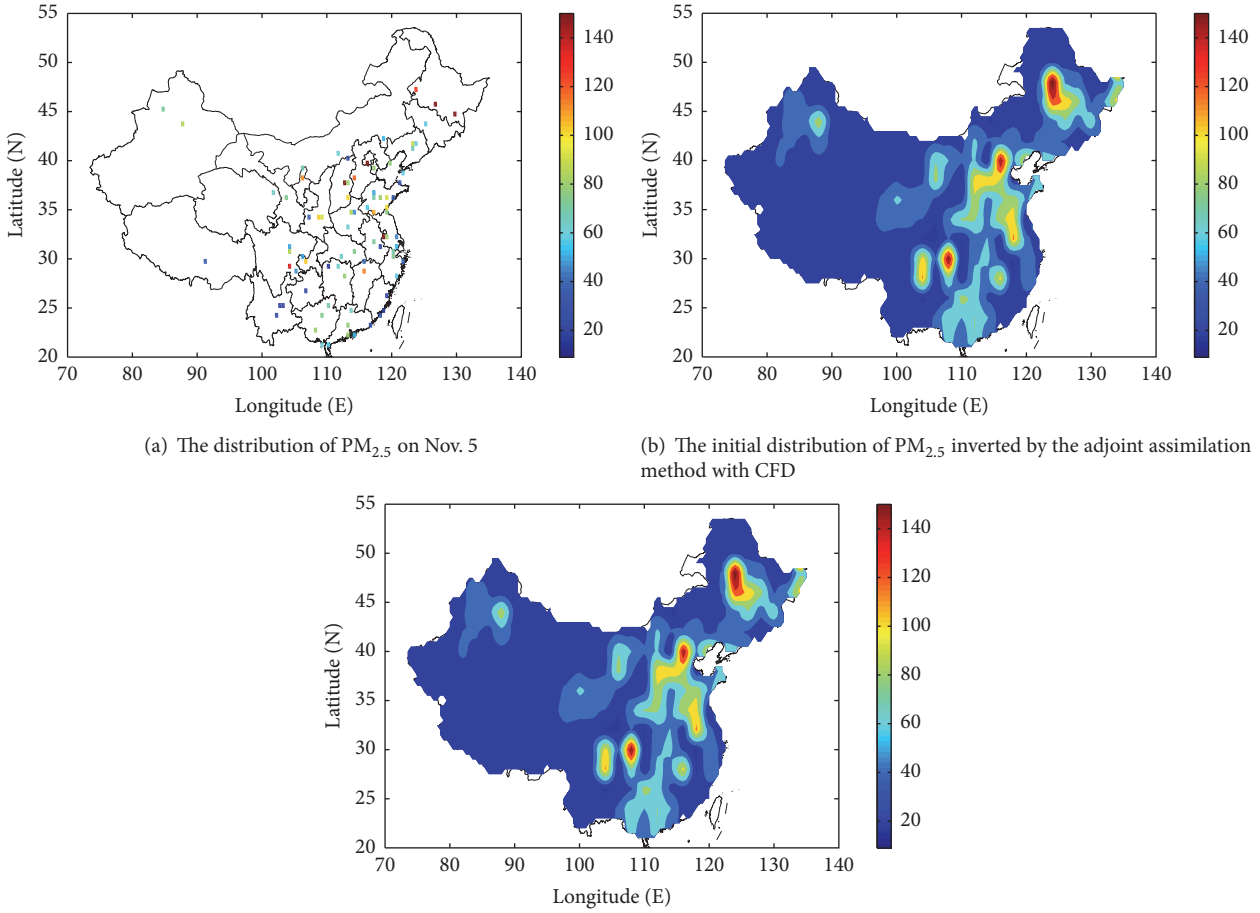

(a) The distribution of $PM_{2.5}$ on Nov. 5

(b) The initial distribution of $PM_{2.5}$ inverted by the adjoint assimilation method with CFD

(c) The initial distribution of $PM_{2.5}$ inverted by the adjoint assimilation method with US1

FIGURE 6: The 2D images of the initial distribution inverted by the adjoint assimilation method with different schemes.

TABLE 5: J_{300}/J_1, errors, and run time inverted by the adjoint assimilation method with different schemes.

Method	$\frac{J_{300}}{J_1}$	MAE ($\mu g/m^3$)		E_∞ ($\mu g/m^3$)	E_2 ($\mu g/m^3$)	Time (s)
		Before assimilation	After assimilation CFD			
CFD	$9.8045e-2$	37.8672	10.8625	41.0113	2.4111	2950.09
US1	$1.0901e-1$	37.8672	12.3036	53.7658	2.7571	45877.78

large time steps is more accurate than the results of first upwind scheme (US1) using small time steps. J_{300} is the final value of cost function and J_1 is the initial value of cost function. Table 5 shows J_{300}/J_1, errors between inverted initial distribution and observations, and run time of the adjoint assimilation method with two difference schemes. When we use adjoint assimilation method with CFD with $\Delta t = 7200$ s, we find J_{300}/J_1 reduces to 9.8045×10^{-2}, mean absolute error (MAE) reduces to 10.8625 $\mu g/m^3$, and E_2 is 2.4111 $\mu g/m^3$. While adjoint assimilation method with US1 gets J_{300}/J_1 of 1.0901×10^{-1}, mean absolute error (MAE) and E_2 are 12.3036 $\mu g/m^3$ and 2.7571 $\mu g/m^3$ using small time step size of $\Delta t = 600$ s.

Further, taking the inverted initial distribution of $PM_{2.5}$ concentration as the initial condition, we simulate the distribution of $PM_{2.5}$ concentration from Nov. 5 to Nov. 11 by the aerosol transport model. Time series of $PM_{2.5}$ concentration simulated by adjoint assimilation method with CFD and US1 in Beijing, Harbin, Shenyang, Xian, Yuxi, and Xiamen during APEC 2014 are shown in Figure 7. It is clear that the simulated $PM_{2.5}$ concentration by our adjoint assimilation method with CFD using large time steps is in good agreement with the observed concentration. Figure 8 gives the comparison of the time-varying of the average $PM_{2.5}$ concentration in China from Nov. 5 to Nov. 11 simulated by two methods. We can see that the adjoint assimilation method with CFD can simulate aerosol concentration using large time steps accurately.

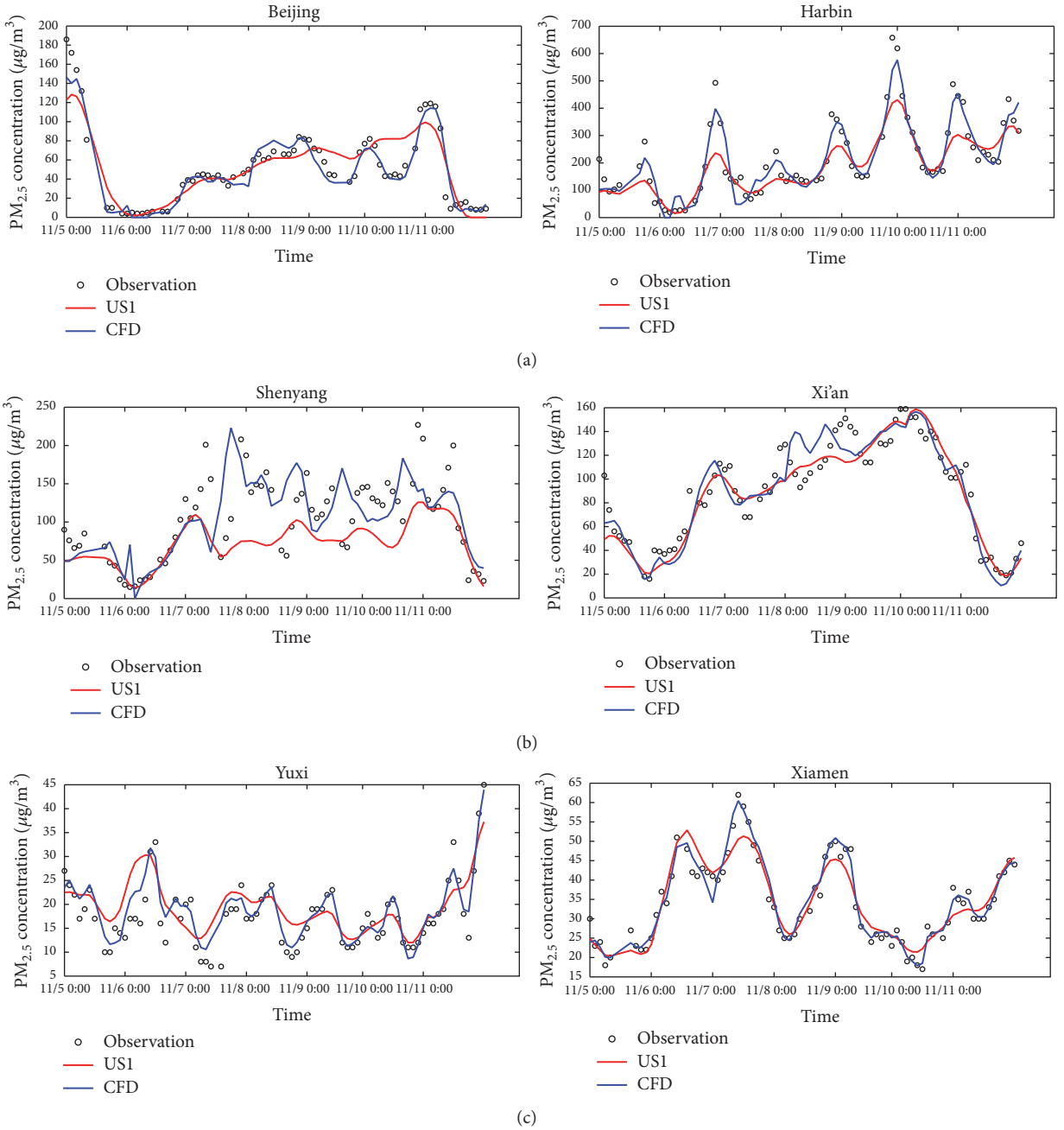

FIGURE 7: Comparisons of the time series of simulated $PM_{2.5}$ concentrations in 6 cities from Nov. 5 to Nov. 11.

4. Conclusions

In this paper, we use the adjoint assimilation method with the characteristic finite difference scheme (CFD) to solve the aerosol transport problem. The adjoint assimilation method with CFD can solve the problem effectively by large time steps. The effectiveness of CFD method was first shown in computing a Gaussian hump. Numerical results exhibit that the CFD method can get good solutions using 10 times time step of the US1 method and get better results. Further, the ideal initial distribution was inverted by adjoint assimilation method with CFD and US1. Comparing to the results of adjoint assimilation method with US1, the adjoint assimilation method with CFD gets better agreements with the ideal initial distribution even using large time steps. At last, a real case of $PM_{2.5}$ concentration distribution in China during the APEC 2014 was simulated and analyzed by using adjoint assimilation method with CFD. The inverted initial distribution of $PM_{2.5}$ concentration by adjoint assimilation method with CFD was in good agreement with the observation. Besides, the adjoint assimilation method with CFD with large time steps can obtain vary good simulations.

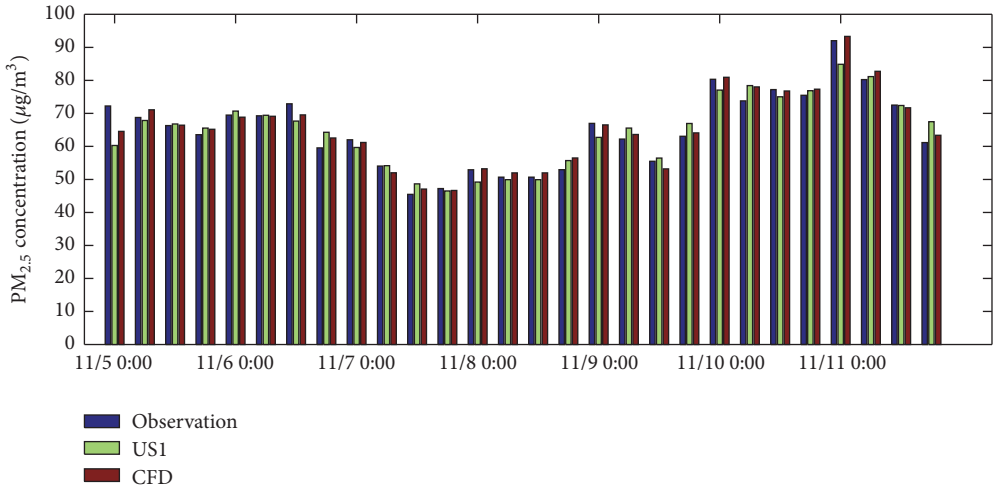

FIGURE 8: The averaged $PM_{2.5}$ concentrations in China from Nov. 5 to Nov. 11.

The adjoint assimilation method with characteristic finite difference scheme can solve large scale aerosol transport problem efficiently.

Conflicts of Interest

The authors declare that there are no conflicts of interest regarding the publication of this paper.

Acknowledgments

This work was partly supported by the Fundamental Research Funds for the Central Universities of China (Grant no. 201513059), the Natural Science Foundation of Shandong Province of China (no. ZR2014DM017), the National Natural Science Foundation of China (no. 11601497, no. 41606006, and no. 41371496), the Natural Science Foundation of Zhejiang Province (no. LY15D060001), the State Ministry of Science and Technology of China (no. 2013AA09A502), the National Science and Technology Support Program (no. 2013BAK05B04), and the Ministry of Education 111 Project (no. B07036).

References

[1] L. D. Bloemsma, G. Hoek, and L. A. M. Smit, "Panel studies of air pollution in patients with COPD: systematic review and meta-analysis," *Environmental Research*, vol. 151, pp. 458–468, 2016.

[2] U. P. Kodavanti, "Stretching the stress boundary: linking air pollution health effects to a neurohormonal stress response," *Biochimica et Biophysica Acta—General Subjects*, vol. 1860, no. 12, pp. 2880–2890, 2016.

[3] W. E. Cascio, "Proposed pathophysiologic framework to explain some excess cardiovascular death associated with ambient air particle pollution: insights for public health translation," *Biochimica et Biophysica Acta (BBA)—General Subjects*, vol. 1860, no. 12, pp. 2869–2879, 2016.

[4] G. A. Grell, S. E. Peckham, R. Schmitz et al., "Fully coupled 'online' chemistry within the WRF model," *Atmospheric Environment*, vol. 39, no. 37, pp. 6957–6975, 2005.

[5] X. Tie, S. Madronich, G. Li et al., "Characterizations of chemical oxidants in Mexico City: a regional chemical dynamical model (WRF-Chem) study," *Atmospheric Environment*, vol. 41, no. 9, pp. 1989–2008, 2007.

[6] S. R. Freitas, K. M. Longo, M. A. F. Silva Dias et al., "The coupled aerosol and tracer transport model to the Brazilian developments on the regional atmospheric modeling system (CATT-BRAMS)-Part 1: model description and evaluation," *Atmospheric Chemistry and Physics*, vol. 9, no. 8, pp. 2843–2861, 2009.

[7] X. Han, M. G. Zhang, and B. R. Zhou, "Modeling nitrate aerosol distributions and its direct radiative forcing in East Asia with RAMS-CMAQ," *Particuology*, vol. 11, no. 3, pp. 256–263, 2013.

[8] A. B. Hudischewskyj and C. Seigneur, "Mathematical modeling of the chemistry and physics of aerosols in plumes," *Environmental Science and Technology*, vol. 23, no. 4, pp. 413–421, 1989.

[9] K. Fu and D. Liang, "The conservative characteristic FD methods for atmospheric aerosol transport problems," *Journal of Computational Physics*, vol. 305, pp. 494–520, 2016.

[10] A. Hakami, D. K. Henze, J. H. Seinfeld et al., "Adjoint inverse modeling of black carbon during the Asian Pacific Regional Aerosol Characterization Experiment," *Journal of Geophysical Research D: Atmospheres*, vol. 110, no. 14, pp. 85–90, 2005.

[11] D. K. Henze, J. H. Seinfeld, and D. T. Shindell, "Inverse modeling and mapping US air quality influences of inorganic $PM_{2.5}$ precursor emissions using the adjoint of GEOS-Chem," *Atmospheric Chemistry and Physics*, vol. 9, no. 16, pp. 5877–5903, 2009.

[12] R. A. Panofsky, "Objective weather-map analysis," *Journal of Meteorology*, vol. 6, no. 6, pp. 386–392, 1949.

[13] E. M. Constantinescu, A. Sandu, T. F. Chai, and G. R. Carmichael, "Assessment of ensemble-based chemical data assimilation in an idealized setting," *Atmospheric Environment*, vol. 41, no. 1, pp. 18–36, 2007.

[14] K. Yumimoto and I. Uno, "Adjoint inverse modeling of CO emissions over Eastern Asia using four-dimensional variational data assimilation," *Atmospheric Environment*, vol. 40, no. 35, pp. 6836–6845, 2006.

[15] Y.-S. Koo, D.-R. Choi, H.-Y. Kwon, Y.-K. Jang, and J.-S. Han, "Improvement of PM10 prediction in East Asia using inverse modeling," *Atmospheric Environment*, vol. 106, pp. 318–328, 2015.

[16] H. Elbern, H. Schmidt, O. Talagrand, and A. Ebel, "4D-Variational data assimilation with an adjoint air quality model for emission analysis," *Environmental Modelling and Software*, vol. 15, no. 6-7, pp. 539–548, 2000.

[17] C. H. Wang, X. Y. Li, and X. Q. Lv, "Adjoint assimilation of seawifs data into a marine ecosystem dynamical model of the bohai sea and the north yellow sea," *Procedia Environmental Sciences*, vol. 13, pp. 2045–2061, 2012.

[18] K. Baba and M. Tabata, "On a conservative upwind finite element scheme for convective diffusion equations," *RAIRO Analyse Numérique*, vol. 15, no. 1, pp. 3–25, 1981.

[19] M. Tabata, "A finite element approximation corresponding to the upwind finite differencing," *Memoirs of Numerical Mathematics*, vol. 4, no. 4, pp. 47–63, 1977.

[20] J. Douglas Jr. and T. F. Russell, "Numerical methods for convection-dominated diffusion problems based on combining the method of characteristics with finite element or finite difference procedures," *SIAM Journal on Numerical Analysis*, vol. 19, no. 5, pp. 871–885, 1982.

[21] O. Pironneau and M. Tabata, "Stability and convergence of a Galerkin-characteristics finite element scheme of lumped mass type," *International Journal for Numerical Methods in Fluids*, vol. 64, no. 10–12, pp. 1240–1253, 2010.

[22] H. Rui and M. Tabata, "A second order characteristic finite element scheme for convection-diffusion problems," *Numerische Mathematik*, vol. 92, no. 1, pp. 161–177, 2002.

[23] J. Zhang and Y. P. Wang, "A method for inversion of periodic open boundary conditions in two-dimensional tidal models," *Computer Methods in Applied Mechanics and Engineering*, vol. 275, pp. 20–38, 2014.

[24] C. Cai, C. Hogrefe, P. Katsafados et al., "Performance evaluation of an air quality forecast modeling system for a summer and winter season—photochemical oxidants and their precursors," *Atmospheric Environment*, vol. 42, no. 37, pp. 8585–8599, 2008.

[25] J. Chen, J. Vaughan, J. Avise, S. O'Neill, and B. Lamb, "Enhancement and evaluation of the AIRPACT ozone and $PM_{2.5}$ forecast system for the Pacific Northwest," *Journal of Geophysical Research Atmospheres*, vol. 113, no. 14, pp. 762–770, 2008.

[26] D. Wang, N. Li, Y. Shen, and X. Lv, "The parameters estimation for a PM2.5 transport model with the Adjoint method," *Advances in Meteorology*, vol. 2016, Article ID 9873815, 2016.

[27] H. B. Chen, A. Z. Cao, J. C. Zhang, C. B. Miao, and X. Q. Lv, "Estimation of spatially varying open boundary conditions for a numerical internal tidal model with adjoint method," *Mathematics and Computers in Simulation*, vol. 97, pp. 14–38, 2014.

[28] K. Yoshida and T. Ishikawa, "Flood hydrograph estimation using an adjoint shallow-water model," *Journal of Hydro-Environment Research*, vol. 9, no. 3, pp. 429–440, 2015.

[29] D. Liang, K. Fu, and W. Wang, "Modelling multi-component aerosol transport problems by the efficient splitting characteristic method," *Atmospheric Environment*, vol. 144, pp. 297–314, 2016.

[30] V. T. Nguyen, D. Georges, and G. Besançon, "State and parameter estimation in 1-D hyperbolic PDEs based on an adjoint method," *Automatica*, vol. 67, pp. 185–191, 2016.

[31] Q. Zhao and X. Lu, "Parameter estimation in a three-dimensional marine ecosystem model using the adjoint technique," *Journal of Marine Systems*, vol. 74, no. 1-2, pp. 443–452, 2008.

[32] D. Fang, Q. G. Wang, H. M. Li, Y. Y. Yu, Y. Lu, and X. Qian, "Mortality effects assessment of ambient $PM_{2.5}$ pollution in the 74 leading cities of China," *Science of The Total Environment*, vol. 569–570, pp. 1545–1552, 2016.

[33] M. Tao, L. Chen, R. Li et al., "Spatial oscillation of the particle pollution in eastern China during winter: implications for regional air quality and climate," *Atmospheric Environment*, vol. 144, pp. 100–110, 2016.

Hindawi
Advances in Mathematical Physics
Volume 2017, Article ID 1843179, 8 pages
https://doi.org/10.1155/2017/1843179

Research Article

Adaptive Modified Function Projective Lag Synchronization of Memristor-Based Five-Order Chaotic Circuit Systems

Qiaoping Li and Sanyang Liu

School of Mathematics and Statistics, Xidian University, Xi'an 710071, China

Correspondence should be addressed to Qiaoping Li; liqiaoping1981@126.com

Received 27 October 2016; Revised 22 February 2017; Accepted 8 March 2017; Published 23 March 2017

Academic Editor: Zhi-Yuan Sun

The modified function projective lag synchronization of the memristor-based five-order chaotic circuit system with unknown bounded disturbances is investigated. Based on the LMI approach and Lyapunov stability theorem, an adaptive control law is established to make the states of two different memristor-based five-order chaotic circuit systems asymptotically synchronized up to a desired scaling function matrix, while the parameter controlling strength update law is designed to estimate the parameters well. Finally, the simulation is put forward to demonstrate the correctness and effectiveness of the proposed methods. The control method involved is simple and practical.

1. Introduction

The memristor, an abbreviation for memory resistor studied by Chua in 1971 [1], is described as the missing 4th passive fundamental circuit element along with resistors, capacitors, and inductors. The memristor is a two-terminal element, either a charge-controlled memristor or a flux-controlled memristor. More than forty years later, on the first day of May 2008, the Hewlett-Packard (HP) research team proudly announced their realization of a memristor prototype, with an official publication in Nature [2, 3]. This new circuit element shares many properties of resistors and shares the same unit of measurement, ohm. Much attention has been attracted to this novel device for its resistance upon turning off the power source; in other words, it depends on the integral of its entire past current waveform. At present, research on chaotic system based on memristor becomes a focal topic [3–10]. Itoh and Chua proposed the possible nonlinear circuits, with a memristor which replaces Chua's diode in 2008 [4], showed a memristor-based four-order Chua's circuit which is derived from Chua's circuit using a PWL memristor. By replacing Chua's diode with an active flux-controlled memristor circuit, a memristor-based five-order chaotic circuit is derived from four-order Chua's oscillator By Bao et al. [10].

As is known to all, the synchronization of chaotic systems has been a subject of active research field due to its potential applications for secure communications and control. Up to now, many types of synchronization methods have been put forward in dynamical systems, such as complete synchronization (CS) [11, 12], antisynchronization (AS) [13], phase synchronization (PS) [14], lag synchronization (LS) [15], intermittent lag synchronization [16], generalized synchronization (GS) [17], intermittent generalized synchronization [18], time scale synchronization [19], projective synchronization [20, 21], modified projective synchronization (MPS) [22], and function projective synchronization (FPS) [23].

Recently a more general form of FPS called modified function projective synchronization (MFPS) [24–26] in which master and slave systems are synchronized up to a desired scaling function matrix has attracted attention of researchers as it can provide more security in secure communication. Therefore, the research on MFPS is more valuable in practice. Considering time-delays exist widely in engineering, recently, a general method called modified function projective lag synchronization (MFPLS) for chaotic systems has been proposed in [27].

To the best of our knowledge, the MFPLS of memristor-based five-order chaotic circuit system with unknown disturbances has not been reported yet. Motivated by the above

discussion, we will give a comprehensive study on this topic in this article. Based on the parameter modulation, the adaptive control technique, and Lyapunov stability theorem, the adaptive control laws are designed to make the states of two different memristor-based five-order chaotic circuit systems asymptotically synchronized up to a desired scaling function matrix.

2. Memristor-Based Five-Order Chaotic Circuit System

By replacing Chua's diode with an active flux-controlled memristor circuit, Bao derived a memristor-based five-order chaotic circuit from four-order Chua's oscillator. This new chaotic circuit can be shown in Figure 1 and it can be described by the following nonlinear equations:

$$\begin{aligned}
\frac{dv_1(t)}{dt} &= \frac{1}{C_1}\left(i_3(t) - W\left(\varphi(t)\right)v_1(t)\right)\\
\frac{dv_2(t)}{dt} &= \frac{1}{C_2}\left(-i_3(t) + i_4(t)\right)\\
\frac{di_3(t)}{dt} &= \frac{1}{L_1}\left(v_2(t) - v_1(t) - Ri_3(t)\right)\\
\frac{di_4(t)}{dt} &= -\frac{1}{L_2}v_2(t)\\
\frac{d\varphi(t)}{dt} &= v_1(t),
\end{aligned} \tag{1}$$

in which $W(\varphi(t)) = -a + 3b\varphi^2(t)$.

Denote

$$\begin{aligned}
x(t) &= \left[x_1(t), x_2(t), x_3(t), x_4(t), x_5(t)\right]^T\\
&= \left[v_1(t), v_2(t), i_3(t), i_4(t), \varphi(t)\right]^T,
\end{aligned} \tag{2}$$

and then system (2) can be written as

$$\begin{aligned}
\dot{x}_1(t) &= \frac{1}{C_1}\left(x_3(t) - W\left(x_5(t)\right)x_1(t)\right)\\
\dot{x}_2(t) &= \frac{1}{C_2}\left(-x_3(t) + x_4(t)\right)\\
\dot{x}_3(t) &= \frac{1}{L_1}\left(x_2(t) - x_1(t) - Rx_3(t)\right)\\
\dot{x}_4(t) &= -\frac{1}{L_2}x_2(t)\\
\dot{x}_5(t) &= x_1(t).
\end{aligned} \tag{3}$$

If we set

$$\begin{aligned}
\frac{1}{C_1} &= 9,\\
C_2 &= 1,\\
\frac{1}{L_1} &= 30,\\
\frac{1}{L_2} &= 15,\\
R &= 1,\\
a &= 1.2,\\
b &= 0.4,
\end{aligned} \tag{4}$$

and the initial value is chosen as

$$x(0) = [0, 0.2, 0, 0, 0]^T, \tag{5}$$

system (3) is chaotic and multiscroll attractor as shown in Figures 2–5.

3. MFPLS in Memristor-Based Five-Order Chaotic Circuit Systems

Taking into account the external disturbances, for the sake of convenience, we reexpress system (3) as

$$\dot{x}(t) = Ax(t) + f(x(t)) + w(t), \tag{6}$$

where

$$\begin{aligned}
A &= \begin{bmatrix}
\frac{a}{C_1} & 0 & \frac{1}{C_1} & 0 & 0\\
0 & 0 & -\frac{1}{C_2} & \frac{1}{C_2} & 0\\
-\frac{1}{L_1} & \frac{1}{L_1} & -\frac{R}{L_1} & 0 & 0\\
0 & -\frac{1}{L_2} & 0 & 0 & 0\\
1 & 0 & 0 & 0 & 0
\end{bmatrix},\\
f(x(t)) &= \left[-\frac{b}{C_1}x_1(t)\,x_5{}^2(t), 0, 0, 0, 0\right]^T,\\
w(t) &= \left[w_1(t), w_2(t), w_3(t), w_4(t), w_5(t)\right]^T.
\end{aligned} \tag{7}$$

Taking system (6) as the drive system, the response system can be written as

$$\dot{y}(t) = By(t) + g\left(y(t)\right) + d(t) + u(t), \tag{8}$$

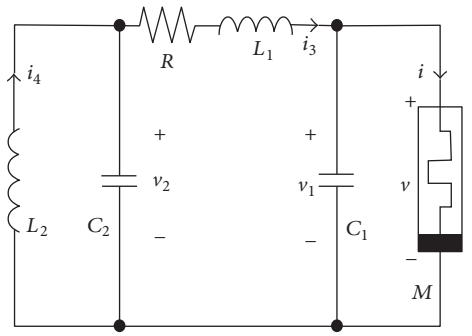

FIGURE 1: Memristor-based five-order chaotic circuit.

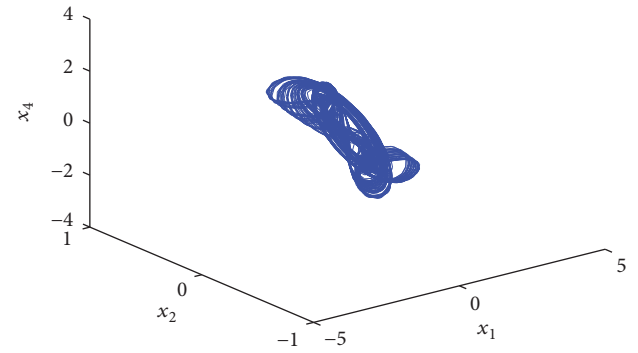

FIGURE 2: Attractor of the memristor-based five-order chaotic circuit (a).

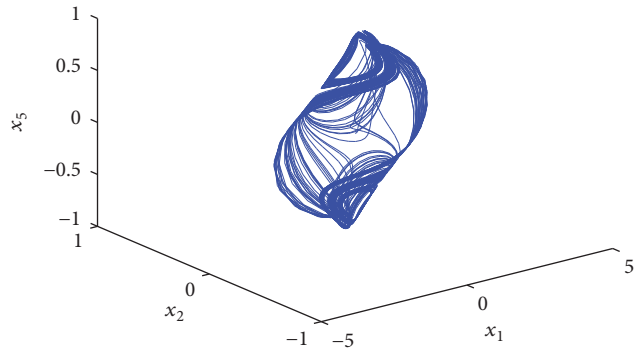

FIGURE 3: Attractor of the memristor-based five-order chaotic circuit (b).

where

$$y(t) = \left[y_1(t), y_2(t), y_3(t), y_4(t), y_5(t)\right]^T,$$

$$B = \begin{bmatrix} \frac{\overline{a}}{\overline{C}_1} & 0 & \frac{1}{\overline{C}_1} & 0 & 0 \\ 0 & 0 & -\frac{1}{\overline{C}_2} & \frac{1}{\overline{C}_2} & 0 \\ -\frac{1}{\overline{L}_1} & \frac{1}{\overline{L}_1} & -\frac{\overline{R}}{\overline{L}_1} & 0 & 0 \\ 0 & -\frac{1}{\overline{L}_2} & 0 & 0 & 0 \\ 1 & 0 & 0 & 0 & 0 \end{bmatrix}, \tag{9}$$

$$g\left(y(t)\right) = \left[-\frac{\overline{b}}{\overline{C}_1} y_1(t)\, {y_5}^2(t), 0, 0, 0, 0\right]^T,$$

$$d(t) = \left[d_1(t), d_2(t), d_3(t), d_4(t), d_5(t)\right]^T.$$

Assumption 1. The unknown external time-varying disturbances $w(t)$ and $d(t)$ are bounded; in other words, there exist nonnegative constants l_1^i and l_2^i such that

$$\begin{aligned} \left|w_i(t)\right| &\le l_1^i, \\ \left|d_i(t)\right| &\le l_2^i. \\ (i = 1, \ldots, 5) \end{aligned} \tag{10}$$

Denoting $l_1 = \sum_{i=1}^5 l_1^i$, $l_2 = \sum_{i=1}^5 l_2^i$, we can further obtain that

$$\begin{aligned} \|w(t)\| &\le l_1, \\ \|d(t)\| &\le l_2, \end{aligned} \tag{11}$$

where $\|\cdot\|$ stands for the 1-norm.

Definition 2 (MFPLS, [27]). For the drive system (6) and the response system (8), it is said that these two systems are modified function projective lag synchronization (MFPLS), if there exist a delay time τ and a scaling function matrix $\Lambda(t)$ such that

$$\lim_{t\to\infty} \left\|x(t-\tau) - \Lambda(t)\, y(t)\right\| = 0, \tag{12}$$

or

$$\lim_{t\to\infty} \left\|y(t) - \Lambda(t)\, x(t-\tau)\right\| = 0, \tag{13}$$

where $\Lambda(t) = \mathrm{diag}\{\lambda_1(t), \ldots, \lambda_5(t)\}$ is reversible and differentiable and $\lambda_i(t) \ne 0$ is a bounded continuously differentiable function.

Remark 3. It is clear that (12) and (13) are equivalent in the form.

Remark 4. When $\tau = 0$, $\lambda_1(t) = \lambda_2(t) = \cdots = \lambda_5(t)$, or $\lambda_1(t) = \lambda_2(t) = \cdots = \lambda_5(t) = 1$, MFPLS is simplified to MFPS, FPS, or complete synchronization, respectively.

Denote $\Lambda_1(t) = \mathrm{diag}\{|\lambda_1(t)|, \ldots, |\lambda_5(t)|\}$, $D = \mathrm{diag}\{\mathrm{sign}(\lambda_1(t)), \ldots, \mathrm{sign}(\lambda_5(t))\}$, and then the diagonal matrix $\Lambda(t)$ can be decomposed as

$$\Lambda(t) = \Lambda_1(t) \cdot D. \tag{14}$$

It is obvious that

$$D \cdot D = I, \tag{15}$$

in which I is an unit matrix.

Noted that $\lambda_i(t) \ne 0$ is a continuously differentiable function with bound, we further pose the following assumption.

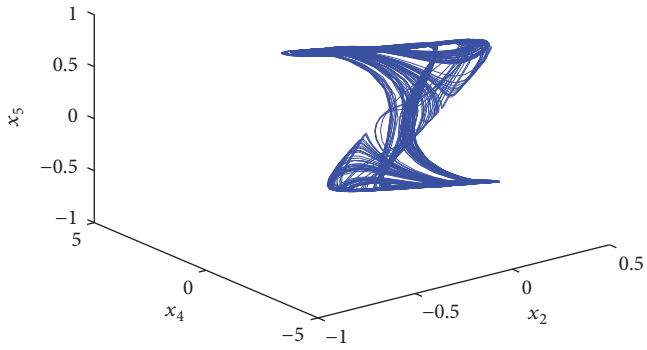

Figure 4: Attractor of the memristor-based five-order chaotic circuit (c).

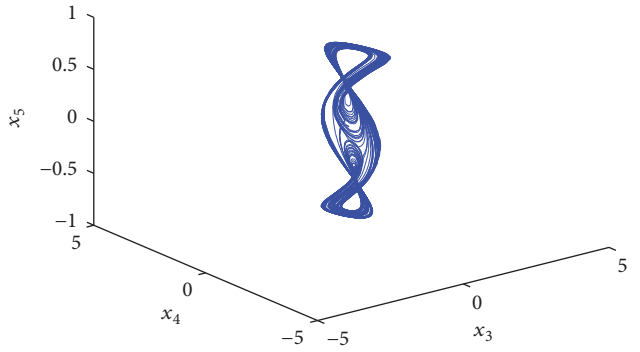

Figure 5: Attractor of the memristor-based five-order chaotic circuit (d).

Assumption 5. There exist three nonnegative constants α, β, and γ such that

$$\alpha \le \left\|\Lambda_1^{-1}(t)\right\| \le \beta, \qquad \left\|\left(\dot{\Lambda_1^{-1}}\right)(t)\right\| \le \gamma. \tag{16}$$

The main purpose of this paper is to design an appropriate controller $u(t)$ to ensure systems (6) and (8) are modified function projective lag synchronization.

Let us define the MFPLS error vector

$$e(t) = x(t-\tau) - \Lambda(t)\, y(t). \tag{17}$$

Combining systems (6) and (8) with the MFPLS error (17), the following error dynamical system can be obtained:

$$\dot{e}(t) = Ae(t) + h(x,y) + w(t-\tau) - \Lambda(t)\, d(t) - \Lambda(t)\, u(t), \tag{18}$$

where

$$h(x,y) = \left[A\Lambda(t) - \Lambda(t)\, B - \dot{\Lambda}(t)\right] y(t) + f(x(t-\tau)) - \Lambda(t)\, g(y(t)). \tag{19}$$

Furthermore, we can obtain

$$\Lambda_1^{-1}(t)\,\dot{e}(t) = \Lambda_1^{-1}(t)\, Ae(t) + \Lambda_1^{-1}(t)\, h(x,y) + \Lambda_1^{-1}(t)\, w(t-\tau) - Dd(t) - Du(t). \tag{20}$$

It followed by designing an adaptive controller to achieve MFPLS of systems (6) and (8).

4. Design of the Adaptive Controller

4.1. Case 1. We start with a simple case in which the bounds l_1 and l_2 are known. In order to achieve the MFPLS, the control law is given by

$$u(t) = D\left[\Lambda_1^{-1}(t)\, Ae(t) + \Lambda_1^{-1}(t)\, h(x,y) + Ke(t)\right] + (\beta l_1 + l_2)\, D\,\mathrm{sign}(e), \tag{21}$$

where $K = \mathrm{diag}\{k_1, \ldots, k_5\}$ is the control gain matrix and $\mathrm{sign}(e) = [\mathrm{sign}(e_1(t)), \ldots, \mathrm{sign}(e_5(t))]^T$.

Theorem 6. *If there exists symmetric positive definite matrix Q, such that the following LMI holds:*

$$-K + \gamma I = -Q, \tag{22}$$

then systems (6) and (8) are MFPLS.

Proof. Substituting the control law (21) into (20), we can obtain

$$\Lambda_1^{-1}(t)\,\dot{e}(t) = \Lambda_1^{-1}(t)\, w(t-\tau) - Dd(t) - Ke(t) - (\beta l_1 + l_2)\,\mathrm{sign}(e). \tag{23}$$

Since $\Lambda_1^{-1}(t)$ is positive definite matrix, we design the following Lyapunov function:

$$V(t) = \frac{1}{2} e^T(t)\, \Lambda_1^{-1}(t)\, e(t). \tag{24}$$

Calculating the time derivative of $V(t)$ along the trajectory of the error system (18), it can be found that

$$\begin{aligned}\dot{V}(t) &= e^T \Lambda_1^{-1}\dot{e} + \frac{1}{2} e^T\left(\dot{\Lambda_1^{-1}}\right)e = e^T\left[\Lambda_1^{-1} w(t-\tau) - Dd(t) - Ke - (\beta l_1 + l_2)\,\mathrm{sign}(e)\right] + \frac{1}{2} e^T\left(\dot{\Lambda_1^{-1}}\right)e \\ &\le \left(\left\|\Lambda_1^{-1} w(t-\tau)\right\| + \|d(t)\|\right)\|e\| - (\beta l_1 + l_2)\,\|e\| \\ &\quad - e^T Ke + e^T(t)\,(\gamma I)\, e \le -e^T(K - \gamma I)\, e = -e^T Qe \\ &< 0.\end{aligned} \tag{25}$$

Utilizing Lyapunov stability theorem, we get

$$\lim_{t\to\infty} \|e(t)\| = 0, \tag{26}$$

which means that systems (6) and (8) are MFPLS. This completes the proof. □

4.2. Case 2. We now consider the general case in which the bounds l_1 and l_2 are unknown; denote $\rho = \beta l_1 + l_2$ and $\widehat{\rho}$ stands

for the estimated value of ρ. Based on the adaptive control method, the controller is designed as

$$u(t) = D\left[\Lambda_1^{-1}(t) Ae(t) + \Lambda_1^{-1}(t) h(x, y) + Ke(t)\right] + q\hat{\rho} D \operatorname{sign}(e), \tag{27}$$

while the parameter adaptive law is given by

$$\dot{\hat{\rho}} = q\|e\|, \tag{28}$$

where constant $q > 0$ is the adjustable gain.

Theorem 7. *If there exist a positive constant η and a symmetric positive definite matrix Q such that the following LMIs hold:*

$$\begin{aligned} \beta l_1 + l_2 - \rho q &= -\eta, \\ -K + \gamma I &= -Q, \end{aligned} \tag{29}$$

then the two systems (6) and (8) are MFPLS.

Proof. Substituting the controller (27) and the adaptive update law (28) into (20), we can obtain

$$\Lambda_1^{-1}(t)\dot{e}(t) = \Lambda_1^{-1}(t) w(t-\tau) - Dd(t) - Ke(t) - q\hat{\rho} \operatorname{sign}(e). \tag{30}$$

Choose the following Lyapunov function:

$$V(t) = \frac{1}{2} e^T(t) \Lambda_1^{-1}(t) e(t) + \frac{1}{2}(\hat{\rho} - \rho)^2. \tag{31}$$

Taking the time derivative of $V(t)$ along the error system leads to

$$\begin{aligned} \dot{V}(t) &= e^T \Lambda_1^{-1} \dot{e} + \frac{1}{2} e^T (\dot{\Lambda_1^{-1}}) e + (\hat{\rho} - \rho)\dot{\hat{\rho}} \\ &= e^T\left[\Lambda_1^{-1} w(t-\tau) - Dd(t) - Ke - q\hat{p} \operatorname{sign}(e)\right] \\ &\quad + \frac{1}{2} e^T (\dot{\Lambda_1^{-1}}) e + (\hat{\rho} - \rho)\dot{\hat{\rho}} \\ &\le \left(\left\|\Lambda_1^{-1} w(t-\tau)\right\| + \|d(t)\|\right)\|e\| - q\rho\|e\| \\ &\quad - e^T(K - \gamma I) e \\ &\le (\beta l_1 + l_2)\|e\| - q\rho\|e\| - e^T(K - \gamma I) e \\ &= (\beta l_1 + l_2 - q\rho)\|e\| - e^T(K - \gamma I) e \\ &= -\eta\|e\| - e^T Q e < 0. \end{aligned} \tag{32}$$

Applying Lyapunov stability theorem, we can obtain

$$\lim_{t\to\infty} \|e\| = 0, \tag{33}$$

which means that systems (6) and (8) are MFPLS. Hence, the proof is completed. □

4.3. Case 3. More generally, if all the bounds l_1^i and $l_2^i (i = 1, 2, \ldots, 5)$ are unknown, let us denote

$$\begin{aligned} \rho &= (\rho_1, \ldots, \rho_5)^T, \\ \rho_i &= \beta l_1^i + l_2^i, \\ &\qquad (i = 1, 2, \ldots, 5) \end{aligned} \tag{34}$$

with the vector $\hat{\rho} = (\hat{\rho}_1, \ldots, \hat{\rho}_5)^T$ standing for the estimated value of ρ.

For this case, the adaptive control law and parameter update rule is chosen by

$$\begin{aligned} u(t) &= D\left[\Lambda_1^{-1}(t) Ae(t) + \Lambda_1^{-1}(t) h(x, y) + Ke(t)\right] \\ &\quad + D\left[q_1\hat{\rho}_1 \operatorname{sign}(e_1), \ldots, q_5\hat{\rho}_5 \operatorname{sign}(e_5)\right]^T, \end{aligned} \tag{35}$$

with

$$\dot{\hat{\rho}}_i = q_i\|e\|, \quad (i = 1, \ldots, 5), \tag{36}$$

where q_i is adjustable gain.

Theorem 8. *If there exist positive constants η_i and a symmetric positive definite matrix Q, such that the following LMIs hold:*

$$\begin{aligned} \beta l_1^i + l_2^i - \rho_i q_i &= -\eta_i, \quad (i = 1, \ldots, 5) \\ -K + \gamma I &= -Q, \end{aligned} \tag{37}$$

then systems (6) and (8) are MFPLS.

Proof. Substituting the controller (35) and the adaptive update law (36) into (20), we obtain

$$\begin{aligned} &\Lambda_1^{-1}(t)\dot{e}(t) \\ &\quad = \Lambda_1^{-1}(t) w(t-\tau) - Dd(t) - Ke(t) \\ &\qquad - \left[q_1\hat{\rho}_1 \operatorname{sign}(e_1), \ldots, q_5\hat{\rho}_5 \operatorname{sign}(e_5)\right]^T. \end{aligned} \tag{38}$$

The Lyapunov function is designed as

$$V(t) = \frac{1}{2} e^T \Lambda_1^{-1}(t) e + \frac{1}{2}(\hat{\rho} - \rho)^T(\hat{\rho} - \rho). \tag{39}$$

The time derivative of $V(t)$ is given by

$$\dot{V}(t) = e^T \Lambda_1^{-1} \dot{e} + \frac{1}{2} e^T (\dot{\Lambda_1^{-1}}) e + (\hat{\rho} - \rho)^T \dot{\hat{\rho}}. \tag{40}$$

Substituting (38) into (40), it follows that

$$\begin{aligned}\dot{V}(t) &= e^T\left\{\Lambda_1^{-1}w(t-\tau) - Dd(t)\right.\\ &\quad \left.-\left[q_1\widehat{\rho}_1\,\mathrm{sign}(e_1),\ldots,q_5\widehat{\rho}_5\,\mathrm{sign}(e_5)\right]^T\right\}\\ &\quad +\sum_{i=1}^{5}\left(q_i\widehat{\rho}_i|e_i| - q_i\rho_i|e_i|\right) - e^TKe + \frac{1}{2}e^T(\dot{\Lambda_1^{-1}})e\\ &\le \sum_{i=1}^{5}\left(\left(\beta {l_1}^i + {l_2}^i\right)|e_i| - q_i\widehat{\rho}_i|e_i|\right)\\ &\quad +\sum_{i=1}^{5}\left(q_i\widehat{\rho}_i|e_i| - q_i\rho_i|e_i|\right) - e^T(K-\gamma I)e\\ &= \sum_{i=1}^{5}\left(\left(\left(\beta {l_1}^i + {l_2}^i\right) - q_i\rho_i\right)|e_i|\right) - e^T(K-\gamma I)e\\ &= -\sum_{i=1}^{5}\eta_i|e_i| - e^TQe < 0.\end{aligned} \tag{41}$$

According to Lyapunov stability theorem, we can get

$$\lim_{t\to\infty}\|e\| = 0, \tag{42}$$

which means that the two systems (6) and (8) are MFPLS. Hence, the proof is completed. □

5. Simulation

In this section, two different memristor-based five-order chaotic circuit systems with unknown bounded disturbances are considered as the master system and the slave system, respectively, which can be described by

$$\begin{aligned}\dot{x}(t) &= Ax(t) + f(x(t)) + w(t),\\ \dot{y}(t) &= By(t) + g(y(t)) + d(t) + u(t),\end{aligned} \tag{43}$$

where

$$A = \begin{bmatrix} 10.8 & 0 & 9 & 0 & 0\\ 0 & 0 & -1 & 1 & 0\\ -30 & 30 & -30 & 0 & 0\\ 0 & -15 & 0 & 0 & 0\\ 1 & 0 & 0 & 0 & 0\end{bmatrix},$$

$$B = \begin{bmatrix} 9 & 0 & 10 & 0 & 0\\ 0 & 0 & -1 & 1 & 0\\ -28 & 28 & -33.6 & 0 & 0\\ 0 & -11 & 0 & 0 & 0\\ 1 & 0 & 0 & 0 & 0\end{bmatrix},$$

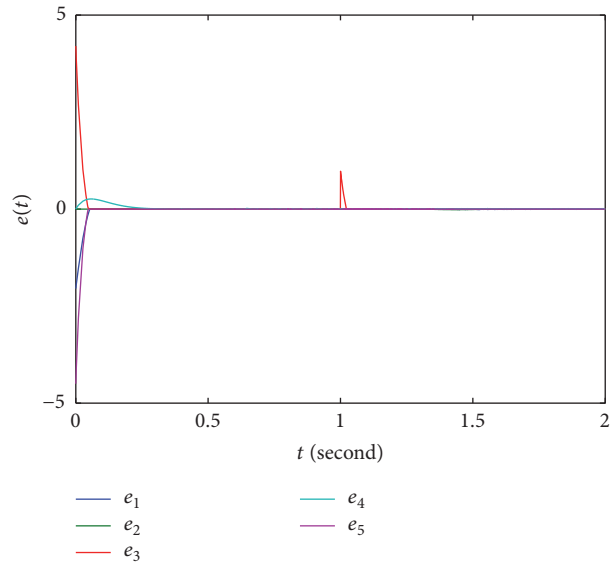

Figure 6: Time response of MFPLS error $e_i(t)$.

$$\begin{aligned}f(x(t)) &= \left[-10.8x_1{x_5}^2, 0, 0, 0, 0\right]^T,\\ g(y(t)) &= \left[-9y_1{y_5}^2, 0, 0, 0, 0\right]^T,\\ w(t) &= [\sin 10t, 0, 0, 0, 0]^T,\\ d(t) &= [0.1\sin t, 0.2\sin t, 0.5\cos 2t, 0.2\\ &\quad -0.1\sin t, 0.1 + 0.2\cos t]^T.\end{aligned} \tag{44}$$

The delay time is chosen as $\tau = 1$, and the scaling function matrix is given by

$$\begin{aligned}\Lambda(t) &= \mathrm{diag}\{3.1 + \cos t, 3.1 + \sin t, 4.2 - \sin t, 3.2\\ &\quad + \sin 5t, 4.5 - 0.5\sin t\},\end{aligned} \tag{45}$$

with the control gain

$$\begin{aligned}K &= \mathrm{diag}\{10, 10, 10, 10, 10\},\\ q_1 &= \cdots = q_5 = 10.\end{aligned} \tag{46}$$

The drive system is initialized with

$$x(0) = (0, 0, 1, 0, 0), \tag{47}$$

and the response system is started with

$$y(0) = (0.5, 0, -1, 0, 1). \tag{48}$$

Using the control method proposed in Theorem 8, the MFPLS error state trajectories are depicted in Figure 6, which illustrate that the error can quickly approach zero while the controller $u(t)$ is maintained in a reasonable range which is shown in Figure 7. At the meantime, as is shown in Figure 8, all of the unknown parameters can be tracked well under the parameter adaptive update law.

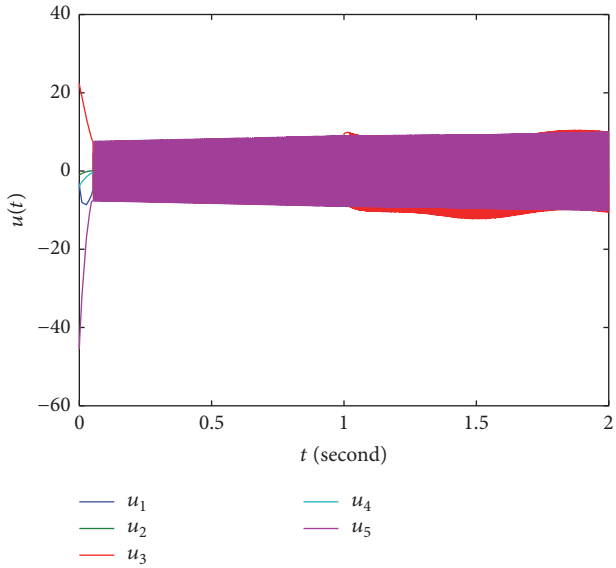

FIGURE 7: Time response of the input controller $u_i(t)$.

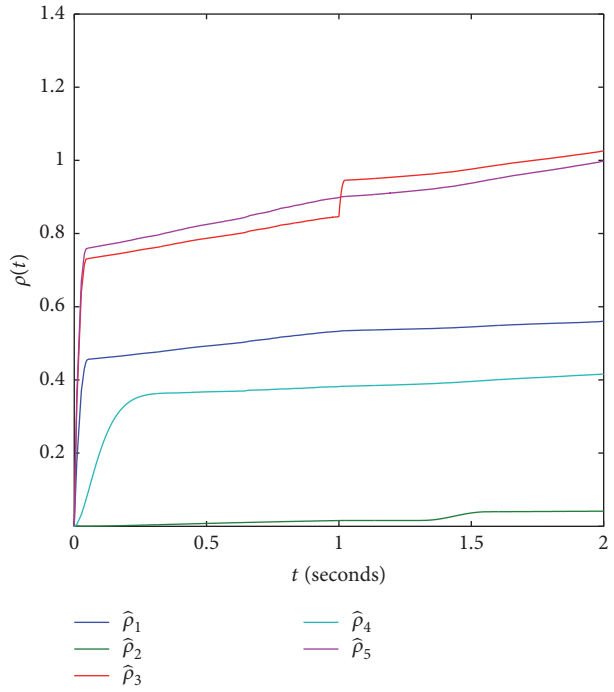

FIGURE 8: Time response of the estimated value of $\rho_i(t)$.

6. Conclusion

In this paper, the problem of MFPLS of memristor-based five-order chaotic circuit systems with unknown bounded disturbances has been addressed. Combining the LMI approach with Lyapunov stability theory, an adaptive control law is designed to make the states of two different memristor-based five-order chaotic circuit systems asymptotically synchronized up to a desired scaling function matrix and the unknown parameters can be estimated accurately. At the end of the paper, the corresponding numerical simulations have been given to verify the effectiveness of the proposed control techniques. The proposed method is also suitable for the MFPLS of other chaotic systems and has broad application in secure communication, image processing, and other fields.

Conflicts of Interest

The authors declare that there are no conflicts of interest regarding the publication of this paper.

Acknowledgments

This paper is supported by the National Natural Science Foundation of China (61373174 and 11301409), and thanks are due to all the references authors.

References

[1] L. O. Chua, "Memoristor-the missing circuit element," *IEEE Transactions on Circuit Theory*, vol. 18, pp. 507–519, 1971.

[2] D. B. Strukov, G. S. Snider, G. R. Stewart, and R. S. Williams, "The missing memoristor found," *Nature*, vol. 453, pp. 80–83, 2008.

[3] B. C. Bao and Z. Liu, "Transient chaos in smooth memristor oscillator," *Chinese Physics B*, vol. 19, Article ID 030510, 2010.

[4] M. Itoh and L. O. Chua, "Memristor oscillators," *International Journal of Bifurcation and Chaos*, vol. 18, no. 11, pp. 3183–3206, 2008.

[5] S. Benderli and T. A. Wey, "On SPICE macromodelling of TiO_2 memristors," *Electronics Letters*, vol. 45, no. 7, pp. 377–379, 2009.

[6] Y. N. Joglekar and S. J. Wolf, "The elusive memristor: properties of basic electrical circuits," *European Journal of Physics*, vol. 30, no. 4, pp. 661–675, 2009.

[7] B. Muthuswamy, "Memristor based chaotic circuits," *IETE Technical Review*, vol. 26, pp. 415–426, 2009.

[8] A. Wu, J. Zhang, and Z. Zeng, "Dynamic behaviors of a class of memristor-based Hopfield networks," *Physics Letters. A*, vol. 375, no. 15, pp. 1661–1665, 2011.

[9] S. Wen, Z. Zeng, and T. Huang, "Adaptive synchronization of memristor-based Chua's circuits," *Physics Letters A: General, Atomic and Solid State Physics*, vol. 376, no. 44, pp. 2775–2780, 2012.

[10] B. C. Bao, Q. H. Wang, and J. P. Xu, *Chin. Journal of Circuits and Systems*, vol. 16, pp. 66–69, 2011.

[11] L. M. Pecora and T. L. Carroll, "Synchronization in chaotic systems," *Physical Review Letters*, vol. 64, no. 8, pp. 821–824, 1990.

[12] H. J. Yu and Y. Z. Liu, "Chaotic synchronization based on stability criterion of linear systems," *Physics Letters A*, vol. 314, no. 4, pp. 292–298, 2003.

[13] C.-M. Kim, S. Rim, W.-H. Kye, J.-W. Ryu, and Y.-J. Park, "Anti-synchronization of chaotic oscillators," *Physics Letters A*, vol. 320, no. 1, pp. 39–46, 2003.

[14] E.-H. Park, M. A. Zaks, and J. Kurths, "Phase synchronization in the forced Lorenz system," *Physical Review E. Statistical, Nonlinear, and Soft Matter Physics*, vol. 60, no. 6, pp. 6627–6638, 1999.

[15] M. G. Rosenblum, A. S. Pikovsky, and J. Kurths, "From phase to lag synchronization in coupled chaotic oscillators," *Physical Review Letters*, vol. 78, no. 22, pp. 4193–4196, 1997.

[16] S. Boccaletti and D. L. Valladares, "Characterization of intermittent lag synchronization," *Physical Review E*, vol. 62, no. 5, pp. 7497–7500, 2000.

[17] S. S. Yang and C. K. Duan, "Generalized synchronization in chaotic systems," *Chaos, Solitons & Fractals*, vol. 9, no. 10, pp. 1703–1707, 1998.

[18] A. E. Hramov, A. A. Koronovskii, and O. I. Moskalenko, "Generalized synchronization onset," *Europhysics Letters*, vol. 72, no. 6, pp. 901–907, 2005.

[19] A. E. Hramov and A. A. Koronovskii, "An approach to chaotic synchronization," *Chaos*, vol. 14, no. 3, pp. 603–610, 2004.

[20] R. Mainieri and J. Rehacek, "Projective synchronization in three-dimensional chaotic systems," *Physical Review Letters*, vol. 82, no. 15, pp. 3042–3045, 1999.

[21] G. Wen and D. Xu, "Nonlinear observer control for full-state projective synchronization in chaotic continuous-time systems," *Chaos, Solitons and Fractals*, vol. 26, no. 1, pp. 71–77, 2005.

[22] N. Cai, Y. Jing, and S. Zhang, "Modified projective synchronization of chaotic systems with disturbances via active sliding mode control," *Communications in Nonlinear Science and Numerical Simulation*, vol. 15, no. 6, pp. 1613–1620, 2010.

[23] H. Du, Q. Zeng, and C. Wang, "Function projective synchronization of different chaotic systems with uncertain parameters," *Physics Letters, Section A: General, Atomic and Solid State Physics*, vol. 372, no. 33, pp. 5402–5410, 2008.

[24] H. Du, Q. Zeng, and C. Wang, "Modified function projective synchronization of chaotic system," *Chaos, Solitons and Fractals*, vol. 42, no. 4, pp. 2399–2404, 2009.

[25] K. S. Sudheer and M. Sabir, "Switched modified function projective synchronization of hyperchaotic Qi system with uncertain parameters," *Communications in Nonlinear Science and Numerical Simulation*, vol. 15, no. 12, pp. 4058–4064, 2010.

[26] K. S. Sudheer and M. Sabir, "Adaptive modified function projective synchronization of multiple time-delayed chaotic Rossler system," *Physics Letters, Section A: General, Atomic and Solid State Physics*, vol. 375, no. 8, pp. 1176–1178, 2011.

[27] H. Du, Q. Zeng, and N. Lü, "A general method for modified function projective lag synchronization in chaotic systems," *Physics Letters A*, vol. 374, no. 13-14, pp. 1493–1496, 2010.

Hindawi
Advances in Mathematical Physics
Volume 2017, Article ID 5210708, 10 pages
https://doi.org/10.1155/2017/5210708

Research Article

Numerical Simulations of the Square Lid Driven Cavity Flow of Bingham Fluids Using Nonconforming Finite Elements Coupled with a Direct Solver

R. Mahmood,[1] N. Kousar,[1] M. Yaqub,[2] and K. Jabeen[2]

[1]*Department of Mathematics, Air University, Islamabad, Pakistan*
[2]*Department of Mathematics, Riphah International University, Islamabad, Pakistan*

Correspondence should be addressed to N. Kousar; nabeela@mail.au.edu.pk

Received 20 December 2016; Accepted 28 February 2017; Published 20 March 2017

Academic Editor: Xin Yu

In this paper, numerical simulations are performed in a single and double lid driven square cavity to study the flow of a Bingham viscoplastic fluid. The governing equations are discretized with the help of finite element method in space and the nonconforming Stokes element $\widetilde{Q}_1/Q_0$ is utilized which gives 2nd-order accuracy for velocity and 1st-order accuracy for pressure. The discretized systems of nonlinear equations are treated by using the Newton method and the inner linear subproablems are solved by the direct solver UMFPACK. A qualitative comparison is done with the results reported in the literature. In addition to these comparisons, some new reference data for the kinetic energy is generated. All these implementations are done in the open source software package FEATFLOW which is a general purpose finite element based solver package for solving partial differential equations.

1. Introduction

The study of non-Newtonian fluids gained much importance in view of its extensive industrial and technological applications. Examples of such fluids include slurries, shampoo, paints, clay coating and suspensions, grease, cosmetic products, and body fluids. Among the non-Newtonian fluids, the viscoplastic fluids are those that exhibit a yield stress and thus combine the behavior of solids and liquids in different flow regimes. The idea of yield stress was first given by Shwedov [1]. Afterwards, Bingham [2] presented the flow shear diagram showing a linear relationship between stress and strain to explain the nature of plastic. A detailed review of viscoplastic behavior of materials is carried out by Barnes [3]. The behavior of such materials is like a solid (elastic or inelastic) below the certain value of shear stress and a liquid otherwise. This critical value of stress is termed as yield stress. Based on this fact the flow field of such materials is divided into unyielded (solid) and yielded (fluid) regions.

The simple version of the constitutive equation describing the viscoplasticity is that proposed by Bingham [2]

$$\begin{aligned} \dot{\boldsymbol{\gamma}} &= \mathbf{0}, \quad \tau \le \tau_y \\ \boldsymbol{\tau} &= \left(\frac{\tau_y}{\dot{\gamma}} + \mu\right)\dot{\boldsymbol{\gamma}}, \quad \tau > \tau_y, \end{aligned} \tag{1}$$

where τ_y is the yield stress, μ is the plastic viscosity, $\boldsymbol{\tau}$ is stress tensor, and $\dot{\boldsymbol{\gamma}}$ is the rate of strain tensor given by

$$\dot{\boldsymbol{\gamma}} \equiv \nabla \mathbf{u} + (\nabla \mathbf{u})^T. \tag{2}$$

$\mathbf{u}$ is the velocity vector, and superscript T denotes the transpose of the velocity-gradient tensor $\nabla \mathbf{u}$. The symbols τ and $\dot{\gamma}$ denote the magnitudes of the stress and rate-of strain tensors, respectively:

$$\begin{aligned} \tau &\equiv \left[\frac{1}{2}\boldsymbol{\tau} : \boldsymbol{\tau}\right]^{1/2}, \\ \dot{\gamma} &\equiv \left[\frac{1}{2}\dot{\boldsymbol{\gamma}} : \dot{\boldsymbol{\gamma}}\right]^{1/2}. \end{aligned} \tag{3}$$

Despite its simplicity, this model contains all the ingredients of viscoplastic materials, namely, a yield stress and a nonlinear variation of the effective viscosity. It is also observed while

dealing with Bingham Model; three different zones in the flow domain can be identified

(i) Shear zone $\|D\| \neq 0$.

(ii) Plug zone $\|D\| = 0$ and u = constant.

(iii) Dead zone $\|D\| = 0$ and $u = 0$.

All these regions are analyzed with great detail in the flow problems considered in this paper.

To date, a large number of research papers are devoted to simulate quantitatively and qualitatively these fluids; see, for example, [4–7]. Due to their yield stress property, the numerical solution of Bingham flows is difficult because the interface between the yielded and unyielded regions is a priori not known. To circumvent this difficulty, there are two approaches. One approach includes methods which approximate equation by a regularized constitutive equation, treating the whole material as fluid of variable viscosity and it is applicable throughout the domain. For such methods a very high value is assigned to the viscosity locally in unyielded regions as discussed by Bercovier and Engelman [7] and by Papanastasiou [8]. The Papanastasiou regularization introduces an exponential term to replace the discontinuous constitutive equation(1) by a single equation as

$$\boldsymbol{\tau} = \left[\frac{\tau_y}{\dot{\gamma}}\left\{1 - \exp\left(-m\dot{\gamma}\right)\right\} + \mu\right]\dot{\boldsymbol{\gamma}} \tag{4}$$

applicable throughout the material. Here m is a stress growth parameter, which should be "sufficiently" large so that the ideal Bingham behavior is approximated with satisfactory accuracy. In view of (4), the viscosity is given by

$$\eta = \frac{\tau_y}{\dot{\gamma}}\left\{1 - \exp\left(-m\dot{\gamma}\right)\right\} + \mu \tag{5}$$

that can be used over the entire flow domain.

The other approach includes methods which start by deriving variational inequalities and minimizing the rate of strain or maximizing the stress [9, 10]. A good review giving comparisons of numerical methods based on variational inequality approach is given in [11].

The rest of the paper is organized as follows. In Section 2, the mathematical formulations of the governing equations are presented. In Section 3, the numerical approach is presented. The numerical results for single and double lid driven cavity flow are presented by means of velocity, viscosity, and stream function plots in Section 4. Finally, Section 5 contains our concluding remarks.

2. Mathematical Formulation

The general form governing the incompressible behavior of these fluids can be written as

$$\begin{gathered}\nabla \cdot \mathbf{u} = 0 \\ \frac{\partial \mathbf{u}}{\partial t} + \mathbf{u} \cdot \nabla \mathbf{u} + \nabla p = \nabla \cdot \boldsymbol{\tau} + \mathbf{f},\end{gathered} \tag{6}$$

where $\mathbf{u}$ is the velocity vector, p is the pressure scaled by density ρ, $\mathbf{f}$ is the body forces, and $\boldsymbol{\tau}$ is the stress tensor which is responsible for categorizing different fluids. Assuming the flow as steady-state, two-dimensional isothermal, and incompressible and using nondimensional variables $\mathbf{u}^*$, p^*, and $\boldsymbol{\tau}^*$ and some reference velocity and reference length as U_{ref} and L_{ref}, respectively, the dimensionless form of the governing equations in the absence of body forces becomes

$$\begin{gathered}\nabla \cdot \mathbf{u}^* = 0 \\ \operatorname{Re} \mathbf{u}^* \cdot \nabla \mathbf{u}^* = -\nabla p^* + \nabla \cdot \boldsymbol{\tau}^*\end{gathered} \tag{7}$$

in which

$$\boldsymbol{\tau}^* = \left[\frac{\mathrm{Bn}}{\dot{\gamma}^*}\left\{1 - \exp\left(-M\dot{\gamma}^*\right)\right\} + 1\right]\dot{\boldsymbol{\gamma}}^*; \tag{8}$$

the nondimensionalization procedure introduces the following important dimensionless numbers: the Reynolds number

$$\mathrm{Re} \equiv \frac{\rho U_{\text{ref}} L_{\text{ref}}}{\mu} \tag{9}$$

and the Bingham number Bn

$$\mathrm{Bn} \equiv \frac{\tau_y L_{\text{ref}}}{\mu U_{\text{ref}}} \tag{10}$$

and M is the dimensionless stress growth parameter, given as

$$M \equiv \frac{m U_{\text{ref}}}{L_{\text{ref}}}. \tag{11}$$

The dimensionless viscosity is now given as

$$\eta^* = \frac{\mathrm{Bn}}{\dot{\gamma}^*}\left\{1 - \exp\left(-M\dot{\gamma}^*\right)\right\} + 1. \tag{12}$$

The higher the value of M is, the better (8) approximates the actual Bingham constitutive equation, $\boldsymbol{\tau} = [\mathrm{Bn}/\dot{\gamma} + 1]\dot{\boldsymbol{\gamma}}$ in the yielded regions of the flow field ($\tau > \mathrm{Bn}$), and the higher the apparent viscosity is in the unyielded regions, making them behave approximately as solid bodies. For practical reasons though, M must not be so high as to cause convergence problems to the numerical methods used to solve the above equations [4, 5].

3. Numerical Approach

Our numerical approach is based on the Galerkin weighted residual finite element method for the solution of the governing equations for the velocity and pressure. The equations are discretized with the help of finite element method using the nonconforming LBB stable Stokes element $\widetilde{Q}_1/Q_0$ of 2nd-order accuracy for velocity and 1st-order accuracy for pressure. This quadrilateral Stokes element is based on "rotated" bilinear shape functions having four local degrees of freedom (DOFs) for velocity component and one DOF for a piecewise constant pressure approximation (see [12, 13]

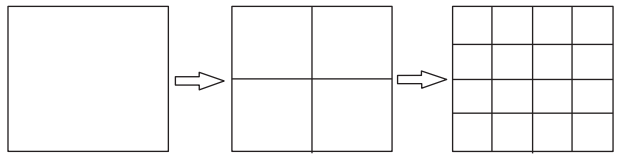

Figure 1: Sequence of grids on space mesh level: 1, 2, and 3 (from left to right).

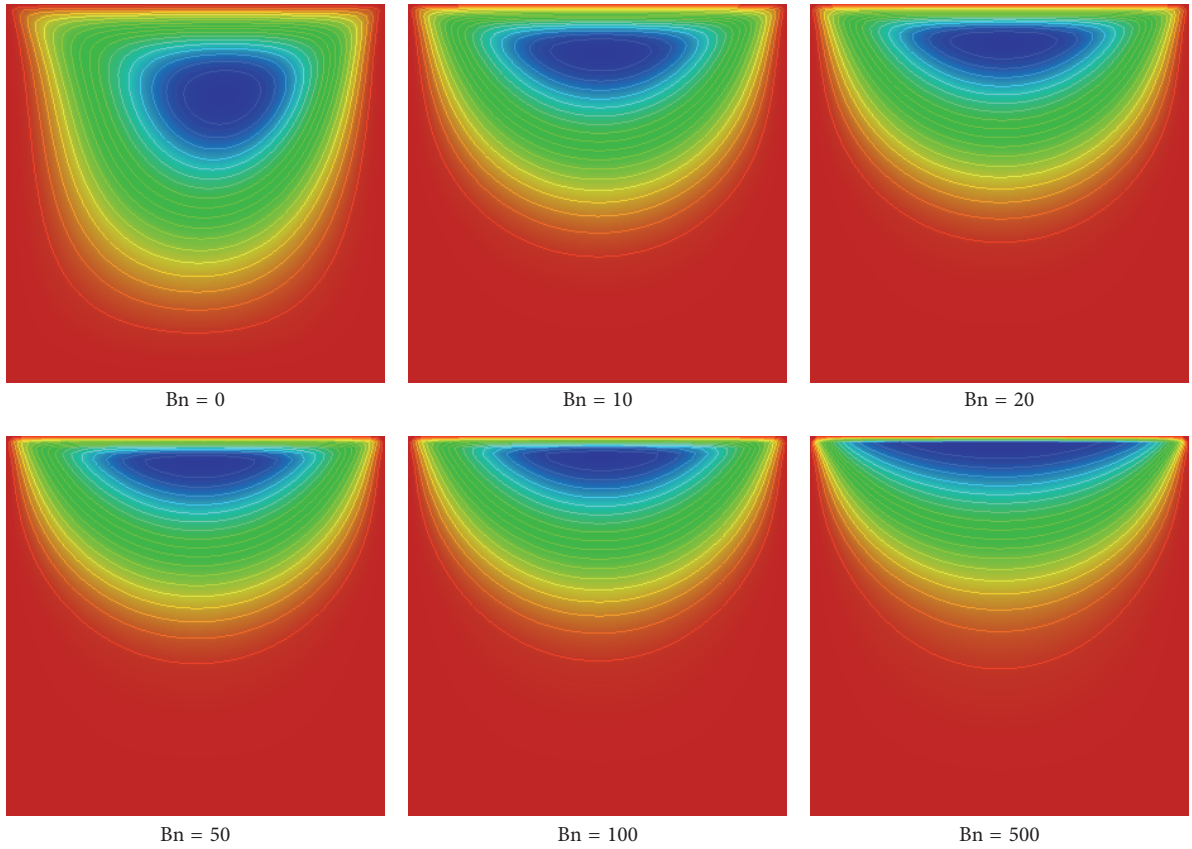

Figure 2: Stream function contours for different values of Bingham number Bn.

for details). The chosen nonconforming $\widetilde{Q}_1$ element requires additional stabilization for handling the deformation tensor formulation due to missing Korn's inequality [13]. To this end we employ the standard edge oriented stabilization [14, 15] in our simulations. Newton's method is applied to solve discrete nonlinear algebraic systems and the direct solver UMFPACK [16] is used as an inner linear solver. For grid refinement, we generate a sequence of grids by uniform refinement from a coarsest mesh. Starting from the mesh level $l = 1$, we generate grid of mesh level $l + 1$ by dividing each quadrilateral cell of grid level l into four new quadrilaterals connecting the mid points of opposite edges. Figure 1 shows the grid on level $l = 1, 2, 3$, respectively, and the mesh size on grid level l is $h = 2^{-l+1}$. The libraries of the open source software package FEATFLOW [17] are used in the simulations.

4. Results and Discussions

4.1. Lid Driven Cavity Flow. Using the methodology described in the previous section, the lid driven cavity problem is simulated. This important benchmark problem is considered by many researchers [5, 6, 18]. Consider a square cavity domain $\Omega = [0, 1]\times[0, 1]$, filled with a Bingham fluid which is set to motion by the upper lid of the cavity which moves with a uniform horizontal velocity U. The zero Dirichlet boundary conditions are given on all other walls. The velocity of the upper lid and length of the cavity are taken as U_{ref} and L_{ref}, respectively, appearing in (9)–(11). The mesh statistic for this benchmark problem is provided in Table 1.

Figure 2 depicts the stream function contour snapshots which indicate the effect of yield stress on the primary vortex. It can be visualized that the main vortex shrinks and approaching to the upper lid with an increase in the value

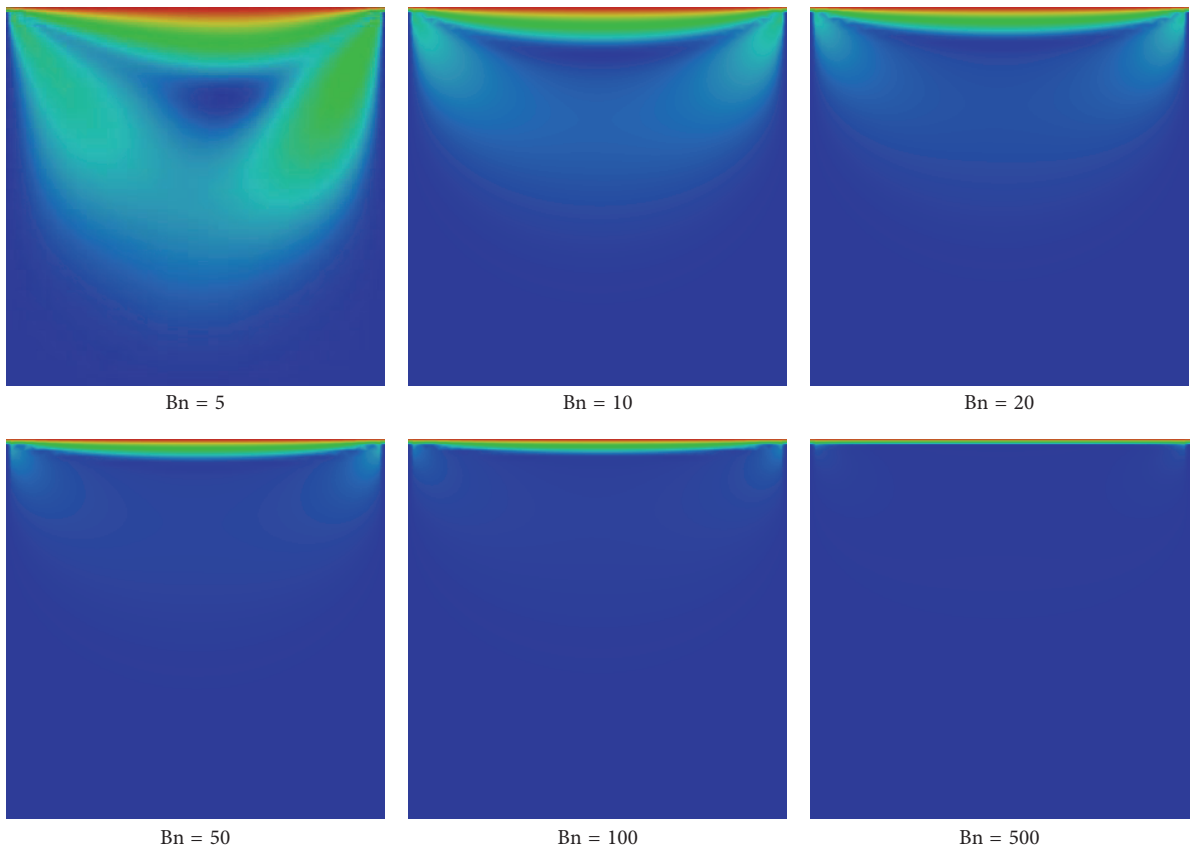

Figure 3: Velocity profiles for different values of Bingham numbers Bn.

Table 1: Mesh statistics at different refinement levels.

Refinement level	Number of elements	Degrees of freedom
3	16	96
4	64	352
5	256	1344
6	1024	5248
7	4096	20736

of Bingham number Bn indicating that as the yield limit increases, the dead region increases and it occupies more of the cavity and the shear region is moved to be close to the moving lid.

Effect of Bingham number Bn on velocity profile is shown in Figure 3 which also confirms that at higher values of Bingham number Bn the velocity is nonzero only in the region close to the upper moving lid. The numeric data for these snapshots of velocity along a vertical centerline is presented in Figure 4.

In Figure 4(a), we plot horizontal velocity along a vertical center line. The curve Bn $= 0$ corresponds to Newtonian case. For all other cases, the yielded and unyielded zones can be identified by decomposing each curve into two segments. The horizontal segment with $u = 0$ from $y = 0$ up to a certain height corresponds to unyielded zone due to increase in Bingham number. The velocity is extremely low throughout the lower portion of the cavity for higher Bn numbers. The other segment corresponds to the upper yielded zone. Such behavior is also observed in [4, 5] and is in good agreement concerning qualitative analysis. The vertical velocity components for all cases are plotted in Figure 4(b).

The dimensionless viscosity as a function of Bingham number Bn is displayed in Figure 5. The progressive growth of unyielded regions can be seen in the bottom of the cavity due to an increase in the plasticity effects produced at higher Bingham numbers Bn.

In addition to the local quantities like velocity, pressure, and viscosity we have also computed the kinetic energy in the cavity which is one of the global quantities of interest. Kinetic energy is defined by

$$E = \frac{1}{2}\int_{\Omega} \|u\|^2 \, dx. \tag{13}$$

To see the Newtonian results of this benchmark quantity we refer to the results of Bruneau and Saad [19]. Table 2 shows kinetic energy for the single lid driven cavity. The results are grid independent after level 7. It is also noted that an increase in Bingham number results in the decrease of kinetic energy due to the enhanced plasticity effect producing unyielded regions.

4.2. Double Lid Driven Cavity Flow. This section presents numerical results for double lid driven cavity flow. The

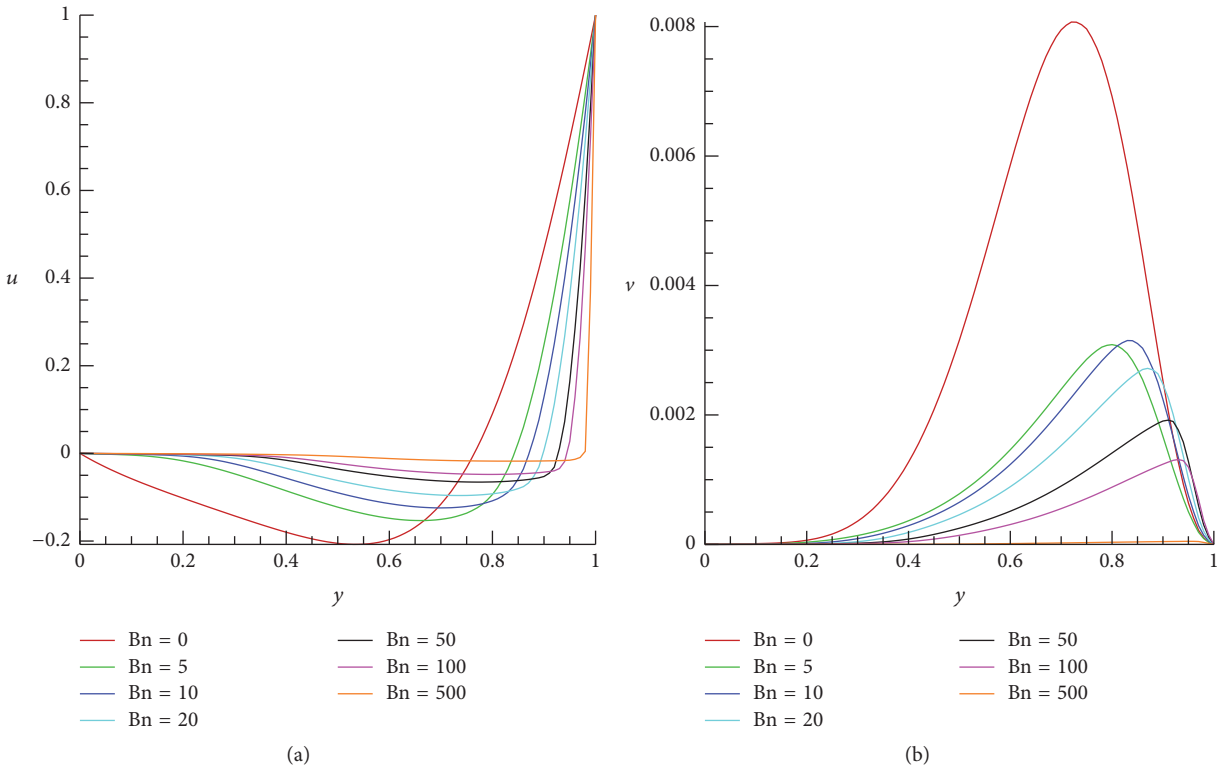

Figure 4: Vertical cut-lines at $x = 0.5$ for u velocity and v velocity for different values of Bingham number.

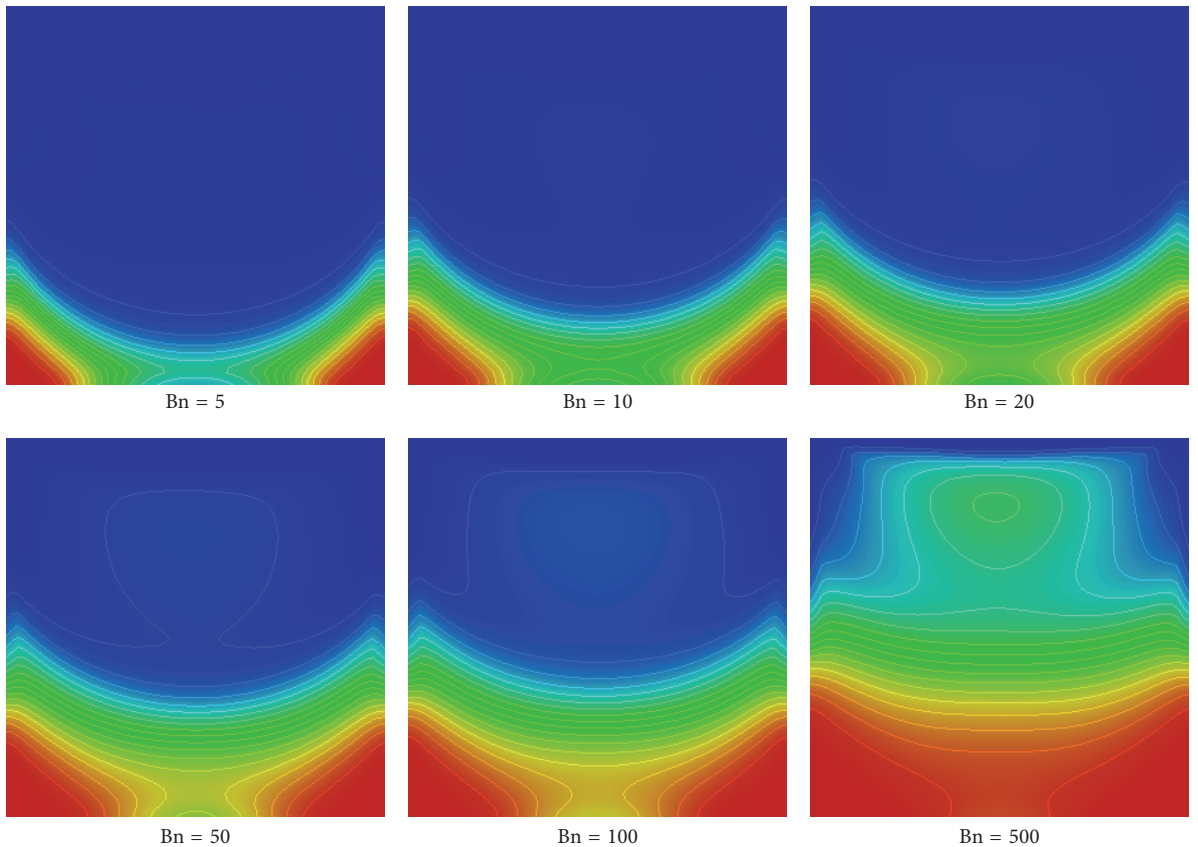

Figure 5: Viscosity contours for different values of Bingham numbers Bn.

Table 2: Kinetic energy at different refinement levels for different Bingham numbers.

Level	Bn = 0	Bn = 10	Bn = 20	Bn = 50	Bn = 100	Bn = 500
2	$5.285538E-02$	$4.285017E-02$	$4.277462E-02$	$4.275709E-02$	$4.275291E-02$	$4.274996E-02$
3	$3.841554E-02$	$2.417936E-02$	$2.257387E-02$	$2.206525E-02$	$2.202012E-02$	$2.198380E-02$
4	$3.480833E-02$	$1.750518E-02$	$1.536717E-02$	$1.401530E-02$	$1.342773E-02$	$1.284529E-02$
5	$3.365933E-02$	$1.579714E-02$	$1.218378E-02$	$8.984129E-03$	$8.415416E-03$	$8.015731E-03$
6	$3.359881E-02$	$1.540207E-02$	$1.152689E-02$	$7.721842E-03$	$5.705813E-03$	$4.536025E-03$
7	$3.358246E-02$	$1.529102E-02$	$1.137576E-02$	$7.450573E-03$	$5.383305E-03$	$2.441167E-03$

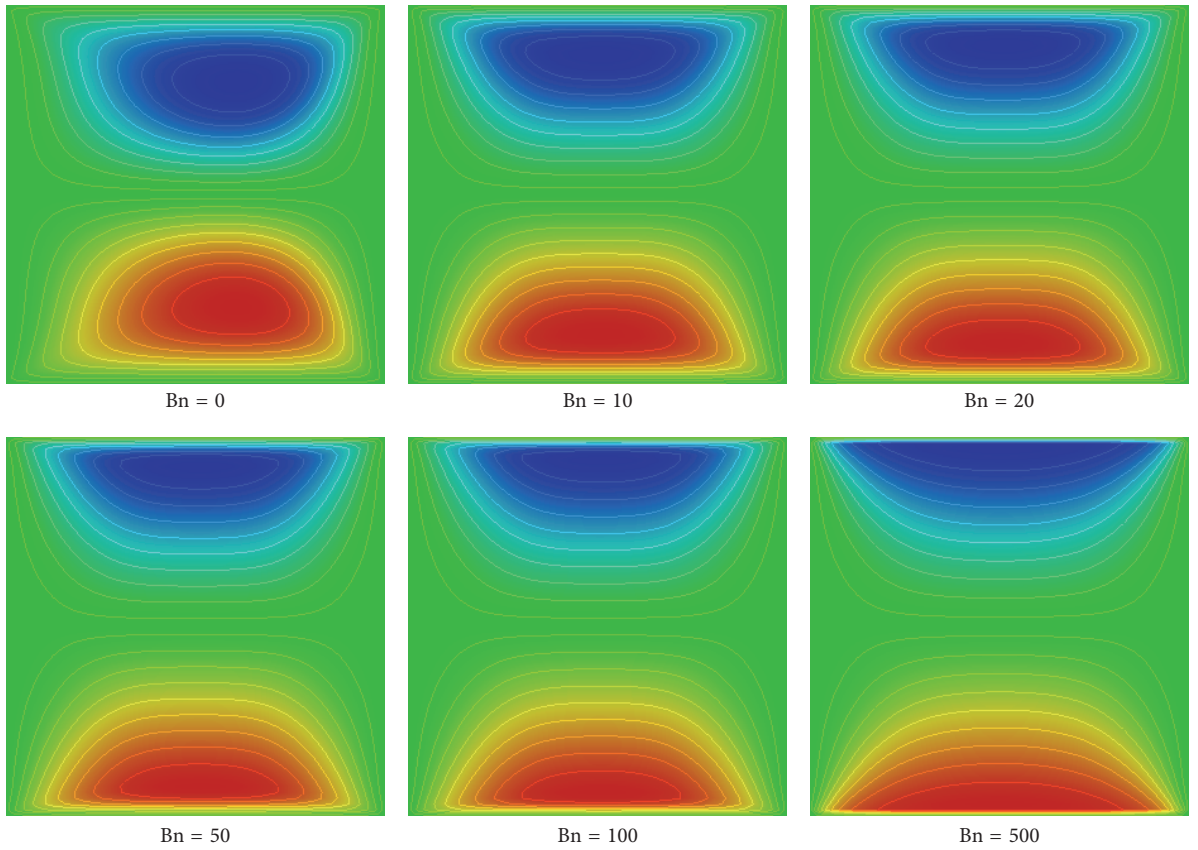

Figure 6: Stream function contours for double lid driven cavity at different values of Bingham number Bn.

geometry of the problem is again a unit square but now the upper and lower walls of the cavity are moving with the constant speed $u = U = 1$, $v = 0$ from left to right. Further studies on this problem can be found in [20–22].

In case of double lid driven cavity the two primary vertices are generated as shown in the stream function plots in Figure 6. These vertices move along to the upper and lower walls with increasing the Bingham numbers. The velocity profile snapshots are presented in Figure 7 and vertical cutlines along the center line at $x = 0.5$ in Figure 8.

Figure 8(a) reflects the evolution of horizontal velocity along the vertical centerline and in Figure 8(b) the plots for vertical velocity along the same centerline are given. The profiles for horizontal velocity become more and more flat in region near to the center showing that the motion of lids cannot penetrate towards the center of cavity due to the enhanced plasticity effects at higher Bn numbers.

In Figure 9, the viscosity contours are presented to show the effect of Bingham numbers on the viscosity. In contrast to the single lid driven cavity, we now see the creation of unyielded regions in the center of the cavity due to distance from the source of motion. These snapshots also reveal the presence of side eddies in the center attached to the stationary walls. An increase in the Bn number limits the yielded region closer to the moving lids.

The kinetic energy is tabulated in Table 3. The convergence of the results can be seen by moving up to down in each column. After level 7 the results are the same which shows grid independency. It is also noted that an increase in Bingham number results in the decrease of kinetic energy due to the expansion in the dead zones.

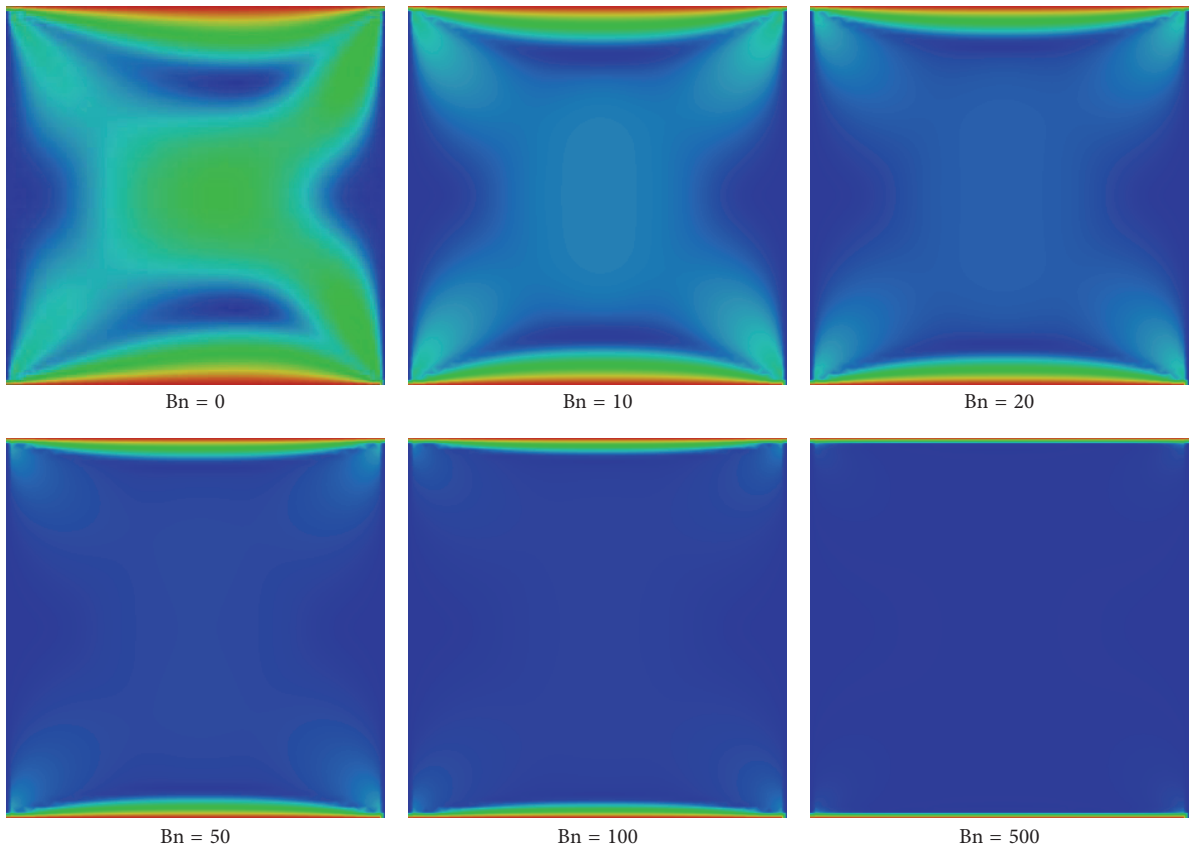

Figure 7: Velocity profiles for double lid driven cavity at different values of Bingham number Bn.

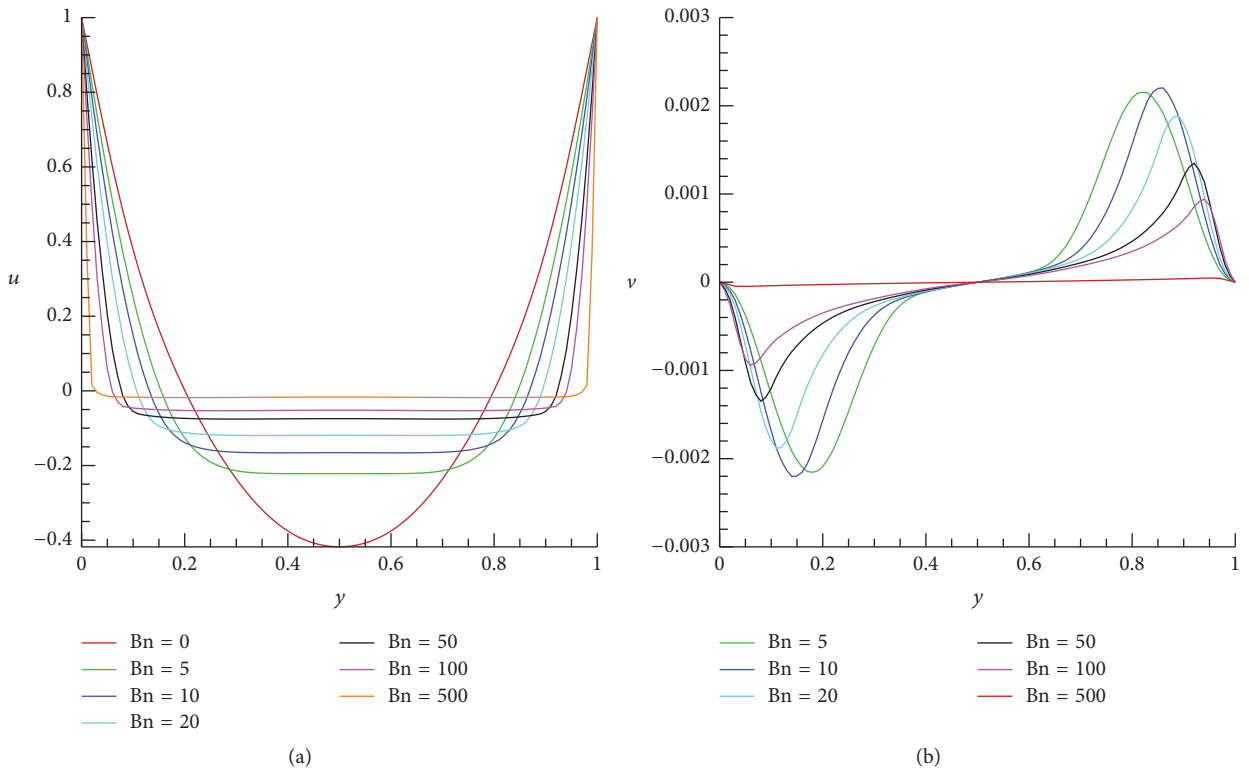

Figure 8: Vertical cut-lines at $x = 0.5$ for u velocity and v velocity for different values of Bingham number.

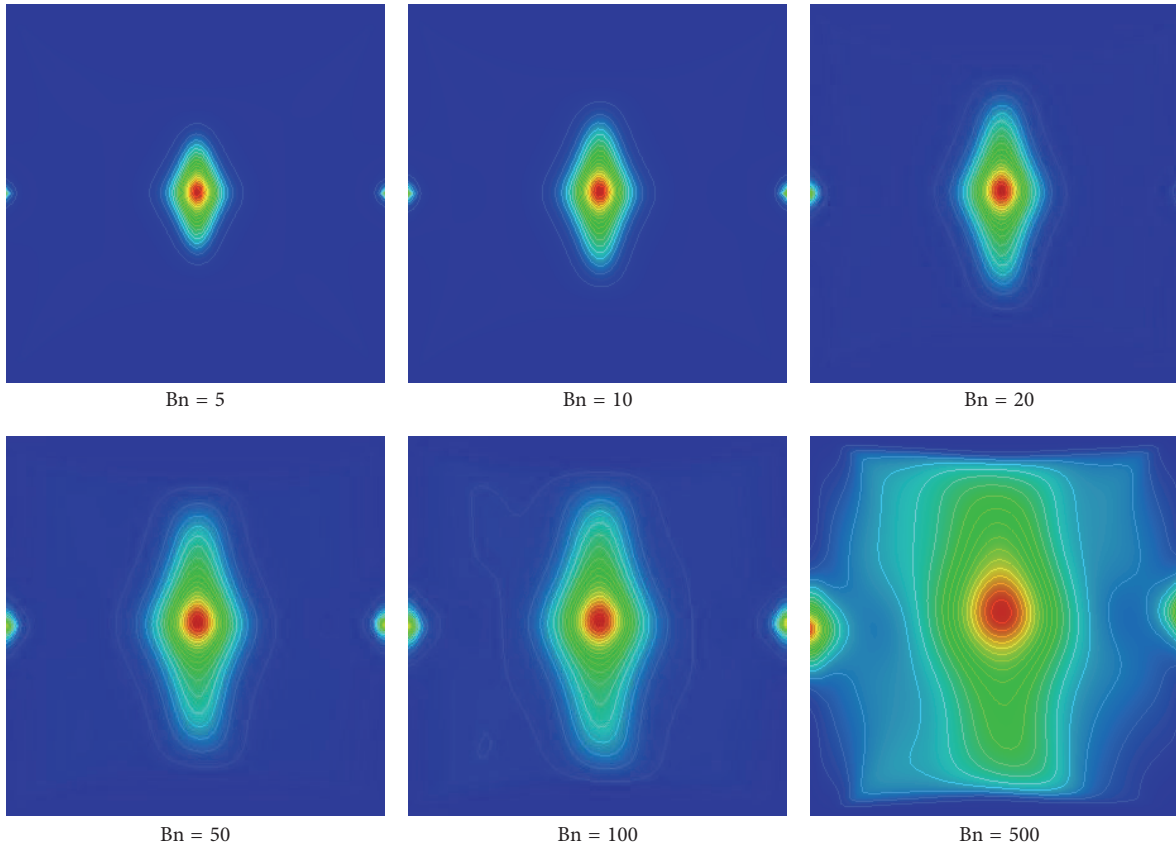

Figure 9: Viscosity contours for double lid driven cavity at different values of Bingham number Bn.

Table 3: Kinetic energy for double lid driven cavity at different Bingham numbers Bn.

Level	Bn = 0	Bn = 10	Bn = 20	Bn = 50	Bn = 100	Bn = 500
2	$9.422139E-02$	$8.561376E-02$	$8.560186E-02$	$8.559770E-02$	$8.559568E-02$	$8.559568E-02$
3	$7.213333E-02$	$5.170203E-02$	$4.909028E-02$	$4.675238E-02$	$4.580014E-02$	$4.505332E-02$
4	$6.531628E-02$	$3.784316E-02$	$3.265451E-02$	$2.988453E-02$	$2.879644E-02$	$2.773203E-02$
5	$6.357059E-02$	$3.438146E-02$	$2.649637E-02$	$1.926139E-02$	$1.748698E-02$	$1.667230E-02$
6	$6.314135E-02$	$3.359117E-02$	$2.531207E-02$	$1.686371E-02$	$1.266649E-02$	$9.243272E-03$
7	$6.302763E-02$	$3.337230E-02$	$2.502079E-02$	$1.632972E-02$	$1.171277E-02$	$5.139763E-03$

The x-component of the velocity (u) is tabulated at the chosen points in Tables 4 and 5 for selected values of Bingham numbers to show the influence of the parameter M and refinement level on the solution. The present choices of M do not have a significant effect on the solution. It is also worth mentioning that the coarser grid level is a larger source of error than the smallness of M. This observation is also noted in [4].

We close this section by showing the dependence of the maximum nonlinear iterations on Bingham number in Table 6. An increase in the number of nonlinear iterations (# NL) is observed with an increase in the non-Newtonian dimensionless parameter Bn.

5. Conclusions

This work presents an insight into the behavior of numerical simulations for Bingham viscoplastic fluid flows in benchmark configurations. The implementations are done via finite element methods in the framework of a monolithic approach. The results obtained for the Bingham Models are able to describe the viscosity function accurately for the configurations of single and double lid driven cavity flows. Results have been obtained for Bingham numbers in the range of 0–500 and are presented by means of velocity, viscosity, and stream function plots. Beside these local quantities, the tabular data for the kinetic energy in the cavity is also generated. It is also noted that number of iterations for

Table 4: Values of the x-component of the velocity along the vertical center line for Bn = 10.

y	$M = 100$			$M = 200$			$M = 400$		
	Level 2	Level 5	Level 7	Level 2	Level 5	Level 7	Level 2	Level 5	Level 7
0.00	0.000000	0.000000	0.000000	0.000000	0.000000	0.000000	0.000000	0.000000	0.000000
0.05	−0.013251	−0.0010289	−0.0010116	−0.013028	−0.0005843	−0.0005535	−0.012885	−0.0003243	−0.0002947
0.10	−0.026501	−0.0020266	−0.0019455	−0.026055	−0.0011590	−0.0010759	−0.025771	−0.0006451	−0.0005783
0.15	−0.039752	−0.0033673	−0.0032162	−0.039083	−0.0020363	−0.0018627	−0.038656	−0.0012314	−0.0010568
0.20	−0.053003	−0.0059797	−0.0057659	−0.052111	−0.0044433	−0.0041157	−0.051542	−0.0035617	−0.0033013
0.25	−0.066254	−0.0113470	−0.0122350	−0.065138	−0.0105230	−0.0112940	−0.064427	−0.0103240	−0.0109420
0.30	−0.079504	−0.0237110	−0.0240660	−0.078166	−0.0234810	−0.0238490	−0.077312	−0.0234520	−0.0238150
0.35	−0.092755	−0.0389840	−0.0395680	−0.091194	−0.0391150	−0.0397450	−0.090198	−0.0392330	−0.0398780
0.40	−0.106010	−0.0557910	−0.0567500	−0.104220	−0.0561110	−0.0571140	−0.103080	−0.0563100	−0.0573210
0.45	−0.119260	−0.0728560	−0.0739620	−0.117250	−0.0732490	−0.0743940	−0.115970	−0.0734660	−0.0746230
0.50	−0.132510	−0.0889990	−0.0899600	−0.130280	−0.0894080	−0.0904000	−0.128850	−0.0896280	−0.0906270
0.55	−0.019256	−0.1023800	−0.1037600	−0.017249	−0.1027800	−0.1041800	−0.015968	−0.102980	−0.1044000
0.60	0.093994	−0.1128200	−0.1146200	0.095779	−0.113200	−0.1150200	0.096917	−0.113400	−0.1152300
0.65	0.207240	−0.1197600	−0.1218100	0.208810	−0.120130	−0.122200	0.209800	−0.120320	−0.1224000
0.70	0.320500	−0.1225400	−0.1244700	0.321830	−0.122910	−0.124860	0.322690	−0.123100	−0.1250500
0.75	0.433750	−0.1203500	−0.1212400	0.434860	−0.120740	−0.121650	0.435570	−0.120950	−0.1218600
0.80	0.547000	−0.1078300	−0.1082700	0.547890	−0.108310	−0.108750	0.548460	−0.108550	−0.1089800
0.85	0.660250	−0.0405360	−0.0578980	0.660920	−0.041105	−0.058487	0.661340	−0.041380	−0.0587660
0.90	0.773500	0.1480600	0.1287800	0.773940	0.147500	0.128200	0.774230	0.147230	0.1279300
0.95	0.886750	0.4934200	0.4848400	0.886970	0.493040	0.484440	0.887110	0.492860	0.4842500
0.97	0.932050	0.6960500	0.6724000	0.932180	0.695820	0.672130	0.932270	0.695720	0.6720100
0.98	0.954700	0.7973700	0.7766300	0.954790	0.797220	0.776440	0.954850	0.797140	0.7763500
0.99	0.977350	0.8986800	0.8862300	0.977390	0.898610	0.886130	0.977420	0.898570	0.8860800
1.00	1.000000	1.000000	1.000000	1.000000	1.000000	1.000000	1.000000	1.000000	1.000000

Table 5: Values of the x-component of the velocity along the vertical center line for Bn = 100.

y	$M = 100$			$M = 200$			$M = 400$		
	Level 2	Level 5	Level 7	Level 2	Level 5	Level 7	Level 2	Level 5	Level 7
0.00	0.00000	0.00000	0.00000	0.000000	0.000000	0.0000000	0.0000000	0.0000000	0.0000000
0.05	−0.01276	−0.0004015	−0.00040	−0.012632	−0.0002256	−0.0002200	−0.012567	−0.0001239	−0.0001164
0.10	−0.02552	−0.0007936	−0.00078	−0.025265	−0.0004461	−0.0004284	−0.025134	−0.0002451	−0.0002267
0.15	−0.03828	−0.0012214	−0.00120	−0.037897	−0.0006895	−0.0006578	−0.037701	−0.0003803	−0.0003491
0.20	−0.05104	−0.0017347	−0.00170	−0.050530	−0.0009877	−0.0009424	−0.050268	−0.0005491	−0.0005036
0.25	−0.06379	−0.0023872	−0.00238	−0.063162	−0.0013773	−0.0013403	−0.062835	−0.0007745	−0.0007269
0.30	−0.07655	−0.0034638	−0.00341	−0.075795	−0.0020713	−0.0020025	−0.075402	−0.0012027	−0.0011303
0.35	−0.08931	−0.0054841	−0.00524	−0.088427	−0.0037121	−0.0034697	−0.087969	−0.0026646	−0.0023786
0.40	−0.10207	−0.0100510	−0.00902	−0.101060	−0.0088888	−0.0077991	−0.100540	−0.0083352	−0.0073288
0.45	−0.11483	−0.0176790	−0.01558	−0.113690	−0.0178200	−0.0156190	−0.113100	−0.0181320	−0.0158290
0.50	−0.12759	−0.0277930	−0.02323	−0.126320	−0.028356	−0.0237720	−0.125670	−0.0287160	−0.0241450
0.55	−0.01483	−0.0369840	−0.03037	−0.013692	−0.037644	−0.0309950	−0.013103	−0.0380350	−0.0313710
0.60	0.09792	−0.0448550	−0.03652	0.098941	−0.045507	−0.0371250	0.099464	−0.0458770	−0.0374760
0.65	0.21069	−0.0512220	−0.04149	0.211570	−0.051834	−0.0420640	0.212030	−0.0521730	−0.0423870
0.70	0.32345	−0.0559550	−0.04517	0.324210	−0.056536	−0.0457100	0.324600	−0.0568550	−0.0460110
0.75	0.43621	−0.0589840	−0.04743	0.436840	−0.059545	−0.0479510	0.437170	−0.0598500	−0.0482400
0.80	0.54896	−0.0595660	−0.04808	0.549470	−0.060137	−0.0486150	0.549730	−0.0604460	−0.0489040
0.85	0.66172	−0.0579270	−0.04688	0.662100	−0.058539	−0.0474550	0.662300	−0.0588640	−0.0477610
0.90	0.77448	−0.0594230	−0.04293	0.774740	−0.060227	−0.0436020	0.774870	−0.0606400	−0.0439500
0.95	0.88724	0.1492400	0.02744	0.887370	0.148400	0.0257970	0.887430	0.1479700	0.0250270
0.97	0.93234	0.4895400	0.26696	0.932420	0.489040	0.2649700	0.932460	0.4887800	0.2640800
0.98	0.95490	0.6597000	0.47095	0.954950	0.659360	0.4693400	0.954970	0.6591900	0.4686200
0.99	0.97745	0.8298500	0.71853	0.977470	0.829680	0.7176000	0.977490	0.8295900	0.7171900
1.00	1.000000	1.000000	1.000000	1.000000	1.000000	1.000000	1.000000	1.000000	1.000000

Table 6: The number of nonlinear iterations (level 7) required to reduce nonlinear defect up to 10^{-6}.

Bn	# NL
10	63
20	72
50	78
100	83
500	88

Newton's solver increased at larger values of Bingham number due to enhanced nonlinearity.

Conflicts of Interest

The authors declare that there are no conflicts of interest regarding the publication of this paper.

References

[1] F. N. Shwedov, "La Rigidite de liquides," *Rapport Congr. Intern. Phys. Paris*, vol. 1, pp. 478–486, 1900.

[2] E. C. Bingham, *Fluidity and Plasticity*, McGraw-Hill, New York, NY, USA, 1922.

[3] H. A. Barnes, "The yield stress—a review or '$\pi\alpha\nu\tau\alpha\rho\epsilon\iota$'—everything flows?" *Journal of Non-Newtonian Fluid Mechanics*, vol. 81, no. 1-2, pp. 133–178, 1999.

[4] A. Syrakos, G. C. Georgiou, and A. N. Alexandrou, "Solution of the square lid-driven cavity flow of a Bingham plastic using the finite volume method," *Journal of Non-Newtonian Fluid Mechanics*, vol. 195, pp. 19–31, 2013.

[5] A. Syrakos, G. C. Georgiou, and A. N. Alexandrou, "Performance of the finite volume method in solving regularised Bingham flows: inertia effects in the lid-driven cavity flow," *Journal of Non-Newtonian Fluid Mechanics*, vol. 208-209, pp. 88–107, 2014.

[6] E. Mitsoulis and T. Zisis, "Flow of Bingham plastics in a lid-driven square cavity," *Journal of Non-Newtonian Fluid Mechanics*, vol. 101, no. 1-3, pp. 173–180, 2001.

[7] M. Bercovier and M. Engelman, "A finite element method for incompressible non-Newtonian flows," *Journal of Computational Physics*, vol. 36, no. 3, pp. 313–326, 1980.

[8] T. C. Papanastasiou, "Flows of materials with yield," *Journal of Rheology*, vol. 31, no. 5, pp. 385–404, 1987.

[9] M. Fortin and R. Glowinski, *Augmented Lagrangian Methods: Applications to the Numerical Solution of Boundary-Value Problems*, North-Holland, Amsterdam, The Netherlands, 1983.

[10] R. Glowinski, *Numerical Methods for Nonlinear Variational Problems*, Springer, New York, NY, USA, 1984.

[11] E. J. Dean, R. Glowinski, and G. Guidoboni, "On the numerical simulation of Bingham visco-plastic flow: old and new results," *Journal of Non-Newtonian Fluid Mechanics*, vol. 142, no. 1–3, pp. 36–62, 2007.

[12] S. Turek and R. Rannacher, "A simple nonconforming quadrilinear stokes element," *Numerical Methods for Partial Differential Equations*, vol. 8, no. 2, pp. 97–111, 1992.

[13] P. Knobloch, "On Korn's inequality for non-conforming finite elements," *Technisshe Mechanik*, vol. 20, pp. 205–214, 2000.

[14] S. Turek, A. Ouazzi, and R. Schmachtel, "Multigrid methods for stabilized nonconforming finite elements for incompressible flow involving the deformation tensor formulation," *Journal of Numerical Mathematics*, vol. 10, no. 3, pp. 235–248, 2002.

[15] S. Turek and A. Ouazzi, "Unified edge-oriented stabilization of nonconforming FEM for incompressible flow problems: numerical investigations," *Journal of Numerical Mathematics*, vol. 15, no. 4, pp. 299–322, 2007.

[16] T. A. Davis, "Algorithm 832: UMFPACK V4.3—an unsymmetric-pattern multifrontal method," *ACM Transactions on Mathematical Software*, vol. 30, no. 2, pp. 196–199, 2004.

[17] S. Turek, *FEATFLOW Finite Element Software for the Incompressible Navier-Stokes Equations: User Manual*, Release 1.2, University of Dortmund, 2000, http://www.featflow.de.

[18] U. Ghia, K. N. Ghia, and C. T. Shin, "High-Re solutions for incompressible flow using the Navier-Stokes equations and a multigrid method," *Journal of Computational Physics*, vol. 48, no. 3, pp. 387–411, 1982.

[19] C.-H. Bruneau and M. Saad, "The 2D lid-driven cavity problem revisited," *Computers and Fluids*, vol. 35, no. 3, pp. 326–348, 2006.

[20] J. Zhang, "Bifurcation of bingham streamline topologies in rectangular double-lid-driven cavities," *Journal of Applied Mathematics and Physics*, vol. 2, no. 12, pp. 1069–1072, 2014.

[21] G. R. Kefayati, "FDLBM simulation of magnetic field effect on non-Newtonian blood flow in a cavity driven by the motion of two facing lids," *Powder Technology*, vol. 253, pp. 325–337, 2014.

[22] S. Arun and A. Satheesh, "Analysis of flow behaviour in a two sided lid driven cavity using lattice Boltzmann technique," *Alexandria Engineering Journal*, vol. 54, no. 4, pp. 795–806, 2015.

Hindawi
Advances in Mathematical Physics
Volume 2017, Article ID 6976205, 7 pages
https://doi.org/10.1155/2017/6976205

Research Article

The Convergence Ball and Error Analysis of the Relaxed Secant Method

Rongfei Lin,[1] Qingbiao Wu,[2] Minhong Chen,[3] and Lu Liu[2]

[1]*Department of Mathematics, Taizhou University, Linhai, Zhejiang 317000, China*
[2]*Department of Mathematics, Zhejiang University, Hangzhou, Zhejiang 310027, China*
[3]*Department of Mathematics, Zhejiang Sci-Tech University, Hangzhou, Zhejiang 310012, China*

Correspondence should be addressed to Qingbiao Wu; qbwu@zju.edu.cn

Received 4 November 2016; Revised 17 January 2017; Accepted 12 February 2017; Published 8 March 2017

Academic Editor: Kaliyaperumal Nakkeeran

A relaxed secant method is proposed. Radius estimate of the convergence ball of the relaxed secant method is attained for the nonlinear equation systems with Lipschitz continuous divided differences of first order. The error estimate is also established with matched convergence order. From the radius and error estimate, the relation between the radius and the speed of convergence is discussed with parameter. At last, some numerical examples are given.

1. Introduction

Many scientific problems can be concluded to the form of nonlinear systems. Finding the solutions of nonlinear systems is widely required in both mathematical physics and nonlinear dynamical systems. In this paper, we will establish the convergence ball and error analysis of the relaxed secant method of nonlinear systems. Consider

$$F(x) = 0, \tag{1}$$

where F is a nonlinear operator defined on a convex subset Ω of a Banach space X with values in another Banach space Y. When F is nonlinear, iterative methods are generally adopted to solve the system:

$$x_{n+1} = \Psi(x_n), \quad x_0 \text{ is given.} \tag{2}$$

The most widely used iterative method is Newton's method which can be described as

$$x_{n+1} = x_n - F(x_n)^{-1} F(x_n), \quad x_0 \text{ is given.} \tag{3}$$

This method and Newton-like methods have been studied well by many authors (see [1–12]).

Newton's method requires that F is differentiable. Thus, when F is nondifferentiable, Newton method cannot be applied on it. We have to turn to other methods that do not need to evaluate derivatives. In their algorithms, instead of derivatives, divided differences are always used. The classical method of this type is the secant method.

Let $\Phi(X, Y)$ denote the space of the bounded linear maps from X to Y. If the following equality holds,

$$[X, Y; F](x - y) = F(x) - F(y), \tag{4}$$

then, we call the operator $[X, Y; F] \in \Phi(X, Y)$, at the points x and y $(x \neq y)$, a divided difference of order one of the nonlinear operator F.

By the above definition, secant method can be generalized to Banach spaces, it is described as the following scheme:

$$x_{n+1} = x_n - [x_{n-1}, x_n; F]^{-1} F(x_n), \quad (n > 0) \ \ x_0, x_{-1} \in \Omega. \tag{5}$$

An interesting issue here is to estimate the radius of the convergence ball of an iterative method. Suppose x_* is a solution of the nonlinear system (1). Denote with $B(x_*, r) \subset X$ an open ball with center x_* and radius r. The open ball $B(x_*, r) \subset X$ is called a convergence ball of an iteration, if the sequence generated by the iterative method converges with any initial value in the ball. Under the assumption that the

nonlinear operator F has Fréchet derivatives satisfying the Hölder condition,

$$\begin{aligned}&\left\|F'(x_*)^{-1}\left([x,y;F]-F'(z)\right)\right\|\\&\quad\leqslant K\left(\|x-z\|^p+\|y-z\|^p\right),\\&\qquad\qquad\forall x,y,z\in\Omega \text{ for some } K>0.\end{aligned}\tag{6}$$

Ren and Wu [13] have given the radius of the convergence ball which is $r_p=\sqrt[p]{(1+p)/K(1+2p)}$.

The convergence ball, the semilocal convergence of secant method, and secant-like method have been studied by many other authors (see [13–18]). In this paper, similar to the relaxed Newton's method in [7], we considered the relaxed secant method which can be written as the following form:

$$x_{n+1}=x_n-\lambda\left[x_{n-1},x_n;F\right]^{-1}F(x_n),\quad x_0,x_{-1}\in\Omega;\tag{7}$$

here, $\lambda\in(0,2)$ is called the relaxed parameter. When $\lambda=1$, it will be the normal secant method.

In this paper, we will study the convergence ball of (7) under the assumption that the nonlinear operator F has Fréchet derivatives satisfying the following Lipschitz condition:

$$\begin{aligned}&\left\|F'(x_*)^{-1}\left([x,y;F]-[v,w;F]\right)\right\|\\&\quad\leqslant K\left(\|x-v\|+\|y-w\|\right),\\&\qquad\qquad\forall x,y,v,w\in\Omega \text{ for some } K>0.\end{aligned}\tag{8}$$

Under the Lipschitz condition, the radius r_{λ_1} of the relaxed method is proved to be $\lambda/4K$ when $0<\lambda\leqslant 1$; and the radius r_{λ_2} of the relaxed method is proved to be $(2-\lambda)/4K\lambda$ when $1<\lambda<2$. The error estimate is also given.

2. Convergence Ball

Theorem 1. *Suppose $F(x_*)=0$, where the nonlinear operator F is Fréchet differentiable on Ω, $F'(x_*)^{-1}$ exists, the Lipschitz condition (8) holds, and $0<\lambda<2$. Denote*

$$\begin{aligned}r_{\lambda_1}&=\frac{\lambda}{4K},\\r_{\lambda_2}&=\frac{(2-\lambda)}{4K\lambda}.\end{aligned}\tag{9}$$

When $0<\lambda\leqslant 1$, starting from any two initial points x_0,x_{-1} in ball $B(x_*,r_{\lambda_1})$, the sequence $\{x_n\}$ generated by the relaxed secant method (7) converges to the solution x_*. When $1<\lambda<2$, the sequence $\{x_n\}$ generated by the relaxed secant method (7) converges to the solution x_*, with any two initial points x_0,x_{-1} in ball $B(x_*,r_{\lambda_2})$. x_* is the unique solution in ball $B(x_*,1/K)$, that is bigger than ball $B(x_*,r_{\lambda_1})$ and ball $B(x_*,r_{\lambda_2})$. Moreover, we have the following error estimate:

$$\begin{aligned}&\|x_n-x_*\|\leqslant\left(\frac{2-\lambda}{1-2K\theta}-1\right)^n,\quad \text{if } 0<\lambda\leqslant 1,\\&\|x_n-x_*\|\leqslant\left(\frac{(4\lambda-2)K\theta+\lambda-1}{1-2K\theta}\right)^n,\quad \text{if } 1<\lambda<2,\end{aligned}\tag{10}$$

where $\theta=\max\{\|x_0-x_*\|,\|x_{-1}-x_*\|\}$.

Proof. We will prove the above theorem by induction. Firstly, when $0<\lambda<2$, by Lipschitz condition, it is easy to get

$$\begin{aligned}&\left\|I-F'(x_*)^{-1}\left[x_{-1},x_0;F\right]\right\|\\&\quad=\left\|F'(x_*)^{-1}\left(F'(x_*)-\left[x_{-1},x_0;F\right]\right)\right\|\\&\quad\leqslant K\left(\|x_{-1}-x_*\|+\|x_0-x_*\|\right)<1.\end{aligned}\tag{11}$$

By Banach lemma, we can know $[x_{-1},x_0;F]$ is invertible. Since x_1 is well defined and

$$\begin{aligned}&\left\|\left(F'(x_*)^{-1}\left[x_{-1},x_0;F\right]\right)^{-1}\right\|\\&\quad\leqslant\frac{1}{1-K\left(\|x_{-1}-x_*\|+\|x_0-x_*\|\right)},\end{aligned}\tag{12}$$

we can conduct

$$\begin{aligned}&\left\|F'(x_*)^{-1}\left[x_{-1},x_0;F\right]\right\|\\&\quad=\left\|F'(x_*)^{-1}\left(\left[x_{-1},x_0;F\right]-F'(x_*)+F'(x_*)\right)\right\|\\&\quad\leqslant K\left(\|x_{-1}-x_*\|+\|x_0-x_*\|\right)+1.\end{aligned}\tag{13}$$

Then, we can give the estimate of $\|x_1-x_*\|$ when $0<\lambda\leqslant 1$. From $F(x_*)=0$, we have

$$\begin{aligned}\|x_1-x_*\|&=\left\|x_0-x_*-\lambda\left[x_{-1},x_0;F\right]^{-1}F(x_0)\right\|\\&=\Big\|\left(F'(x_*)^{-1}\left[x_{-1},x_0;F\right]\right)^{-1}F'(x_*)^{-1}\\&\quad\cdot\left(\left[x_{-1},x_0;F\right](x_0-x_*)-\lambda\left(F(x_0)-F(x_*)\right)\right)\Big\|\\&\leqslant\left\|\left(F'(x_*)^{-1}\left[x_{-1},x_0;F\right]\right)^{-1}\right\|\Big\|F'(x_*)^{-1}\\&\quad\cdot\left(\left[x_{-1},x_0;F\right](x_0-x_*)\right)\\&\quad-\lambda\int_0^1F'\left(tx_0+(1-t)x_*\right)\mathrm{d}t\,(x_0-x_*)\Big\|\\&\leqslant\left\|\left(F'(x_*)^{-1}\left[x_{-1},x_0;F\right]\right)^{-1}\right\|\|x_0-x_*\|\\&\quad\cdot\Bigg(\lambda\left\|F'(x_*)^{-1}\right.\\&\quad\cdot\left.\left(\left[x_{-1},x_0;F\right]-\int_0^1F'\left(tx_0+(1-t)x_*\right)\mathrm{d}t\right)\right\|+(1\\&\quad-\lambda)\left\|F'(x_*)^{-1}\left[x_{-1},x_0;F\right]\right\|\Bigg).\end{aligned}\tag{14}$$

Using Lipschitz condition with (12) and (13), we have

$$\begin{aligned}\|x_1 - x_*\| &\leqslant \frac{r_{\lambda_1}}{1-2Kr_{\lambda_1}}\left(\int_0^1 \lambda K\left(\|x_{-1} - tx_0 - (1-t)x_*\|\right.\right.\\ &\quad + \|x_0 - tx_0 - (1-t)x_*\|)\,dt + (1-\lambda)\left(K\left(\|x_{-1} - x_*\|\right.\right.\\ &\quad \left.\left.+ \|x_0 + x_*\|\right) + 1\right)\Bigg)\\ &= \frac{r_{\lambda_1}}{1-2Kr_{\lambda_1}}\left(\int_0^1 \lambda K\left(\|t(x_{-1} - x_0) + (1-t)(x_{-1} - x_*)\|\right.\right.\\ &\quad + (1-t)\|x_0 - x_*\|)\,dt + (1-\lambda)\left(K\left(\|x_{-1} - x_*\|\right.\right.\\ &\quad \left.\left.+ \|x_0 + x_*\|\right) + 1\right)\Bigg).\end{aligned} \tag{15}$$

Obviously, we have

$$\|x_{-1} - x_0\| \leqslant \|x_0 - x_*\| + \|x_{-1} - x_*\|. \tag{16}$$

From $x_{-1}, x_0 \in B(x_*, r_{\lambda_1})$, together with (15), (16), and $r_{\lambda_1} = \lambda/4K$, we have

$$\begin{aligned}&\|x_1 - x_*\|\\ &\quad < \frac{r_{\lambda_1}}{1-2Kr_{\lambda_1}}\left(2K\lambda r_{\lambda_1} + (1-\lambda)\left(2Kr_{\lambda_1} + 1\right)\right)\\ &\quad = r_{\lambda_1}.\end{aligned} \tag{17}$$

This means $x_1 \in B(x_*, r_{\lambda_1})$.

Similar to the procession above, when $1 < \lambda < 2$, we can get that

$$\begin{aligned}\|x_1 - x_*\| &= \left\|x_0 - x_* - \lambda\left[x_{-1}, x_0; F\right]^{-1} F(x_0)\right\|\\ &\leqslant \left\|\left(F'(x_*)^{-1}\left[x_{-1}, x_0; F\right]\right)^{-1}\right\| \|x_0 - x_*\|\\ &\quad \cdot \left(\lambda\left\|F'(x_*)\right.\right.\\ &\quad \left.\left.\cdot\left(\left[x_{-1}, x_0; F\right] - \int_0^1 F'(tx_0 + (1-t)x_*)\,dt\right)\right\| + (\lambda\right.\\ &\quad \left.- 1)\left\|F'(x_*)^{-1}\left[x_{-1}, x_0; F\right]\right\|\right).\end{aligned} \tag{18}$$

By (13) and (18) and Lipschitz condition we can get

$$\begin{aligned}\|x_1 - x_*\| &\leq \frac{r_{\lambda_2}}{1-2Kr_{\lambda_2}}\left(\int_0^1 \lambda K\left(\|x_{-1} - tx_0 - (1-t)x_*\|\right.\right.\\ &\quad + \|x_0 - tx_0 - (1-t)x_*\|)\,dt + (\lambda-1)\left(K\left(\|x_{-1} - x_*\|\right.\right.\\ &\quad \left.\left.+ \|x_0 - x_*\|\right) + 1\right)\Bigg)\\ &= \frac{r_{\lambda_2}}{1-2Kr_{\lambda_2}}\left(\int_0^1 \lambda K\left(\|t(x_{-1} - x_0) + (1-t)(x_{-1} - x_*)\|\right.\right.\\ &\quad + (1-t)\|x_0 - x_*\|)\,dt + (\lambda-1)\left(K\left(\|x_{-1} - x_*\|\right.\right.\\ &\quad \left.\left.+ \|x_0 - x_*\|\right) + 1\right)\Bigg) \leqslant \frac{r_{\lambda_2}}{1-2K\lambda_2}\left(2K\lambda r_{\lambda_2} + (\lambda-1)\left(2Kr_{\lambda_2}\right.\right.\\ &\quad \left.\left.+ 1\right)\right).\end{aligned} \tag{19}$$

For $x_{-1}, x_0 \in B(x_*, r_{\lambda_2})$,

$$\begin{aligned}&\|x_1 - x_*\|\\ &\quad \leqslant \frac{Kr_{\lambda_2}}{1-2K\lambda_2}\left(2K\lambda r_{\lambda_2} + (\lambda-1)\left(2Kr_{\lambda_2} + 1\right)\right)\\ &\quad = r_{\lambda_2}.\end{aligned} \tag{20}$$

This means that $x_1 \in B(x_*, r_{\lambda_2})$ when $1 < \lambda < 2$.

Now, suppose $\{x_k\}$ $(k = 1, 2, \ldots, n)$ is well defined, $x_k \in B(x_*, r_{\lambda_1})$, when $0 < \lambda \leqslant 1$; $\{x_k\}$ $(k = 1, 2, \ldots, n)$ is well defined, $x_k \in B(x_*, r_{\lambda_2})$, when $1 < \lambda < 2$. Similar to the argumentation about x_{-1} and x_0, when $0 < \lambda < 2$,

$$\begin{aligned}&\left\|I - F'(x_*)^{-1}\left[x_{n-1}, x_n; F\right]\right\|\\ &\quad \leqslant K\left(\|x_{n-1} - x_*\| + \|x_n - x_*\|\right) < 1.\end{aligned} \tag{21}$$

By the Banach lemma, it is obviously known that $[x_{n-1}, x_n; F]$ is invertible. Hence, x_{n+1} is well defined. We also get

$$\begin{aligned}&\left\|\left(F'(x_*)^{-1}\left[x_{n-1}, x_n; F\right]\right)^{-1}\right\|\\ &\quad \leq \frac{1}{1 - K\left(\|x_{n-1} - x_*\| + \|x_n - x_*\|\right)}.\end{aligned} \tag{22}$$

When $0 < \lambda \leqslant 1$,

$$\begin{aligned}\|x_{n+1} - x_*\| &\leqslant \frac{\|x_n - x_*\|}{1 - K\left(\|x_n - x_*\| + \|x_{n-1} - x_*\|\right)}\\ &\quad \times \left(\lambda K\int_0^1 \left(\|t(x_{n-1} - x_n) + (1-t)(x_{n-1} - x_*)\|\right.\right.\\ &\quad \left.\left.+ (1-t)\|x_n - x_*\|\right)dt + (1-\lambda)\right.\\ &\quad \left.\cdot\left(K\left(\|x_{n-1} - x_*\| + \|x_n - x_*\|\right) + 1\right)\right).\end{aligned} \tag{23}$$

And when $1 < \lambda < 2$, we have

$$\begin{aligned}\|x_{n+1} - x_*\| &\leqslant \frac{\|x_n - x_*\|}{1 - K\left(\|x_n - x_*\| + \|x_{n-1} - x_*\|\right)}\\ &\quad \times \left(\lambda K\int_0^1 \left(\|t(x_{n-1} - x_n) + (1-t)(x_{n-1} - x_*)\|\right.\right.\\ &\quad \left.\left.+ (1-t)\|x_n - x_*\|\right)dt + (\lambda-1)\right.\\ &\quad \left.\cdot\left(K\left(\|x_{n-1} - x_*\| + \|x_n - x_*\|\right) + 1\right)\right).\end{aligned} \tag{24}$$

By the assumptions that $x_{n-1}, x_n \in B(x_*, r_{\lambda_1})$ when $0 < \lambda \leqslant 1$ and $x_{n-1}, x_n \in B(x_*, r_{\lambda_2})$ when $1 < \lambda < 2$, similar to the discussions about x_1, it is known that $x_{n+1} \in B(x_*, r_{\lambda_1})$ when $0 < \lambda \leqslant 1$ and $x_{n+1} \in B(x_*, r_{\lambda_2})$ when $1 < \lambda < 2$.

Therefore, starting from any two initial points x_{-1}, x_0, x_n, the sequence $\{x_n\}$, generated by the relaxed secant method, is well defined when $0 < \lambda \leqslant 1$, $x_n \in B(x_*, r_{\lambda_1})$, and when $1 < \lambda < 2$, $x_n \in B(x_*, r_{\lambda_2})$. It means that the following holds:

$$\|x_n - x_*\| < r_{\lambda_1}, \quad (0 < \lambda \leqslant 1,\ n \geq -1), \tag{25}$$

$$\|x_n - x_*\| < r_{\lambda_2}, \quad (1 < \lambda < 2,\ n \geq -1). \tag{26}$$

Denote

$$\theta_n = \|x_n - x_*\|, \tag{27}$$

$$\theta = \max\{\theta_0, \theta_{-1}\}. \tag{28}$$

When $0 < \lambda \leqslant 1$, from (14) we can get

$$\begin{aligned}\|x_{n+1} - x_*\| &\leqslant \frac{\|x_n - x_*\|}{1 - K(\|x_n - x_*\| + \|x_{n-1} - x_*\|)} \\ &\times (\lambda K(\|x_n - x_*\| + \|x_{n-1} - x_*\|) \\ &+ (1-\lambda)(K(\|x_n - x_*\| + \|x_{n-1} - x_*\|) + 1)).\end{aligned} \tag{29}$$

Then, by (27), we have

$$\begin{aligned}\theta_{n+1} &\leqslant \frac{\theta_n}{1 - K(\theta_n + \theta_{n-1})}(\lambda K(\theta_n + \theta_{n-1}) \\ &+ (1-\lambda)(K(\theta_n + \theta_{n-1}) + 1)).\end{aligned} \tag{30}$$

By (23), we know $\theta_n < r_{\lambda_1}$ for all n. Then by (29) and (30), we can induct

$$\theta_{n+1} < \theta_n < \theta_{n-1} < \cdots < \theta_1 < \theta. \tag{31}$$

Then we can see

$$\begin{aligned}\theta_{n+1} &\leqslant \frac{\theta_n}{1 - K(\theta_n + \theta_{n-1})}(K(\theta_n + \theta_{n-1}) + 1 - \lambda) \\ &= \theta_n \frac{K(\theta_n + \theta_{n-1}) - 1 + 2 - \lambda}{1 - K(\theta_n + \theta_{n-1})} \\ &= \theta_n \left(\frac{2-\lambda}{1 - K(\theta_n + \theta_{n-1})} - 1\right) \\ &< \theta_n \left(\frac{2-\lambda}{1 - 2K\theta} - 1\right) < \theta \left(\frac{2-\lambda}{1-2K\theta} - 1\right)^{n+1}.\end{aligned} \tag{32}$$

Obviously, $0 < (2-\lambda)/(1-2K\theta) - 1 < 1$. The sequence $\{x_n\}$ converges to the exact solution x_* from (32).

When $1 < \lambda < 2$, from (24),

$$\begin{aligned}\|x_{n+1} - x_*\| &\leqslant \frac{\|x_n - x_*\|}{1 - K(\|x_n - x_*\| + \|x_{n-1} - x_*\|)} \\ &\times \left(\lambda K \int_0^1 (\|t(x_{n-1} - x_n) + (1-t)(x_{n-1} - x_*)\| \right. \\ &+ (1-t)\|x_n - x_*\|)\,dt + (\lambda - 1) \\ &\left. \cdot (K(\|x_{n-1} - x_*\| + \|x_n - x_*\|) + 1)\right).\end{aligned} \tag{33}$$

Then, by (27), we have

$$\begin{aligned}\theta_{n+1} &\leqslant \frac{\theta_n}{1 - K(\theta_n + \theta_{n-1})}(\lambda K(\theta_n + \theta_{n-1}) \\ &+ (\lambda - 1)(K(\theta_n + \theta_{n-1}) + 1)) \\ &= \frac{\theta_n}{1 - K(\theta_n + \theta_{n-1})}((2\lambda - 1)K(\theta_n + \theta_{n-1}) + \lambda \\ &- 1).\end{aligned} \tag{34}$$

By (24) and (26), we know $\theta_n < r_{\lambda_2}$ for all n. Then by (26) and (34), when $1 < \lambda < 2$, we can induct

$$\theta_{n+1} < \theta_n < \theta_{n-1} < \cdots < \theta_1 < \theta. \tag{35}$$

So we have

$$\begin{aligned}\theta_{n+1} &\leqslant \theta_n \left(\frac{2(2\lambda - 1)K\theta - 1}{1 - 2K\theta}\right) \\ &< \theta \left(\frac{(4\lambda - 2)K\theta + \lambda - 1}{1 - 2K\theta}\right)^{n+1}.\end{aligned} \tag{36}$$

It is easy to proof that $0 < ((4\lambda - 2)K\theta + \lambda - 1)/(1 - 2K\theta) < 1$. So the sequence $\{x_n\}$ converges to the solution x_*.

Now we show the uniqueness. Assume that there exists another solution $y_* \in B(x_*, 1/K)$. Consider the operator $A = [x_*, y_*; F]$. Because $A[y_* - x_*] = F(y_*) - F(x_*)$, we can get $y_* = x_*$ if the operator A is invertible. From (4), we get

$$\begin{aligned}\left\|I - F'(x_*)^{-1} A\right\| &= \left\|F'(x_*)^{-1}\left(F'(x_*) - A\right)\right\| \\ &\leqslant K\|y_* - x_*\| < 1.\end{aligned} \tag{37}$$

So, we can tell that operator A is invertible by Banach lemma. From the definition of r_λ and (9), it is easy to verify that ball $B(x_*, 1/K)$ is bigger than ball $B(x_*, r_{\lambda_1})$ and ball $B(x_*, r_{\lambda_2})$. Proof completes. □

Remark 2. When $\lambda = 1$, the radius of the convergence ball is $1/4K$. We denote $r_1 = 1/4K$. From (9), we know when $0 < \lambda < 1$, $r_{\lambda_1} < r_1$, and when $1 < \lambda < 2$, $r_{\lambda_2} < r_1$. So we have the biggest convergence ball when $\lambda = 1$.

3. Numerical Examples

In this section, we applied the convergence ball result given in Section 2 to solve some numerical problems.

Table 1: Relaxed secant method with different λ.

λ	n	x_n	$\|x_n - x_*\|$	CPU time
0.9	1	1.0315	0.0315	0.000877
	2	1.0057	0.0057	
	3	1.0006	6.4804×10^{-4}	
	4	1.0001	6.6458×10^{-5}	
	5	1.0000	6.6652×10^{-6}	
	6	1.0000	6.6672×10^{-7}	
1	1	1.0128	0.0128	0.000864
	2	1.0012	0.0012	
	3	1.0000	7.3141×10^{-6}	
	4	1.0000	4.2172×10^{-7}	
1.1	1	0.9940	0.006	0.000095
	2	1.0000	1.6176×10^{-6}	
	3	1.0000	1.6708×10^{-7}	

Example 1. Let us consider

$$F(x) = x^2 - 1, \quad x \in [0, 2]. \tag{38}$$

Then $F'(x) = 2x$. $F(x) = 0$ has a root $x_* = 1$ and $F'(x_*) = 2$. It is easy to obtain

$$\begin{aligned} &\left\| F'(x_*)^{-1} ([x, y; F] - [u, v; F]) \right\| \\ &\leqslant \frac{1}{2} \left(\|x - u\| + \|y - v\| \right). \end{aligned} \tag{39}$$

Set $\lambda_1 = 0.9$, $\lambda_2 = 1$, $\lambda_3 = 1.1$. Then the radius of the convergence balls is $r_1 = 9/20$, $r_2 = 1/2$, $r_3 = 9/22$. Choose the initial points $x_{-1} = 1.15$, $x_0 = 1.2$ and they are in the convergence ball of the relaxed secant method. From Table 1, we can see the sequence $\{x_n\}$ converges to x_* with different λ.

As we know, when $\lambda = 1$, the relaxed secant method reduces to normal secant method. From Table 1, we can see that relaxed secant method in the case of $\lambda = 1.1$ outperforms the normal secant method in the sense of iteration number and CPU time.

Example 2. Let us consider the following numerical problem which has been studied in [3, 17, 18]:

$$\begin{aligned} F(x) &= e^x - 1, \\ D &= [-1, 1]. \end{aligned} \tag{40}$$

Then $F'(x) = e^x$, $x_* = 0$, and $F'(x_*) = 1$.

Similar to the process in [17], we know $|e^x - e^y| \leqslant e|x - y|$. Then,

$$\left| \int_0^1 \left(e^{tx+(1-t)y} - e^{tu+(1-t)v} \right) dt \right| \leqslant \frac{e}{2} \left(|x - u| + |y - v| \right). \tag{41}$$

For $[x, y; F] = \int_0^1 e^{tx+(1-t)y} dt$ and $\|F'(x_*)^{-1}([x, y; F] - [u, v; F])\| \leqslant \|[x, y; F] - [u, v; F]\|$, we can get

$$\begin{aligned} &\left\| F'(x_*)^{-1} ([x, y; F] - [u, v; F]) \right\| \\ &\leqslant \frac{e}{2} \left(\|x - u\| + \|y - v\| \right). \end{aligned} \tag{42}$$

Table 2: Relaxed secant method with different λ.

λ	n	x_n	$\|x_n - x_*\|$	CPU time
0.999	1	0.0038	0.0038	0.000094
	2	1.8245×10^{-4}	1.8245×10^{-4}	
	3	1.6290×10^{-7}	1.6290×10^{-7}	
1	1	0.0039	0.0039	0.000094
	2	1.9078×10^{-4}	1.9078×10^{-4}	
	3	3.7011×10^{-4}	3.7011×10^{-4}	
1.01	1	0.0048	0.0048	0.000108
	2	2.8301×10^{-4}	2.8301×10^{-4}	
	3	3.4788×10^{-6}	3.4788×10^{-6}	
	4	3.4931×10^{-8}	3.4931×10^{-8}	

So $K = e/2$ in this problem. Set $\lambda_1 = 0.999$, $\lambda_2 = 1$, $\lambda_3 = 1.01$. Then, the radius of the convergence balls is $r_1 = 999/2000e$, $r_2 = 1/2e$, $r_3 = 99/202e$. Set the initial points $x_{-1} = 0.08$, $x_0 = 0.1$, and they are in the convergence ball of the relaxed secant method. From Table 2, we can see the sequence $\{x_n\}$ converges to the solution x_*.

From Table 2, we can know that the relaxed scant method ($\lambda = 0.999$) performs the same as the normal secant method in the sense of the iteration number and CPU time, while the solution gotten by the relaxed secant method is closer to the exact solution than that by the normal secant method.

Example 3. Let us consider the nonlinear system:

$$\begin{aligned} 2x_1 - \frac{1}{9}x_1^2 - x_2 &= 0, \\ -x_1 + 2x_2 - \frac{1}{9}x_2^2 &= 0. \end{aligned} \tag{43}$$

It comes from the following nonlinear boundary value problem of second order:

$$\begin{aligned} x'' + x^2 &= 0, \\ x(0) = x(1) &= 0, \end{aligned} \tag{44}$$

which has been studied by many authors [5, 13, 16].

Now, define the operator $F : R^2 \to R^2$ such that $F = (F_1, F_2)$. We take $F_1(x_1, x_2) = 2x_1 - (1/9)x_1^2 - x_2 = 0$, $F_2(x_1, x_2) = -x_1 + 2x_2 - (1/9)x_2^2 = 0$, $x = (x_1, x_2) \in R^2$. Then, notice $0 < \lambda \leqslant 1$; it is easy to know F is Fréchet differentiable in R^2 and we get

$$F'(x) = \begin{pmatrix} 2 - \frac{2}{9}x_1 & -1 \\ -1 & 2 - \frac{2}{9}x_2 \end{pmatrix}. \tag{45}$$

Let $x = (x_1, x_2) \in R^2$ and $\|x\| = \|x\|_\infty = \max_{1 \leqslant i \leqslant 2} |x_i|$. The corresponding norm on $A \in R^2 \times R^2$ is

$$\|A\| = \max_{1 \leqslant i \leqslant 2} \sum_{j=1}^{2} \left| a_{ij} \right|. \tag{46}$$

Table 3: Relaxed secant method with different λ.

λ	n	x_n	$\|x_n - x_*\|$	CPU time
0.9999	1	(8.9732, 8.9732)	0.0277	0.000288
	2	(9.0016, 9.0016)	0.0016	
	3	(9.0000, 9.0000)	5.2307×10^{-6}	
	4	(9.0000, 9.0000)	4.2965×10^{-10}	
1	1	(8.9722, 8.9722)	0.0278	0.001643
	2	(9.0016, 9.0016)	0.0016	
	3	(9.0000, 9.0000)	5.0744×10^{-6}	
	4	(9.0000, 9.0000)	9.2414×10^{-10}	
0.8	1	(8.9455, 8.9455)	0.545	0.001608
	2	(9.0000, 9.0000)	4.0974×10^{-5}	
	3	(9.0000, 9.0000)	2.0838×10^{-6}	
	4	(9.0000, 9.0000)	1.1794×10^{-7}	

It can be verified easily that $x_* = (9, 9)$ is a solution of (24) and from (26) we get

$$F'(x) = \begin{pmatrix} 0 & -1 \\ -1 & 0 \end{pmatrix}. \tag{47}$$

$F'(x)$ is invertible. Similar to [13], we can deduce that Lipschitz continuous condition is satisfied for $K = 1/9$. Set $\lambda_1 = 0.9999$, $\lambda_2 = 1$, $\lambda_3 = 1.06$. Then the radius of the convergence ball is $r_1 = 2.499975$, $r_2 = 9/4$, $r_3 = 326/212$. Set the two initial points $x_{-1} = (9.5, 9.5)$, $x_0 = (8.5, 8.5)$ and they are in the convergence ball. For results, see Table 3.

Table 3 shows the sequence $\{x_n\}$ generated by the relaxed secant method. From this table, it is known that the sequence $\{x_n\}$ converges, and also the error estimation holds. Moreover, relaxed secant method has more choices than secant method, and optimal parameter λ makes the presented method outperforms the normal secant method.

Example 4. Consider the nonlinear conservative system given in [15]:

$$\begin{aligned} \frac{d^2x(t)}{dt^2} &= -e^{x(t)}, \\ x(0) &= x(1) = 0. \end{aligned} \tag{48}$$

Applying the centered finite difference scheme, we can get the nonlinear system:

$$F(x) = Mx + h^2\phi(x), \tag{49}$$

where $h = 1/(N+1)$ is the step-size and N is a prescribed positive integer. x, $\phi(x)$ are vectors with forms of

$$\begin{aligned} x &= \begin{pmatrix} x_1 \\ x_2 \\ \vdots \\ x_m \end{pmatrix}, \\ \phi(x) &= \begin{pmatrix} e^{x_1} \\ e^{x_2} \\ \vdots \\ e^{x_m} \end{pmatrix}, \end{aligned} \tag{50}$$

Table 4: Numerical results for nonlinear conservative systems.

λ	IT	$\|x_{n+1} - x_n\|$	CPU time
0.99	75	8.7445×10^{-7}	0.002581
1	94	1.9319×10^{-7}	0.002931
0.001	63	9.3315×10^{-7}	0.001471

Table 5: Approximated solution.

i	x_i^*
1	0.026205377
2	0.049844664
3	0.070856372
4	0.089184975
5	0.104780806
6	0.117601571
7	0.127610864
8	0.134780833
9	0.139090798
10	0.140529159
11	0.139090906
12	0.134780768
13	0.127610728
14	0.117601588
15	0.104780816
16	0.089184869
17	0.070856314
18	0.049844674
19	0.026205359

and the matrix M has the form

$$A = \begin{pmatrix} -2 & 1 & 0 & \cdots & 0 \\ 1 & -2 & 1 & \cdots & 0 \\ 0 & 1 & -2 & \cdots & 0 \\ \vdots & \vdots & \vdots & \ddots & \vdots \\ 0 & 0 & 0 & \cdots & -2 \end{pmatrix}. \tag{51}$$

Take the same parameters used in [15], $N = 19$, $h = 1/20$, and the initial points $x_{-1}(t) = (5/2)t(1-t)$ and $x_0(t) = (1/2)t(1-t)$, $t \in [0, 1]$. Then, we can solve this problem by our relaxed secant method, and we compare it with normal secant method. For the results, see Table 4.

From the results, we can know that, in this example, the relaxed secant method performs better. And we list the approximation solution which is gotten by the relaxed secant method in the situation $\lambda = 0.99$ in Table 5.

Competing Interests

The authors declare that they have no competing interests.

Acknowledgments

This work is supported by National Natural Science Foundation of China (Grant nos. 11371320, 11632015), Zhejiang Natural Science Foundation (Grant no. LZ14A010002), and Scientific Research Fund of Zhejiang Provincial Education Department (Grant no. FX2016073).

References

[1] I. K. Argyros, "A new semilocal convergence theorem for Newton's method in Banach space using hypotheses on the second Fréchet-derivative," *Journal of Computational and Applied Mathematics*, vol. 130, no. 1-2, pp. 369–373, 2001.

[2] I. K. Argyros, "On the Newton-Kantorovich hypothesis for solving equations," *Journal of Computational and Applied Mathematics*, vol. 169, no. 2, pp. 315–332, 2004.

[3] I. K. Argyros and S. Hilout, "On the local convergence of fast two-step Newton-like methods for solving nonlinear equations," *Journal of Computational and Applied Mathematics*, vol. 245, pp. 1–9, 2013.

[4] M. A. Hernández and M. J. Rubio, "A modifcation of Newton's method for nondiferentiable equations," *Journal of Computational and Applied Mathematics*, vol. 164, pp. 409–417, 2004.

[5] M. A. Hernández and M. J. Rubio, "A uniparametric family of iterative processes for solving nondifferentiable equations," *Journal of Mathematical Analysis and Applications*, vol. 275, no. 2, pp. 821–834, 2002.

[6] M. T. Darvishi, "A two-step high order Newton-like method for solving systems of nonlinear equations," *International Journal of Pure and Applied Mathematics*, vol. 57, no. 4, pp. 543–555, 2009.

[7] S. Amat, A. Magreñán, and N. Romero, "On a two-step relaxed Newton-type method," *Applied Mathematics and Computation*, vol. 219, no. 24, pp. 11341–11347, 2013.

[8] I. K. Argyros and Á. A. Magreñán, "On the convergence of inexact two-point Newton-like methods on Banach spaces," *Applied Mathematics and Computation*, vol. 265, Article ID 21248, pp. 893–902, 2015.

[9] I. K. Argyros, A. Cordero, A. Magreñán, and J. R. Torregrosa, "On the convergence of a damped Newton-like method with modified right hand side vector," *Applied Mathematics and Computation*, vol. 266, Article ID 21280, pp. 927–936, 2015.

[10] J. A. Ezquerro, D. González, and M. A. Hernández-Verón, "A semilocal convergence result for Newton's method under generalized conditions of Kantorovich," *Journal of Complexity*, vol. 30, no. 3, pp. 309–324, 2014.

[11] O. P. Ferreira, "A robust semi-local convergence analysis of Newton's method for cone inclusion problems in Banach spaces under affine invariant majorant condition," *Journal of Computational and Applied Mathematics*, vol. 279, pp. 318–335, 2015.

[12] I. K. Argyros and S. George, "Unified convergence domains of Newton-like methods for solving operator equations," *Applied Mathematics and Computation*, vol. 286, pp. 106–114, 2016.

[13] H. M. Ren and Q. B. Wu, "The convergence ball of the Secant method under Hölder continuous divided differences," *Journal of Computational and Applied Mathematics*, vol. 194, no. 2, pp. 284–293, 2006.

[14] I. K. Argyros and S. K. Khattri, "On the Secant method," *Journal of Complexity*, vol. 29, no. 6, pp. 454–471, 2013.

[15] J. A. Ezquerro, M. Grau-Sánchez, M. A. Hernández, and M. Noguera, "Semilocal convergence of secant-like methods for differentiable and nondifferentiable operator equations," *Journal of Mathematical Analysis and Applications*, vol. 398, no. 1, pp. 100–112, 2013.

[16] M. A. Hernandez and M. J. Rubio, "The secant method and divided differences Holder continuous," *Applied Mathematics and Computation*, vol. 124, no. 2, pp. 139–149, 2001.

[17] H. M. Ren, S. J. Yang, and Q. B. Wu, "A new semilocal convergence theorem for the Secant method under Hölder continuous divided differences," *Applied Mathematics and Computation*, vol. 182, no. 1, pp. 41–48, 2006.

[18] H. M. Ren and Q. B. Wu, "Mysovskii-type theorem for the secant method under Hölder continuous Fréchet derivative," *Journal of Mathematical Analysis and Applications*, vol. 320, no. 1, pp. 415–424, 2006.

Hindawi
Advances in Mathematical Physics
Volume 2017, Article ID 9648538, 9 pages
https://doi.org/10.1155/2017/9648538

Research Article

Turing Bifurcation and Pattern Formation of Stochastic Reaction-Diffusion System

Qianiqian Zheng,[1] Zhijie Wang,[1] Jianwei Shen,[2] and Hussain Muhammad Ather Iqbal[1]

[1]*College of Information Science and Technology, Donghua University, Shanghai 201620, China*
[2]*Institute of Applied Mathematics, Xuchang University, Xuchang, Henan 461000, China*

Correspondence should be addressed to Zhijie Wang; wangzj@dhu.edu.cn and Jianwei Shen; xcjwshen@gmail.com

Received 28 August 2016; Revised 18 November 2016; Accepted 15 December 2016; Published 12 February 2017

Academic Editor: Zhi-Yuan Sun

Noise is ubiquitous in a system and can induce some spontaneous pattern formations on a spatially homogeneous domain. In comparison to the Reaction-Diffusion System (RDS), Stochastic Reaction-Diffusion System (SRDS) is more complex and it is very difficult to deal with the noise function. In this paper, we have presented a method to solve it and obtained the conditions of how the Turing bifurcation and Hopf bifurcation arise through linear stability analysis of local equilibrium. In addition, we have developed the amplitude equation with a pair of wave vector by using Taylor series expansion, multiscaling, and further expansion in powers of small parameter. Our analysis facilitates finding regions of bifurcations and understanding the pattern formation mechanism of SRDS. Finally, the simulation shows that the analytical results agree with numerical simulation.

1. Introduction

The pattern formation was first investigated and interpreted by Turing sixty years ago [1]. Othmer and Scriven [2] proposed that the Turing instability which is initially stable steady-state of a dynamical system can become unstable if we consider diffusion in the system. It is also possible in network-organized systems which is important for understanding of multicellular morphogenesis. Recently Turing bifurcation, amplitude equation, and secondary bifurcation have become more significant to study the pattern formation [3–5]; Lee and Cho found that the shape and type of Turing patterns depend on dynamical parameters and external periodic forcing [6]. Moreover, Peña and Pérez-García showed that slightly squeezed hexagons are locally stable in a full range of distorted angles [7]. The domain coarsening process is strongly affected by the spatial separation between groups created by the Turing pattern formation process [8] and the robustness problem is also investigated [9]. The effects of cross-diffusion, the phenomenon in which a gradient in the concentration of one species induces the change of other species, on pattern formation in Reaction-Diffusion Systems have been discussed in many theoretical papers [10]. Fanelli et al. [11] showed that cross-diffusion can destabilize uniform equilibrium which is stable for the kinetic and self-diffusion reaction systems. On the other hand, cross-diffusion can also stabilize a uniform equilibrium which is stable for the kinetic system but unstable for the self-diffusion reaction system [12]. In conclusion, spatial patterns in Reaction-Diffusion Systems have attracted the interest of experimentalists and theorists during the last few decades. However, until now, no general theoretical analysis has been proposed for the possible role of noise in dissipative pattern formation.

Noise is a ubiquitous phenomenon in nature and is always deemed to play a very important role in natural synthetic system [13]. Coherence resonance and stochastic resonance in a noise-driven gene network regulated by small RNA [14, 15]. Viney and Reece [16] treated noise as adaptive and suggested that applying evolutionary rigour to the study of noise is necessary to fully understand organismal phenotypes. Scarsoglio et al. [17] presented different stochastic mechanisms of spatial pattern formation with a variable as noise-induced phenomena. Hori and Hara provided a mechanistic basis of Turing pattern formation that is induced by intrinsic noise

and derived an efficient computation tool to examine the spatial power spectrum of the intrinsic noise [18]. Sun et al. [19] revealed that noise can make the regular circle pattern to be a target wave-like pattern by numerical simulations. A stochastic version of the Brusselator model is proposed and studied via the system size expansion [20] and the mesoscopic equations governing the dynamics were derived and used to special models [21]. Many studies have been presented in these research areas [22–28], as practice shows that theory on Turing bifurcation and pattern formation in dynamical system was rarely studied.

It is known that amplitude equation is not only a promising tool to investigate the RDS but also the main focus of the pattern dynamics [29, 30]. However, the amplitude equation is a complex process [31], and only a few systems have been chosen in the past for amplitude equation [32–35]. In this paper, we studied pattern selection of amplitude equation with a pair of wave vector by using the standard multiple scale analysis [36, 37]. Previously, the researchers did not take into account the effect of noise when deriving the amplitude equation but we will include it.

Besides the study of patterns, it can offer useful information on the underlying processes causing possible changes in the system. In order to better understand the reaction diffusion model, first, we proposed to study the pattern formation with noise based on the theory. In this paper, we obtained some interesting results explaining biological mechanism in a modified system. Moreover, we also investigated the relationship between the Reaction-Diffusion System and noise, revealing how the dynamics of the model regulation is affected by noise which provides a way to investigate the mechanism of pattern formation.

The paper is organized as follows. In Section 2, we present the general reaction diffusion with noise and derive the condition of Hopf bifurcation and Turing bifurcation. In Section 3, we derive the amplitude equation from Reaction-Diffusion System with noise. In Section 4, we utilize an example to illustrate the application of these ideas and using simulations validate theoretical results and present some interesting pattern dynamical phenomena. Finally, we summarize our results and conclude.

2. Turing Bifurcation with SRDS

Since we know that noise plays an important role in the nonlinear systems, some promising results have been presented [11, 12, 32]. However, most people investigated noise by simulation and seldom put forward the theoretical conclusion, especially on pattern formation. In this paper, we study the effect of noise on pattern formation by deriving the Turing bifurcation, to know how it affects the pattern formation. The general diffusion form with noise is as follows:

$$\begin{aligned}\frac{\partial u}{\partial t} &= f(u,v) + d_1\nabla^2 u + d_2 R_1(u,v)\,\xi_1,\\ \frac{\partial v}{\partial t} &= g(u,v) + d_3\nabla^2 v + d_4 R_2(u,v)\,\xi_2,\end{aligned} \tag{1}$$

where ξ is the noise and ∇^2 is the Laplace operator; d_1, d_3 and d_2, d_4 are diffusion parameters and noise magnitude, respectively.

For convenience, we just consider $R_1(u,v) = u - u_0$, $R_2(u,v) = v - v_0$, $\xi_1 = (1/\sqrt{2\pi}\sigma)e^{-(u-u_0)^2/2\sigma^2}$, $\xi_2 = (1/\sqrt{2\pi}\sigma)e^{-(v-v_0)^2/2\sigma^2}$ as random variable in this system. In order to obtain the stability of this spatially uniform solution, we consider a perturbation of the form in the following:

$$P(t) = \begin{pmatrix} u(t) \\ v(t) \end{pmatrix} = \begin{pmatrix} u(t) - u_0 \\ v(t) - v_0 \end{pmatrix}. \tag{2}$$

In the convergence domain, we can obtain the linear system of stochastic system as (3) at (u_0, v_0) which satisfy $f(u_0, v_0) = 0$, $g(u_0, v_0) = 0$.

$$\begin{aligned}\frac{\partial u}{\partial t} &= a_{11}u + a_{12}v + d_1\nabla^2 u + d_{21}u,\\ \frac{\partial v}{\partial t} &= a_{21}u + a_{22}v + d_3\nabla^2 v + d_{41}v,\end{aligned} \tag{3}$$

where the matrix a is the partial derivative of $f(u,v)$, $g(u,v)$ at (u_0, v_0) and $d_{21} = d_2(1/\sqrt{2\pi}\sigma)$, $d_{41} = d_4(1/\sqrt{2\pi}\sigma)$.

For convenience, we can get the linearized system governing the dynamics of P is defined by

$$P_t = AP + D\Delta P, \tag{4}$$

where the coefficient matrix is given by

$$\begin{aligned}A &= \begin{pmatrix} A_{11} & A_{12} \\ A_{21} & A_{22} \end{pmatrix},\\ D &= \begin{pmatrix} d_1 & 0 \\ 0 & d_3 \end{pmatrix},\end{aligned} \tag{5}$$

where

$$\begin{aligned}\mathrm{A}_{11} &= a_{11} + d_{21},\\ A_{12} &= a_{12},\\ A_{22} &= a_{22} + d_{41},\\ A_{21} &= a_{21}.\end{aligned} \tag{6}$$

In the standard way, we assume that P take the form as

$$P = \begin{pmatrix} c_1 \\ c_2 \end{pmatrix} e^{\lambda t + ikr} \tag{7}$$

and get the characteristic equation from system (4) as follows:

$$\begin{vmatrix} \lambda_k - A_{11} + k^2 d_1 & -A_{12} \\ -A_{21} & \lambda_k - A_{22} + k^2 d_3 \end{vmatrix} = 0. \tag{8}$$

Finally, we solve the characteristic equation and obtain the eigenvalues

$$\begin{aligned}\lambda_k^2 - \mathrm{Tr}_k\lambda + \delta\left(k^2\right) &= 0\\ \lambda_k &= \frac{1}{2}\left(\mathrm{Tr}_k \pm \sqrt{\mathrm{Tr}_k^2 - 4\delta_k}\right),\end{aligned} \tag{9}$$

where

$$\begin{aligned}
\mathrm{Tr}_k &= A_{11} + A_{22} - k^2\left(d_1 + d_3\right) \\
&= a_{11} + d_{21} + a_{22} + d_{41} - k^2\left(d_1 + d_3\right), \\
\mathrm{Tr}_0 &= A_{11} + A_{22} = a_{11} + d_{21} + a_{22} + d_{41} \\
\delta\left(k^2\right) &= A_{11}A_{22} - A_{12}A_{21} - \left(A_{11}d_3 + A_{22}d_1\right)k^2 \\
&\quad + d_1 d_3 k^4 \\
&= a_{11}a_{22} + a_{11}d_{41} + d_{21}a_{22} + d_{21}d_{41} - a_{12}a_{21} \\
&\quad - \left(a_{11}d_3 + d_{21}d_3 + a_{22}d_1 + d_1 d_{41}\right)k^2 \\
&\quad + d_1 d_3 k^4 \\
\det(P) &= \delta_0 \\
&= a_{11}a_{22} + a_{11}d_{41} + d_{21}a_{22} + d_{21}d_{41} - a_{12}a_{21}.
\end{aligned} \tag{10}$$

Based on the bifurcation theory, we obtain new conditions of bifurcation with noise.

(1) Hopf bifurcation occurs in the Reaction-Diffusion System (3) which should satisfy the following critical conditions here:

(i) $a_{11} + d_{21} + a_{22} + d_{41} = 0$,

(ii) $a_{11}a_{22} + a_{11}d_{41} + d_{21}a_{22} + d_{21}d_{41} - a_{12}a_{21} > 0$,

(iii) $\mathrm{Re}(\lambda_k)$ is not a constant.

(2) Turing bifurcation (diffusion-driven instability) occurs in the Reaction-Diffusion System (3) which should satisfy the following conditions here:

(i) $a_{11} + d_{21} + a_{22} + d_{41} < 0$,

(ii) $a_{11}a_{22} + a_{11}d_{41} + d_{21}a_{22} + d_{21}d_{41} - a_{12}a_{21} > 0$,

(iii) $a_{11}d_3 + d_{21}d_3 + a_{22}d_1 + d_{41}d_1 > 0$,

(iv) $a_{11}d_3 + d_{21}d_3 + a_{22}d_1 + d_{41}d_1 > 2\sqrt{d_1 d_3(a_{11}a_{22} + a_{11}d_{41} + d_{21}a_{22} + d_{21}d_{41} - a_{12}a_{21})}$.

And the critical condition where $k \neq 0$ is

$$\begin{aligned}
&a_{11}a_{22} + a_{11}d_{41} + d_{21}a_{22} + d_{21}d_{41} - a_{12}a_{21} \\
&\quad - \left(a_{11}d_3 + d_{21}d_3 + a_{22}d_1 + d_1 d_{41}\right)k^2 + d_1 d_3 k^4 \\
&= 0.
\end{aligned} \tag{11}$$

3. Amplitude Equation with a Pair of Wave Vector

For a modified model [38] with the external stimulus γuv, the following is obtained:

$$\begin{aligned}
\frac{\partial u}{\partial t} &= u - u^3 - \alpha v - \gamma uv + d_1\nabla^2 u + d_2 R_1(u,v)\,\xi_1, \\
\frac{\partial v}{\partial t} &= u - \beta v + d_3\nabla^2 v + d_4 R_2(u,v)\,\xi_2.
\end{aligned} \tag{12}$$

In this paper, we expanded (12) at equilibrium $(0,0)$ by using the Taylor expansion and then we truncated the expansion at third order; it is found that only third order $ue^{-u^2} = u - u^3 + \cdots$ will be included and higher order will not affect the amplitude equation in the process. And it can be written as

$$\begin{aligned}
\frac{\partial u}{\partial t} &= u - u^3 - \alpha v - \gamma uv + d_{21}u - d_{22}u^3 + d_1\nabla^2 u, \\
\frac{\partial v}{\partial t} &= u - \beta v + d_{41}v - d_{42}v^3 + d_3\nabla^2 v.
\end{aligned} \tag{13}$$

In the following, we use multiple scale analysis to derive the amplitude equations with a pair of wave vector when $|k| = k_c$. Denote β as the controlled parameters. When the controlled parameter is larger than the critical value of Turing point, the solutions of the systems (13) can be expanded as

$$c = c_0 + Ze^{ik_c r} + \overline{Z}e^{-ik_c r}. \tag{14}$$

Close to onset $\beta = \beta_c$, one has that $\partial Z/\partial t = sZ + F(Z)$.

Based on the center manifold near the Turing bifurcation point, it can be concluded that amplitude Z satisfies $\partial Z/\partial t = F(Z, \overline{Z})$.

From the standard multiple scale analysis, up to the third order in the perturbations, the spatiotemporal evolution of the amplitudes can be described as

$$\begin{aligned}
\tau_0\frac{\partial Z}{\partial t} &= \mu Z + b\overline{Z} + cZ^2 + d|Z|^2 + e\overline{Z}^2 + fZ^3 \\
&\quad + g|Z|^2 Z + h|Z|^2\overline{Z} + i\overline{Z}^3 + O\left(Z^4\right).
\end{aligned} \tag{15}$$

Due to spatial translational symmetry, we have the following equation:

$$\begin{aligned}
\tau_0 e^{i\phi}\frac{\partial Z}{\partial t} &= e^{i\phi}\mu Z + e^{-i\phi}b\overline{Z} + e^{i2\phi}cZ^2 + d|Z|^2 \\
&\quad + e^{-i2\phi}e\overline{Z}^2 + e^{i3\phi}fZ^3 + e^{i\phi}g|Z|^2 Z \\
&\quad + e^{-i\phi}h|Z|^2\overline{Z} + e^{-i3\phi}i\overline{Z}^3 + O\left(Z^4\right).
\end{aligned} \tag{16}$$

Comparing (15) with (16) and from the center manifold theory, we know that amplitude equation does not include the amplitude with unstable mode. As a result, we have the following equations:

$$\tau_0\frac{\partial Z}{\partial t} = \mu Z - g|Z|^2 Z. \tag{17}$$

In the following, we will give the expressions of τ_0, μ, and g. Let system (13) be written as

$$\frac{\partial c}{\partial t} = Lc + N(c,c), \tag{18}$$

where

$$c = \begin{pmatrix} u \\ v \end{pmatrix} \tag{19}$$

is the variable,

$$L = \begin{pmatrix} d_{21} + 1 + d_1\nabla^2 & -\alpha \\ 1 & d_{41} - \beta + d_3\nabla^2 \end{pmatrix} \tag{20}$$

is the linear operator, and

$$N = \begin{pmatrix} \gamma uv - u^3 - d_{22}u^3 \\ -d_{42}v^3 \end{pmatrix} \tag{21}$$

is the nonlinear term, where $d_{22} = (1/2\sigma^2)d_{21}$ and $d_{42} = (1/2\sigma^2)d_{41}$.

We need to investigate the dynamical behavior when β is close to β_c, and then we expand β as

$$\beta_c - \beta = \varepsilon\beta_1 + \varepsilon^2\beta_2 + \cdots, \tag{22}$$

where ε is a small enough parameter. We expand c and N as the series form of ε:

$$c = \begin{pmatrix} u_1 \\ v_1 \end{pmatrix}\varepsilon + \begin{pmatrix} u_2 \\ v_2 \end{pmatrix}\varepsilon^2 + \cdots \tag{23}$$

and N in the Appendix.

Linear operator L can be expanded as

$$L = L_c + (\gamma_c - \gamma)M \tag{24}$$

and L_c and M in the Appendix.

Let

$$\begin{aligned} T_0 &= t, \\ T_1 &= \varepsilon t, \\ T_2 &= \varepsilon^2 t, \\ &\vdots \end{aligned} \tag{25}$$

and T_i is a dependent variable. For the derivation of time, we have that

$$\frac{\partial}{\partial t} = \varepsilon\frac{\partial}{\partial T_1} + \varepsilon^2\frac{\partial}{\partial T_2} + \cdots. \tag{26}$$

The solutions of systems (13) have the following form:

$$c = \begin{pmatrix} u \\ v \end{pmatrix} = \begin{pmatrix} x \\ y \end{pmatrix} e^{ik_c r} + c.c. \tag{27}$$

This expression implies that the bases of the solutions have nothing to do with time and the amplitude W is a variable that changes slowly. As a result, it can be written generally as the following equation:

$$\frac{\partial W}{\partial t} = \varepsilon\frac{\partial W}{\partial T_1} + \varepsilon^2\frac{\partial W}{\partial T_2} + \cdots. \tag{28}$$

Substituting the above equations into (24) and expanding (24) according to different orders of ε, we can obtain three equations as follows:

$$\begin{aligned} \varepsilon &: L_c \begin{pmatrix} u_1 \\ v_1 \end{pmatrix} = 0, \\ \varepsilon^2 &: L_c \begin{pmatrix} u_2 \\ v_2 \end{pmatrix} = N_1, \\ \varepsilon^3 &: L_c \begin{pmatrix} u_3 \\ v_3 \end{pmatrix} = N_2 \end{aligned} \tag{29}$$

and N_1, N_2 in the Appendix.

We first consider the case of the first order of ε. Since L_c is the linear operator of the system close to the onset, $(u_1, v_1)^T$ is the linear combination of the eigenvectors that corresponds to the zero eigenvalue since that

$$\begin{pmatrix} u_1 \\ v_1 \end{pmatrix} = \begin{pmatrix} x_1 \\ y_1 \end{pmatrix} We^{ik_c r} + c.c. \tag{30}$$

Let $x_1 = p$ by assuming $y_1 = 1$; then,

$$\begin{pmatrix} u_1 \\ v_1 \end{pmatrix} = \begin{pmatrix} p \\ 1 \end{pmatrix} \left(We^{ik_c r} + c.c.\right), \tag{31}$$

where p in the Appendix and W is the amplitude of the mode $e^{ik_c r}$.

Now, we consider the case of the second order of ε^2. According to the Fredholm solubility condition [32], the vector function of the right hand of the above equation must be orthogonal with the zero eigenvectors of operator L_c^+. And the zero eigenvectors of adjoint operator L_c^+ are

$$\begin{pmatrix} 1 \\ q \end{pmatrix} e^{-ik_c r} \tag{32}$$

and q in the Appendix.

It can be obtained from the orthogonality condition that

$$\tau_0\frac{\partial}{\partial T_1}(W) = \beta_1 W. \tag{33}$$

By using the same methods, we deduce

$$\begin{pmatrix} u_2 \\ v_2 \end{pmatrix} = \begin{pmatrix} a_0 \\ b_0 \end{pmatrix} + \begin{pmatrix} a_1 \\ b_1 \end{pmatrix} e^{ik_c r} + \begin{pmatrix} a_{ii} \\ b_{ii} \end{pmatrix} e^{i2k_c r} \tag{34}$$

and coefficients in the Appendix.

For the case of the third order of ε^3, replace u_1, v_1, u_2, and v_2 by their expression

$$L_c \begin{pmatrix} u_2 \\ v_2 \end{pmatrix} = B = C \tag{35}$$

and B, C in the Appendix. Using the Fredholm solubility condition again, we can obtain

$$\tau_0\frac{\partial b_1}{\partial T_1} + \tau_0\frac{\partial W}{\partial T_2} = \beta_1 v_2 + \beta_2 v_1 - g|W|^2 W. \tag{36}$$

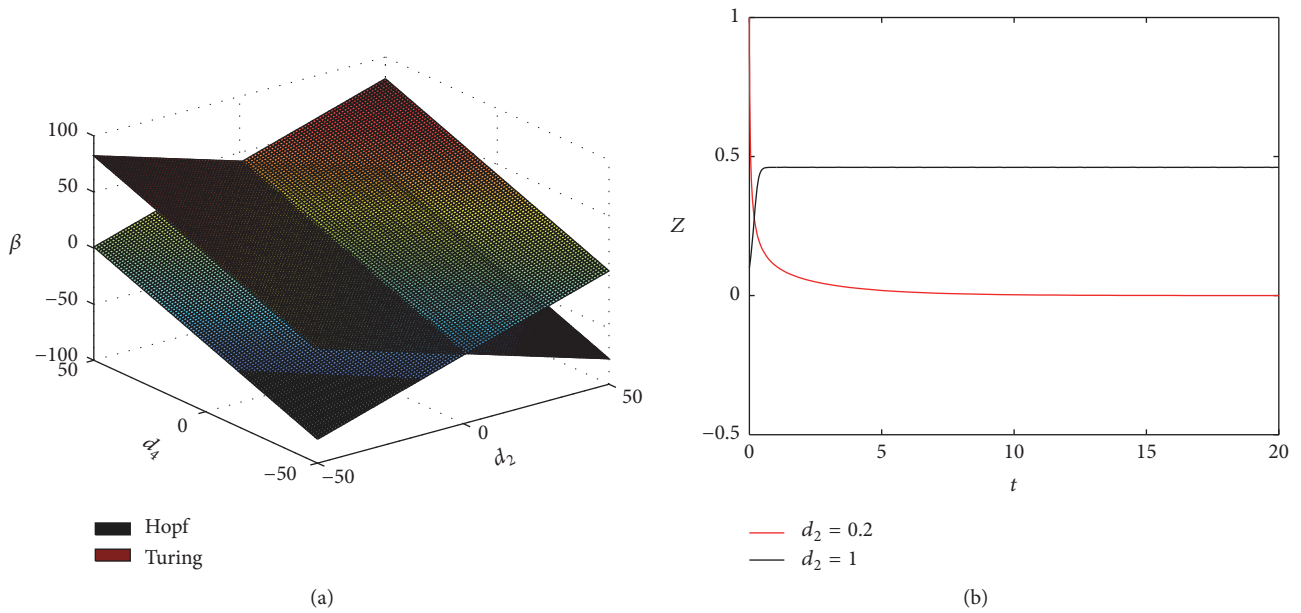

FIGURE 1: (a) The bifurcation space diagram. (b) The bifurcation space diagram based on (38) when $\alpha = 3$, $\gamma = 1$, $d_1 = 1$, $d_3 = 1$, $\sigma = 1/2$, and $\beta = 2$.

And then we substitute system (28) and (33) into (24) to simplify [32]; we obtain the expressions of the coefficients of τ_0, g, and μ in the Appendix.

And

$$Z_i = \varepsilon W_i + \varepsilon^2 b_i + \cdots . \tag{37}$$

So the equation of amplitude is as follows:

$$\tau_0 \frac{\partial Z}{\partial t} = \mu Z - g |Z|^2 Z. \tag{38}$$

Here, we will investigate the dynamics of amplitude equation by using the linear stability analysis [30, 32] and study the different pattern. The dynamical systems (38) possess two kinds of solution as follows.

(i) The stationary solution $Z = 0$ is stable for $\mu < 0$ and unstable for $\mu > 0$.

(ii) The solution $Z = \sqrt{\mu/g}$ is only unstable for $\mu < 0$.

4. Simulation

As the examples of Reaction-Diffusion System with noise, we use the following:

$$\begin{aligned} \frac{\partial u}{\partial t} &= f(u,v) + d_1 \nabla^2 u + d_2 R_1(u,v)\,\xi_1, \\ \frac{\partial v}{\partial t} &= g(u,v) + d_3 \nabla^2 u + d_4 R_2(u,v)\,\xi_2, \end{aligned} \tag{39}$$

where $R_1(u,v) = u - u_0$, $R_2(u,v) = v - v_0$, $f(u,v) = u - u^3 - \alpha v - \gamma uv$, and $g(u,v) = u - \beta v$, and obtain the characteristic equation at $(u_0, v_0) = (0,0)$. Here, we denote $\alpha = 3$, $\gamma = 1$, $d_1 = 1$, $d_3 = 1$, and $\sigma = 1/2$ and get the critical value of Hopf bifurcation when $\beta = 1 + 2d_2/\sqrt{2\pi} + 2d_4/\sqrt{2\pi}$ and Turing bifurcation when $\beta = -2d_2/\sqrt{2\pi} + 2d_4/\sqrt{2\pi} + 2\sqrt{3} - 1$ based on the bifurcation theory in Section 2.

The model is simulated numerically in two spatial dimensions and employ the zero-flux boundary conditions in (39). We set time step and space step as 0.02 and 1, respectively. The bifurcation space divide the space into four domains (Figure 1(a)). On bottom domain, locating below two bifurcation spaces, the system lies in the steady state (Figure 3(d)). The middle domain are regions of pure Turing and pure Hopf in stabilities (Figures 3(b) and 3(c)). On the top, two bifurcation spaces interact (Figure 3(a)). It is found that noise contribute to Turing bifurcation and Hopf bifurcation.

In addition, We find $\tau_0 = -1.0721$, $g = -31.5212$, $\beta_c = 2.3843$, and $\beta = 2$ when $d_2 = 0.2$, $d_4 = 0.1$ and $\tau_0 = 0.1149$, $g = 3.5556$, $\beta_c = 1.7560$, and $\beta = 2$ when $d_2 = 1, d_4 = 0.1$. We get the stability of amplitude equation (Figure 1(b)) and the corresponding pattern formation (Figures 2(a) and 2(b)). In a nutshell, noise plays an important role in the type of pattern formation and the stability in the system, which provides a new way to investigate the mechanism of pattern formation.

5. Conclusion

As we all know, noise could make a bistable system which switches and regulates relevant mechanism [39]. Similarly, it was presented in [40] to understand the biological pattern formation and we presented the spatial pattern with different noise intensities, which gave results supporting that noise could make pattern formation switch (Figures 2(a) and 2(b)) for the Stochastic Reaction-Diffusion Systems. Later some special biological models [21] have been studied and its

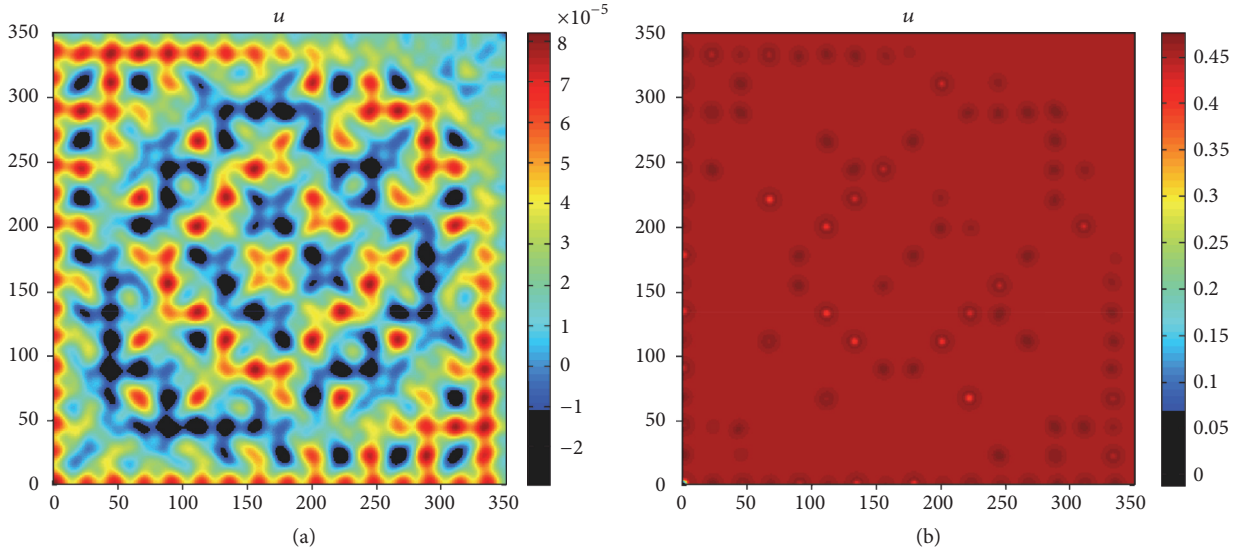

FIGURE 2: Parameter values and initial perturbation, respectively: $\alpha = 3$, $\gamma = 1$, $d_1 = 1$, $d_3 = 1$, $\sigma = 1/2$, $d_4 = 0.1$, $\beta = 2$, $\sin(xy)$, and $\cos(xy)$. (a) Pattern formation on the top domain when $d_2 = 0.2$. (b) Pattern formation on the top domain when $d_2 = 1$. Although the amplitude equation is stable, the effect of noise is crucial.

biological mechanism was explained by the type of pattern formation. For example, the system will exhibit a characteristic excursion in phase space before the variables u and v relax back to their rest values [38]. The only spot pattern existing in Figure 2(b) means that the noise exceeds the maximum value that a biological system could bear and makes the biological system worse. Instead, the appropriate noise could keep a biological system working towards better development. For the Turing instability, the different pattern formation occurs in different condition (Figure 3), especially, the pure Turing domain (Figure 3(b)) and the pure Hopf domain (Figure 3(c)), which shows that not only Turing bifurcation but also Hopf bifurcation makes the system vary and decides whether to relax back to their rest values, then keeping good condition. The patterns discussed above show that the distribution and interaction of ion density and electric potential are caused by noise and diffusion. As a result, we can control the distribution of ion by noise, diffusion, and so on. Our research may help cure some diseases caused by the conduction of electrical impulses along a nerve fiber in future.

To summarise, noise effects have been paid much attention due to its strong impact on pattern formation [19–25]. In this article, we presented the theoretical, analytical, and numerical study of the Turing instability accompanied with noise. We examined the effects of noise on pattern formation and the interaction between Hopf bifurcation space and Turing bifurcation space. It is found that the systems with noise effect have rich spatial dynamics by performing a series of numerical simulations. Thus we know that noise plays an important role in Turing bifurcation and Hopf bifurcation. Moreover, we derive the amplitude equation with a pair of wave vector and analyze the stability. It should be noted that noise contribute to the type of pattern formation and the stability. For future study, we would use the theoretical concepts to solve some other problems and find out a general way to deal with it.

Appendix

$$N = \begin{pmatrix} \gamma u_1 v_1 \varepsilon^2 + \left(\gamma u_1 v_2 + \gamma v_1 u_2 - u_1^3 - d_{22} u_1^3\right)\varepsilon^3 + o\left(\varepsilon^4\right) \\ -d_{42} v_1^3 \varepsilon^3 \end{pmatrix},$$

$$L_c = \begin{pmatrix} d_{21} + 1 + d_1 \nabla^2 & -\alpha \\ 1 & d_{41} - \beta_c + d_3 \nabla^2 \end{pmatrix},$$

$$M = \begin{pmatrix} 0 & 0 \\ 0 & 1 \end{pmatrix},$$

$$N_1 = \frac{\partial}{\partial T_1} \begin{pmatrix} u_1 \\ v_1 \end{pmatrix} - \beta_1 M \begin{pmatrix} u_1 \\ v_1 \end{pmatrix} - \begin{pmatrix} \gamma u_1 v_1 \\ 0 \end{pmatrix},$$

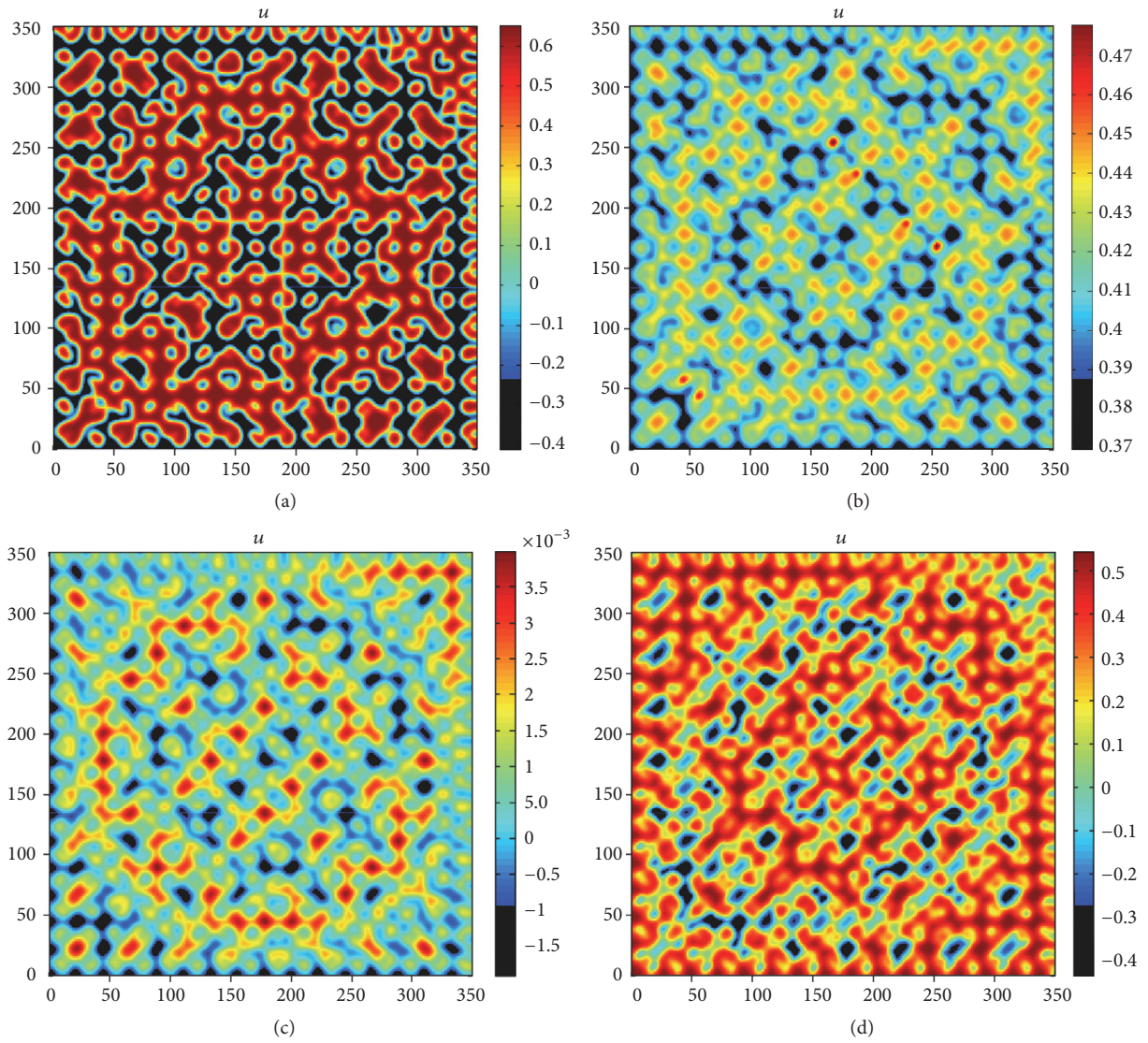

FIGURE 3: Parameter values and initial perturbation, respectively: $\alpha = 3$, $\gamma = 1$, $d_1 = 1$, $d_3 = 1$, $\sigma = 1/2$, $d_2 = 0.1$, $\sin(xy)$, and $\cos(xy)$. (a) Pattern formation on the top domain when $d_4 = 0.1$, $\beta = 4$. (b) Pattern formation on the right domain when $d_4 = 1$, $\beta = 2$. (c) Pattern formation on the left domain when $d_4 = 0.1$, $\beta = 2$. (d) Pattern formation on the bottom domain when $d_4 = 1$, $\beta = 2$.

$$N_2 = \frac{\partial}{\partial T_1}\begin{pmatrix} u_2 \\ v_2 \end{pmatrix} + \frac{\partial}{\partial T_2}\begin{pmatrix} u_1 \\ v_1 \end{pmatrix} - \beta_1 M \begin{pmatrix} u_2 \\ v_2 \end{pmatrix} - \beta_2 M \begin{pmatrix} u_1 \\ v_1 \end{pmatrix} \begin{pmatrix} \gamma u_1 v_2 + \gamma u_2 v_1 - u_1^3 - d_{22} u_1^3 \\ d_{42} v_1^3 \end{pmatrix},$$

$$x_1 = p y_1,$$

$$p = \beta_c - d_{41} + d_3 k_c^2,$$

$$q = d_1 k_c^2 - d_{21} - 1,$$

$$a_0 = (d_{41} - \beta_c) b_0,$$

$$b_0 = \frac{2|Z|^2 \gamma p}{(d_{21} + 1)(d_{41} - \beta_c) - \alpha},$$

$$a_1 = p b_1,$$

$$a_{ii} = \left(\beta_c + 4 d_3 k_c^2 - d_{41}\right) b_{ii},$$

$$
\begin{aligned}
b_{ii} &= \frac{\gamma p |Z|^2}{\left(d_{21} + 1 - 4d_1 k_c^2\right)\left(\beta_c + 4d_3 k_c^2 - d_{41}\right) - \alpha}, \\
B &= \begin{pmatrix} \left(d_{21}+1\right) X_0 - \alpha Y_0 + \left(\left(d_{21} + 1 - d_1 k_c^2\right) X_1 - \alpha Y_1\right) e^{ik_c r} + \left(\left(d_{21} + 1 - 4d_1 k_c^2\right) X_{11} - \alpha Y_{11}\right) e^{i2k_c r} + c.c \\ X_0 + \left(-\beta_c + d_{41}\right) Y_0 + \left(X_1 - \left(\beta_c - d_{41} + d_3 k_c^2\right) Y_1\right) e^{ik_c r} + \left(X_{11} - \left(\beta_c - d_{41} + 4d_3 k_c^2\right) Y_{11}\right) e^{i2k_c r} + c.c \end{pmatrix}, \\
\tau_0 &= \frac{p+q}{q}, \\
gq &= -\frac{a_0 + a_{ii} + pb_0 + pb_{ii}}{|Z|^2} + p^3 + d_{22} p^3 + d_{42} q, \\
\mu &= \beta_c - \beta, \\
C &= \frac{\partial}{\partial T_1} \begin{pmatrix} u_1 \\ v_1 \end{pmatrix} - \beta_1 \begin{pmatrix} 0 \\ Z e^{ik_c r} + c.c. \end{pmatrix} - \begin{pmatrix} \gamma u_1 v_1 \\ 0 \end{pmatrix}.
\end{aligned}
\tag{A.1}
$$

Fredholm Solubility Condition. The perturbation equation has $O(1) : Lu_0 = 0$, $O(\varepsilon^i) : Lu_i = q_i$, q_i which is nonlinear function about $x_0, \ldots, x_{i-1}$. In order to remove the resonance term, q_i cannot resonate with the nontrivial null space of linear operator L, namely, u_0. Then every linear operator defines an adjoint operator L^*. The consistency of the solution of equation $Lu = q$ requires $u^+ q = 0$, where $L^* u^+ = 0, l_{ij}^* = \bar{l}_{ji}$. Simply put, Fredholm solubility condition is $u^+ q = 0$.

Competing Interests

The authors declare that there is no conflict of interests regarding the publication of this paper.

Acknowledgments

This work is supported by the National Natural Science Foundation of China (11272277, 11572278, and 11572084) and Innovation Scientists and Technicians Troop Construction Projects of Henan Province (2017JR0013).

References

[1] A. M. Turing, "The chemical basis of morphogenesis," *Philosophical Transactions of the Royal Society of London, Series B: Biological Sciences*, vol. 237, no. 641, pp. 37–72, 1952.

[2] H. G. Othmer and L. E. Scriven, "Instability and dynamic pattern in cellular networks," *Journal of Theoretical Biology*, vol. 32, no. 3, pp. 507–537, 1971.

[3] H. Liu and W. Wang, "The amplitude equations of an epidemic model," *Science Technology and Engineering*, vol. 10, no. 8, pp. 1929–1933, 2010.

[4] E. Ahmed, H. A. Abdusalam, and E. S. Fahmy, "On telegraph coupled map lattice and its applications," *International Journal of Modern Physics C*, vol. 12, no. 10, pp. 1525–1535, 2001.

[5] Q. Zheng and J. Shen, "Dynamics and pattern formation in a cancer network with diffusion," *Communications in Nonlinear Science and Numerical Simulation*, vol. 27, no. 1–3, pp. 93–109, 2015.

[6] I. Lee and U. I. Cho, "Pattern formations with Turing and Hopf oscillating pattern," *Bulletin of the Korean Chemical Society*, vol. 21, no. 12, pp. 1213–1216, 2000.

[7] B. Peña and C. Pérez-García, "Stability of turing patterns in the Brusselator model," *Physical Review E. Statistical, Nonlinear, and Soft Matter Physics*, vol. 64, no. 5, 2001.

[8] H. Sayama, M. A. de Aguiar, Y. Bar-Yam, and M. Baranger, "Interplay between Turing pattern formation and domain coarsening in spatially extended population models," *Forma*, vol. 18, no. 1, pp. 19–36, 2003.

[9] P. K. Maini, T. E. Woolley, R. E. Baker, E. A. Gaffney, and S. Seirin Lee, "Turing's model for biological pattern formation and the robustness problem," *Interface Focus*, vol. 2, no. 4, pp. 487–496, 2012.

[10] V. K. Vanag and I. R. Epstein, "Cross-diffusion and pattern formation in reaction-diffusion systems," *Physical Chemistry Chemical Physics*, vol. 11, no. 6, pp. 897–912, 2009.

[11] D. Fanelli, C. Cianci, and F. Di Patti, "Turing instabilities in reaction-diffusion systems with cross diffusion," *The European Physical Journal B*, vol. 86, no. 4, article 142, 8 pages, 2013.

[12] J. Shi, Z. Xie, and K. Little, "Cross-diffusion induced instability and stability in reaction-diffusion systems," *The Journal of Applied Analysis and Computation*, vol. 1, no. 1, pp. 95–119, 2011.

[13] M. Thattai and A. Van Oudenaarden, "Intrinsic noise in gene regulatory networks," *Proceedings of the National Academy of Sciences of the United States of America*, vol. 98, no. 15, pp. 8614–8619, 2001.

[14] Y. Zhu, J. Shen, and Y. Xu, "Coherence resonance in a noise-driven gene network regulated by small RNA," *Theoretical and Applied Mechanics Letters*, vol. 4, no. 1, Article ID 013008, 2014.

[15] Y. Zhu, J. Shen, and Y. Xu, "Mechanism of stochastic resonance in a quorum sensing network regulated by small RNAs," *Abstract and Applied Analysis*, vol. 2013, Article ID 105724, 6 pages, 2013.

[16] M. Viney and S. Reece, "Adaptive noise," *Proceedings of the Royal Society of London B*, vol. 280, no. 1767, 2013.

[17] S. Scarsoglio, F. Laio, P. D'Odorico, and L. Ridolfi, "Spatial pattern formation induced by Gaussian white noise," *Mathematical Biosciences*, vol. 229, no. 2, pp. 174–184, 2011.

[18] Y. Hori and S. Hara, "Noise-induced spatial pattern formation in stochastic reaction-diffusion systems," in *Proceedings of the 51st IEEE Conference on Decision and Control (CDC '12)*, pp. 1053–1058, Maui, Hawaii, USA, December 2012.

[19] G. Sun, Z. Jin, L. Li, and Q. Liu, "The role of noise in a predator–prey model with Allee effect," *Journal of Biological Physics*, vol. 35, no. 2, pp. 185–196, 2009.

[20] T. Biancalani, D. Fanelli, and F. Di Patti, "Stochastic turing patterns in the Brusselator model," *Physical Review E*, vol. 81, no. 4, Article ID 046215, 2010.

[21] A. J. McKane, T. Biancalani, and T. Rogers, "Stochastic pattern formation and spontaneous polarisation: the linear noise approximation and beyond," *Bulletin of Mathematical Biology*, vol. 76, no. 4, pp. 895–921, 2014.

[22] T. Butler and N. Goldenfeld, "Fluctuation-driven Turing patterns," *Physical Review E—Statistical, Nonlinear, and Soft Matter Physics*, vol. 84, Article ID 011112, 2011.

[23] Z.-P. Fu, X.-H. Xu, H.-L. Wang, and Q. Ouyang, "Stochastic simulation of turing patterns," *Chinese Physics Letters*, vol. 25, no. 4, pp. 1220–1223, 2008.

[24] C. Marr and M.-T. Hütt, "Similar impact of topological and dynamic noise on complex patterns," *Physics Letters, Section A: General, Atomic and Solid State Physics*, vol. 349, no. 5, pp. 302–305, 2006.

[25] J.-H. Huh and S. Kai, "Pure noise-induced pattern formations in a nematic liquid crystal," *Journal of the Physical Society of Japan*, vol. 78, no. 4, Article ID 043601, 2009.

[26] Z. Song, C. Y. Ko, M. Nivala, J. N. Weiss, and Z. Qu, "Calcium-voltage coupling in the genesis of early and delayed afterdepolarizations in cardiac myocytes," *Biophysical Journal*, vol. 108, no. 8, pp. 1908–1921, 2015.

[27] Z. Song, A. Karma, J. N. Weiss, and Z. Qu, "Long-lasting sparks: multi-metastability and release competition in the calcium release unit network," *PLoS Computational Biology*, vol. 12, no. 1, Article ID e1004671, 2016.

[28] E. Lau, K. Kossidas, T. Kim et al., "Spatially discordant alternans and arrhythmias in tachypacing-induced cardiac myopathy in transgenic LQT1 rabbits: the importance of I Ks and Ca2+ cycling," *PLoS ONE*, vol. 10, no. 5, Article ID e0122754, 2015.

[29] W. Wang, H. Liu, Y. Cai, and Z. Li, "Turing pattern selection in a reaction-diffusion epidemic model," *Chinese Physics B*, vol. 20, no. 7, Article ID 074702, 2011.

[30] Q. Zheng and J. Shen, "Pattern formation in the FitzHugh-Nagumo model," *Computers & Mathematics with Applications*, vol. 70, no. 5, pp. 1082–1097, 2015.

[31] A. K. Dutt, "Amplitude equation for a diffusion-reaction system: the reversible Sel'kov model," *AIP Advances*, vol. 2, no. 4, pp. 1–24, 2012.

[32] Q. Ouyang, *Introduction to Nonlinear Science and Pattern Dynamics*, Peking University Press, Beijing, China, 2010.

[33] C. Mayol, R. Toral, and C. R. Mirasso, "Derivation of amplitude equations for nonlinear oscillators subject to arbitrary forcing," *Physical Review E—Statistical, Nonlinear, and Soft Matter Physics*, vol. 69, no. 6, Article ID 066141, 2004.

[34] J. Murray, *Mathematical Biology: I. An Introduction*, Interdisciplinary Applied Mathematics, Springer, 2007.

[35] Y. Kuramoto, *Chemical Oscillations, Waves and Turbulence*, Dover, Mineola, NY, USA, 2003.

[36] G. H. Gunaratne, Q. Ouyang, and H. L. Swinney, "Pattern formation in the presence of symmetries," *Physical Review E*, vol. 50, no. 4, pp. 2802–2820, 1994.

[37] G.-Q. Sun, L. Li, Z. Jin, Z.-K. Zhang, and T. Zhou, "Pattern dynamics in a spatial predator-prey system with Allee effect," *Abstract and Applied Analysis*, vol. 2013, Article ID 921879, 12 pages, 2013.

[38] R. FitzHugh, "Impulses and physiological states in theoretical models of nerve membrane," *Biophysical Journal*, vol. 1, no. 6, pp. 445–466, 1961.

[39] Y. Xu, Y.-N. Zhu, J. W. Shen, and J. B. Su, "Switch dynamics for stochastic model of genetic toggle switch," *Physica A: Statistical Mechanics and Its Applications*, vol. 416, pp. 461–466, 2014.

[40] A. T. Winfree, "Varieties of spiral wave behavior: an experimentalist's approach to the theory of excitable media," *Chaos. An Interdisciplinary Journal of Nonlinear Science*, vol. 1, no. 3, pp. 303–334, 1991.

Hindawi
Advances in Mathematical Physics
Volume 2017, Article ID 3094173, 11 pages
https://doi.org/10.1155/2017/3094173

Research Article

The General Solution of Differential Equations with Caputo-Hadamard Fractional Derivatives and Noninstantaneous Impulses

Xianzhen Zhang,[1] Zuohua Liu,[2] Hui Peng,[3] Xianmin Zhang,[3] and Shiyong Yang[3]

[1]*School of Chemical and Environmental Engineering, Jiujiang University, Jiujiang, Jiangxi 332005, China*
[2]*School of Chemistry and Chemical Engineering, Chongqing University, Chongqing 400044, China*
[3]*School of Electronic Engineering, Jiujiang University, Jiujiang, Jiangxi 332005, China*

Correspondence should be addressed to Xianmin Zhang; z6x2m@126.com

Received 25 September 2016; Accepted 22 November 2016; Published 9 February 2017

Academic Editor: Kaliyaperumal Nakkeeran

Based on some recent works about the general solution of fractional differential equations with instantaneous impulses, a Caputo-Hadamard fractional differential equation with noninstantaneous impulses is studied in this paper. An equivalent integral equation with some undetermined constants is obtained for this fractional order system with noninstantaneous impulses, which means that there is general solution for the impulsive systems. Next, an example is given to illustrate the obtained result.

1. Introduction

Impulsive differential equations are used in modeling of biology and physics and engineering and so forth to describe abrupt changes of the state at certain instants. However, the classical impulsive models in which instantaneous impulses were mainly considered in most of the existing papers can not describe some processes such as evolution processes in pharmacotherapy. Hence, Hernández and O'Regan [1] and Pierri et al. [2] presented and studied a kind of differential equations with noninstantaneous impulses. Next, the fractional differential equations with noninstantaneous impulses were considered in [3, 4].

Recently, Hadamard fractional calculus is getting attention which is an important part of theory of fractional calculus [5]. The works in [6–11] made development in fundamental theorem of Hadamard fractional calculus. A Caputo-type modification of Hadamard fractional derivative which is called Caputo-Hadamard fractional derivative was given in [12], and its fundamental theorems were proved in [13, 14].

Furthermore, some works in [15–21] uncover that there is general solution for several fractional differential equations with instantaneous impulses. Therefore, we will try to consider the general solution for differential equations with Caputo-Hadamard fractional derivatives and noninstantaneous impulses:

$$\begin{aligned} {}_{\text{C-H}}D^{q}_{a^+}u(t) &= f(t,u(t)), \\ &\qquad t \in (s_k, t_{k+1}],\ k = 0,1,\ldots,N, \\ u(t) &= g_k(t,u(t)), \\ &\qquad t \in (t_k, s_k],\ k = 1,2,\ldots,N, \\ u(a) &= u_a \in \mathbb{C}, \end{aligned} \tag{1}$$

where $q \in \mathbb{C}$, $\Re(q) \in (0,1)$, and $a > 0$ and ${}_{\text{C-H}}D^{q}_{a^+}$ is the left-side Caputo-Hadamard fractional derivative of order q. $f : [a,T] \times \mathbb{C} \to \mathbb{C}$ and $g_k : (t_k, s_k] \times \mathbb{C} \to \mathbb{C}$ (here $k = 1,2,\ldots,N$) are some appropriate functions, and g_k denote noninstantaneous impulses. $a = t_0 = s_0 < t_1 \le s_1 \le t_2 \le \cdots \le t_N \le s_N \le t_{N+1} = T$.

Firstly, we only consider ${}_{\text{C-H}}D^{q}_{a^+}u(t) = f(t,u(t))$ in each interval $(s_k, t_{k+1}]$ $(k = 0, 1, \ldots, N)$ in (1), and then

$$\begin{aligned} &{}_{\text{C-H}}D^{q}_{a^+}u(t) = f(t,u(t)), \quad \text{for } t \in (s_k, t_{k+1}] \\ &= {}_{\text{C-H}}D^{q}_{s_k^+}u(t) = f(t,u(t)), \quad \text{for } t \in (s_k, t_{k+1}] \Longleftrightarrow \\ &u(t) = u(s_k) + \frac{1}{\Gamma(q)} \int_{s_k}^{t} \left(\ln\frac{t}{\tau}\right)^{q-1} f(\tau,u(\tau)) \frac{d\tau}{\tau}, \quad \text{for } t \in (s_k, t_{k+1}]. \end{aligned} \tag{2}$$

Substituting (2) into (1), we obtain

$$\widetilde{u}(t) = \begin{cases} u_a + \dfrac{1}{\Gamma(q)} \displaystyle\int_a^t \left(\ln\frac{t}{\tau}\right)^{q-1} f(\tau,u(\tau)) \frac{d\tau}{\tau}, & \text{for } t \in (a, t_1], \\ g_k(t,u(t)), & \text{for } t \in (t_k, s_k],\ k = 1, 2, \ldots, N, \\ g_k(s_k,u(s_k)) + \dfrac{1}{\Gamma(q)} \displaystyle\int_{s_k}^t \left(\ln\frac{t}{\tau}\right)^{q-1} f(\tau,u(\tau)) \frac{d\tau}{\tau}, & \text{for } t \in (s_k, t_{k+1}],\ k = 1, 2, \ldots, N. \end{cases} \tag{3}$$

In fact, $\widetilde{u}(t)$ satisfies conditions of fractional derivative and noninstantaneous impulses in system (1). However, we will illustrate that $\widetilde{u}(t)$ is not an equivalent integral equations of system (1).

For system (1), we have

$$\{\text{system (1)}\} \xrightarrow[\text{for } t\in(t_k,s_k],\ \forall k\in\{1,2,\ldots,N\}]{g_k(t,u(t))=u_a+(1/\Gamma(q))\int_a^t(\ln(t/\tau))^{q-1}f(\tau,u(\tau))(d\tau/\tau)}$$

$$\begin{cases} {}_{\text{C-H}}D^{q}_{a^+}u(t) = f(t,u(t)), & t \in (s_k, t_{k+1}],\ k = 0, 1, \ldots, N, \\ u(t) = u_a + \dfrac{1}{\Gamma(q)} \displaystyle\int_a^t \left(\ln\frac{t}{\tau}\right)^{q-1} f(\tau,u(\tau)) \frac{d\tau}{\tau}, & t \in (t_k, s_k],\ k = 1, 2, \ldots, N \\ u(a) = u_a \in \mathbb{C}, \end{cases} \Longleftrightarrow \tag{4}$$

$$\begin{cases} {}_{\text{C-H}}D^{q}_{a^+}u(t) = f(t,u(t)), \quad t \in (a, T], \\ u(a) = u_a \in \mathbb{C}, \end{cases} \quad (\text{using Lemma 5}) \Longleftrightarrow$$

$$u(t) = u_a + \frac{1}{\Gamma(q)} \int_a^t \left(\ln\frac{t}{\tau}\right)^{q-1} g(\tau,u(\tau)) \frac{d\tau}{\tau}, \quad \text{for } t \in (a, T]. \tag{5}$$

On the other hand, letting $g_k(t,u(t)) = u_a + (1/\Gamma(q))\int_a^t (\ln(t/\tau))^{q-1} f(\tau,u(\tau))(d\tau/\tau)$ for $t \in (t_k, s_k]$ and all $k \in \{1,2,\ldots,N\}$ in (3), we get

$$\widetilde{u}(t) = \begin{cases} u_a + \dfrac{1}{\Gamma(q)}\displaystyle\int_a^t \left(\ln\frac{t}{\tau}\right)^{q-1} f(\tau,u(\tau))\,\frac{d\tau}{\tau}, & \text{for } t \in (a,t_1], \\ u_a + \dfrac{1}{\Gamma(q)}\displaystyle\int_a^t \left(\ln\frac{t}{\tau}\right)^{q-1} f(\tau,u(\tau))\,\frac{d\tau}{\tau} & \text{for } t \in (t_k,s_k],\ k = 1,2,\ldots,N, \\ u_a + \dfrac{1}{\Gamma(q)}\left[\displaystyle\int_a^{s_k} \left(\ln\frac{s_k}{\tau}\right)^{q-1} f(\tau,u(\tau))\,\frac{d\tau}{\tau} + \int_{s_k}^t \left(\ln\frac{t}{\tau}\right)^{q-1} f(\tau,u(\tau))\,\frac{d\tau}{\tau}\right], & \text{for } t \in (s_k,t_{k+1}],\ k = 1,2,\ldots,N. \end{cases} \tag{6}$$

If $\widetilde{u}(t)$ is equivalent to system (1), then (5) is equivalent to (6). Therefore, some unfit equations can be obtained as

$$\int_a^t \left(\ln\frac{t}{\tau}\right)^{q-1} f(\tau,u(\tau))\,\frac{d\tau}{\tau} = \int_a^{s_k} \left(\ln\frac{s_k}{\tau}\right)^{q-1} f(\tau,u(\tau))\,\frac{d\tau}{\tau} + \int_{s_k}^t \left(\ln\frac{t}{\tau}\right)^{q-1} f(\tau,u(\tau))\,\frac{d\tau}{\tau}, \tag{7}$$

and here $t \in (s_k, t_{k+1}]$, $k = 1,2,\ldots,N$. Therefore, $\widetilde{u}(t)$ is not equivalent with system (1), and $\widetilde{u}(t)$ will be regarded as an *approximate solution* of system (1).

Next, considering ${}_{\text{C-H}}D^q_{a^+}u(t) = f(t,u(t))$ for $t \in (s_k, t_{k+1}]$ $(k = 0,1,\ldots,N)$ in whole interval $[a,T]$, we have

$$\begin{aligned} &{}_{\text{C-H}}D^q_{a^+}u(t) = f(t,u(t)), \quad \text{for } t \in (s_k,t_{k+1}] \subset [a,T] \Longleftrightarrow \\ &u(t) = C_k + u_a + \frac{1}{\Gamma(q)}\int_a^t \left(\ln\frac{t}{\tau}\right)^{q-1} f(\tau,u(\tau))\,\frac{d\tau}{\tau}, \quad \text{for } t \in (s_k,t_{k+1}] \subset [a,T], \text{ here } C_k \text{ are some constants.} \end{aligned} \tag{8}$$

Substituting (8) into (1), we obtain $C_0 = 0$ and

$$C_k = g_k(s_k,u(s_k)) - u_a - \frac{1}{\Gamma(q)}\int_a^{s_k} \left(\ln\frac{s_k}{\tau}\right)^{q-1} f(\tau,u(\tau))\,\frac{d\tau}{\tau}, \quad k = 1,2,\ldots,N. \tag{9}$$

Hence, substituting (8) and (9) into (1), we get

$$u(t) = \begin{cases} u_a + \dfrac{1}{\Gamma(q)}\displaystyle\int_a^t \left(\ln\frac{t}{\tau}\right)^{q-1} f(\tau,u(\tau))\,\frac{d\tau}{\tau}, & \text{for } t \in (a,t_1], \\ g_k(t,u(t)), & \text{for } t \in (t_k,s_k],\ k = 1,2,\ldots,N, \\ g_k(s_k,u(s_k)) + \dfrac{1}{\Gamma(q)}\left[\displaystyle\int_a^t \left(\ln\frac{t}{\tau}\right)^{q-1} f(\tau,u(\tau))\,\frac{d\tau}{\tau} - \int_a^{s_k} \left(\ln\frac{s_k}{\tau}\right)^{q-1} f(\tau,u(\tau))\,\frac{d\tau}{\tau}\right] & \text{for } t \in (s_k,t_{k+1}],\ k = 1,2,\ldots,N. \end{cases} \tag{10}$$

Obviously, (10) satisfies the conditions in system (1) and

$$\lim_{\substack{g_k(t,u(t))=u_a+(1/\Gamma(q))\int_a^t(\ln(t/\tau))^{q-1}f(\tau,u(\tau))(d\tau/\tau)\\ \text{for } t\in(t_k,s_k],\ \forall k\in\{1,2,\ldots,N\}}} \{\text{Eq. (10)}\} \Longleftrightarrow \lim_{\substack{g_k(t,u(t))=u_a+(1/\Gamma(q))\int_a^t(\ln(t/\tau))^{q-1}f(\tau,u(\tau))(d\tau/\tau)\\ \text{for } t\in(t_k,s_k],\ \forall k\in\{1,2,\ldots,N\}}} \{\text{system (1)}\}. \tag{11}$$

Therefore, (10) is a solution of system (1).

Remark 1. Equation (10) is only a *particular solution* of system (1) because it does not contain the important part $\int_{s_k}^{t}(\ln(t/\tau))^{q-1}f(\tau,u(\tau))(d\tau/\tau)$ of the approximate solution $\widetilde{u}(t)$.

Next, some definitions and conclusions are introduced in Section 2, the equivalent integral equation will be given for differential equation with Caputo-Hadamard fractional derivatives and noninstantaneous impulses in Section 3, and an example will show that there exists the general solution for this fractional differential equation with noninstantaneous impulses in Section 4.

2. Preliminaries

Definition 2 (see [5, p. 110]). Let $0 \le a \le b \le \infty$ be finite or infinite interval of the half-axis $\mathbb{R}^+$. The left-sided Hadamard fractional integral of order $\alpha \in \mathbb{C}$ $(\Re(\alpha) > 0)$ of function $\varphi(x)$ is defined by

$${}_{\mathrm{H}}\mathcal{J}_{a^+}^{\alpha}\varphi(x) = \frac{1}{\Gamma(\alpha)}\int_a^x \left(\ln\frac{x}{s}\right)^{\alpha-1}\varphi(s)\frac{ds}{s}, \quad (a < x < b), \tag{12}$$

where $\Gamma(\cdot)$ is the Gamma function.

The left-sided Caputo-Hadamard fractional derivative ${}_{\mathrm{C\text{-}H}}D_{a^+}^{\alpha}\varphi(x)$ is presented in [12] by the following.

Definition 3 (see [12, p. 4]). Let $\Re(\alpha) \ge 0$ and $n = [\Re(\alpha)] + 1$ and $\varphi \in \{\varphi : [a,b] \to \mathbb{C} : \delta^{(n-1)}\varphi(x) \in AC[a,b]\}$, $0 < a < b < \infty$. Then ${}_{\mathrm{C\text{-}H}}D_{a^+}^{\alpha}\varphi(x)$ exist everywhere on $[a,b]$ and if $\alpha \notin \mathbb{N}_0$,

$$\begin{aligned} {}_{\mathrm{C\text{-}H}}D_{a^+}^{\alpha}\varphi(x) &= \frac{1}{\Gamma(n-\alpha)}\int_a^x \left(\ln\frac{x}{s}\right)^{n-\alpha-1}\delta^n\varphi(s)\frac{ds}{s} \\ &= {}_{\mathrm{H}}\mathcal{J}_{a^+}^{n-\alpha}\delta^n\varphi(x), \end{aligned} \tag{13}$$

where differential operator $\delta = x(d/dx)$ and $\delta^0 y(x) = y(x)$.

Lemma 4 (see [12, p. 5]). *Let $\Re(\alpha) > 0$, $n = [\Re(\alpha)] + 1$, and $\varphi \in C[a,b]$. If $\Re(\alpha) \ne 0$ or $\alpha \in \mathbb{N}$, then*

$${}_{C\text{-}H}D_{a^+}^{\alpha}\left({}_{H}\mathcal{J}_{a^+}^{\alpha}\varphi\right)(x) = \varphi(x). \tag{14}$$

Lemma 5 (see [12, p. 6]). *Let $\varphi \in AC_{\delta}^{n}[a,b]$ or $C_{\delta}^{n}[a,b]$ and $\alpha \in \mathbb{C}$, then*

$${}_{H}\mathcal{J}_{a^+}^{\alpha}\left({}_{C\text{-}H}D_{a^+}^{\alpha}\varphi\right)(x) = \varphi(x) - \sum_{k=0}^{n-1}\frac{\delta^k\varphi(a)}{k!}\left(\ln\frac{x}{a}\right)^k. \tag{15}$$

Lemma 6 (see [15, p 4]). *Let $0 < \Re(q) < 1$ and ξ is a constant. A function $u(t) : [a,T] \to \mathbb{C}$ is general solution of the system*

$$\begin{aligned} &{}_{C\text{-}H}D_{a^+}^{q}u(t) = h(t,u(t)), \quad t \in (a,T],\ t \ne t_k\ (k = 1,2,\ldots,m), \\ &\Delta u|_{t=t_k} = u(t_k^+) - u(t_k^-) = \Delta_k(u(t_k^-)) \in \mathbb{C}, \quad k = 1,2,\ldots,m, \\ &u(a) = u_a, \quad u_a \in \mathbb{C}, \end{aligned} \tag{16}$$

if and only if $u(t)$ satisfies the fraction integral equation

$$u(t) = \begin{cases} u_a + \dfrac{1}{\Gamma(q)}\displaystyle\int_a^t\left(\ln\frac{t}{s}\right)^{q-1}h\frac{ds}{s}, & \text{for } t \in (a,t_1], \\ u_a + \displaystyle\sum_{i=1}^{k}\Delta_i(u(t_i^-)) + \dfrac{1}{\Gamma(q)}\displaystyle\int_a^t\left(\ln\frac{t}{s}\right)^{q-1}h\frac{ds}{s} & \\ \quad + \xi\displaystyle\sum_{i=1}^{k}\dfrac{\Delta_i(u(t_i^-))}{\Gamma(q)}\left[\displaystyle\int_a^{t_i}\left(\ln\frac{t_i}{s}\right)^{q-1}h\frac{ds}{s} + \int_{t_i}^{t}\left(\ln\frac{t}{s}\right)^{q-1}h\frac{ds}{s} - \int_a^t\left(\ln\frac{t}{s}\right)^{q-1}h\frac{ds}{s}\right] & \text{for } t \in (t_k,t_{k+1}],\ k = 1,2,\ldots,m. \end{cases} \tag{17}$$

provided that the integral in (17) exists, and here $h = h(s, u(s))$.

3. Main Result

Theorem 7. *Let* ξ_k *(here* $k = 1, 2, \ldots, N$*) be some arbitrary constants. System (1) is equivalent to*

$$u(t) = \begin{cases} u_a + \dfrac{1}{\Gamma(q)} \displaystyle\int_a^t \left(\ln \frac{t}{\tau}\right)^{q-1} f \frac{d\tau}{\tau} & \text{for } t \in (a, t_1], \\ g_k(t, u(t)) & \text{for } t \in (t_k, s_k],\ k = 1, 2, \ldots, N, \\ g_k(s_k, u(s_k)) - \dfrac{1}{\Gamma(q)} \displaystyle\int_a^{s_k} \left(\ln \frac{s_k}{\tau}\right)^{q-1} f \frac{d\tau}{\tau} + \dfrac{1}{\Gamma(q)} \displaystyle\int_a^t \left(\ln \frac{t}{\tau}\right)^{q-1} f \frac{d\tau}{\tau} & \\ \quad + \dfrac{\xi_k}{\Gamma(q)} \left[g_k(s_k, u(s_k)) - u_a - \dfrac{1}{\Gamma(q)} \displaystyle\int_a^{s_k} \left(\ln \frac{s_k}{\tau}\right)^{q-1} f \frac{d\tau}{\tau} \right] & \\ \quad \times \left[\displaystyle\int_a^{s_k} \left(\ln \frac{s_k}{\tau}\right)^{q-1} f \frac{d\tau}{\tau} + \int_{s_k}^t \left(\ln \frac{t}{\tau}\right)^{q-1} f \frac{d\tau}{\tau} - \int_a^t \left(\ln \frac{t}{\tau}\right)^{q-1} f \frac{d\tau}{\tau} \right] & \text{for } t \in (s_k, t_{k+1}],\ k = 1, 2, \ldots, N, \end{cases} \tag{18}$$

provided that the integral in (18) exists, and here $f = f(\tau, u(\tau))$.

Proof.

Step 1 (Necessity). We will verify that (18) satisfies all conditions of system (1). For convenience, we divide this section into three steps.

Step 1.1. Equation (18) satisfies the fractional derivative in system (1).

By (18), for $t \in (s_k, t_{k+1}]$ (here $k = 0, 1, \ldots, N$), we get

$$\begin{aligned} {}_{\text{C-H}}D^q_{a^+} u(t) = {}& {}_{\text{C-H}}D^q_{a^+} \left\{ g_k(s_k, u(s_k)) - \frac{1}{\Gamma(q)} \right. \\ & \cdot \int_a^{s_k} \left(\ln \frac{s_k}{\tau}\right)^{q-1} f \frac{d\tau}{\tau} + \frac{1}{\Gamma(q)} \int_a^t \left(\ln \frac{t}{\tau}\right)^{q-1} f \frac{d\tau}{\tau} \\ & + \frac{\xi_k}{\Gamma(q)} \left(g_k(s_k, u(s_k)) - u_a \right. \\ & \left. - \frac{1}{\Gamma(q)} \int_a^{s_k} \left(\ln \frac{s_k}{\tau}\right)^{q-1} f \frac{d\tau}{\tau} \right) \\ & \times \left[\int_a^{s_k} \left(\ln \frac{s_k}{\tau}\right)^{q-1} f \frac{d\tau}{\tau} + \int_{s_k}^t \left(\ln \frac{t}{\tau}\right)^{q-1} f \frac{d\tau}{\tau} \right. \\ & \left. \left. - \int_a^t \left(\ln \frac{t}{\tau}\right)^{q-1} f \frac{d\tau}{\tau} \right] \right\} = f(t, u(t))\big|_{t \in (s_k, t_{k+1}]} \\ & + \frac{\xi_k}{\Gamma(q)} \left(g_k(s_k, u(s_k)) - u_a - \frac{1}{\Gamma(q)} \right. \\ & \left. \cdot \int_a^{s_k} \left(\ln \frac{s_k}{\tau}\right)^{q-1} f \frac{d\tau}{\tau} \right) \\ & \times \left[{}_{\text{C-H}}D^q_{s_k^+} \left(\int_{s_k}^t \left(\ln \frac{t}{\tau}\right)^{q-1} f \frac{d\tau}{\tau} \right) \right. \\ & \left. - {}_{\text{C-H}}D^q_{a^+} \left(\int_a^t \left(\ln \frac{t}{\tau}\right)^{q-1} f \frac{d\tau}{\tau} \right) \right]_{t \in (s_k, t_{k+1}]} \\ = {}& f(t, u(t))\big|_{t \in (s_k, t_{k+1}]}. \end{aligned} \tag{19}$$

So, (18) satisfies the fractional derivative in system (1).

Step 1.2. We can verify that (18) satisfies noninstantaneous impulses and initial value in system (1).

Step 1.3. Verify that (18) satisfies a hidden condition of system (1).

Letting $g_k(t, u(t)) = u_a + (1/\Gamma(q)) \int_a^t (\ln(t/\tau))^{q-1} f(d\tau/\tau)$ for $t \in (t_k, s_k]$ and all $k \in \{1, 2, \ldots, N\}$ in (18), we obtain

$$\lim_{\substack{g_k(t,u(t)) = u_a + (1/\Gamma(q)) \int_a^t (\ln(t/\tau))^{q-1} f(d\tau/\tau) \\ \forall k \in \{1,2,\ldots,N\},\, t \in (t_k, s_k]}} u(t)$$

$$= \lim_{\substack{g_k(t,u(t)) = u_a + (1/\Gamma(q)) \int_a^t (\ln(t/\tau))^{q-1} f(d\tau/\tau) \\ \forall k \in \{1,2,\ldots,N\},\, t \in (t_k, s_k]}} \begin{cases} u_a + \dfrac{1}{\Gamma(q)} \displaystyle\int_a^t \left(\ln \frac{t}{\tau}\right)^{q-1} f \frac{d\tau}{\tau}, & \text{for } t \in (a, t_1], \\ g_k(t, u(t)), & \text{for } t \in (t_k, s_k],\ k = 1, 2, \ldots, N, \\ g_k(s_k, u(s_k)) - \dfrac{1}{\Gamma(q)} \displaystyle\int_a^{s_k} \left(\ln \frac{s_k}{\tau}\right)^{q-1} f \frac{d\tau}{\tau} + \dfrac{1}{\Gamma(q)} \displaystyle\int_a^t \left(\ln \frac{t}{\tau}\right)^{q-1} f \frac{d\tau}{\tau} & \\ \quad + \dfrac{\xi_k}{\Gamma(q)} \left(g_k(s_k, u(s_k)) - u_a - \dfrac{1}{\Gamma(q)} \displaystyle\int_a^{s_k} \left(\ln \frac{s_k}{\tau}\right)^{q-1} f \frac{d\tau}{\tau} \right) & \\ \quad \times \left[\displaystyle\int_a^{s_k} \left(\ln \frac{s_k}{\tau}\right)^{q-1} f \frac{d\tau}{\tau} + \int_{s_k}^t \left(\ln \frac{t}{\tau}\right)^{q-1} f \frac{d\tau}{\tau} - \int_a^t \left(\ln \frac{t}{\tau}\right)^{q-1} f \frac{d\tau}{\tau} \right] & \text{for } t \in (s_k, t_{k+1}],\ k = 1, 2, \ldots, N, \end{cases}$$

$$= \begin{cases} u_a + \dfrac{1}{\Gamma(q)} \displaystyle\int_a^t \left(\ln \frac{t}{\tau}\right)^{q-1} f \frac{d\tau}{\tau} & \text{for } t \in (a, t_1], \\ u_a + \dfrac{1}{\Gamma(q)} \displaystyle\int_a^t \left(\ln \frac{t}{\tau}\right)^{q-1} f \frac{d\tau}{\tau} & \text{for } t \in (t_k, s_k],\ k = 1, 2, \ldots, N, \\ u_a + \dfrac{1}{\Gamma(q)} \displaystyle\int_a^t \left(\ln \frac{t}{\tau}\right)^{q-1} f \frac{d\tau}{\tau} & \text{for } t \in (s_k, t_{k+1}],\ k = 1, 2, \ldots, N. \end{cases} \tag{20}$$

Moreover, it is sure that (20) is the solution of system (4) by Lemma 5. Thus, (18) satisfies all conditions of system (1).

Step 2 (Sufficiency). We will verify that the solution of system (1) satisfies (18). For convenience, we divide this section into three steps.

Step 2.1. Verify that the solution of system (1) satisfies (18) in intervals $(a, t_1]$ and $(t_1, s_1]$.

By Lemma 5, the solution of (1) satisfies

$$u(t) = u_a + \frac{1}{\Gamma(q)} \int_a^t \left(\ln \frac{t}{\tau}\right)^{q-1} f \frac{d\tau}{\tau} \quad \text{for } t \in (a, t_1], \tag{21}$$

and $u(t) = g_1(t, u(t))$ for $t \in (t_1, s_1]$.

Step 2.2. Verify that the solution of system (1) satisfies (18) in intervals $(s_1, t_2]$ and $(t_2, s_2]$.

For $t \in (s_1, t_2]$, the approximate solution (by the above discussion about $\widetilde{u}(t)$) is given as

$$\widetilde{u}(t) = g_1(s_1, u(s_1)) + \frac{1}{\Gamma(q)} \int_{s_1}^t \left(\ln \frac{t}{\tau}\right)^{q-1} f \frac{d\tau}{\tau} \quad \text{for } t \in (s_1, t_2], \tag{22}$$

with error $e_1(t) = u(t) - \widetilde{u}(t)$ for $t \in (s_1, t_2]$. By the particular solution (10), the exact solution $u(t)$ of system (1) satisfies

$$\lim_{[g_1(s_1,u(s_1))-u_a-(1/\Gamma(q))\int_a^{s_1}(\ln(s_1/\tau))^{q-1} f(d\tau/\tau)]\to 0} u(t) = u_a + \frac{1}{\Gamma(q)} \int_a^t \left(\ln \frac{t}{\tau}\right)^{q-1} f \frac{d\tau}{\tau} \quad \text{for } t \in (s_1, t_2]. \tag{23}$$

Thus,

$$\lim_{[g_1(s_1,u(s_1))-u_a-(1/\Gamma(q))\int_a^{s_1}(\ln(s_1/\tau))^{q-1} f(d\tau/\tau)]\to 0} e_1(t) = \lim_{[g_1(s_1,u(s_1))-u_a-(1/\Gamma(q))\int_a^{s_1}(\ln(s_1/\tau))^{q-1} f(d\tau/\tau)]\to 0} \{u(t) - \widetilde{u}(t)\} = \frac{1}{\Gamma(q)} \left[\int_a^t \left(\ln \frac{t}{\tau}\right)^{q-1} f \frac{d\tau}{\tau} - \int_a^{s_1} \left(\ln \frac{s_1}{\tau}\right)^{q-1} f \frac{d\tau}{\tau} - \int_{s_1}^t \left(\ln \frac{t}{\tau}\right)^{q-1} f \frac{d\tau}{\tau}\right]. \tag{24}$$

Therefore, suppose

$$\begin{aligned} e_1(t) = \frac{1}{\Gamma(q)} \gamma \Bigg(& g_1(s_1, u(s_1)) - u_a \\ & - \frac{1}{\Gamma(q)} \int_a^{s_1} \left(\ln \frac{s_1}{\tau}\right)^{q-1} f \frac{d\tau}{\tau} \Bigg) \\ & \times \left[\int_a^t \left(\ln \frac{t}{\tau}\right)^{q-1} f \frac{d\tau}{\tau} - \int_a^{s_1} \left(\ln \frac{s_1}{\tau}\right)^{q-1} f \frac{d\tau}{\tau} \right. \\ & \left. - \int_{s_1}^t \left(\ln \frac{t}{\tau}\right)^{q-1} f \frac{d\tau}{\tau}\right], \end{aligned} \tag{25}$$

where γ is an undetermined function with $\gamma(0) = 1$. Thus,

$$\begin{aligned} u(t) = \widetilde{u}(t) + e_1(t) = & g_1(s_1, u(s_1)) - \frac{1}{\Gamma(q)} \\ & \cdot \int_a^{s_1} \left(\ln \frac{s_1}{\tau}\right)^{q-1} f \frac{d\tau}{\tau} + \frac{1}{\Gamma(q)} \int_a^t \left(\ln \frac{t}{\tau}\right)^{q-1} f \frac{d\tau}{\tau} \\ & + \frac{1}{\Gamma(q)} \left[1 - \gamma \Bigg(g_1(s_1, u(s_1)) - u_a \right. \\ & \left. - \frac{1}{\Gamma(q)} \int_a^{s_1} \left(\ln \frac{s_1}{\tau}\right)^{q-1} f \frac{d\tau}{\tau} \Bigg)\right] \\ & \times \left[\int_a^{s_1} \left(\ln \frac{s_1}{\tau}\right)^{q-1} f \frac{d\tau}{\tau} + \int_{s_1}^t \left(\ln \frac{t}{\tau}\right)^{q-1} f \frac{d\tau}{\tau} \right. \\ & \left. - \int_a^t \left(\ln \frac{t}{\tau}\right)^{q-1} f \frac{d\tau}{\tau}\right] \quad \text{for } t \in (s_1, t_2]. \end{aligned} \tag{26}$$

On the other hand, letting $t_1 \to s_1$, we get

$$\begin{aligned}
&\lim_{t_1 \to s_1} \begin{cases} \left({}_{\text{C-H}}D^{q}_{a+}u\right)(t) = f\left(t, u\left(t\right)\right), & t \in \left(s_k, t_{k+1}\right], \ k = 0, 1, \\ u\left(t\right) = g_1\left(t, u\left(t\right)\right), & t \in \left(t_1, s_1\right], \\ u\left(a\right) = u_a \in \mathbb{C}, \end{cases} \\
&= \begin{cases} \left({}_{\text{C-H}}D^{q}_{a+}u\right)(t) = f\left(t, u\left(t\right)\right), & t \in \left(s_k, t_{k+1}\right], \ k = 0, 1, \\ u\left(s_1\right) = g_1\left(s_1, u\left(s_1\right)\right), \\ u\left(a\right) = u_a \in \mathbb{C}, \end{cases} \\
&= \begin{cases} \left({}_{\text{C-H}}D^{q}_{a+}u\right)(t) = f\left(t, u\left(t\right)\right), & t \in \left(s_k, t_{k+1}\right], \ k = 0, 1, \\ u\left(s_1^{+}\right) - u\left(s_1^{-}\right) = g_1\left(s_1, u\left(s_1\right)\right) - u_a - \dfrac{1}{\Gamma\left(q\right)} \displaystyle\int_a^{s_1} \left(\ln \frac{s_1}{\tau}\right)^{q-1} f \frac{d\tau}{\tau}, \\ u\left(a\right) = u_a \in \mathbb{C}. \end{cases}
\end{aligned} \tag{27}$$

By using Lemma 6 to (27), we get $1 - \gamma(z) = \xi_1 z, \forall z \in \mathbb{C}$, and here ξ_1 is an arbitrary constant. Thus,

$$\begin{aligned}
u\left(t\right) &= g_1\left(s_1, u\left(s_1\right)\right) - \frac{1}{\Gamma\left(q\right)} \int_a^{s_1} \left(\ln \frac{s_1}{\tau}\right)^{q-1} f \frac{d\tau}{\tau} \\
&+ \frac{1}{\Gamma\left(q\right)} \int_a^{t} \left(\ln \frac{t}{\tau}\right)^{q-1} f \frac{d\tau}{\tau} + \frac{\xi_1}{\Gamma\left(q\right)} \Bigg(g_1\left(s_1, u\left(s_1\right)\right) \\
&- u_a - \frac{1}{\Gamma\left(q\right)} \int_a^{s_1} \left(\ln \frac{s_1}{\tau}\right)^{q-1} f \frac{d\tau}{\tau} \Bigg) \\
&\times \left[\int_a^{s_1} \left(\ln \frac{s_1}{\tau}\right)^{q-1} f \frac{d\tau}{\tau} + \int_{s_1}^{t} \left(\ln \frac{t}{\tau}\right)^{q-1} f \frac{d\tau}{\tau} \right. \\
&\left. - \int_a^{t} \left(\ln \frac{t}{\tau}\right)^{q-1} f \frac{d\tau}{\tau} \right] \quad \text{for } t \in \left(s_1, t_2\right].
\end{aligned} \tag{28}$$

And $u(t) = g_2(t, u(t))$ for $t \in (t_2, s_2]$.

Step 2.3. Verify that the solution of system (1) satisfies (18) in intervals $(s_k, t_{k+1}]$ and $(t_{k+1}, s_{k+1}]$.

The approximate solution as $t \in (s_k, t_{k+1}]$ is given by

$$\begin{aligned}
\widetilde{u}\left(t\right) &= g_k\left(s_k, u\left(s_k\right)\right) + \frac{1}{\Gamma\left(q\right)} \int_{s_k}^{t} \left(\ln \frac{t}{\tau}\right)^{q-1} f \frac{d\tau}{\tau} \\
&\qquad \text{for } t \in \left(s_k, t_{k+1}\right], \ k = 1, 2, \ldots, N,
\end{aligned} \tag{29}$$

with error $e_k(t) = u(t) - \widetilde{u}(t)$ for $t \in (s_k, t_{k+1}]$. Moreover, by the particular solution (10), the exact solution of system (1) satisfies

$$\begin{aligned}
&\lim_{[g_k(s_k, u(s_k)) - u_a - (1/\Gamma(q)) \int_a^{s_k} (\ln(s_k/\tau))^{q-1} f(d\tau/\tau)] \to 0} u\left(t\right) \\
&= u_a + \frac{1}{\Gamma\left(q\right)} \int_a^{t} \left(\ln \frac{t}{\tau}\right)^{q-1} f \frac{d\tau}{\tau} \\
&\qquad \text{for } t \in \left(s_k, t_{k+1}\right].
\end{aligned} \tag{30}$$

Thus,

$$\begin{aligned}
&\lim_{[g_k(s_k, u(s_k)) - u_a - (1/\Gamma(q)) \int_a^{s_k} (\ln(s_k/\tau))^{q-1} f(d\tau/\tau)] \to 0} e_k\left(t\right) \\
&= \lim_{[g_k(s_k, x(s_k)) - u_a - (1/\Gamma(q)) \int_a^{s_k} (\ln(s_k/\tau))^{q-1} f(d\tau/\tau)] \to 0} \{u\left(t\right) \\
&- \widetilde{u}\left(t\right)\} = \frac{1}{\Gamma\left(q\right)} \left[\int_a^{t} \left(\ln \frac{t}{\tau}\right)^{q-1} f \frac{d\tau}{\tau} \right. \\
&\left. - \int_a^{s_k} \left(\ln \frac{s_k}{\tau}\right)^{q-1} f \frac{d\tau}{\tau} - \int_{s_k}^{t} \left(\ln \frac{t}{\tau}\right)^{q-1} f \frac{d\tau}{\tau} \right].
\end{aligned} \tag{31}$$

Therefore, suppose

$$\begin{aligned}
e_k\left(t\right) &= \varpi \Bigg(g_k\left(s_k, u\left(s_k\right)\right) - u_a \\
&- \frac{1}{\Gamma\left(q\right)} \int_a^{s_k} \left(\ln \frac{s_k}{\tau}\right)^{q-1} f \frac{d\tau}{\tau} \Bigg) \\
&\cdot \lim_{[g_k(s_k, u(s_k)) - u_a - (1/\Gamma(q)) \int_a^{s_k} (\ln(s_k/\tau))^{q-1} f(d\tau/\tau)] \to 0} e_k\left(t\right) \\
&= \frac{-1}{\Gamma\left(q\right)} \varpi \Bigg(g_k\left(s_k, u\left(s_k\right)\right) - u_a \\
&- \frac{1}{\Gamma\left(q\right)} \int_a^{s_k} \left(\ln \frac{s_k}{\tau}\right)^{q-1} f \frac{d\tau}{\tau} \Bigg) \\
&\times \left[\int_a^{s_k} \left(\ln \frac{s_k}{\tau}\right)^{q-1} f \frac{d\tau}{\tau} + \int_{s_k}^{t} \left(\ln \frac{t}{\tau}\right)^{q-1} f \frac{d\tau}{\tau} \right. \\
&\left. - \int_a^{t} \left(\ln \frac{t}{\tau}\right)^{q-1} f \frac{d\tau}{\tau} \right],
\end{aligned} \tag{32}$$

where ϖ is an undetermined function with $\varpi(0) = 1$. Therefore,

$$\begin{aligned} u(t) &= \widetilde{u}(t) + e_k(t) = g_k(s_k, u(s_k)) - \frac{1}{\Gamma(q)} \\ &\cdot \int_a^{s_k} \left(\ln \frac{s_k}{\tau}\right)^{q-1} f \frac{d\tau}{\tau} + \frac{1}{\Gamma(q)} \int_a^t \left(\ln \frac{t}{\tau}\right)^{q-1} f \frac{d\tau}{\tau} \\ &+ \frac{1}{\Gamma(q)} \left\{ 1 - \varpi \left(g_k(s_k, u(s_k)) - u_a \right. \right. \\ &\left. \left. - \frac{1}{\Gamma(q)} \int_a^{s_k} \left(\ln \frac{s_k}{\tau}\right)^{q-1} f \frac{d\tau}{\tau} \right) \right\} \\ &\times \left[\int_a^{s_k} \left(\ln \frac{s_k}{\tau}\right)^{q-1} f \frac{d\tau}{\tau} + \int_{s_k}^t \left(\ln \frac{t}{\tau}\right)^{q-1} f \frac{d\tau}{\tau} \right. \\ &\left. - \int_a^t \left(\ln \frac{t}{\tau}\right)^{q-1} f \frac{d\tau}{\tau} \right] \quad \text{for } t \in (s_k, t_{k+1}]. \end{aligned} \tag{33}$$

On the other hand, consider a special case of system (1) as

$$\begin{aligned} &\lim_{t_k \to s_k} \begin{cases} {}_{\text{C-H}}D_{a+}^q u(t) = f(t, u(t)), & t \in (s_i, t_{i+1}],\ i = 0, 1, \ldots, k, \\ u(t) = u_a + \dfrac{1}{\Gamma(q)} \displaystyle\int_a^t \left(\ln \frac{t}{\tau}\right)^{q-1} f(\tau, u(\tau)) \frac{d\tau}{\tau}, & t \in (t_i, s_i],\ i = 1, 2, \ldots, k-1, \\ u(t) = g_k(t, u(t)), & t \in (t_k, s_k], \\ u(a) = u_a \in \mathbb{C}, \end{cases} \\ &= \begin{cases} \left({}_{\text{C-H}}D_{a+}^q u\right)(t) = f(t, u(t)), & t \in (s_i, t_{i+1}],\ i = 0, 1, \ldots, k, \\ u(t) = u_a + \dfrac{1}{\Gamma(q)} \displaystyle\int_a^t \left(\ln \frac{t}{\tau}\right)^{q-1} f(\tau, u(\tau)) \frac{d\tau}{\tau}, & t \in (t_i, s_i],\ i = 1, 2, \ldots, k-1, \\ u(s_k) = g_k(s_k, u(s_k)), \\ u(a) = u_a \in \mathbb{C}, \end{cases} \\ &= \begin{cases} \left({}_{\text{C-H}}D_{a+}^q u\right)(t) = f(t, u(t)), & t \in (s_i, t_{i+1}],\ i = 0, 1, \ldots, k, \\ u(t) = u_a + \dfrac{1}{\Gamma(q)} \displaystyle\int_a^t \left(\ln \frac{t}{\tau}\right)^{q-1} f(\tau, u(\tau)) \frac{d\tau}{\tau}, & t \in (t_i, s_i],\ i = 1, 2, \ldots, k-1, \\ u(s_k^+) - u(s_k^-) = g_k(s_k, u(s_k)) - u_a - \dfrac{1}{\Gamma(q)} \displaystyle\int_a^{s_k} \left(\ln \frac{s_k}{\tau}\right)^{q-1} f(\tau, u(\tau)) \frac{d\tau}{\tau}, \\ u(a) = u_a \in \mathbb{C}. \end{cases} \end{aligned} \tag{34}$$

Using Lemma 6 for system (34), we obtain $1 - \varpi(z) = \xi_k z$, $\forall z \in \mathbb{C}$, and here ξ_k is an arbitrary constant. Thus

$$\begin{aligned} u(t) &= g_k(s_k, u(s_k)) - \frac{1}{\Gamma(q)} \int_a^{s_k} \left(\ln \frac{s_k}{\tau}\right)^{q-1} f \frac{d\tau}{\tau} \\ &+ \frac{1}{\Gamma(q)} \int_a^t \left(\ln \frac{t}{\tau}\right)^{q-1} f \frac{d\tau}{\tau} + \frac{\xi_k}{\Gamma(q)} \left(g_k(s_k, u(s_k)) \right. \\ &\left. - u_a - \frac{1}{\Gamma(q)} \int_a^{s_k} \left(\ln \frac{s_k}{\tau}\right)^{q-1} f \frac{d\tau}{\tau} \right) \\ &\times \left[\int_a^{s_k} \left(\ln \frac{s_k}{\tau}\right)^{q-1} f \frac{d\tau}{\tau} + \int_{s_k}^t \left(\ln \frac{t}{\tau}\right)^{q-1} f \frac{d\tau}{\tau} \right. \\ &\left. - \int_a^t \left(\ln \frac{t}{\tau}\right)^{q-1} f \frac{d\tau}{\tau} \right] \quad \text{for } t \in (s_k, t_{k+1}]. \end{aligned} \tag{35}$$

By "Sufficiency" and "Necessity," system (1) is equivalent to (18). The proof is completed. □

4. Examples

In this section, we will give an impulsive fractional system to illustrate that there exists general solution for fractional differential equations with noninstantaneous impulses.

Example 1. Let us consider the following impulsive linear fractional system:

$$\begin{aligned} \left({}_{\text{C-H}}D_{1+}^{1/2} u\right)(t) &= \ln t, \quad t \in \left(1, \frac{\pi}{2}\right] \cup (\pi, 2\pi], \\ u(t) &= \sin t, \quad t \in \left(\frac{\pi}{2}, \pi\right], \\ u(1) &= 1. \end{aligned} \tag{36}$$

By Theorem 7, system (36) has general solution

$$u(t)=\begin{cases}1+\dfrac{1}{\Gamma(1/2)}\displaystyle\int_1^t\left(\ln\frac{t}{\tau}\right)^{1/2-1}\ln\tau\frac{d\tau}{\tau}, & \text{for } t\in\left(1,\dfrac{\pi}{2}\right],\\ \sin t, & \text{for } t\in\left(\dfrac{\pi}{2},\pi\right],\\ -\dfrac{1}{\Gamma(1/2)}\displaystyle\int_1^\pi\left(\ln\frac{\pi}{\tau}\right)^{1/2-1}\ln\tau\frac{d\tau}{\tau}+\dfrac{1}{\Gamma(1/2)}\displaystyle\int_1^t\left(\ln\frac{t}{\tau}\right)^{1/2-1}\ln\tau\frac{d\tau}{\tau} & \\ \quad+\dfrac{\xi}{\Gamma(1/2)}\left[-1-\dfrac{1}{\Gamma(1/2)}\displaystyle\int_1^\pi\left(\ln\frac{\pi}{\tau}\right)^{1/2-1}\ln\tau\frac{d\tau}{\tau}\right] & \\ \quad\times\left[\displaystyle\int_1^\pi\left(\ln\frac{\pi}{\tau}\right)^{1/2-1}\ln\tau\frac{d\tau}{\tau}+\int_\pi^t\left(\ln\frac{t}{\tau}\right)^{1/2-1}\ln\tau\frac{d\tau}{\tau}-\int_1^t\left(\ln\frac{t}{\tau}\right)^{1/2-1}\ln\tau\frac{d\tau}{\tau}\right], & \text{for } t\in(\pi,2\pi],\end{cases}\tag{37}$$

where ξ is a constant. After some elementary computation, (37) can be rewritten by

$$u(t)=\begin{cases}1+\dfrac{4}{3\sqrt{\pi}}(\ln t)^{3/2}, & \text{for } t\in\left(1,\dfrac{\pi}{2}\right],\\ \sin t, & \text{for } t\in\left(\dfrac{\pi}{2},\pi\right],\\ -\dfrac{4}{3\sqrt{\pi}}(\ln\pi)^{3/2}+\dfrac{4}{3\sqrt{\pi}}(\ln t)^{3/2}\Big|_{t>1}+\dfrac{2\xi}{3\sqrt{\pi}}\left[-1-\dfrac{4}{3\sqrt{\pi}}(\ln\pi)^{3/2}\right] & \\ \quad\times\left[2(\ln\pi)^{3/2}+\left(\ln\dfrac{t}{\pi}\right)^{1/2}(2\ln t+\ln\pi)\Big|_{t>\pi}-2(\ln t)^{3/2}\Big|_{t>1}\right], & \text{for } t\in(\pi,2\pi].\end{cases}\tag{38}$$

Next, let us verify that (38) satisfies all conditions of system (36). By Definition 3, we have

$$\begin{aligned}
&{}_{\text{C-H}}D_{1+}^{1/2}\left(\frac{4}{3\sqrt{\pi}}(\ln t)^{3/2}\right)=\frac{1}{\Gamma(1-1/2)}\frac{4}{3\sqrt{\pi}}\\
&\quad\cdot\int_1^t\left(\ln\frac{t}{s}\right)^{1-1/2-1}\delta\left((\ln s)^{3/2}\right)\frac{ds}{s}=\frac{1}{\Gamma(1/2)}\\
&\quad\cdot\frac{4}{3\sqrt{\pi}}\int_1^t\left(\ln\frac{t}{s}\right)^{1-1/2-1}\frac{3}{2}(\ln s)^{1/2}\frac{ds}{s}=\ln t\\
&{}_{\text{C-H}}D_{1+}^{1/2}\left[\left(\ln\frac{t}{\pi}\right)^{1/2}(2\ln t+\ln\pi)\Big|_{t>\pi}\right]\\
&\quad=\frac{1}{\Gamma(1-1/2)}\int_1^t\left(\ln\frac{t}{s}\right)^{1-1/2-1}\\
&\quad\cdot\delta\left[\left(\ln\frac{s}{\pi}\right)^{1/2}(2\ln s+\ln\pi)\Big|_{t>\pi}\right]\frac{ds}{s}\\
&\quad=\frac{1}{\Gamma(1/2)}\int_\pi^t\left(\ln\frac{t}{s}\right)^{1-1/2-1}\\
&\quad\cdot\delta\left[\left(\ln\frac{s}{\pi}\right)^{1/2}(2\ln s+\ln\pi)\right]\frac{ds}{s}=\frac{1}{\Gamma(1/2)}\\
&\quad\cdot\int_\pi^t\left(\ln\frac{t}{s}\right)^{1-1/2-1}\left[2\left(\ln\frac{s}{\pi}\right)^{1/2}\right.\\
&\quad\left.+\frac{1}{2}\left(\ln\frac{s}{\pi}\right)^{-1/2}(2\ln s+\ln\pi)\right]\frac{ds}{s}\\
&\quad=\frac{1}{\Gamma(1/2)}\int_\pi^t\left(\ln\frac{t}{s}\right)^{1-1/2-1}\left[2\left(\ln\frac{s}{\pi}\right)^{1/2}\right.\\
&\quad\left.+\frac{1}{2}\left(\ln\frac{s}{\pi}\right)^{-1/2}\left(2\ln\frac{s}{\pi}+3\ln\pi\right)\right]\frac{ds}{s}\\
&\quad=\frac{3}{\Gamma(1/2)}\int_\pi^t\left(\ln\frac{t}{s}\right)^{1-1/2-1}\left(\ln\frac{s}{\pi}\right)^{1/2}\frac{ds}{s}\\
&\quad+\frac{(3/2)\ln\pi}{\Gamma(1/2)}\int_\pi^t\left(\ln\frac{t}{s}\right)^{1-1/2-1}\left(\ln\frac{s}{\pi}\right)^{-1/2}\frac{ds}{s}=\frac{3}{2}\\
&\quad\cdot\Gamma\left(\frac{1}{2}\right)\ln\frac{t}{\pi}+\frac{3}{2}\Gamma\left(\frac{1}{2}\right)\ln\pi=\frac{3}{2}\Gamma\left(\frac{1}{2}\right)\ln t\Big|_{t>\pi}.
\end{aligned}\tag{39}$$

Therefore, for $t \in (1, \pi/2]$ and $t \in (\pi, 2\pi]$ in (38), we have

$$
\begin{aligned}
&{}_{\text{C-H}}D_{1+}^{1/2} u(t) = {}_{\text{C-H}}D_{1+}^{1/2}\left(1 + \frac{4}{3\sqrt{\pi}}(\ln t)^{3/2}\right) = \ln t, \\
&\qquad\qquad\qquad\qquad\qquad\qquad \text{for } t \in \left(1, \frac{\pi}{2}\right], \\
&{}_{\text{C-H}}D_{1+}^{1/2} u(t)\Big|_{t\in(\pi,2\pi]} = {}_{\text{C-H}}D_{1+}^{1/2}\left\{-\frac{4}{3\sqrt{\pi}}(\ln\pi)^{3/2}\right. \\
&\quad + \frac{4}{3\sqrt{\pi}}(\ln t)^{3/2}\Big|_{t>1} + \frac{2\xi}{3\sqrt{\pi}}\left[-1 - \frac{4}{3\sqrt{\pi}}(\ln\pi)^{3/2}\right] \\
&\quad \times \left[2(\ln\pi)^{3/2} + \left(\ln\frac{t}{\pi}\right)^{1/2}(2\ln t + \ln\pi)\Big|_{t>\pi}\right. \\
&\quad \left.\left. - 2(\ln t)^{3/2}\Big|_{t>1}\right]\right\}_{t\in(\pi,2\pi]} \\
&= {}_{\text{C-H}}D_{1+}^{1/2}\left\{\frac{4}{3\sqrt{\pi}}(\ln t)^{3/2}\Big|_{t>1} + \frac{2\xi}{3\sqrt{\pi}}\left[-1\right.\right. \\
&\quad \left.\left. - \frac{4}{3\sqrt{\pi}}(\ln\pi)^{3/2}\right] \times \left[\left(\ln\frac{t}{\pi}\right)^{1/2}(2\ln t + \ln\pi)\Big|_{t>\pi}\right. \\
&\quad \left.\left. - 2(\ln t)^{3/2}\Big|_{t>1}\right]\right\}_{t\in(\pi,2\pi]} = \left\{\ln t|_{t>1} + \frac{2\xi}{3\sqrt{\pi}}\left[-1\right.\right. \\
&\quad \left.\left. - \frac{4}{3\sqrt{\pi}}(\ln\pi)^{3/2}\right]\left[\frac{3}{2}\Gamma\left(\frac{1}{2}\right)\ln t\Big|_{t>\pi}\right. \right. \\
&\quad \left.\left. - \frac{3}{2}\Gamma\left(\frac{1}{2}\right)\ln t\Big|_{t>1}\right]\right\}_{t\in(\pi,2\pi]} = \left\{\ln t|_{t>1}\right\}_{t\in(\pi,2\pi]}, \\
&\qquad\qquad\qquad\qquad\qquad\qquad \text{for } t \in (\pi, 2\pi].
\end{aligned}
\tag{40}
$$

Thus, (38) satisfies fractional derivative and noninstantaneous impulses in system (36). Therefore, (38) is general solution of system (36).

Competing Interests

The authors declare that they have no competing interests.

Acknowledgments

The work described in this paper is financially supported by the National Natural Science Foundation of China (Grant nos. 21576033, 21636004, 61563023, and 61362038) and the Research Foundation of Education Bureau of Jiangxi Province, China (Grant no. GJJ14738).

References

[1] E. Hernández and D. O'Regan, "On a new class of abstract impulsive differential equations," *Proceedings of the American Mathematical Society*, vol. 141, no. 5, pp. 1641–1649, 2013.

[2] M. Pierri, D. O'Regan, and V. Rolnik, "Existence of solutions for semi-linear abstract differential equations with not instantaneous impulses," *Applied Mathematics and Computation*, vol. 219, no. 12, pp. 6743–6749, 2013.

[3] J. Wang, Y. Zhou, and Z. Lin, "On a new class of impulsive fractional differential equations," *Applied Mathematics and Computation*, vol. 242, pp. 649–657, 2014.

[4] P.-L. Li and C.-J. Xu, "Mild solution of fractional order differential equations with not instantaneous impulses," *Open Mathematics*, vol. 13, pp. 436–443, 2015.

[5] A. A. Kilbas, H. H. Srivastava, and J. J. Trujillo, *Theory and Applications of Fractional Differential Equations*, Elsevier, Amsterdam, The Netherlands, 2006.

[6] A. A. Kilbas, "Hadamard-type fractional calculus," *Journal of the Korean Mathematical Society*, vol. 38, no. 6, pp. 1191–1204, 2001.

[7] P. L. Butzer, A. A. Kilbas, and J. J. Trujillo, "Compositions of Hadamard-type fractional integration operators and the semigroup property," *Journal of Mathematical Analysis and Applications*, vol. 269, no. 2, pp. 387–400, 2002.

[8] P. L. Butzer, A. A. Kilbas, and J. J. Trujillo, "Mellin transform analysis and integration by parts for Hadamard-type fractional integrals," *Journal of Mathematical Analysis and Applications*, vol. 270, no. 1, pp. 1–15, 2002.

[9] P. Thiramanus, S. K. Ntouyas, and J. Tariboon, "Existence and uniqueness results for Hadamard-type fractional differential equations with nonlocal fractional integral boundary conditions," *Abstract and Applied Analysis*, Article ID 902054, Art. ID 902054, 9 pages, 2014.

[10] M. Klimek, "Sequential fractional differential equations with Hadamard derivative," *Communications in Nonlinear Science and Numerical Simulation*, vol. 16, no. 12, pp. 4689–4697, 2011.

[11] B. Ahmad and S. K. Ntouyas, "A fully Hadamard type integral boundary value problem of a coupled system of fractional differential equations ," *Fractional Calculus and Applied Analysis*, vol. 17, no. 2, pp. 348–360, 2014.

[12] F. Jarad, T. Abdeljawad, and D. Baleanu, "Caputo-type modification of the Hadamard fractional derivatives," *Advances in Difference Equations*, 2012:142, 8 pages, 2012.

[13] Y. Y. Gambo, F. Jarad, D. Baleanu, and T. Abdeljawad, "On Caputo modification of the Hadamard fractional derivatives," *Advances in Difference Equations*, vol. 2014, article no. 10, 12 pages, 2014.

[14] Y. Adjabi, F. Jarad, D. Baleanu, and T. Abdeljawad, "On Cauchy problems with CAPuto Hadamard fractional derivatives," *Journal of Computational Analysis and Applications*, vol. 21, no. 4, pp. 661–681, 2016.

[15] X. Zhang, "The general solution of differential equations with Caputo-Hadamard fractional derivatives and impulsive effect," *Advances in Difference Equations*, vol. 2015, article 215, 16 pages, 2015.

[16] X. Zhang, Z. Liu, H. Peng, T. Shu, and S. Yang, "The general solution of impulsive systems with caputo- hadamard fractional derivative of order $q \in \mathbb{C}(\Re(q) \in (1,2))$," *Mathematical Problems in Engineering*, vol. 2016, Article ID 8101802, 20 pages, 2016.

[17] X. Zhang, X. Zhang, and M. Zhang, "On the concept of general solution for impulsive differential equations of fractional order $q \epsilon (0, 1)$," *Applied Mathematics and Computation*, vol. 247, pp. 72–89, 2014.

[18] X. Zhang, "On the concept of general solutions for impulsive differential equations of fractional order $q \in (1, 2)$," *Applied Mathematics and Computation*, vol. 268, pp. 103–120, 2015.

[19] X. Zhang, P. Agarwal, Z. Liu, and H. Peng, "The general solution for impulsive differential equations with Riemann-Liouville fractional-order $q(1, 2)$," *Open Mathematics*, vol. 13, pp. 908–930, 2015.

[20] X. Zhang, T. Shu, H. Cao, Z. Liu, and W. Ding, "The general solution for impulsive differential equations with Hadamard fractional derivative of order $q \in (1, 2)$," *Advances in Difference Equations*, vol. 2016, article 14, 2016.

[21] X. Zhang, X. Zhang, Z. Liu, W. Ding, H. Cao, and T. Shu, "On the general solution of impulsive systems with Hadamard fractional derivatives," *Mathematical Problems in Engineering*, vol. 2016, Article ID 2814310, 12 pages, 2016.

Hindawi
Advances in Mathematical Physics
Volume 2017, Article ID 7396063, 14 pages
https://doi.org/10.1155/2017/7396063

Research Article

Closed-Form Exact Solutions for the Unforced Quintic Nonlinear Oscillator

Augusto Beléndez,[1,2] Enrique Arribas,[3] Tarsicio Beléndez,[1,2] Carolina Pascual,[1,2] Encarnación Gimeno,[1,2] and Mariela L. Álvarez[1,2]

[1] *Instituto Universitario de Física Aplicada a las Ciencias y las Tecnologías, Universidad de Alicante, Apartado 99, 03080 Alicante, Spain*
[2] *Departamento de Física, Ingeniería de Sistemas y Teoría de la Señal, Universidad de Alicante, Apartado 99, 03080 Alicante, Spain*
[3] *Departamento de Física Aplicada, Universidad de Castilla-La Mancha, Avda. España s/n, 02071 Albacete, Spain*

Correspondence should be addressed to Augusto Beléndez; a.belendez@ua.es

Received 6 November 2016; Accepted 5 January 2017; Published 2 February 2017

Academic Editor: Zhi-Yuan Sun

Closed-form exact solutions for the periodic motion of the one-dimensional, undamped, quintic oscillator are derived from the first integral of the nonlinear differential equation which governs the behaviour of this oscillator. Two parameters characterize this oscillator: one is the coefficient of the linear term and the other is the coefficient of the quintic term. Not only the common case in which both coefficients are positive but also all possible combinations of positive and negative values of these coefficients which provide periodic motions are considered. The set of possible combinations of signs of these coefficients provides four different cases but only three different pairs of period-solution. The periods are given in terms of the complete elliptic integral of the first kind and the solutions involve Jacobi elliptic function. Some particular cases obtained varying the parameters that characterize this oscillator are presented and discussed. The behaviour of the periods as a function of the initial amplitude is analysed and the exact solutions for several values of the parameters involved are plotted. An interesting feature is that oscillatory motions around the equilibrium point that is not at $x = 0$ are also considered.

1. Introduction

Mathematical models based on nonlinear oscillators have been widely used in physics, engineering, applied mathematics, and related fields [1, 2]. These nonlinear systems have been the focus of attention for many years and several methods have been used to find approximate solutions to them [1, 3]. In conservative nonlinear oscillators the restoring force is not dependent on time, the total energy is constant [1], and any oscillation is stationary. The aim of this paper is to obtain closed-form exact periodic solutions to the quintic equation corresponding to a nonlinear oscillator described by a differential equation with fifth-power nonlinearity. Due to the presence of the fifth-power nonlinearity, this oscillator is difficult to handle and has not been studied as extensively as the Duffing oscillator with cubic nonlinearity. For this reason, several techniques have been used to obtain analytical approximate expressions for the period and the solution of the quintic oscillator. Lin [4] proposed a new parameter iteration technique to solve the Duffing equation with strong and higher-order nonlinearity. Ramos [5] approximately solved the quintic equation using some Lindstedt-Poincaré techniques. Pirbodaghi et al. [6] obtained an accurate analytical approximate solution to Duffing equations with cubic and quintic nonlinearities using the homotopy analysis method and homotopy Padé technique. Wu et al. [7] approximately solved this nonlinear oscillator using a method that incorporates salient features of both Newton's method and the harmonic balance method. Later, Lai et al. [8] used a Newton-harmonic balancing approach to obtain accurate approximate analytical higher-order solutions for strong nonlinear Duffing oscillators with cubic-quintic restoring force. They also discussed the effect of strong quantic nonlinearity on accuracy as compared to cubic

nonlinearity. Beléndez et al. [9] approximately solved the quintic oscillator using a cubication method which allowed them to obtain approximate analytical expressions for the period and the solution in terms of elementary functions. Scarpello and Ritelli [10] exactly solved the quintic oscillator, but only when the coefficient for the linear term is equal to one and the coefficient for the nonlinear term is positive. Elías-Zúñiga [11] derived the exact solution of the cubic-quintic Duffing equation based on the use of Jacobi elliptic functions by the same method that he used to obtain the exact solution of the mixed-parity Helmholtz-Duffing oscillator [12]. However, in both cases he did not solve the nonlinear differential equation but assumed that its exact solution is given by a rational equation which includes the cn Jacobian elliptic function and five unknown parameters that need to be determined. Based on his pervious results, Elías-Zúñiga obtained the analytical approximate solution of the damped cubic-quintic Duffing oscillator [13] and also developed a "quintication" method [14] to obtain approximate analytical solutions of conservative nonlinear oscillators. Recently, Beléndez et al. [15] have exactly solved the unforced cubic-quintic Duffing oscillator, providing exact expressions for the period and the solution, but only for oscillations around $x = 0$ and taken into account that the coefficients for the linear and the nonlinear terns are positive.

In this paper we obtain the closed-form exact expressions for the period and the solution of the quintic Duffing nonlinear oscillator modelled by the second-order differential equation $d^2x/dt^2 + a_1x + a_5x^5 = 0$, where a_1 and a_5 are the coefficients of the linear and the nonlinear terms, respectively, considering all possible combinations of signs of a_1 and a_5 that provide oscillatory motions. Unlike the procedure considered by Elías-Zúñiga [11, 12], we do not assume an expression for the solution but solve the nonlinear differential equation exactly as was done in [15]. This is done using elliptic functions so that, after inversion, the solution x is provided as an explicit function of time t. When $a_1 = 0$ and $a_5 > 0$, the system becomes a truly nonlinear oscillator [16] for which the exact expressions for the period and the solution have been already obtained [17]. The particular situation in which coefficients a_1 and a_5 are both positive is the most common case analysed. However, we obtain closed-form exact solutions not only for the case in which both coefficients are positive, but also for all possible combinations of positive and negative values of these coefficients which provide periodic motions. The set of possible combinations of signs of these coefficients gives rise to four different cases. In three of these combinations ((a) $a_1 \geq 0$, $a_5 > 0$, and $x_0 > 0$, (b) $a_1 < 0$, $a_5 > 0$ and $x_0 > (-3a_1/a_5)^{1/4}$, and (d) $a_1 > 0$, $a_5 < 0$ and $0 < x_0 < (-a_1/a_5)^{1/4}$) the system oscillates around the equilibrium position $x = 0$ with $x \in [-x_0, x_0]$, where $x_0 > 0$ is the oscillation amplitude. However, there is still one more case ((c) $a_1 > 0$, $a_5 < 0$, and $0 < x_0 < (-3a_1/a_5)^{1/4}$ or $-(-3a_1/a_5)^{1/4} < x_0 < 0$) in which the system does not oscillate around the position $x = 0$ with $x \in [-x_0, x_0]$, but around the equilibrium position $x = (-a_1/a_5)^{1/4}$ with $x \in [x_1, x_0]$. Three different sets of closed-form expressions for the exact period and solution were obtained. Following the procedure considered by Lai and Chow [18], some examples are analysed and plots including periods, solutions, or phase-diagrams are presented and discussed.

2. Formulation and Solution Procedure

A quintic oscillator is an example of a conservative autonomous oscillatory system, which is modelled by the following second-order differential equation:

$$\frac{d^2x}{dt^2} + a_1x + a_5x^5 = 0 \tag{1}$$

with initial conditions

$$x(0) = x_0 > 0, \qquad \frac{dx}{dt}(0) = 0. \tag{2}$$

In (1) x and t are generalized dimensionless displacement and time variables, and we assume that the coefficients for the linear and the nonlinear terms satisfy. In order to obtain the exact period and periodic solution for (1), we take into account that this is a conservative system and has the following first integral:

$$\left(\frac{dx}{dt}\right)^2 + a_1x^2 + \frac{1}{3}a_5x^6 = a_1x_0^2 + \frac{1}{3}x_0^6 \tag{3}$$

which can be written as follows:

$$v^2 = \left(\frac{dx}{dt}\right)^2 = a_1\left(x_0^2 - x^2\right) + \frac{1}{3}a_5\left(x_0^6 - x^6\right) \geq 0. \tag{4}$$

The dynamical study [19] of the nonlinear differential equation given in (1) showed that its motion is periodic in the following situations:

(a) $a_1 \geq 0$, $a_5 > 0$, and $x_0 > 0$: the system oscillates around the equilibrium position $x = 0$ and the periodic solution x satisfies $x \in [-x_0, x_0]$.

(b) $a_1 < 0$, $a_5 > 0$, and $x_0 > (-3a_1/a_5)^{1/4}$: the system oscillates around the equilibrium position $x = 0$ and the periodic solution x satisfies $x \in [-x_0, x_0]$.

(c) $a_1 < 0$, $a_5 > 0$, and $0 < x_0 < (-3a_1/a_5)^{1/4}$: the system oscillates around the equilibrium position $x = (-3a_1/a_5)^{1/4}$ and the periodic solution satisfies $x \in [x_1, x_0]$ with $0 < x_1 \leq x \leq x_0$ (or around the equilibrium position $x = -(-3a_1/a_5)^{1/4}$ with $x \in [x_0, x_1]$ when $-(-3a_1/a_5)^{1/4} < x_0 < 0$).

(d) $a_1 > 0$, $a_5 < 0$, and $0 < x_0 < (-a_1/a_5)^{1/4}$: the system oscillates around the equilibrium position $x = 0$ and the periodic solution x satisfies $x \in [-x_0, x_0]$.

The phase plots in Figure 1 illustrate four examples of these situations: (a) $a_1 = 1$, $a_5 = 3$, and $x_0 = 1$, (b) $a_1 = -1$, $a_5 = 3$ with $x_0 = 1.1$ (x_0 must be > 1), (c) $a_1 = -1$, $a_5 = -3$, and $x_0 = 0.95$ (x_0 must be < 1), and (d) $a_1 = 1$, $a_5 = -3$,

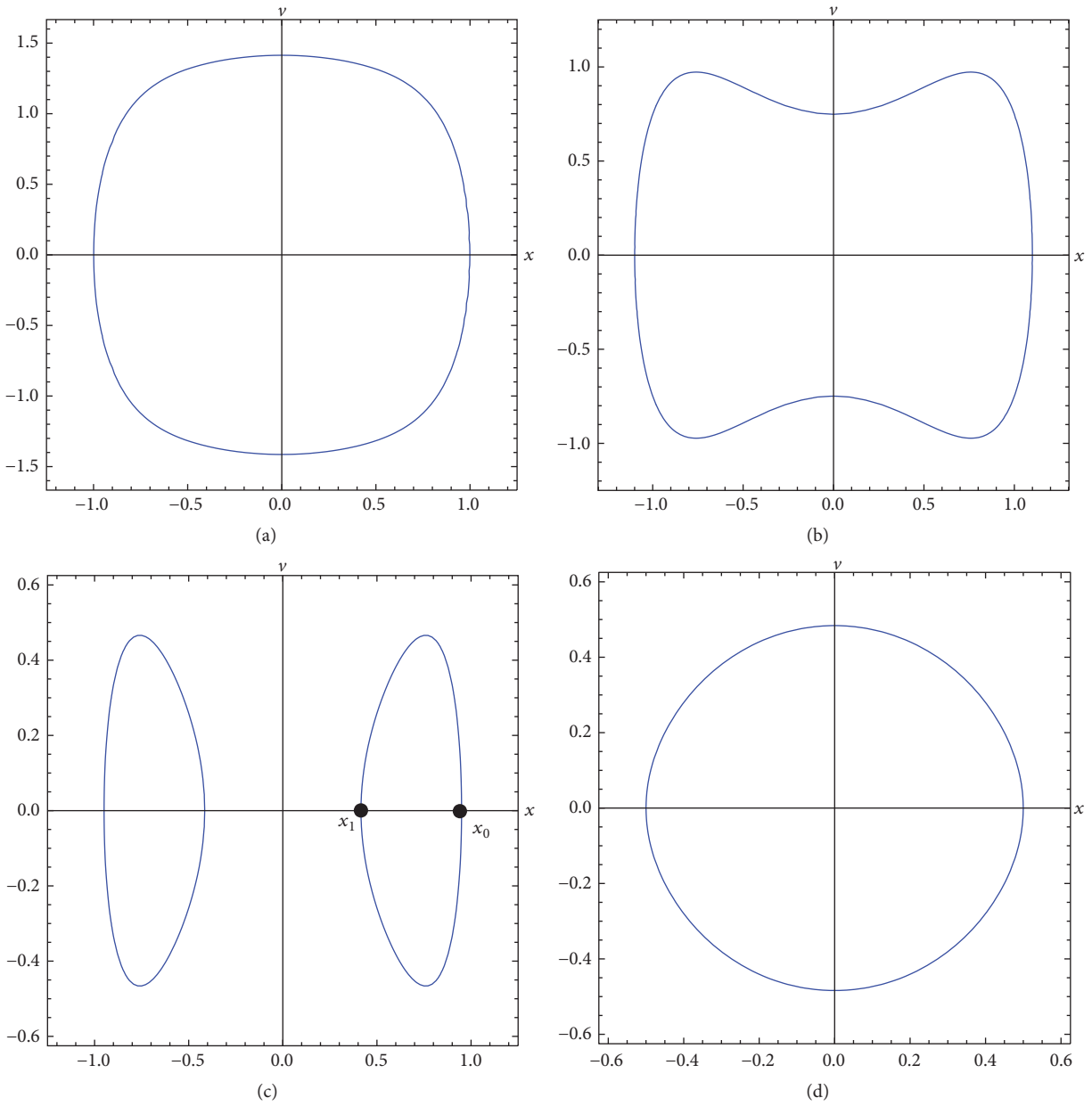

FIGURE 1: Phase space portraits for parameters values of (a) $a_1 = 1$, $a_5 = 3$, and $x_0 = 1$; (b) $a_1 = -1$, $a_5 = 3$, and $x_0 = 1.1$; (c) $a_1 = -1$, $a_5 = 3$, and $x_0 = 0.95$; and (d) $a_1 = 1$, $a_5 = -3$, and $x_0 = 0.5$.

and $x_0 = 0.5$ (x_0 must be $< 3^{-1/4} \approx 0.7598$). As can be seen in these figures, for cases (a), (b), and (d) the system oscillates around the equilibrium position $x = 0$, whereas for case (c) the system oscillates around the equilibrium position $x = (-a_1/a_5)^{1/4}$. In the following sections we obtain the exact expressions for the period and the periodic solution for each of these four cases.

3. Exact Solution When $a_1 \geq 0$, $a_5 > 0$, and $x_0 > 0$

In this situation all the solutions are periodical and the phase space diagram is made up of an infinite number of closed orbits, each of them for each value of the initial amplitude x_0 (as can be seen in Figure 1(a)). This system oscillates around the equilibrium position $x = 0$ with $x \in [-x_0, x_0]$, where $x_0 > 0$ is the initial amplitude and the period, T, and periodic solution, x, are dependent on the oscillation amplitude x_0. This system corresponds to a nonlinear oscillator for which the nonlinear function $f(x) = a_1 x + a_3 x^3 + a_5 x^5$ is odd; that is, $f(-x) = -f(x)$. From (4) we obtain

$$\left(\frac{dt}{dx}\right)^2 = \frac{1}{a_1\left(x_0^2 - x^2\right) + (1/3)\,a_5\left(x_0^6 - x^6\right)} \tag{5}$$

and then

$$dt = \pm \frac{dx}{\sqrt{a_1\left(x_0^2 - x^2\right) + (1/3)\, a_5\left(x_0^6 - x^6\right)}}, \tag{6}$$

where the sign $(\pm)$ is chosen taking into account the sign of dx/dt in each quadrant.

Taking into account that $a_5 > 0$, from (6) we can write

$$\sqrt{\frac{a_5}{3}}\, dt = \pm \frac{dx}{\sqrt{\left(3a_1/a_5\right)\left(x_0^2 - x^2\right) + \left(x_0^6 - x^6\right)}} \tag{7}$$

and after some mathematical operations we obtain

$$\sqrt{\frac{a_5}{3}}\, dt = \pm \frac{dx}{\sqrt{\left(x_0^2 - x^2\right)\left(x^4 + x_0^2 x^2 + 3a_1/a_5 + x_0^2\right)}}. \tag{8}$$

Integrating (8) we obtain

$$\sqrt{\frac{a_5}{3}}\, t = \pm \int_x^{x_0} \frac{dx}{\sqrt{\left(x_0^2 - x^2\right)\left(x^4 + x_0^2 x^2 + 3a_1/a_5 + x_0^2\right)}}. \tag{9}$$

The change of variable $x^2 = u$ gives

$$\sqrt{\frac{a_5}{3}}\, t = \pm \int_{x^2}^{x_0^2} \frac{du}{\sqrt{\left(x_0^2 - u\right) u\left(u^2 + x_0^2 u + 3a_1/a_5 + x_0^2\right)}}. \tag{10}$$

This is an improper integral which contains a square root of a four-degree polynomial in the denominator and so its solution can be expressed as a function of an elliptic integral.

3.1. Calculation of the Exact Period. The symmetry of the problem indicates that the period of the oscillation T is four times the time taken by the oscillator to go from $u = 0$ to $u = x_0^2$. Therefore, from (10) it follows that

$$T = 2\sqrt{\frac{3}{a_5}} \int_{x^2}^{x_0^2} \frac{du}{\sqrt{\left(x_0^2 - u\right) u\left(u^2 + x_0^2 u + 3a_1/a_5 + x_0^2\right)}}. \tag{11}$$

We consider the definite integral [20, section 3.145, formula 2, pages 270-271]

$$\int_\beta^y \frac{du}{\sqrt{(\alpha - u)(u - \beta)\left[(u - \sigma)^2 + \rho^2\right]}} = \frac{1}{\sqrt{pq}} \cdot F\left(2\,\operatorname{arccot}\sqrt{\frac{q(\alpha - y)}{p(y - \beta)}}, \frac{(\alpha - \beta)^2 - (p - q)^2}{4pq}\right), \tag{12}$$

where $\beta < u < \alpha$, $F(\phi, m)$ is the incomplete elliptic integral of the first kind [20]

$$F(\phi, m) = \int_0^\phi \frac{d\theta}{\sqrt{1 - m\sin^2\theta}}, \tag{13}$$

and p, q, and m are defined as

$$p = \sqrt{(\sigma - \alpha)^2 + \rho^2},$$
$$q = \sqrt{(\sigma - \beta)^2 + \rho^2}, \tag{14}$$
$$m = \frac{(\alpha - \beta)^2 - (p - q)^2}{4pq}.$$

By comparing the integrals in (11) and (12) we obtain $y = x_0^2$, $\alpha = x_0^2$, and $= 0$, as well as the following values for the different parameters which appear in (12)

$$\sigma = -\frac{1}{2}x_0^2,$$
$$\rho = \frac{1}{2}\sqrt{\frac{12a_1}{a_5} + 3x_0^2},$$
$$p = \sqrt{\frac{3}{a_5}}\sqrt{a_1 + a_5 x_0^4}, \tag{15}$$
$$q = \frac{1}{\sqrt{a_5}}\sqrt{3a_1 + a_5 x_0^4},$$
$$m = \frac{1}{2} - \frac{\sqrt{3}\left(2a_1 + a_5 x_0^4\right)}{4\sqrt{\left(a_1 + a_5 x_0^4\right)\left(3a_1 + a_5 x_0^4\right)}}.$$

As $y = \alpha = x_0^2$, then $F(2\,\operatorname{arccot} 0, m) = F(\pi, m) = 2K(m)$, where $K(m)$ is the complete elliptic integral of the first kind defined as [20]

$$K(m) = \int_0^{\pi/2} \frac{d\theta}{\sqrt{1 - m\sin^2\theta}}. \tag{16}$$

From (11) to (16) we conclude that the exact period of the quintic nonlinear oscillator can be written in the compact form

$$T = 4\left(\frac{3}{q_1 q_3}\right)^{1/4} K\left(m_a\right), \tag{17}$$

where m_a takes the form

$$m_a = \frac{1}{2} - \frac{q_2}{4}\left(\frac{3}{q_1 q_3}\right)^{1/2} \tag{18}$$

and coefficients q_n—which depend on a_1, a_5, and x_0—are defined as follows:

$$q_n = n a_1 + a_5 x_0^4. \tag{19}$$

Figure 2 shows the period T as a function of the initial amplitude x_0 (17) when $a_1 = 1$ and (a) $a_5 = 0.1$, (b) $a_5 = 0.5$, (c) $a_5 = 5$, and (d) $a_5 = 50$.

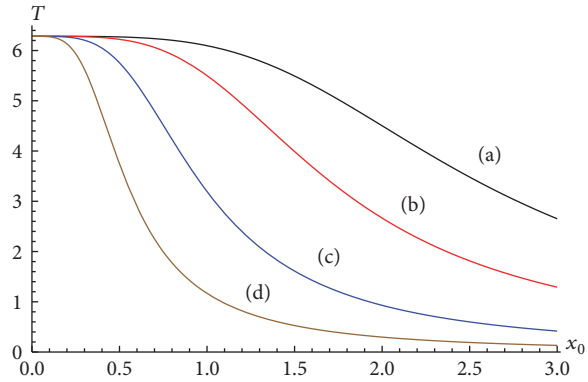

FIGURE 2: Exact period T in (17) as a function of the initial amplitude x_0 when $a_1 = 1$ and (a) $a_5 = 0.1$, (b) $a_5 = 0.5$, (c) $a_5 = 5$, and (d) $a_5 = 50$.

3.2. Calculation of the Exact Solution. From (6) we obtain t as a function of x for the following cases:

Trajectory $1 \to 2$ ($0 \le t \le T/4$ and $x_0 \ge x \ge 0$), x is positive and dx/dt is negative.

Trajectory $2 \to 3$ ($T/4 \le t \le T/2$ and $0 \ge x \ge -x_0$), x is negative and dx/dt is negative.

Trajectory $3 \to 4$ ($T/2 \le t \le 3T/4$ and $-x_0 \le x \le 0$), x is negative and dx/dt is positive.

Trajectory $4 \to 1$ ($3T/4 \le t \le T$ and $0 \le x \le x_0$), x is positive and dx/dt is positive.

From (10), it follows that for trajectory $1 \to 2$ ($0 \le t \le T/4$ and $x_0 \ge x \ge 0$) we have

$$2\sqrt{\frac{a_5}{3}}t = \int_{x^2}^{x_0^2} \frac{du}{\sqrt{(x_0^2-u)\,u\,(u^2+x_0^2u+3a_1/a_5+x_0^2)}}. \quad (20)$$

The definite integral in (20) can be split as follows:

$$2\sqrt{\frac{a_5}{3}}t = \int_0^{x_0^2} \frac{du}{\sqrt{(x_0^2-u)\,u\,(u^2+x_0^2u+3a_1/a_5+x_0^2)}} - \int_0^{x^2} \frac{du}{\sqrt{(x_0^2-u)\,u\,(u^2+x_0^2u+3a_1/a_5+x_0^2)}}. \quad (21)$$

The values of the two integrals on the right-hand side of (21) can be calculated taking into account (11) and (12) and their values are

$$\int_0^{x_0^2} \frac{du}{\sqrt{(x_0^2-u)\,u\,(u^2+x_0^2u+3a_1/a_5+x_0^2)}} = 2\sqrt{\frac{a_5}{3}}\frac{T}{4},$$
$$\int_0^{x^2} \frac{du}{\sqrt{(x_0^2-u)\,u\,(u^2+x_0^2u+3a_1/a_5+x_0^2)}} = \frac{1}{\sqrt{pq}}F\left(2\,\mathrm{arccot}\sqrt{\frac{q\left(A^2-x^2\right)}{px^2}}, m_a\right). \quad (22)$$

Substituting (22) into (21) gives

$$2\sqrt{pq}\sqrt{\frac{a_5}{3}}\left(\frac{T}{4}-t\right) = F\left(2\,\mathrm{arccot}\sqrt{\frac{q\left(A^2-x^2\right)}{px^2}}, m_a\right), \quad (23)$$

and using (15)–(19), (23) can be written as

$$2K(m_a) - \left(\frac{q_1q_3}{3}\right)^{1/4} t = F\left(2\,\mathrm{arccot}\left[\left(\frac{q_3}{3q_1}\right)^{1/4}\left(\frac{x_0^2-x^2}{x^2}\right)^{1/2}\right], m_a\right). \quad (24)$$

The inverse function of $F(\varphi, m)$ is the Jacobi amplitude φ [21, 22]

$$F^{-1}(u,m) = \varphi = \mathrm{am}(u,m) \quad (25)$$

whose cosine is the Jacobi cosine function, cn [21]

$$\cos\varphi = \cos(\mathrm{am}(u,m)) = \mathrm{cn}(u,m). \quad (26)$$

In order to introduce an "arccos" function in (24) we take into account that

$$2\,\mathrm{arccot}\,z = \varphi, \quad (27)$$

where

$$z = \left(\frac{q_3}{3q_1}\right)^{1/4}\left(\frac{x_0^2-x^2}{x^2}\right)^{1/2}. \quad (28)$$

From (28) we obtain

$$\tan^2\frac{\varphi}{2} = \frac{1}{z^2}. \quad (29)$$

Taking into account the relation

$$\tan^2\frac{\varphi}{2}=\frac{1-\cos\varphi}{1+\cos\varphi} \tag{30}$$

we can finally write

$$\cos\varphi=\frac{z^2-1}{z^2+1}=\frac{\sqrt{q_3}\left(x_0^2-x^2\right)-\sqrt{3q_1}x^2}{\sqrt{q_3}\left(x_0^2-x^2\right)+\sqrt{3q_1}x^2} \tag{31}$$

which allows us to write (24) as follows:

$$\begin{aligned}&2K\left(m_a\right)-2\left(\frac{q_1q_3}{3}\right)^{1/4}t\\&=F\left(\arccos\left(\frac{\sqrt{q_3}\left(x_0^2-x^2\right)-\sqrt{3q_1}x^2}{\sqrt{q_3}\left(x_0^2-x^2\right)+\sqrt{3q_1}x^2}\right),m_a\right)\end{aligned} \tag{32}$$

and from (25), (26), and (32) we can write, after some simplifications,

$$\begin{aligned}&\frac{\sqrt{q_3}x_0^2-\left(\sqrt{q_3}+\sqrt{3q_1}\right)x^2}{\sqrt{q_3}x_0^2-\left(\sqrt{q_3}-\sqrt{3q_1}\right)x^2}\\&=\operatorname{cn}\left(2K\left(m_a\right)-2\left(\frac{1}{3}q_1q_3\right)^{1/4}t,m_a\right)\\&=-\operatorname{cn}\left(2\left(\frac{1}{3}q_1q_3\right)^{1/4}t,m_a\right),\end{aligned} \tag{33}$$

where the relation $\operatorname{cn}(2K(m)-u,m)=-\operatorname{cn}(u,m)$ [22] has been taken into account.

Finally we can write

$$\begin{aligned}x_a(t)=x_0\Bigg[&1\\&+\sqrt{\frac{3q_1}{q_3}}\left(\frac{1-\operatorname{cn}\left((1/2)\left((8/3)q_1q_3\right)^{1/4}t,m_a\right)}{1+\operatorname{cn}\left((1/2)\left((8/3)q_1q_2\right)^{1/4}t,m_a\right)}\right)\Bigg]^{-1/2}\end{aligned} \tag{34}$$

which is valid for $0\le t\le T/4$.

From (7), it follows for trajectory $2\to3$ that

$$\begin{aligned}&2\sqrt{\frac{a_5}{3}}\int_{T/4}^{t}dt=2\sqrt{\frac{a_5}{3}}\left(t-\frac{T}{4}\right)\\&=-\int_0^{x^2}\frac{du}{\sqrt{\left(x_0^2-u\right)u\left(u^2+x_0^2u+3a_1/a_5+x_0^2\right)}}\end{aligned} \tag{35}$$

and for trajectory $3\to4(T/4\le t\le T/2)$

$$\begin{aligned}&2\sqrt{\frac{a_5}{3}}\int_{T/2}^{t}dt=2\sqrt{\frac{a_5}{3}}\left(t-\frac{T}{2}\right)\\&=\int_{x_0^2}^{x^2}\frac{du}{\sqrt{\left(x_0^2-u\right)u\left(u^2+x_0^2u+3a_1/a_5+x_0^2\right)}}.\end{aligned} \tag{36}$$

Proceeding in the same manner as for trajectory $1\to2$, it is follows that $x_b(t)=-x_a(t)$ which is valid for $T/4\le t\le3T/4$, because $x<0$ for these values of time.

Finally, for trajectory $4\to1$ we have

$$\begin{aligned}&2\sqrt{\frac{a_5}{3}}\int_{3T/4}^{t}dt=2\sqrt{\frac{a_5}{3}}\left(t-\frac{3T}{4}\right)\\&=\int_0^{x^2}\frac{du}{\sqrt{\left(x_0^2-u\right)u\left(u^2+x_0^2u+3a_1/a_5+x_0^2\right)}}\end{aligned} \tag{37}$$

and we obtain the same value for the solution as that given in (34).

The exact solution of the quintic oscillator can be written as follows:

$$x(t)=\begin{cases}x_a(t) & 0\le t\le\dfrac{T}{4}\\-x_a(t) & \dfrac{T}{4}\le t\le\dfrac{3T}{4}\\x_a(t) & \dfrac{3T}{4}\le t\le T\end{cases} \tag{38}$$

Taking into account the relation [22, formula 16.18.4, page 574]

$$\frac{1-\operatorname{cn}2u}{1+\operatorname{cn}2u}=\frac{\operatorname{sn}^2u\operatorname{dn}^2u}{\operatorname{cn}^2u} \tag{39}$$

and (34) and (38), the exact periodic solution of the quintic oscillator can be written in compact form as follows:

$$x(t)=\frac{x_0\operatorname{cn}\left(\left((1/3)q_1q_3\right)^{1/4}t,m_a\right)}{\left[\operatorname{cn}^2\left(\left((1/3)q_1q_3\right)^{1/4}t,m_a\right)+\left(3q_1/q_3\right)^{1/2}\operatorname{sn}^2\left(\left((1/3)q_1q_3\right)^{1/4}t,m_a\right)\operatorname{dn}^2\left(\left((1/3)q_1q_3\right)^{1/4}t,m_a\right)\right]^{1/2}} \tag{40}$$

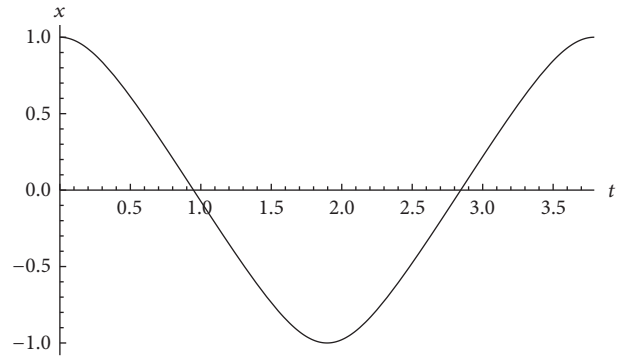

FIGURE 3: Exact solution x in (40) as a function of time t when $a_1 = 1$, $a_5 = 3$, and $x_0 = 1$.

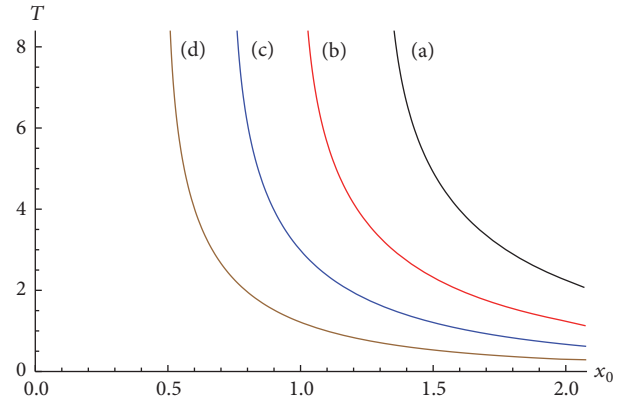

FIGURE 4: Exact period T in (17) as a function of the initial amplitude x_0 when $a_1 = -1$, $x_0 > (-3a_1/a_5)^{1/4}$ and (a) $a_5 = 1$, (b) $a_5 = 3$, (c) $a_5 = 10$, and (d) $a_5 = 50$.

which is valid for all value of t and where cn, sn, and dn are the basic Jacobi elliptic functions [20]. Figure 3 shows the plot of the displacement x as a function of time t when $a_1 = 1$, $a_5 = 3$, and $x_0 = 1$. This displacement was obtained using (40). This figure corresponds to the phase space portrait shown in Figure 1(a).

4. Exact Solution When $a_1 < 0$, $a_5 > 0$, and $x_0 > (-3a_1/a_5)^{1/4}$

Equations (17) and (40) can be used to obtain the period and the solution in case (b), $a_1 < 0$, $a_5 > 0$, and $x_0 > (-3a_1/a_5)^{1/4}$. Figure 4 shows the period T as a function of the initial amplitude x_0 (17) when $a_1 = -1$ and (a) $a_5 = 1$, (b) $a_5 = 3$, (c) $a_5 = 10$, and (d) $a_5 = 50$. Figure 5 shows the plot of the displacement x as a function of time t when $a_1 = -1, a_5 = 3$, and $x_0 = 1.1$. This displacement was obtained using (40). This figure corresponds to the phase space portrait shown in Figure 1(b).

5. Exact Solution When $a_1 < 0$, $a_5 > 0$, and $0 < x_0 < (-3a_1/a_5)^{1/4}$

The phase portrait in Figure 1(c) shows the behaviour of the oscillator when $0 < x_0 < (-3a_1/a_5)^{1/4}$ ($a_1 = -1$, $a_5 = 3$, and

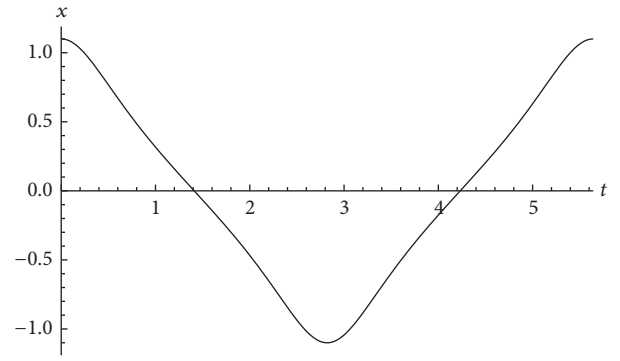

FIGURE 5: Exact solution x in (40) as a function of time t when $a_1 = -1$, $a_5 = 3$, and $x_0 = 1.1$.

$x_0 = 19/20 = 0.95 < 1 = (-3a_1/a_5)^{1/4}$). As was previously mentioned, now the system oscillates around the equilibrium position $x = (-a_1/a_5)^{1/4}$ and the periodic solution satisfies $x \in [x_1, x_0]$ with $0 < x_1 \le x \le x_0$.

5.1. Calculation of the Exact Period. We shall now obtain the period and the solution for the right orbit in Figure 1(c) for which $x > 0$ taking into account that x_0 is the highest value for x. From (7) and considering that $x > 0$, we obtain t as a function of x as follows:

$$2\sqrt{\frac{a_5}{3}}t = \int_{x^2}^{x_0^2} \frac{du}{\sqrt{(x_0^2 - u)\,u\,(u^2 + x_0^2 u + 3a_1/a_5 + x_0^2)}} \tag{41}$$

which can be written as

$$2\sqrt{\frac{a_5}{3}}t = \int_{x^2}^{x_0^2} \frac{du}{\sqrt{(x_0^2 - u)\,(u - u_1)\,u\,(u - u_2)}}, \tag{42}$$

where u_1 and u_2 are defined by the following equations:

$$\begin{aligned} u_1 &= \frac{1}{2\sqrt{a_5}}\left(\sqrt{-3\left(4a_1 + a_5 x_0^4\right)} - \sqrt{a_5 x_0^4}\right) \\ &= \frac{1}{2\sqrt{a_5}}\left(\sqrt{-3q_4} - \sqrt{q_0}\right), \end{aligned} \tag{43}$$

$$\begin{aligned} u_2 &= -\frac{1}{2\sqrt{a_5}}\left(\sqrt{-3\left(4a_1 + a_5 x_0^4\right)} + \sqrt{a_5 x_0^4}\right) \\ &= -\frac{1}{2\sqrt{a_5}}\left(\sqrt{-3q_4} + \sqrt{q_0}\right), \end{aligned} \tag{44}$$

where q_2 and q_4 are defined in (19).

For the right orbit in Figure 1(c) it is easy to verify that it satisfies

$$x_0^2 \ge u \ge u_1 > 0 > u_2. \tag{45}$$

Now the period, T, and the periodic solution, x, are dependent on x_0 and $x \in [x_1, x_0]$, where $x_1 = \sqrt{u_1}$ and u_1 is given in (43). The following integral is valid for $a \geq u \geq b > c > d$ [20, 6th edition, Formula 3.147, Integral 7, page 272]:

$$\int_u^a \frac{dy}{\sqrt{(a-y)(y-b)(y-c)(y-d)}} = \frac{2}{\sqrt{(a-c)(b-d)}} F(\mu, r), \tag{46}$$

where $F(\mu, r)$ is the incomplete elliptic integral of the first kind defined in (13) and μ and r are given by the following equations:

$$\mu = \arcsin\sqrt{\frac{(b-d)(a-u)}{(a-b)(u-d)}}, \qquad r = \frac{(a-b)(c-d)}{(a-c)(b-d)}. \tag{47}$$

We have $a = x_0^2$, $b = u_1$, $c = 0$, and $d = u_2$.

Then the value of the integral in (42) is

$$2\sqrt{\frac{a_5}{3}}t = \frac{2}{\sqrt{x_0^2(u_1-u_2)}} \cdot F\left(\arcsin\sqrt{\frac{(u_1-u_2)(x_0^2-x^2)}{(x_0^2-u_1)(x^2-u_2)}}, \frac{u_2(u_1-x_0^2)}{x_0^2(u_1-u_2)}\right). \tag{48}$$

As can be seen in Figure 1(c), the period of the oscillation is twice the time taken by the oscillator to go from $u = x_0^2$ to $u = u_1$. Therefore,

$$T = 2\left(\frac{-3}{q_0 q_4}\right)^{1/4} K(m_c), \tag{49}$$

where m_c is given by

$$m_c = \frac{1}{2} + \frac{q_2}{2}\left(\frac{-3}{q_0 q_4}\right)^{1/2}. \tag{50}$$

q_0, q_2, and q_4 are defined in (19) and $K(m)$ is the complete elliptic integral of the first kind defined in (16). Figure 6 shows the period T as a function of the initial amplitude x_0 (49) when $a_1 = -1$, $0 < x_0 < (-3a_1/a_5)^{1/4}$ and (a) $a_5 = 1$, (b) $a_5 = 3$, (c) $a_5 = 10$, and (d) $a_5 = 50$. This figure corresponds to the right orbit in the phase space portrait shown in Figure 1(c). Figure 7 shows the variation in the period as a function of the initial position when $a_1 = -1$ and $a_5 = 3$, (a) $x_0 > (-3a_1/a_5)^{1/4} = 1$, Section 4 (17), and (b) $0 < x_0 < (-3a_1/a_5)^{1/4} = 1$, Section 3 (49). As can be seen the motion is not periodic when the initial position is $x = (-3a_1/a_5)^{1/4}$.

5.2. Calculation of the Exact Solution. In order to obtain the solution x as a function of time t, from (48) it follows that

$$\frac{(u_1-u_2)(x_0^2-x^2)}{(x_0^2-u_1)(x^2-u_2)} = \mathrm{sn}^2\left(\sqrt{\frac{1}{3}a_5 x_0^2(u_1-u_2)}\,t, \frac{u_2(u_1-x_0^2)}{x_0^2(u_1-u_2)}\right) \tag{51}$$

and taking into account (19), (43), (44), and (50), (51) allows us to obtain the solution as follows:

$$x(t) = x_0\left[\frac{1-\left(1/2+(q_2/2)(-3/q_0q_4)^{1/2}\right)\mathrm{sn}^2\left(\left(-(1/3)q_0q_4\right)^{1/4}t, m_c\right)}{1-\left(1/2-(1/2)(-3q_0/q_4)^{1/2}\right)\mathrm{sn}^2\left(\left(-(1/3)q_0q_4\right)^{1/4}t, m_c\right)}\right]^{1/2}. \tag{52}$$

When $a_1 < 0$ and $a_5 > 0$, (49) and (52) are valid provided that the initial position x_0 satisfies the condition $0 < x_0 < (-3a_1/a_5)^{1/4}$, except for the equilibrium point (when $x_0 = (-a_1/a_5)^{1/4}$).

The expressions for the period and the exact solution for the left orbit in Figure 1(c), that is, for $x < 0$, can be obtained following the same procedure as that used for $x > 0$ and are not included here.

Figure 8(a) shows the plot of the displacement x as a function of time t when $a_1 = -1$, $a_5 = 3$, and $x_0 = 19/20 = 0.95$. This displacement was obtained using (52). In this example, and from (43), we obtain

$$x_1 = \sqrt{u_1} = \frac{1}{20}\sqrt{\frac{1}{2}\left(-361+\sqrt{249037}\right)} \approx 0.415385. \tag{53}$$

As can easily be verified in Figure 8(a), the oscillatory motion of this system is bounded between $x_1 \approx 0.415385$ and

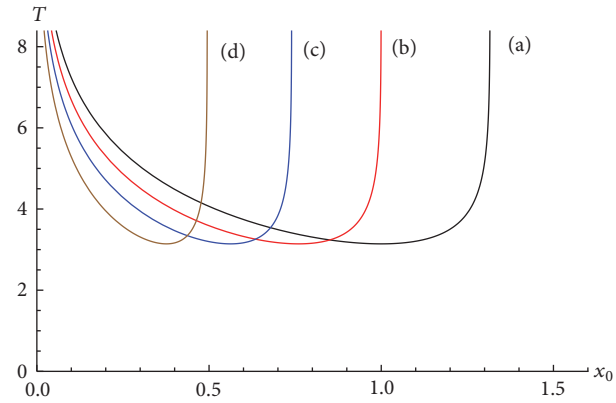

FIGURE 6: Exact period T in (49) as a function of the initial amplitude x_0 when $a_1 = -1$, $0 < x_0 < (-3a_1/a_5)^{1/4}$ and (a) $a_5 = 1$, (b) $a_5 = 3$, (c) $a_5 = 10$, and (d) $a_5 = 50$.

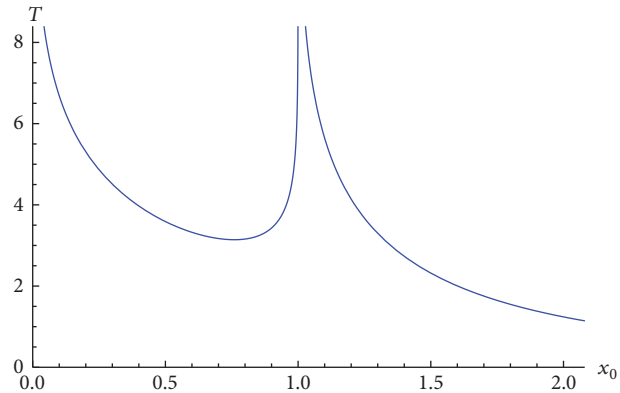

FIGURE 7: Exact period T as a function of the initial position x_0 when $a_1 = -1$ and $a_5 = 3$, (a) $x_0 > (-3a_1/a_5)^{1/4} = 1$, Section 4 (17), and (b) $x_0 < (-3a_1/a_5)^{1/4} = 1$, Section 3 (49). As can be seen the motion is not periodic when the initial position is $x = (-3a_1/a_5)^{1/4}$.

$x_0 = 0.95$ and the equilibrium point is located at $x = (-a_1/a_5)^{1/4} = 3^{-1/4} \approx 0.759839$. Figure 8(b) shows the displacement x as a function of time t when $a_1 = -1$, $a_5 = 3$, and

$$x_0 = \frac{1}{20}\sqrt{\frac{1}{2}\left(-361 + \sqrt{249037}\right)} \approx 0.415385. \tag{54}$$

In this situation we obtained $x_1 = \sqrt{u_1} = 19/20 = 0.95$.

It is easy to verify that in this case the system is equivalent to a mixed-parity nonlinear oscillator. The change of variable

$$y = x - \left(-\frac{a_1}{a_5}\right)^{1/4} \tag{55}$$

gives

$$\frac{d^2y}{dt^2} - 4a_1 y - 10\left(-a_1 a_5^{1/3}\right)^{3/4} y^2 + 10\left(-a_1 a_5\right)^{1/2} y^3 - 5\left(-a_1 a_5^{1/3}\right)^{1/4} y^4 + a_5 y^5 = 0. \tag{56}$$

The system modelled by (56) oscillates around the equilibrium position $y = 0$ and the periodic solution y satisfies $y \in [y_1, y_0]$ with $y_1 = x_1 - (-a_1/a_5)^{1/4}$ and $y_0 = x_0 - (-a_1/a_5)^{1/4}$. Figure 9 shows the phase portrait when $a_1 = -1$, $a_5 = 3$, and $y_0 = x_0 - (-a_1/a_5)^{1/4} = 0.95 - 3^{-1/4} \approx 0.190164$. As can be seen the system oscillates around the equilibrium point $y = 0$.

6. Exact Solution When $a_1 > 0$, $a_5 < 0$, and $0 < x_0 < (-a_1/a_5)^{1/4}$

For case (d) it is necessary to obtain the equation for the period again since if $a_5 < 0$, the root $\sqrt{a_5/3}$ is not a real number and so (7) cannot be used. In order to obtain the exact solution when $a_1 > 0$, $a_5 < 0$, and $0 < x_0 < (-a_1/a_5)^{1/4}$ in which case the system oscillates around the equilibrium position $x = 0$ and the periodic solution x satisfies $x \in [-x_0, x_0]$, we proceed as follows. From (6) we can write

$$\sqrt{-\frac{a_5}{3}}\,dt = \pm\frac{dx}{\sqrt{\left(-3a_1/a_5\right)\left(x_0^2 - x^2\right) + \left(x_0^6 - x^6\right)}}. \tag{57}$$

6.1. Calculation of the Exact Period. We can consider the same four trajectories that we analysed at the beginning of Section 3.2. Doing the change of variable $x^2 = u$, it follows that for trajectory $1 \to 2$ ($0 \le t \le T/4$ and $x_0 \ge x \ge 0$) we have

$$2\sqrt{-\frac{a_5}{3}}\,t = \int_{x^2}^{x_0^2} \frac{du}{\sqrt{\left(x_0^2 - u\right)u\left(-u^2 - x_0^2 u - 3a_1/a_5 - x_0^2\right)}} \tag{58}$$

which can be written as

$$2\sqrt{-\frac{a_5}{3}}\,t = \int_{x^2}^{x_0^2} \frac{du}{\sqrt{\left(w_1 - u\right)\left(x_0^2 - u\right)u\left(u - w_2\right)}}, \tag{59}$$

where w_1 and w_2 are defined by the following equations:

$$\begin{aligned} w_1 &= \frac{1}{2\sqrt{-a_5}}\left(\sqrt{3\left(4a_1 + a_5 x_0^4\right)} - \sqrt{-a_5 x_0^4}\right) \\ &= \frac{1}{2\sqrt{-a_5}}\left(\sqrt{3q_4} - \sqrt{-q_0}\right), \\ w_2 &= -\frac{1}{2\sqrt{-a_5}}\left(\sqrt{3\left(4a_1 + a_5 x_0^4\right)} + \sqrt{-a_5 x_0^4}\right) \\ &= -\frac{1}{2\sqrt{a_5}}\left(\sqrt{3q_4} + \sqrt{-q_0}\right). \end{aligned} \tag{60}$$

It is easy to verify that it satisfies

$$w_1 > x_0^2 \ge u > 0 > w_2. \tag{61}$$

Now the period, T, and the periodic solution, x, are dependent on x_0 and $x \in [-x_0, x_0]$. The following integral is valid

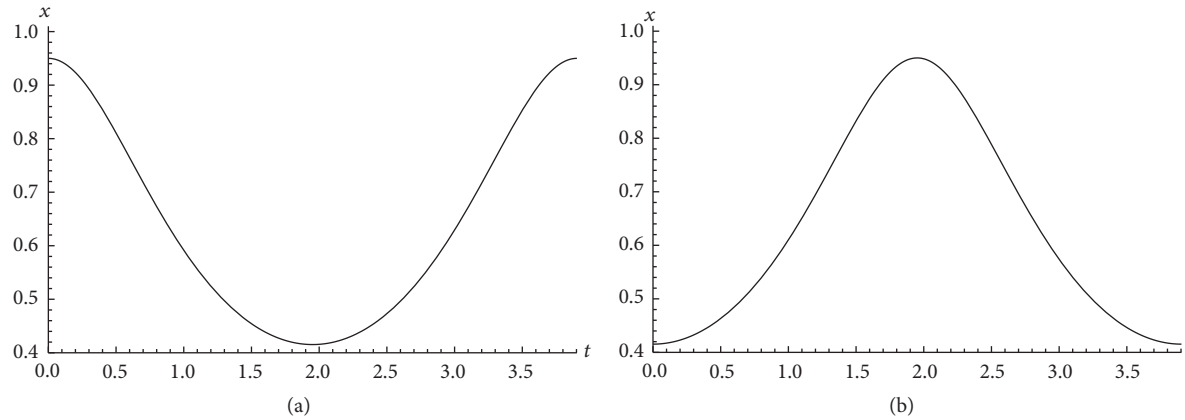

FIGURE 8: (a) Exact periodic solution x in (52) for $a_1 = -1$, $a_5 = 3$, and $x_0 = 19/20 = 0.95$ and (b) $a_1 = -1$, $a_5 = 3$, and $x_0 = (1/20)\sqrt{(1/2)(-361 + \sqrt{249037})}$. In this situation $x_1 = 19/20 = 0.95$ is obtained.

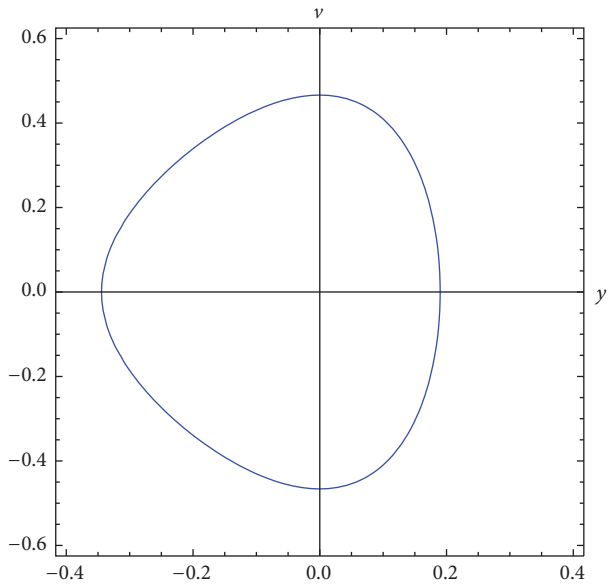

FIGURE 9: Phase space portrait for the mixed-parity nonlinear oscillator in (56) when $a_1 = -1$, $a_1 = 3$ and $y_0 = x_0 - (-a_1/a_5)^{1/4} = 0.95 - 3^{-1/4} \approx 0.190164$. As can be seen the system oscillates around the equilibrium point $y = 0$.

for $a > b \geq u > c > d$ [20, 6th edition, Formula 3.147, Integral 5, page 272]:

$$\int_u^b \frac{dy}{\sqrt{(a-y)(b-y)(y-c)(y-d)}} = \frac{2}{\sqrt{(a-c)(b-d)}} F(\kappa, q), \tag{62}$$

where $F(\kappa, q)$ is the incomplete elliptic integral of the first kind defined in (13) and κ and q are given by the following equations:

$$\kappa = \arcsin\sqrt{\frac{(a-c)(b-u)}{(b-c)(a-u)}},$$

$$q = \frac{(b-c)(a-d)}{(a-c)(b-d)}. \tag{63}$$

We have $a = w_1$, $b = x_0^2$, $c = 0$, and $d = w_2$. Then the value of the integral in (59) is

$$2\sqrt{-\frac{a_5}{3}}t = \frac{2}{\sqrt{w_1(x_0^2 - w_2)}} \cdot F\left(\arcsin\sqrt{\frac{w_1(x_0^2 - x^2)}{x_0^2(w_1 - x^2)}}, \frac{x_0^2(w_1 - w_2)}{w_1(x_0^2 - w_2)}\right). \tag{64}$$

As can be seen in Figure 1(d), the period of the oscillation is four times the time taken by the oscillator to go from $u = 0$ and $u = x_0^2$. Therefore,

$$T = 4\left(\frac{6}{3q_2 - \sqrt{-3q_0q_4}}\right)^{1/2} K(m_d), \tag{65}$$

where m_d is given by

$$m_d = \left(\frac{1}{2} - \frac{3q_2}{2\sqrt{-3q_0q_4}}\right)^{-1}. \tag{66}$$

q_0, q_2, and q_4 are defined in (19) and $K(m)$ is the complete elliptic integral of the first kind defined in (16). Figure 10 shows the period T as a function of the initial amplitude x_0 (65) when $a_1 = 1$, $0 < x_0 < (-a_1/a_5)^{1/4}$ and (a) $a_5 = -1$, (b) $a_5 = -3$, (c) $a_5 = -10$, and (d) $a_5 = -50$. This figure corresponds to the right orbit in the phase space portrait shown in Figure 1(d).

6.2. Calculation of the Exact Solution. In order to obtain the solution x as a function of time t, from (64) it follows that

$$F\left(\arcsin\sqrt{\frac{w_1\left(x_0^2-x^2\right)}{x_0^2\left(w_1-x^2\right)}},\frac{x_0^2\left(w_1-w_2\right)}{w_1\left(x_0^2-w_2\right)}\right) = \sqrt{-\frac{1}{3}a_5w_1\left(x_0^2-w_2\right)}t \tag{67}$$

and then

$$\frac{w_1\left(x_0^2-x^2\right)}{x_0^2\left(w_1-x^2\right)} = \mathrm{sn}^2\left(\sqrt{-\frac{1}{3}a_5w_1\left(x_0^2-w_2\right)}t,\frac{x_0^2\left(w_1-w_2\right)}{w_1\left(x_0^2-w_2\right)}\right) \tag{68}$$

and taking into account (19), (60), (66), and (68) we finally obtain

$$x(t)=\frac{x_0\mathrm{cn}\left(\left((1/2)\,q_2-(1/6)\sqrt{-3q_0q_4}\right)^{1/2}t,m_d\right)}{\left[1+\left(2/\left(1+\left(-3q_4/q_0\right)^{1/2}\right)\right)\mathrm{sn}^2\left(\left((1/2)\,q_2-(1/6)\sqrt{-3q_0q_4}\right)^{1/2}t,m_d\right)\right]^{1/2}}. \tag{69}$$

It is easy to verify that (69) is also valid for trajectories $2\to3$ ($T/4\le t\le T/2$ and $0\ge x\ge -x_0$), $3\to4$ ($T/2\le t\le 3T/4$ and $-x_0\le x\le 0$), and $4\to1$ ($3T/4\le t\le T$ and $0\le x\le x_0$), where the exact period T is given in (65). It is important to point out that when $a_1>0$ and $a_5<0$, (65) and (69) are valid provided that the initial amplitude x_0 satisfies the condition $0<x_0<(-a_1/a_5)^{1/4}$. Figure 11 shows the plot of the displacement x as a function of time t when $a_1=1, a_5=-3$, and $x_0=0.5$. This displacement was obtained using (69). This figure corresponds to the phase space portrait shown in Figure 1(d).

7. Discussion

In this section we briefly discuss the derived solutions presented in this paper compared to the exact one derived by Elías-Zúñiga [11], providing a discussion in which both solutions are compared for all the cases discussed in the manuscript. As it was pointed out in the introduction, Elías-Zúñiga does not solve the nonlinear differential equation exactly as we have done here, but he assumes an expression for the solution. He proposed a solution for (1) with the initial conditions given in (2) which can be written as follows:

$$x^2(t)=\frac{1}{a+b\mathrm{cn}^2(\omega t,m)}. \tag{70}$$

Substituting (70) into (1) it is possible to obtain the values for a, b, ω, and m, whose expressions in terms of a_1, a_5, and x_0 are

$$a=-\frac{2a_5}{a_5x_0^2\pm\sqrt{3}\sqrt{-a_5\left(4a_1a_5+a_5x_0^4\right)}},$$

$$b=\frac{1-ax_0^2}{x_0^2},$$

$$m=\frac{1-a^2x_0^4}{1+2ax_0^2},$$

$$\omega=\sqrt{-\frac{a_1+2aa_1x_0^2}{1+ax_0^2+a^2x_0^4}}. \tag{71}$$

Elías-Zúñiga also concluded that the corresponding exact period of oscillation T of this nonlinear oscillator is given by [11, Eq. (15), page 2576]

$$T=\frac{4K(m)}{\omega} \tag{72}$$

and pointed out that, depending on the system parameter values of a_1, a_5, and x_0, we can have real, complex, or imaginary values for a, b, ω, and m. Now we are going to compare the exact period and solutions presented in this paper with Elías-Zúñiga's paper for all the cases discussed in the manuscript.

7.1. Exact Solution When $a_1\ge0$, $a_5>0$, and $x_0>0$. We have obtained the exact period given in (17) and we have written the exact periodic solution of the quintic oscillator in the compact form given in (40). For this case, Elías-Zúñiga exact period is given in (72) and the exact solution has to be written as a piecewise function as follows:

$$x(t)=\begin{cases}\left(a+b\mathrm{cn}^2(\omega t,m)\right)^{-1/2} & 0\le t\le\dfrac{T}{4}\\ -\left(a+b\mathrm{cn}^2(\omega t,m)\right)^{-1/2} & \dfrac{T}{4}\le t\le\dfrac{3T}{4}\\ \left(a+b\mathrm{cn}^2(\omega t,m)\right)^{-1/2} & \dfrac{3T}{4}\le t\le T.\end{cases} \tag{73}$$

When $a_1=1$, $a_5=3$, and $x_0=1$ we obtain

$$\begin{aligned}a&=-0.25\pm0.661438i,\\ b&=1.25\mp0.661438i,\\ \omega&=0.405233\mp1.63224i,\\ m&=0.5625\pm0.826797i\end{aligned} \tag{74}$$

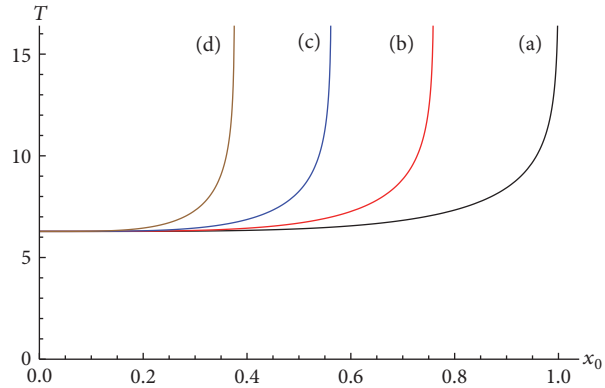

Figure 10: Exact period T in (65) as a function of the initial amplitude x_0 when $a_1 = 1$, $x_0 < (-a_1/a_5)^{1/4}$ and (a) $a_5 = -1$, (b) $a_5 = -3$, (c) $a_5 = -10$, and (d) $a_5 = -50$.

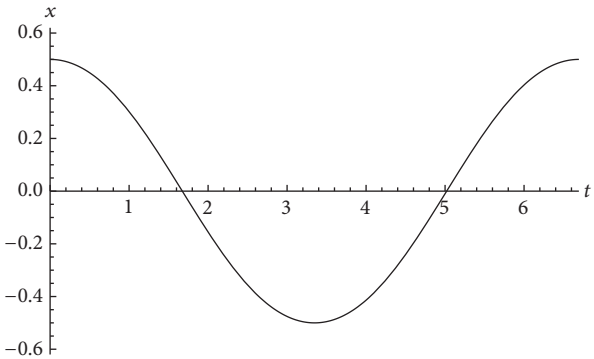

Figure 11: Exact solution x in (69) as a function of time t when $a_1 = 1$, $a_5 = -3$, and $x_0 = 0.5$.

and (72) gives for the period of this nonlinear oscillator the following value:

$$T = 1.89604 \pm 3.37321i \tag{75}$$

which is not a real number and cannot correspond to a period of an oscillatory system. The period we have obtained in this paper by using (17) is $T = 3.79208$ s, which is the correct period. Substituting the values for a, b, ω, and m given in (74) into (73) and plotting x as a function of time, we obtain Figure 3, and it is possible to conclude that the solution given in (40) and the piecewise solution given in (73) are the same exact solution. However, the equation for the exact period given in (72) [11, Eq. (15), page 2576] does not give the exact period.

7.2. Exact Solution When $a_1 < 0$, $a_5 > 0$, and $x_0 > (-3a_1/a_5)^{1/4}$. The exact period is given in (17) and the exact periodic solution is given in (40). For this case, Elías-Zúñiga exact period is given in (72) and the exact solution is written as a piecewise function given in (73).

When $a_1 = -1$, $a_5 = 3$, and $x_0 = 1.1$ we obtain

$$\begin{aligned} a &= -1.3036 \pm 0.674788i, \\ b &= 2.13004 \mp 0.674788i, \\ \omega &= 0.171154 \mp 1.107i, \\ m &= 0.817588 \pm 0.575804i \end{aligned} \tag{76}$$

and (72) gives for the period of this nonlinear oscillator the following value:

$$T = 2.8212 \pm 5.85337i \tag{77}$$

which is not a real number and cannot correspond to a period of a physical oscillatory system. The period we have obtained in this paper by using (17) is $T = 5.64241$ s, which is the correct period. Substituting the values for a, b, ω, and m given in (76) into (73) and plotting x as a function of time, we obtain Figure 5, and it is possible to conclude that the solution given in (40) and the piecewise solution given in (73) are the same exact solution. However, the equation for the exact period given in (72) [11, Eq. (15), page 2576] does not give the exact period.

7.3. Exact Solution When $a_1 < 0$, $a_5 > 0$, and $0 < x_0 < (-3a_1/a_5)^{1/4}$. We have obtained the exact period given in (49) and the exact periodic solution given in (52). For this case, Elías-Zúñiga exact period is given in (72) and the exact solution can be written as follows:

$$x(t) = \frac{1}{\sqrt{a + b\,\mathrm{cn}^2(\omega t, m)}}. \tag{78}$$

When $a_1 = -1$, $a_5 = 3$, and $x_0 = 0.95$ we obtain

$$\begin{aligned} a &= -0.930194, \\ b &= 2.03823, \\ \omega &= 0.885853i, \\ m &= -0.434817 \end{aligned} \tag{79}$$

and (72) gives for the period of this nonlinear oscillator the following value:

$$T = -6.46749i \tag{80}$$

which is an imaginary number and cannot correspond to a period of an oscillatory system. The period we have obtained in this paper by using (49) is $T = 3.90327$ s, which is the correct period. Substituting the values for a, b, ω, and m given in (79) into (78) and plotting x as a function of time, we obtain Figure 8(a), and it is possible to conclude that the solution given in (52) and the solution given in (78) are the same exact solution. However, the equation for the exact period given in (72) [11, Eq. (15), page 2576] does not give the exact period.

7.4. Exact Solution When $a_1 > 0$, $a_5 < 0$, and $0 < x_0 < (-a_1/a_5)^{1/4}$. We have obtained the exact period given in (65)

and the exact periodic solution given in (69). For this case, Elías-Zúñiga exact period is given in (72) and the exact solution is written as a piecewise function given in (73).

When $a_1 = -1$, $a_5 = 3$, and $x_0 = 0.5$ we obtain

$$\begin{aligned} a &= 1.1747, \\ b &= 2.8253, \\ \omega &= 1.07253i, \\ m &= 0.575648 \end{aligned} \tag{81}$$

and (72) gives for the period of this nonlinear oscillator the following value:

$$T = -7.80654i \tag{82}$$

which is an imaginary number and cannot correspond to a period of an oscillatory system. The period we have obtained in this paper by using (65) is $T = 6.69369$ s, which is the correct period. Substituting the values for a, b, ω, and m given in (81) into (73) and plotting x as a function of time, we obtain Figure 11, and it is possible to conclude that the solution we obtained (69) and the solution given in (73) are the same exact solution. However, the equation for the exact period given in (72) [11, Eq. (15), page 2576] does not give the exact period.

7.5. Why the Period Given in [11, Eq. (15), page 2576] Does Not Give the Exact Period? As we have previously pointed out, Elías-Zúñiga concludes that "since the Jacobian elliptic function $\mathrm{cn}(\omega t, m)$ has a period in ωt equal to $4K(m)$, we may see that the corresponding exact period of oscillation T is given by $T = 4K(m)/\omega$" [11, page 2576]. As we have just proved, this equation for the period gives complex and imaginary values for the period of a physical oscillator but not real numbers. However, if Elías-Zúñiga's equations for the exact solution have been proven correct, where is the error in the expression for the period? The answer of this question is that not only the Jacobian elliptic function $\mathrm{cn}(\omega t, m)$ has a period in ωt equal to $4K(m)$, but also periods $4iK'(m)$ and $2K(m) + 2iK'(m)$, where $K'(m) = K(1-m)$ [22].

When $a_1 = 1$, $a_5 = 3$, and $x_0 = 1$, Elías-Zúñiga's period would have to be

$$T = -\frac{4iK'(m)}{\omega} = -\frac{4iK(1-m)}{\omega} = 3.79208 \text{ s} \tag{83}$$

which gives the correct period. When $a_1 = -1$, $a_5 = 3$, and $x_0 = 1.1$, Elías-Zúñiga's period would have to be

$$T = -\frac{4iK'(m)}{\omega} = -\frac{4iK(1-m)}{\omega} = 5.64241 \text{ s} \tag{84}$$

which corresponds to the correct period for these numerical parameters. When $a_1 = -1$, $a_5 = 3$, and $x_0 = 0.95$, the correct expression for Elías-Zúñiga's period would have to be

$$\begin{aligned} T &= \frac{-2K(m) + 2iK'(m)}{\omega} = \frac{-2K(m) + 2iK(1-m)}{\omega} \\ &= 3.90327 \text{ s} \end{aligned} \tag{85}$$

which is the correct period. Finally, when $a_1 = 1$, $a_5 = -3$, and $x_0 = 0.5$, the correct expression for Elías-Zúñiga's period would have to be

$$T = \frac{4iK'(m)}{\omega} = \frac{4iK(1-m)}{\omega} = 6.69369 \text{ s} \tag{86}$$

which corresponds to the correct period for these parameters.

8. Conclusions

Closed-form expressions for the exact periods and solutions of the nonlinear quintic oscillator have been obtained for all possible oscillatory motions of this nonlinear system. Unlike Elías-Zúñiga's procedure [11, 12], we do not assume any expression for the solution but exactly solve the nonlinear differential equation, which allows us to obtain the period and, after inversion, the solution for this conservative nonlinear oscillator. As shown, there are four possible combinations of coefficients a_1 and a_5 which provide periodic motions. In three of them ((a) $a_1 \geq 0$, $a_5 > 0$, and $x_0 > 0$, (b) $a_1 < 0$, $a_5 > 0$, and $x_0 > (-3a_1/a_5)^{1/4} > 0$, and (d) $a_1 > 0$, $a_5 < 0$, and $0 < x_0 < (-a_1/a_5)^{1/4}$) the system oscillates around the equilibrium position $x = 0$ with $x \in [-x_0, x_0]$. However, there is one more case ((c) $a_1 > 0$, $a_5 < 0$, and $0 < x_0 < (-3a_1/a_5)^{1/4}$) in which the system oscillates around the equilibrium position $x = (-a_1/a_5)^{1/4}$ with $x \in [x_1, x_0]$. In all cases the exact periods are given in terms of a complete elliptic integral of the first kind and the exact solutions are expressed in terms of Jacobi elliptic functions. We also showed that making a convenient change of variable to a new variable $y = x - (-a_1/a_5)^{1/4}$ it is possible to verify that case (c) is equivalent to a mixed-parity nonlinear oscillator oscillating around the equilibrium position $y = 0$. Finally, our exact solutions are compared with the exact ones obtained by Elías-Zúñiga [11].

Competing Interests

The authors declare that there is no conflict of interests regarding the publication of this paper.

Acknowledgments

This work was supported by the "Generalitat Valenciana" of Spain, under Project PROMETEOII/2015/015 and by the Universidad de Alicante, Spain, under Project GITE-09006-UA.

References

[1] R. E. Mickens, *Oscillations in Planar Dynamic Systems*, World Scientific, Singapore, 1996.

[2] A. H. Nayfeh and D. T. Mook, *Nonlinear Oscillations*, Wiley-Interscience, New York, NY, USA, 1979.

[3] A. H. Nayfeh, *Problems in Perturbation*, John Wiley & Sons, New York, NY, USA, 1985.

[4] J. Lin, "A new approach to Duffing equation with strong and high order nonlinearity," *Communications in Nonlinear Science and Numerical Simulation*, vol. 4, no. 2, pp. 132–135, 1999.

[5] J. I. Ramos, "On Linstedt-Poincaré technique for the quintic Duffing equation," *Applied Mathematics and Computation*, vol. 193, no. 2, pp. 303–310, 2007.

[6] T. Pirbodaghi, S. H. Hoseini, M. T. Ahmadian, and G. H. Farrahi, "Duffing equations with cubic and quintic nonlinearities," *Computers & Mathematics with Applications*, vol. 57, no. 3, pp. 500–506, 2009.

[7] B. S. Wu, W. P. Sun, and C. W. Lim, "An analytical approximate technique for a class of strongly non-linear oscillators," *International Journal of Non-Linear Mechanics*, vol. 41, no. 6-7, pp. 766–774, 2006.

[8] S. K. Lai, C. W. Lim, B. S. Wu, C. Wang, Q. C. Zeng, and X. F. He, "Newton-harmonic balancing approach for accurate solutions to nonlinear cubic-quintic Duffing oscillators," *Applied Mathematical Modelling*, vol. 33, no. 2, pp. 852–866, 2009.

[9] A. Beléndez, G. Bernabeu, J. Francés, D. I. Méndez, and S. Marini, "An accurate closed-form approximate solution for the quintic Duffing oscillator equation," *Mathematical and Computer Modelling*, vol. 52, no. 3-4, pp. 637–641, 2010.

[10] G. M. Scarpello and D. Ritelli, "Exact solution to a first-fifth power nonlinear unforced oscillator," *Applied Mathematical Sciences*, vol. 4, no. 69-72, pp. 3589–3594, 2010.

[11] A. Elías-Zúñiga, "Exact solution of the cubic-quintic Duffing oscillator," *Applied Mathematical Modelling*, vol. 37, no. 4, pp. 2574–2579, 2013.

[12] A. Elías-Zúñiga, "Exact solution of the quadratic mixed-parity Helmholtz-Duffing oscillator," *Applied Mathematics and Computation*, vol. 218, no. 14, pp. 7590–7594, 2012.

[13] A. Elías-Zúñiga, "Solution of the damped cubic-quintic Duffing oscillator by using Jacobi elliptic functions," *Applied Mathematics and Computation*, vol. 246, pp. 474–481, 2014.

[14] A. Elías-Zúñiga, ""Quintication" method to obtain approximate analytical solutions of non-linear oscillators," *Applied Mathematics and Computation*, vol. 243, pp. 849–855, 2014.

[15] A. Beléndez, T. Beléndez, F. J. Martínez, C. Pascual, M. L. Alvarez, and E. Arribas, "Exact solution for the unforced Duffing oscillator with cubic and quintic nonlinearities," *Nonlinear Dynamics*, vol. 86, no. 3, pp. 1687–1700, 2016.

[16] R. E. Mickens, *Truly Nonlinear Oscillations*, World Scientific, Singapore, 2010.

[17] I. Kovacic and Z. Rakaric, "Oscillators with a fractional-order restoring force: higher-order approximations for motion via a modified Ritz method," *Communications in Nonlinear Science and Numerical Simulation*, vol. 15, no. 9, pp. 2651–2658, 2010.

[18] S. K. Lai and K. W. Chow, "Exact solutions for oscillators with quadratic damping and mixed-parity nonlinearity," *Physica Scripta*, vol. 85, no. 4, Article ID 045006, 2012.

[19] S. L. Perko, *Differential Equations and Dynamical Systems*, Springer, New York, NY, USA, 1991.

[20] I. S. Gradshteyn and I. M. Ryzhik, *Table of Integrals, Series and Products*, Academic Press, San Diego, Calif, USA, 6th edition, 2000.

[21] L. M. Milne-Thomson, "Elliptic integrals," in *Handbook of Mathematical functions with Formulas, Graphics and Mathematical Tables*, M. Abramowitz and I. A. Stegun, Eds., chapter 17, pp. 587–607, Dover, New York, NY, USA, 1972.

[22] L. M. Milne-Thomson, "Jacobian elliptic functions and theta functions," in *Handbook of Mathematical Functions with Formulas, Graphics and Mathematical Tables*, M. Abramowitz and I. A. Stegun, Eds., chapter 16, pp. 567–581, Dover, New York, NY, USA, 1972.

Hindawi
Advances in Mathematical Physics
Volume 2017, Article ID 4538230, 11 pages
https://doi.org/10.1155/2017/4538230

Research Article

Asymptotic Stability and Asymptotic Synchronization of Memristive Regulatory-Type Networks

Jin-E Zhang

Hubei Normal University, Hubei 435002, China

Correspondence should be addressed to Jin-E Zhang; zhang86021205@163.com

Received 31 October 2016; Accepted 10 January 2017; Published 26 January 2017

Academic Editor: Xin Yu

Memristive regulatory-type networks are recently emerging as a potential successor to traditional complementary resistive switch models. Qualitative analysis is useful in designing and synthesizing memristive regulatory-type networks. In this paper, we propose several succinct criteria to ensure global asymptotic stability and global asymptotic synchronization for a general class of memristive regulatory-type networks. The experimental simulations also show the performance of theoretical results.

1. Introduction

Using memristive devices as synapses is a focus in memristive networks. To extract the benefits of high-efficiency memristive memory, various memristive networks have been reported to date [1–18]. Unlike conventional two-terminal devices, memristive networks exhibit pinched memristor hysteresis loop characteristics, making them particularly suitable for linear-drift devices [10]. Moreover, as the modular compact model for memristors, memristive regulatory-type networks are further broadened to memristive systems that exhibit the phenomenon of closed-form sneak paths, which enable nanoscale geometries with short access latencies. A memristive regulatory-type network contains multiply-threshold synapses, which has been heralded as a new paradigm in large-scale circuits. Compared with some memristive systems, a memristive regulatory-type network has the following advantages: (1) it is more biomimetic in behaviors with simple system structure; (2) it simplifies the structure and complication of circuits and is easy to realize. With these coveted properties, memristive regulatory-type networks have the potential of realizations in module-based nanoscale neuromorphic computing systems.

The underlying physics mechanism of memristor models is extremely complex. In order to explore the characteristics and applications of memristive networks, several attempts in [1–4, 6–18] have been made, using nonlinear system theory, to develop behavioral models of memristors. An ideal dynamic property is a critical requirement for the development and validation of memristive networks. Evolutional characteristics of memristive networks are an interesting and prosperous research area. However, deploying nonlinear analysis technology in memristive networks is challenging because a memristive network is basically a switched network cluster [13, 15]. Such switched network cluster thus possesses the synaptic action, in which the synaptic weight can be incrementally ameliorated by adjusting the charge or flux through it. There are two major obstacles to analyze and control the memristive networks, namely, high complexity and switched hybridity [12, 13]. On the other hand, dynamical analysis for memristive networks can explain carrier dynamics and associated transients. Once the electronic properties of memristive networks are revealed, then the circuit models can be implemented based upon the underlying dynamic nature. By tweaking physical structures and bias conditions, system designer can optimize the circuit performance, and then, numerous potential applications of the memristors have been exploited, such as neuromorphic, digital, and quantum computation.

In spite of having significant progress in the area of nonlinear control systems [19–35], memristive regulatory-type networks constituting switched network cluster have received less attention. It has been reasoned that much like neuroevolutionary systems, memristive regulatory-type

networks could be responsible for different neuromorphic architectures [36, 37]. To this end, we focus on the evolution of memristive regulatory-type networks. In this paper, we study global asymptotic stability and global asymptotic synchronization of a class of memristive regulatory-type networks. Based on M-matrix theory, we develop less conservative global asymptotic stability results and global asymptotic synchronization results for memristive regulatory-type networks. Such theoretical analysis can significantly help understand and identify system performance, especially in neuromorphic computing era where stability or synchronization is crucial. In fact, dynamic analysis of memristive regulatory-type networks can provide an overview for optimizing the circuit device and enhancing circuit performances.

The rest of this paper is organized as follows. Section 2 introduces model description and preliminaries. Section 3 gives main results. Section 4 discusses two numerical examples to demonstrate the effectiveness of theoretical results. Finally, Section 5 concludes the paper with some remarks.

2. Model Description and Preliminaries

Consider a general class of memristive regulatory-type networks described by the following delay differential equations: for $i = 1, 2, \ldots, N$, $j = 1, 2, \ldots, M$,

$$\begin{aligned} \dot{p}_i(t) &= -a_i p_i(t) + \sum_{j=1}^{M} b_{ij}\left(q_j(t)\right) f_j\left(q_j\left(t-\rho_{ij}\right)\right), \\ \dot{q}_j(t) &= -c_j q_j(t) + \sum_{i=1}^{N} d_{ji} p_i\left(t-\varrho_{ji}\right), \end{aligned} \tag{1}$$

where $p_i(t)$ and $q_j(t)$ represent the concentration variations of memristive messenger gene i and affiliated organic compound j, respectively, $a_i > 0$ and $c_j > 0$ denote the degradation rates of memristive messenger gene i and affiliated organic compound j, respectively, $d_{ji} \geq 0$ represents the translating rate, nonlinear function $f_j(\cdot)$ is bounded and $f_j(0) = 0$, $0 \leq \rho_{ij} \leq \tau$ and $0 \leq \varrho_{ji} \leq \tau$ ($\tau \geq 0$ is a constant) denote the regulating delay and the translating delay, respectively, and $b_{ij}(q_j(t))$ represents regulatory relationship of the network, which is defined as

$$b_{ij}\left(q_j(t)\right) = \begin{cases} \widehat{b}_{ij}, & q_j(t) < 0, \\ \check{b}_{ij}, & q_j(t) > 0, \end{cases} \tag{2}$$

where $\widehat{b}_{ij}$ and $\check{b}_{ij}$ are constants.

The initial conditions of system (1) are assumed to be

$$\begin{aligned} p_i(s) &= \phi_i(s), \\ q_j(s) &= \varphi_j(s), \\ s &\in [-\tau, 0],\ i = 1, 2, \ldots, N,\ j = 1, 2, \ldots, M, \end{aligned} \tag{3}$$

where $\phi_i(s)$ and $\varphi_j(s)$ are both continuous functions defined on $[-\tau, 0]$.

In addition, we also assume that the nonlinear function $f_j(\cdot)$ ($j = 1, 2, \ldots, M$) satisfies the Lipschitz condition with the Lipschitz constant $l_j > 0$; that is,

$$\begin{aligned} \left|f_j(\chi) - f_j(\widehat{\chi})\right| &\leq l_j\left|\chi - \widehat{\chi}\right|, \\ j &= 1, 2, \ldots, M,\ \forall \chi, \widehat{\chi} \in \mathfrak{R}. \end{aligned} \tag{4}$$

In this paper, solutions of all the systems considered in the following are in Filippov's sense. $K(\mathscr{P})$ denotes closure of the convex hull of set $\mathscr{P}$. $\mathrm{co}\{\widehat{\Pi}, \widehat{\Pi}\}$ denotes closure of the convex hull generated by real numbers $\widehat{\Pi}$ and $\widehat{\Pi}$. Let $\overline{b}_{ij} = \max\{\widehat{b}_{ij}, \check{b}_{ij}\}$, $\underline{b}_{ij} = \min\{\widehat{b}_{ij}, \check{b}_{ij}\}$, and $\widetilde{b}_{ij} = \max\{|\widehat{b}_{ij}|, |\check{b}_{ij}|\}$, for $i = 1, 2, \ldots, N$, $j = 1, 2, \ldots, M$.

When considering memristive regulatory-type networks (1), throughout this paper, let us define the set-valued maps as follows:

$$K\left(b_{ij}\left(q_j(t)\right)\right) = \begin{cases} \widehat{b}_{ij}, & q_j(t) < 0, \\ \mathrm{co}\left\{\widehat{b}_{ij}, \check{b}_{ij}\right\}, & q_j(t) = 0, \\ \check{b}_{ij}, & q_j(t) > 0. \end{cases} \tag{5}$$

Obviously, for $i = 1, 2, \ldots, N$, $j = 1, 2, \ldots, M$,

$$\mathrm{co}\left\{\widehat{b}_{ij}, \check{b}_{ij}\right\} = \left[\underline{b}_{ij}, \overline{b}_{ij}\right]. \tag{6}$$

By the theory of differential inclusions, from (1), then for $i = 1, 2, \ldots, N$, $j = 1, 2, \ldots, M$,

$$\begin{aligned} \dot{p}_i(t) &\in -a_i p_i(t) + \sum_{j=1}^{M} K\left(b_{ij}\left(q_j(t)\right)\right) f_j\left(q_j\left(t-\rho_{ij}\right)\right), \\ \dot{q}_j(t) &= -c_j q_j(t) + \sum_{i=1}^{N} d_{ji} p_i\left(t-\varrho_{ji}\right). \end{aligned} \tag{7}$$

A solution $p(t) = (p_1(t), p_2(t), \ldots, p_N(t))^T$, $q(t) = (q_1(t), q_2(t), \ldots, q_M(t))^T$ in the sense of Filippov of system (1) with initial conditions $p_i(s) = \phi_i(s)$, $q_j(s) = \varphi_j(s)$, and $s \in [-\tau, 0]$, $i = 1, 2, \ldots, N$, $j = 1, 2, \ldots, M$, is absolutely continuous on any compact interval of $[0, +\infty)$, and

$$\begin{aligned} \dot{p}_i(t) &\in -a_i p_i(t) + \sum_{j=1}^{M} K\left(b_{ij}\left(q_j(t)\right)\right) f_j\left(q_j\left(t-\rho_{ij}\right)\right), \\ \dot{q}_j(t) &= -c_j q_j(t) + \sum_{i=1}^{N} d_{ji} p_i\left(t-\varrho_{ji}\right). \end{aligned} \tag{8}$$

Definition 1. The constant vectors $p^* = (p_1^*, p_2^*, \ldots, p_N^*)^T$ and $q^* = (q_1^*, q_2^*, \ldots, q_M^*)^T$ are called an equilibrium point of system (1), if for $i = 1, 2, \ldots, N$, $j = 1, 2, \ldots, M$,

$$\begin{aligned} 0 &\in -a_i p_i^* + \sum_{j=1}^{M} K\left(b_{ij}\left(q_j^*\right)\right) f_j\left(q_j^*\right), \\ 0 &= -c_j q_j^* + \sum_{i=1}^{N} d_{ji} p_i^*. \end{aligned} \tag{9}$$

Definition 2. The equilibrium point of system (1) is said to be globally asymptotically stable if it is locally stable in sense of Lyapunov and globally attractive.

According to Lyapunov direct method, from Definition 2, as we know, if there exists an appropriate Lyapunov function V which is positive definite and radially unbounded, such that the time-derivative of V along the trajectory of system (1) is negative definite, then the equilibrium point of system (1) is globally asymptotically stable.

Definition 3. For drive system $\dot{\mathscr{X}}(t) = \mathscr{F}(t, \mathscr{X})$, $\mathscr{X} \in \mathfrak{R}^n$, response system $\dot{\mathscr{Y}}(t) = \mathscr{G}(t, \mathscr{Y}, U)$, $\mathscr{Y} \in \mathfrak{R}^n$, and $U \in \mathfrak{R}^n$, define the synchronization error signal $\mathscr{E}(t) = \mathscr{X}(t) - \mathscr{Y}(t)$, $\mathscr{E} \in \mathfrak{R}^n$; then the error dynamics can be expressed by the following form:

$$\dot{\mathscr{E}}(t) = \mathscr{F}(t, \mathscr{X}) - \mathscr{G}(t, \mathscr{Y}, U), \tag{10}$$

and we say that the response system can be globally asymptotically synchronized with the drive system if the zero solution of error system is globally asymptotically stable.

3. Main Results

In this section, we will first give two lemmas, which play important role in the analysis and synthesis of memristive regulatory-type networks (1).

Lemma 4. *In system (1) at least one equilibrium point exists:* $p^* = (p_1^*, p_2^*, \ldots, p_N^*)^T$; $q^* = (q_1^*, q_2^*, \ldots, q_M^*)^T$.

Lemma 5. *For system (1), we have*

$$\begin{aligned} &\left|K\left(b_{ij}\left(\mathscr{X}_j\right)\right) f_j\left(\mathscr{X}_j\right) - K\left(b_{ij}\left(\mathscr{Y}_j\right)\right) f_j\left(\mathscr{Y}_j\right)\right| \\ &\quad \le \tilde{b}_{ij} l_j \left|\mathscr{X}_j - \mathscr{Y}_j\right|, \\ &\qquad \forall i = 1, 2, \ldots, N,\ \ j = 1, 2, \ldots, M,\ \ \forall \mathscr{X}_j, \mathscr{Y}_j \in \mathfrak{R}, \end{aligned} \tag{11}$$

where $K(b_{ij}(\mathscr{X}_j))$ and $K(b_{ij}(\mathscr{Y}_j))$ are defined as those in (5).

Using standard arguments as Lemmas 1 and 2 in [15], Lemmas 4 and 5 of this paper can be proved, respectively.

3.1. Global Asymptotic Stability. According to Lemma 4, memristive regulatory-type networks (1) have the equilibrium points $p^* = (p_1^*, p_2^*, \ldots, p_N^*)^T$ and $q^* = (q_1^*, q_2^*, \ldots, q_M^*)^T$; we shift the equilibrium points $p^* = (p_1^*, p_2^*, \ldots, p_N^*)^T$ and $q^* = (q_1^*, q_2^*, \ldots, q_M^*)^T$ to the origin by the translation $x_i(t) = p_i(t) - p_i^*$ and $y_j(t) = q_j(t) - q_j^*$ in the differential inclusion (7), which results in

$$\begin{aligned} \dot{x}_i(t) &\in -a_i x_i(t) \\ &\quad + \sum_{j=1}^{M} K\left(b_{ij}\left(y_j(t)\right)\right) f_j\left(y_j\left(t - \rho_{ij}\right)\right), \\ \dot{y}_j(t) &= -c_j y_j(t) + \sum_{i=1}^{N} d_{ji} x_i\left(t - \varrho_{ji}\right), \end{aligned} \tag{12}$$

where

$$\begin{aligned} &K\left(b_{ij}\left(y_j(t)\right)\right) f_j\left(y_j\left(t - \rho_{ij}\right)\right) \\ &\quad = K\left(b_{ij}\left(y_j(t) + q_j^*\right)\right) f_j\left(y_j\left(t - \rho_{ij}\right) + q_j^*\right) \\ &\qquad - K\left(b_{ij}\left(q_j^*\right)\right) f_j\left(q_j^*\right). \end{aligned} \tag{13}$$

According to Lemma 5,

$$\left|K\left(b_{ij}\left(y_j(t)\right)\right) f_j\left(y_j\left(t - \rho_{ij}\right)\right)\right| \le \tilde{b}_{ij} l_j \left|y_j\left(t - \rho_{ij}\right)\right|. \tag{14}$$

From (12)–(14), for $i = 1, 2, \ldots, N$, $j = 1, 2, \ldots, M$,

$$\begin{aligned} \left|\dot{x}_i(t)\right| &\le -a_i \left|x_i(t)\right| + \sum_{j=1}^{M} \tilde{b}_{ij} l_j \left|y_j\left(t - \rho_{ij}\right)\right|, \\ \left|\dot{y}_j(t)\right| &= -c_j \left|y_j(t)\right| + \sum_{i=1}^{N} d_{ji} \left|x_i\left(t - \varrho_{ji}\right)\right|. \end{aligned} \tag{15}$$

Theorem 6. *The equilibrium points $p^* = (p_1^*, p_2^*, \ldots, p_N^*)^T$ and $q^* = (q_1^*, q_2^*, \ldots, q_M^*)^T$ of system (1) is globally asymptotically stable, if the following matrix*

$$\mathscr{W} = \begin{pmatrix} \mathscr{A} & -\mathscr{B} \\ -\mathscr{D} & \mathscr{C} \end{pmatrix}_{(N+M)\times(N+M)} \tag{16}$$

is a nonsingular M-matrix, where $\mathscr{A} = \operatorname{diag}(a_1, a_2, \ldots, a_N)$, $\mathscr{B} = (\tilde{b}_{ij} l_j)_{N\times M}$, $\mathscr{C} = \operatorname{diag}(c_1, c_2, \ldots, c_M)$, and $\mathscr{D} = (d_{ji})_{M\times N}$.

Proof. Since matrix $\mathscr{W}$ is a nonsingular M-matrix, by the M-matrix theory, it follows that $\mathscr{W}^T$ is a nonsingular M-matrix. Based on the fact that $\mathscr{W}^T$ is a nonsingular M-matrix, then there exists an $(N + M)$-dimensional vector $\eta > 0$ such that $\mathscr{W}^T \eta > 0$; that is,

$$\begin{aligned} a_i \eta_i - \sum_{j=1}^{M} d_{ji} \eta_{N+j} > 0, \quad &\text{for } i = 1, 2, \ldots, N, \\ c_j \eta_{N+j} - \sum_{i=1}^{N} \tilde{b}_{ij} l_j \eta_i > 0, \quad &\text{for } j = 1, 2, \ldots, M. \end{aligned} \tag{17}$$

Choose

$$\begin{aligned} \vartheta_1 &= \min_{1\le i\le N} \left\{ a_i \eta_i - \sum_{j=1}^{M} d_{ji} \eta_{N+j} \right\}, \\ \vartheta_2 &= \min_{1\le j\le M} \left\{ c_j \eta_{N+j} - \sum_{i=1}^{N} \tilde{b}_{ij} l_j \eta_i \right\}, \end{aligned} \tag{18}$$

and then we get

$$\vartheta = \min\{\vartheta_1, \vartheta_2\} > 0. \tag{19}$$

Consider the following positive definite and radially unbounded Lyapunov function:

$$V(x(t), y(t)) = \sum_{i=1}^{N} \eta_i |x_i(t)| + \sum_{j=1}^{M} \eta_{N+j} |y_j(t)| + \sum_{j=1}^{M} \eta_{N+j} \sum_{i=1}^{N} d_{ji} \int_{t-\varrho_{ji}}^{t} |x_i(s)| \, ds + \sum_{i=1}^{N} \eta_i \sum_{j=1}^{M} \widetilde{b}_{ij} l_j \int_{t-\rho_{ij}}^{t} |y_j(s)| \, ds. \tag{20}$$

Calculating the upper right Dini derivative of $V(x(t), y(t))$ along the trajectory of system (12) yields

$$\begin{aligned} &D^+ V(x(t), y(t)) \\ &\le \sum_{i=1}^{N} \eta_i \left[-a_i |x_i(t)| + \sum_{j=1}^{M} \widetilde{b}_{ij} l_j |y_j(t - \rho_{ij})| \right] \\ &\quad + \sum_{j=1}^{M} \eta_{N+j} \left[-c_j |y_j(t)| + \sum_{i=1}^{N} d_{ji} |x_i(t - \varrho_{ji})| \right] \\ &\quad + \sum_{j=1}^{M} \eta_{N+j} \sum_{i=1}^{N} d_{ji} \left[|x_i(t)| - |x_i(t - \varrho_{ji})| \right] \\ &\quad + \sum_{i=1}^{N} \eta_i \sum_{j=1}^{M} \widetilde{b}_{ij} l_j \left[|y_j(t)| - |y_j(t - \rho_{ij})| \right] \\ &= -\sum_{i=1}^{N} \eta_i a_i |x_i(t)| - \sum_{j=1}^{M} \eta_{N+j} c_j |y_j(t)| \\ &\quad + \sum_{j=1}^{M} \eta_{N+j} \sum_{i=1}^{N} d_{ji} |x_i(t)| + \sum_{i=1}^{N} \eta_i \sum_{j=1}^{M} \widetilde{b}_{ij} l_j |y_j(t)| \\ &= \sum_{i=1}^{N} \left[-\eta_i a_i + \sum_{j=1}^{M} \eta_{N+j} d_{ji} \right] |x_i(t)| \\ &\quad + \sum_{j=1}^{M} \left[-\eta_{N+j} c_j + \sum_{i=1}^{N} \eta_i \widetilde{b}_{ij} l_j \right] |y_j(t)| \\ &\le -\vartheta \left[\sum_{i=1}^{N} |x_i(t)| + \sum_{j=1}^{M} |y_j(t)| \right]. \end{aligned} \tag{21}$$

By Lyapunov global asymptotic stability theory, we can conclude system (12) is globally asymptotically stable. Thus, the equilibrium points $p^* = (p_1^*, p_2^*, \ldots, p_N^*)^T$ and $q^* = (q_1^*, q_2^*, \ldots, q_M^*)^T$ of system (1) are globally asymptotically stable. The proof is completed. □

Next we extend Theorem 6 to other possible cases.

Corollary 7. *The equilibrium points $p^* = (p_1^*, p_2^*, \ldots, p_N^*)^T$ and $q^* = (q_1^*, q_2^*, \ldots, q_M^*)^T$ of system (1) are globally asymptotically stable, if*

$$\begin{aligned} a_i &> \sum_{j=1}^{M} d_{ji}, \quad \text{for } i = 1, 2, \ldots, N, \\ c_j &> \sum_{i=1}^{N} \widetilde{b}_{ij} l_j, \quad \text{for } j = 1, 2, \ldots, M. \end{aligned} \tag{22}$$

Proof. Select the $(N + M)$-dimensional unit vector as η in the proof of Theorem 6, from (22); it follows that (17) hold. Therefore, the conclusion of Corollary 7 is obvious. □

Corollary 8. *When $M = N$, the equilibrium points $p^* = (p_1^*, p_2^*, \ldots, p_N^*)^T$ and $q^* = (q_1^*, q_2^*, \ldots, q_M^*)^T$ of system (1) are globally asymptotically stable, if the matrix*

$$\mathscr{W} = \mathscr{A}\mathscr{C} - \mathscr{D}\mathscr{B} \tag{23}$$

is a nonsingular M-matrix, where $\mathscr{A} = \mathrm{diag}(a_1, a_2, \ldots, a_N)$, $\mathscr{B} = (\widetilde{b}_{ij} l_j)_{N \times M}$, $\mathscr{C} = \mathrm{diag}(c_1, c_2, \ldots, c_M)$, and $\mathscr{D} = (d_{ji})_{M \times N}$.

Proof. The proof is a direct result of Theorem 6. □

3.2. Global Asymptotic Synchronization. Let (1) be the drive memristive regulatory-type networks. The response memristive regulatory-type networks are described by the following: for $i = 1, 2, \ldots, N$, $j = 1, 2, \ldots, M$,

$$\begin{aligned} \dot{\mathscr{P}}_i(t) &= -a_i \mathscr{P}_i(t) + \sum_{j=1}^{M} b_{ij} \left(\mathscr{Q}_j(t) \right) f_j \left(\mathscr{Q}_j(t - \rho_{ij}) \right) + \mathscr{U}_i(t), \\ \dot{\mathscr{Q}}_j(t) &= -c_j \mathscr{Q}_j(t) + \sum_{i=1}^{N} d_{ji} \mathscr{P}_i(t - \varrho_{ji}) + \mathscr{V}_j(t), \end{aligned} \tag{24}$$

where $\mathscr{U}_i(t)$, $\mathscr{V}_j(t)$, $i = 1, 2, \ldots, N$, $j = 1, 2, \ldots, M$, denote the appropriate control inputs that will be designed in order to obtain a certain control objective.

Next, the linear feedback scheme is used to achieve synchronization between drive memristive regulatory-type networks (1) and response memristive regulatory-type networks (24); that is, the controllers $\mathscr{U}_i(t)$, $\mathscr{V}_j(t)$, $i = 1, 2, \ldots, N$, $j = 1, 2, \ldots, M$, are designed as follows:

$$\begin{aligned} \mathscr{U}_i(t) &= \mathscr{K}_i \left(p_i(t) - \mathscr{P}_i(t) \right), \\ \mathscr{V}_j(t) &= \mathscr{H}_j \left(q_j(t) - \mathscr{Q}_j(t) \right), \end{aligned} \tag{25}$$

where $\mathscr{K}_i > 0$, $\mathscr{H}_j > 0$ denote the control gains.

Let

$$\begin{aligned} e_i(t) &= p_i(t) - \mathscr{P}_i(t), \\ \mathscr{E}_j(t) &= q_j(t) - \mathscr{Q}_j(t), \end{aligned} \tag{26}$$

for $i = 1, 2, \ldots, N$, $j = 1, 2, \ldots, M$. Then by drive memristive regulatory-type networks (1), response memristive regulatory-type networks (24), and the controllers (25), the error system can be described by

$$\begin{aligned}\dot{e}_i(t) &= -a_i e_i(t) + \left[\sum_{j=1}^{M} b_{ij}\left(q_j(t)\right) f_j\left(q_j\left(t-\rho_{ij}\right)\right)\right. \\ &\quad \left. - \sum_{j=1}^{M} b_{ij}\left(\mathcal{Q}_j(t)\right) f_j\left(\mathcal{Q}_j\left(t-\rho_{ij}\right)\right)\right] - \mathcal{K}_i e_i(t), \\ \dot{\mathcal{E}}_j(t) &= -c_j \mathcal{E}_j(t) + \sum_{i=1}^{N} d_{ji} e_i\left(t-\varrho_{ji}\right) - \mathcal{H}_j \mathcal{E}_j(t),\end{aligned} \tag{27}$$

for $i = 1, 2, \ldots, N$, $j = 1, 2, \ldots, M$.

To apply the theories of set-valued maps and differential inclusions, (27) is equivalent to

$$\begin{aligned}\dot{e}_i(t) &\in -a_i e_i(t) \\ &\quad + \left[\sum_{j=1}^{M} K\left(b_{ij}\left(q_j(t)\right)\right) f_j\left(q_j\left(t-\rho_{ij}\right)\right)\right. \\ &\quad \left. - \sum_{j=1}^{M} K\left(b_{ij}\left(\mathcal{Q}_j(t)\right)\right) f_j\left(\mathcal{Q}_j\left(t-\rho_{ij}\right)\right)\right] - \mathcal{K}_i e_i(t), \\ \dot{\mathcal{E}}_j(t) &= -c_j \mathcal{E}_j(t) + \sum_{i=1}^{N} d_{ji} e_i\left(t-\varrho_{ji}\right) - \mathcal{H}_j \mathcal{E}_j(t).\end{aligned} \tag{28}$$

According to Lemma 5,

$$\begin{aligned}&\left|K\left(b_{ij}\left(q_j(t)\right)\right) f_j\left(q_j\left(t-\rho_{ij}\right)\right)\right. \\ &\quad \left. - K\left(b_{ij}\left(\mathcal{Q}_j(t)\right)\right) f_j\left(\mathcal{Q}_j\left(t-\rho_{ij}\right)\right)\right| \\ &\quad \le \tilde{b}_{ij} l_j \left|\mathcal{E}_j\left(t-\rho_{ij}\right)\right|.\end{aligned} \tag{29}$$

From (28) and (29), for $i = 1, 2, \ldots, N$, $j = 1, 2, \ldots, M$,

$$\begin{aligned}\left|\dot{e}_i(t)\right| &\le -\left(a_i + \mathcal{K}_i\right)\left|e_i(t)\right| + \sum_{j=1}^{M} \tilde{b}_{ij} l_j \left|\mathcal{E}_j\left(t-\rho_{ij}\right)\right|, \\ \left|\dot{\mathcal{E}}_j(t)\right| &= -\left(c_j + \mathcal{H}_j\right)\left|\mathcal{E}_j(t)\right| + \sum_{i=1}^{N} d_{ji}\left|e_i\left(t-\varrho_{ji}\right)\right|.\end{aligned} \tag{30}$$

Theorem 9. *The zero solution of system (28) is globally asymptotically stable; that is, the response system (24) can be globally asymptotically synchronized with the drive system (1), if the following matrix*

$$\mathcal{W} = \begin{pmatrix} \mathcal{A} & -\mathcal{B} \\ -\mathcal{D} & \mathcal{C} \end{pmatrix}_{(N+M)\times(N+M)} \tag{31}$$

is a nonsingular M-matrix, where $\mathcal{A} = \operatorname{diag}(a_1 + \mathcal{K}_1, a_2 + \mathcal{K}_2, \ldots, a_N + \mathcal{K}_N)$, $\mathcal{B} = (\tilde{b}_{ij} l_j)_{N\times M}$, $\mathcal{C} = \operatorname{diag}(c_1 + \mathcal{H}_1, c_2 + \mathcal{H}_2, \ldots, c_M + \mathcal{H}_M)$, *and* $\mathcal{D} = (d_{ji})_{M\times N}$.

Proof. Since matrix $\mathcal{W}$ is a nonsingular M-matrix, by the M-matrix theory, it follows that $\mathcal{W}^T$ is a nonsingular M-matrix. Based on the fact that $\mathcal{W}^T$ is a nonsingular M-matrix, then there exists an $(N + M)$-dimensional vector $\eta > 0$ such that $\mathcal{W}^T \eta > 0$; that is,

$$\begin{aligned}&\left(a_i + \mathcal{K}_i\right)\eta_i - \sum_{j=1}^{M} d_{ji}\eta_{N+j} > 0, \quad \text{for } i = 1, 2, \ldots, N, \\ &\left(c_j + \mathcal{H}_j\right)\eta_{N+j} - \sum_{i=1}^{N} \tilde{b}_{ij} l_j \eta_i > 0, \quad \text{for } j = 1, 2, \ldots, M.\end{aligned} \tag{32}$$

Choose

$$\begin{aligned}\vartheta_1 &= \min_{1\le i\le N}\left\{\left(a_i + \mathcal{K}_i\right)\eta_i - \sum_{j=1}^{M} d_{ji}\eta_{N+j}\right\}, \\ \vartheta_2 &= \min_{1\le j\le M}\left\{\left(c_j + \mathcal{H}_j\right)\eta_{N+j} - \sum_{i=1}^{N} \tilde{b}_{ij} l_j \eta_i\right\},\end{aligned} \tag{33}$$

and then we get

$$\vartheta = \min\{\vartheta_1, \vartheta_2\} > 0. \tag{34}$$

Consider the following positive definite and radially unbounded Lyapunov function:

$$\begin{aligned}V(e(t), \mathcal{E}(t)) &= \sum_{i=1}^{N} \eta_i \left|e_i(t)\right| + \sum_{j=1}^{M} \eta_{N+j}\left|\mathcal{E}_j(t)\right| \\ &\quad + \sum_{j=1}^{M} \eta_{N+j} \sum_{i=1}^{N} d_{ji} \int_{t-\varrho_{ji}}^{t} \left|e_i(s)\right| ds \\ &\quad + \sum_{i=1}^{N} \eta_i \sum_{j=1}^{M} \tilde{b}_{ij} l_j \int_{t-\rho_{ij}}^{t} \left|\mathcal{E}_j(s)\right| ds.\end{aligned} \tag{35}$$

Calculating the upper right Dini derivative of $V(e(t), \mathcal{E}(t))$ along the trajectory of system (28) yields

$$\begin{aligned}D^+V(e(t), \mathcal{E}(t)) &\le \sum_{i=1}^{N} \eta_i \left[-\left(a_i + \mathcal{K}_i\right)\left|e_i(t)\right|\right. \\ &\quad \left. + \sum_{j=1}^{M} \tilde{b}_{ij} l_j \left|\mathcal{E}_j\left(t-\rho_{ij}\right)\right|\right] \\ &\quad + \sum_{j=1}^{M} \eta_{N+j} \left[-\left(c_j + \mathcal{H}_j\right)\left|\mathcal{E}_j(t)\right|\right. \\ &\quad \left. + \sum_{i=1}^{N} d_{ji}\left|e_i\left(t-\varrho_{ji}\right)\right|\right] + \sum_{j=1}^{M} \eta_{N+j} \sum_{i=1}^{N} d_{ji} \left[\left|e_i(t)\right|\right. \\ &\quad \left. - \left|e_i\left(t-\varrho_{ji}\right)\right|\right] + \sum_{i=1}^{N} \eta_i \sum_{j=1}^{M} \tilde{b}_{ij} l_j \left[\left|\mathcal{E}_j(t)\right|\right. \\ &\quad \left. - \left|\mathcal{E}_j\left(t-\rho_{ij}\right)\right|\right] = -\sum_{i=1}^{N} \eta_i \left(a_i + \mathcal{K}_i\right)\left|e_i(t)\right|\end{aligned}$$

$$
\begin{aligned}
&- \sum_{j=1}^{M} \eta_{N+j} \left(c_j + \mathscr{H}_j\right) \left|\mathscr{E}_j(t)\right| + \sum_{j=1}^{M} \eta_{N+j} \sum_{i=1}^{N} d_{ji} \left|e_i(t)\right| \\
&+ \sum_{i=1}^{N} \eta_i \sum_{j=1}^{M} \tilde{b}_{ij} l_j \left|\mathscr{E}_j(t)\right| = \sum_{i=1}^{N} \Bigg[-\eta_i \left(a_i + \mathscr{K}_i\right) \\
&+ \sum_{j=1}^{M} \eta_{N+j} d_{ji} \Bigg] \left|e_i(t)\right| + \sum_{j=1}^{M} \Bigg[-\eta_{N+j} \left(c_j + \mathscr{H}_j\right) \\
&+ \sum_{i=1}^{N} \eta_i \tilde{b}_{ij} l_j \Bigg] \left|\mathscr{E}_j(t)\right| \le -\vartheta \Bigg[\sum_{i=1}^{N} \left|e_i(t)\right| \\
&+ \sum_{j=1}^{M} \left|\mathscr{E}_j(t)\right| \Bigg].
\end{aligned} \tag{36}
$$

By Lyapunov global asymptotic stability theory, we can conclude that system (28) is globally asymptotically stable. Thus, the response system (24) can be globally asymptotically synchronized with the drive system (1). The proof is completed. □

Next we extend Theorem 9 to other possible cases.

Corollary 10. *The zero solution of system (28) is globally asymptotically stable; that is, the response system (24) can be globally asymptotically synchronized with the drive system (1), if*

$$
\begin{aligned}
a_i + \mathscr{K}_i &> \sum_{j=1}^{M} d_{ji}, \quad \text{for } i = 1, 2, \ldots, N, \\
c_j + \mathscr{H}_j &> \sum_{i=1}^{N} \tilde{b}_{ij} l_j, \quad \text{for } j = 1, 2, \ldots, M.
\end{aligned} \tag{37}
$$

Proof. Select the $(N + M)$-dimensional unit vector as η in the proof of Theorem 9, from (37), it follows that (32) hold. Therefore, the conclusion of Corollary 10 is obvious. □

Corollary 11. *When $M = N$, the zero solution of system (28) is globally asymptotically stable; that is, the response system (24) can be globally asymptotically synchronized with the drive system (1), if the matrix*

$$
\mathscr{W} = \mathscr{A}\mathscr{C} - \mathscr{D}\mathscr{B} \tag{38}
$$

is a nonsingular M-matrix, where $\mathscr{A} = \operatorname{diag}(a_1 + \mathscr{K}_1, a_2 + \mathscr{K}_2, \ldots, a_N + \mathscr{K}_N)$, $\mathscr{B} = (\tilde{b}_{ij} l_j)_{N\times M}$, $\mathscr{C} = \operatorname{diag}(c_1 + \mathscr{H}_1, c_2 + \mathscr{H}_2, \ldots, c_M + \mathscr{H}_M)$, and $\mathscr{D} = (d_{ji})_{M\times N}$.

Proof. The proof is a direct result of Theorem 9. □

Remark 12. Theorem 9 and Corollaries 10 and 11 show the feasibility of linear feedback scheme for designing a perfect control in memristive regulatory-type networks, and the sufficient conditions only depend on some system parameters, which are easy to be checked.

Remark 13. Compared with many other control strategies, linear feedback scheme is more suitable for implementation in memristive regulatory-type networks. For one thing, transient states are quite prevalent in memristive regulatory-type networks; that is, state-dependent jump abruptly spikes up or down with uncertainty. For another thing, linear feedback scheme itself is relatively cheaper and simpler to operate. It is more reasonable and implementable for linear feedback scheme only carried out at finite gain and bandwidth.

Remark 14. The asymptotic synchronization strategy contains more general synchronization behaviors. Through the node cluster, asymptotic synchronization in each group can achieve complete synchronization.

4. Illustrative Examples

In this section, we discuss two numerical examples to illustrate the theoretical results.

Example 1. Consider the following memristive regulatory-type networks:

$$
\begin{aligned}
\dot{p}_i(t) &= -p_i(t) + \sum_{j=1}^{2} b_{ij}\left(q_j(t)\right) f_j\left(q_j(t - 0.1)\right), \\
\dot{q}_j(t) &= -q_j(t) + \sum_{i=1}^{3} 0.2 p_i(t - 0.3),
\end{aligned} \tag{39}
$$

where $i = 1, 2, 3$, $j = 1, 2$, $f_j(\nu) = (|\nu + 1| - |\nu - 1|)/2$,

$$
b_{ij}\left(q_j(t)\right) = \begin{cases} 0.3, & q_j(t) < 0, \\ -0.3, & q_j(t) > 0, \end{cases} \quad i = 1, 2, 3, \ j = 1, 2. \tag{40}
$$

Obviously, we can calculate that

$$
\begin{aligned}
\mathscr{A} &= \begin{pmatrix} 1 & 0 & 0 \\ 0 & 1 & 0 \\ 0 & 0 & 1 \end{pmatrix}_{3\times 3}, \\
-\mathscr{B} &= \begin{pmatrix} -0.3 & -0.3 \\ -0.3 & -0.3 \\ -0.3 & -0.3 \end{pmatrix}_{3\times 2}, \\
\mathscr{C} &= \begin{pmatrix} 1 & 0 \\ 0 & 1 \end{pmatrix}_{2\times 2}, \\
-\mathscr{D} &= \begin{pmatrix} -0.2 & -0.2 & -0.2 \\ -0.2 & -0.2 & -0.2 \end{pmatrix}_{2\times 3},
\end{aligned} \tag{41}
$$

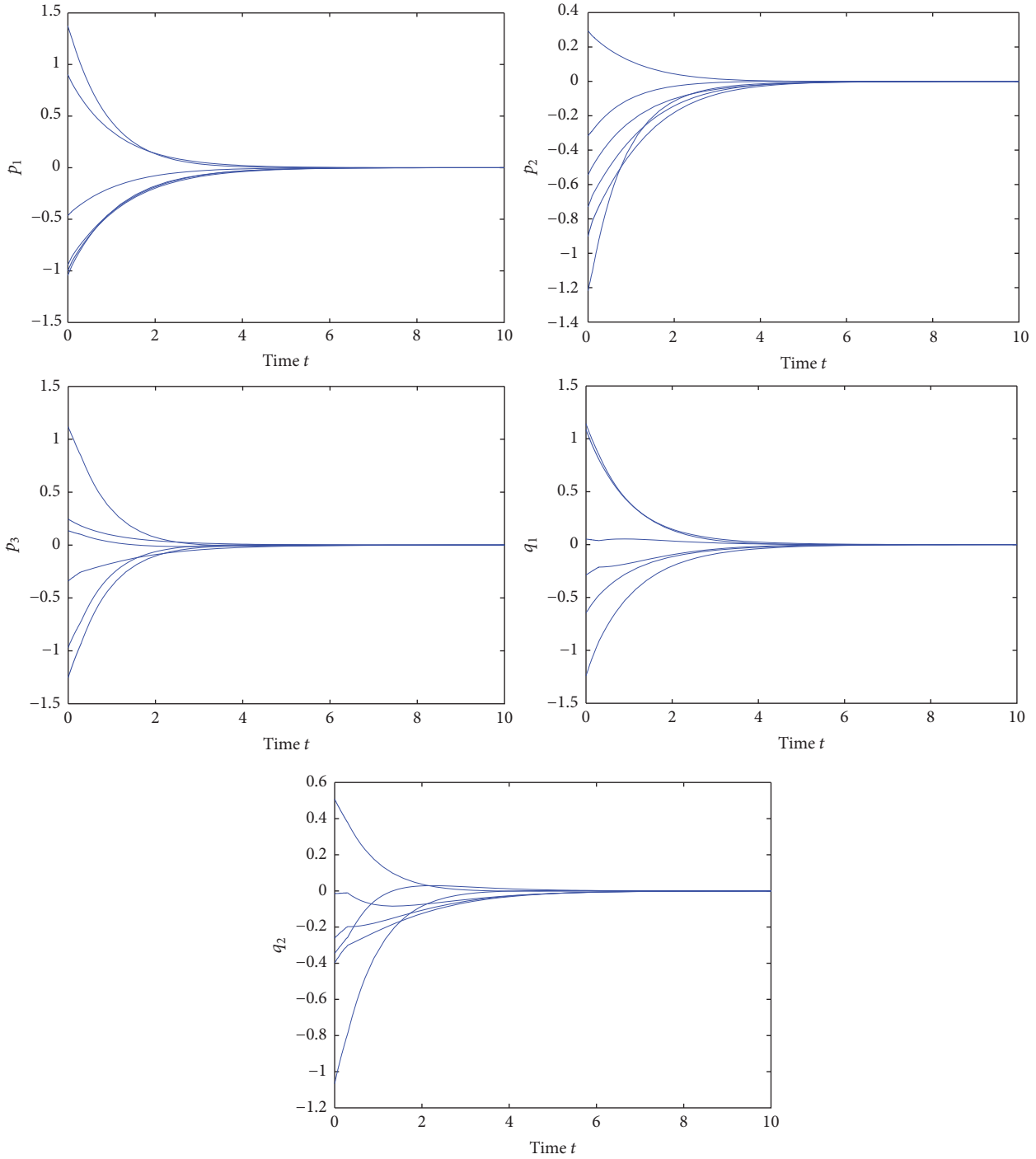

Figure 1: Transient behaviors of system (39).

and then

$$\mathscr{W} = \begin{pmatrix} 1 & 0 & 0 & -0.3 & -0.3 \\ 0 & 1 & 0 & -0.3 & -0.3 \\ 0 & 0 & 1 & -0.3 & -0.3 \\ -0.2 & -0.2 & -0.2 & 1 & 0 \\ -0.2 & -0.2 & -0.2 & 0 & 1 \end{pmatrix}_{5\times 5}, \quad (42)$$

and the eigenvalues of matrix $\mathscr{W}$ are 0.4, 1, 1, 1, and 1.6; thus the matrix $\mathscr{W}$ is a nonsingular M-matrix. According to Theorem 6, system (39) is globally asymptotically stable.

The simulation results of system (39) with some initial values are depicted in Figures 1 and 2. Based on the dynamical evolutions in Figures 1 and 2, we can see that the experimental results agree with the theory very well.

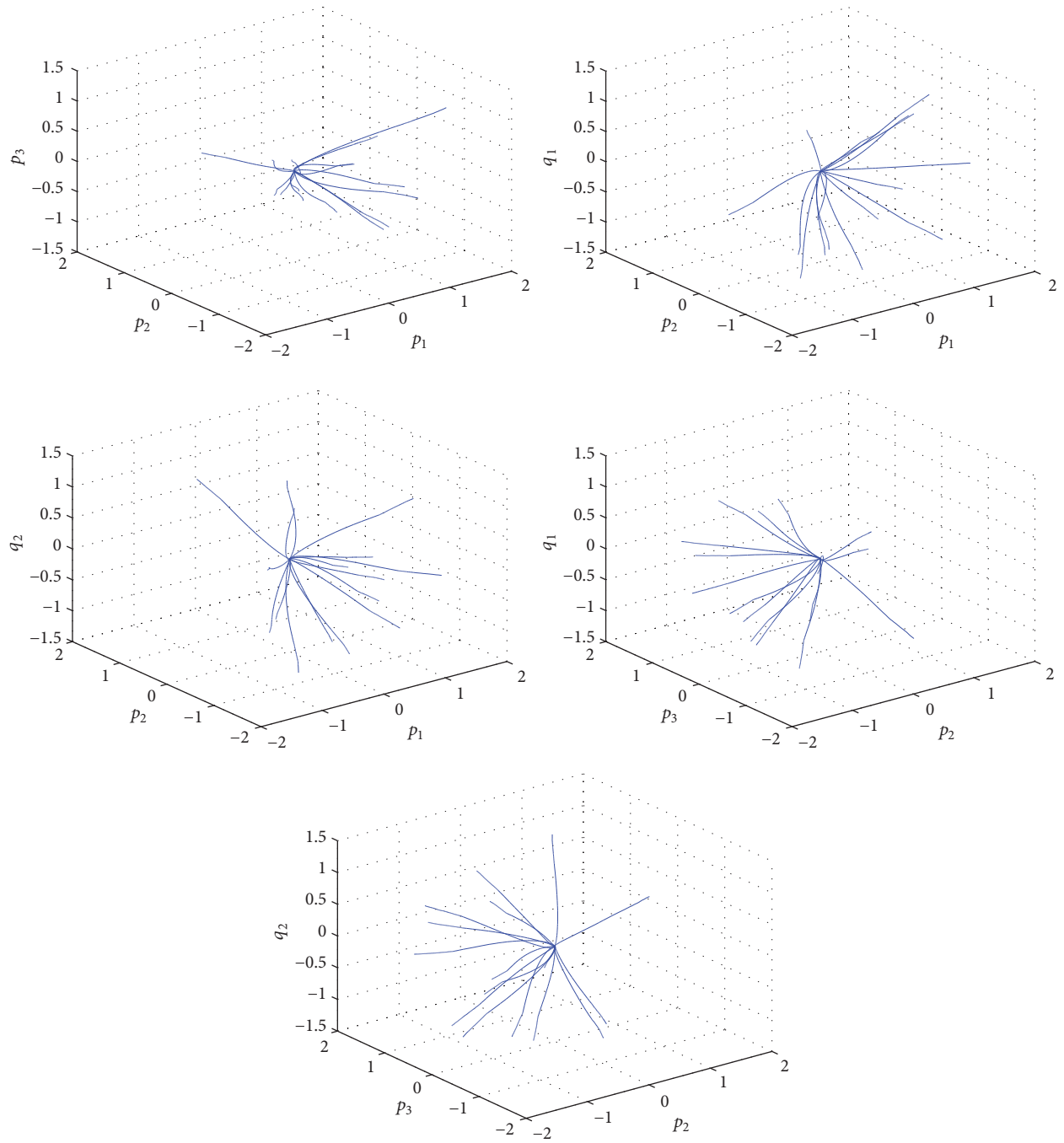

Figure 2: Phase portraits of system (39) in the three-dimensional space.

Example 2. Consider the following memristive regulatory-type networks:

$$\begin{aligned}\dot{p}_i(t) &= -0.2p_i(t) + \sum_{j=1}^{2} b_{ij}\left(q_j(t)\right) f_j\left(q_j(t-0.1)\right),\\ \dot{q}_j(t) &= -0.2q_j(t) + \sum_{i=1}^{3} 0.2p_i(t-0.3),\end{aligned} \tag{43}$$

where $i = 1, 2, 3$, $j = 1, 2$, $f_j(v) = (|v+1| - |v-1|)/2$,

$$b_{ij}\left(q_j(t)\right) = \begin{cases} 0.3, & q_j(t) < 0,\\ -0.3, & q_j(t) > 0,\end{cases} \tag{44}$$

$$i = 1, 2, 3, \quad j = 1, 2.$$

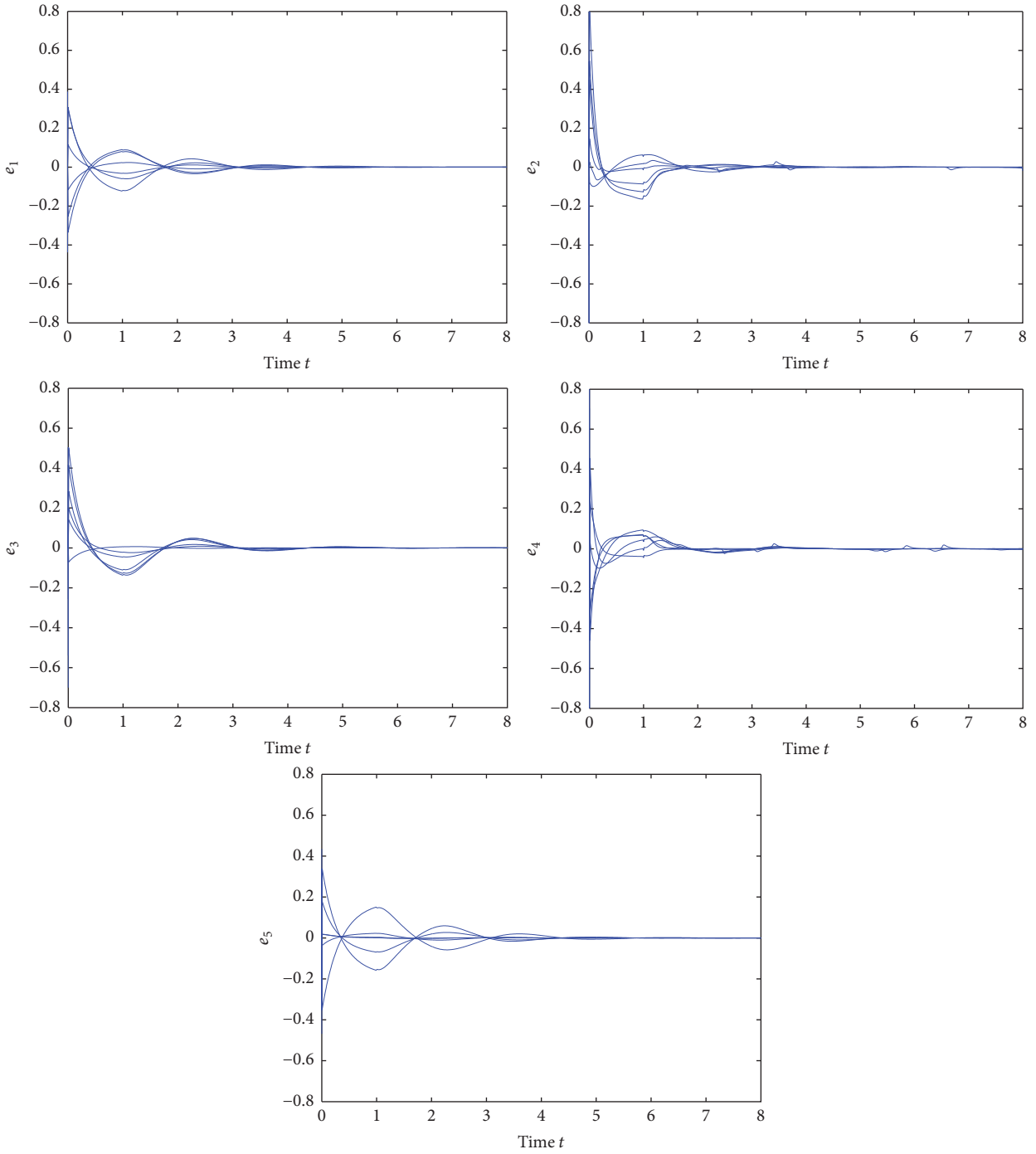

FIGURE 3: The error dynamics $e_1(t) = p_1(t) - \mathscr{P}_1(t)$, $e_2(t) = p_2(t) - \mathscr{P}_2(t)$, $e_3(t) = p_3(t) - \mathscr{P}_3(t)$, $e_4(t) = q_1(t) - \mathscr{Q}_1(t)$, and $e_5(t) = q_2(t) - \mathscr{Q}_2(t)$.

Let (43) be the drive system. The response system is described by

$$\dot{\mathscr{P}}_i(t) = -0.2\mathscr{P}_i(t) + \sum_{j=1}^{2} b_{ij}\left(\mathscr{Q}_j(t)\right) f_j\left(\mathscr{Q}_j(t-0.1)\right) + \mathscr{U}_i(t), \tag{45}$$

$$\dot{\mathscr{Q}}_j(t) = -0.2\mathscr{Q}_j(t) + \sum_{i=1}^{3} 0.2\mathscr{P}_i(t-0.3) + \mathscr{V}_j(t),$$

where $i = 1, 2, 3$, $j = 1, 2$, $f_j(v) = (|v+1| - |v-1|)/2$,

$$b_{ij}\left(\mathscr{Q}_j(t)\right) = \begin{cases} 0.3, & \mathscr{Q}_j(t) < 0, \\ -0.3, & \mathscr{Q}_j(t) > 0, \end{cases} \quad i = 1, 2, 3, \ j = 1, 2. \tag{46}$$

The controllers $\mathscr{U}_i(t)$, $\mathscr{V}_j(t)$, $i = 1, 2, 3$, $j = 1, 2$, are designed as follows:

$$\mathscr{U}_i(t) = 0.8\left(p_i(t) - \mathscr{P}_i(t)\right),$$

$$\mathscr{V}_j(t) = 0.8\left(q_j(t) - \mathscr{Q}_j(t)\right), \tag{47}$$

and to apply Theorem 9, then we can calculate that

$$\mathscr{A} = \begin{pmatrix} 1 & 0 & 0 \\ 0 & 1 & 0 \\ 0 & 0 & 1 \end{pmatrix}_{3\times 3},$$
$$-\mathscr{B} = \begin{pmatrix} -0.3 & -0.3 \\ -0.3 & -0.3 \\ -0.3 & -0.3 \end{pmatrix}_{3\times 2}, \tag{48}$$
$$\mathscr{C} = \begin{pmatrix} 1 & 0 \\ 0 & 1 \end{pmatrix}_{2\times 2},$$
$$-\mathscr{D} = \begin{pmatrix} -0.2 & -0.2 & -0.2 \\ -0.2 & -0.2 & -0.2 \end{pmatrix}_{2\times 3},$$

and then

$$\mathscr{W} = \begin{pmatrix} 1 & 0 & 0 & -0.3 & -0.3 \\ 0 & 1 & 0 & -0.3 & -0.3 \\ 0 & 0 & 1 & -0.3 & -0.3 \\ -0.2 & -0.2 & -0.2 & 1 & 0 \\ -0.2 & -0.2 & -0.2 & 0 & 1 \end{pmatrix}_{5\times 5}, \tag{49}$$

and the eigenvalues of matrix $\mathscr{W}$ are 0.4, 1, 1, 1, and 1.6; thus the matrix $\mathscr{W}$ is a nonsingular M-matrix. According to Theorem 9, the response system (45) can be globally asymptotically synchronized with the drive system (43). The simulation result on the error dynamics $e_1(t) = p_1(t) - \mathscr{P}_1(t)$, $e_2(t) = p_2(t) - \mathscr{P}_2(t)$, $e_3(t) = p_3(t) - \mathscr{P}_3(t)$, $e_4(t) = q_1(t) - \mathscr{Q}_1(t)$, and $e_5(t) = q_2(t) - \mathscr{Q}_2(t)$, with some initial values, is depicted in Figure 3. The dynamical evolutions in Figure 3 clearly indicate that the controller designed performs well.

5. Conclusion

Memristive network can achieve more expedient goal-finding behavior in spiking networks via memristive connections, which has aroused considerable interest by electronics researchers. The practical applications of memristive network popularizes real-time processing and recognition of natural signals. It is of great significance to investigate its nonlinear dynamics. In this paper, we study global asymptotic stability and global asymptotic synchronization for memristive regulatory-type networks, based on the M-matrix theory and Lyapunov stability theory. These criteria, which can be directly derived from the system parameters, are easily verified. The theoretical results developed in this paper may be applied to the synthesis of memristive regulatory-type networks.

Competing Interests

The author declares that there is no conflict of interests regarding the publication of this paper.

Acknowledgments

The work is supported by the Research Project of Hubei Provincial Department of Education of China under Grant T201412.

References

[1] T. Li, S. Duan, J. Liu, L. Wang, and T. Huang, "A spintronic memristor-based neural network with radial basis function for robotic manipulator control implementation," *IEEE Transactions on Systems, Man, and Cybernetics: Systems*, vol. 46, no. 4, pp. 582–588, 2016.

[2] S. P. Adhikari, H. Kim, R. K. Budhathoki, C. Yang, and L. O. Chua, "A circuit-based learning architecture for multilayer neural networks with memristor bridge synapses," *IEEE Transactions on Circuits and Systems I: Regular Papers*, vol. 62, no. 1, pp. 215–223, 2015.

[3] Z. Y. Guo, J. Wang, and Z. Yan, "Global exponential dissipativity and stabilization of memristor-based recurrent neural networks with time-varying delays," *Neural Networks*, vol. 48, pp. 158–172, 2013.

[4] Z. Guo, J. Wang, and Z. Yan, "Attractivity analysis of memristor-based cellular neural networks with time-varying delays," *IEEE Transactions on Neural Networks and Learning Systems*, vol. 25, no. 4, pp. 704–717, 2014.

[5] Y. V. Pershin and M. Di Ventra, "Experimental demonstration of associative memory with memristive neural networks," *Neural Networks*, vol. 23, no. 7, pp. 881–886, 2010.

[6] X. Wang, C. Li, and T. Huang, "Delay-dependent robust stability and stabilization of uncertain memristive delay neural networks," *Neurocomputing*, vol. 140, pp. 155–161, 2014.

[7] X. Wang, C. Li, T. Huang, and S. Duan, "Global exponential stability of a class of memristive neural networks with time-varying delays," *Neural Computing and Applications*, vol. 24, no. 7-8, pp. 1707–1715, 2014.

[8] X. S. Yang and D. W. C. Ho, "Synchronization of delayed memristive neural networks: robust analysis approach," *IEEE Transactions on Cybernetics*, vol. 46, no. 12, pp. 3377–3387, 2016.

[9] Z. Wang, S. Ding, Z. Huang, and H. Zhang, "Exponential stability and stabilization of delayed memristive neural networks based on quadratic convex combination method," *IEEE Transactions on Neural Networks and Learning Systems*, vol. 27, no. 11, pp. 2337–2350, 2016.

[10] A. Wu and Z. Zeng, "Global Mittag–Leffler stabilization of fractional-order memristive neural networks," *IEEE Transactions on Neural Networks and Learning Systems*, vol. 28, no. 1, pp. 206–217, 2017.

[11] L. M. Wang and Y. Shen, "Finite-time stabilizability and instabilizability of delayed memristive neural networks with nonlinear discontinuous controller," *IEEE Transactions on Neural Networks and Learning Systems*, vol. 26, no. 11, pp. 2914–2924, 2015.

[12] S. Yang, Z. Guo, and J. Wang, "Robust synchronization of multiple memristive neural networks with uncertain parameters via

nonlinear coupling," *IEEE Transactions on Systems, Man, and Cybernetics: Systems*, vol. 45, no. 7, pp. 1077–1086, 2015.

[13] A. Wu and Z. Zhigang, "Lagrange stability of memristive neural networks with discrete and distributed delays," *IEEE Transactions on Neural Networks and Learning Systems*, vol. 25, no. 4, pp. 690–703, 2014.

[14] D. Querlioz, O. Bichler, P. Dollfus, and C. Gamrat, "Immunity to device variations in a spiking neural network with memristive nanodevices," *IEEE Transactions on Nanotechnology*, vol. 12, no. 3, pp. 288–295, 2013.

[15] A. Wu and Z. Zeng, "An improved criterion for stability and attractability of memristive neural networks with time-varying delays," *Neurocomputing*, vol. 145, pp. 316–323, 2014.

[16] M. Al-Shedivat, R. Naous, G. Cauwenberghs, and K. N. Salama, "Memristors empower spiking neurons with stochasticity," *IEEE Journal on Emerging and Selected Topics in Circuits and Systems*, vol. 5, no. 2, pp. 242–253, 2015.

[17] G. D. Zhang and Y. Shen, "New algebraic criteria for synchronization stability of chaotic memristive neural networks with time-varying delays," *IEEE Transactions on Neural Networks and Learning Systems*, vol. 24, no. 10, pp. 1701–1707, 2013.

[18] G. Zhang, Y. Shen, Q. Yin, and J. Sun, "Global exponential periodicity and stability of a class of memristor-based recurrent neural networks with multiple delays," *Information Sciences*, vol. 232, pp. 386–396, 2013.

[19] H. Huang, G. Feng, and J. Cao, "Robust state estimation for uncertain neural networks with time-varying delay," *IEEE Transactions on Neural Networks*, vol. 19, no. 8, pp. 1329–1339, 2008.

[20] T. Huang, "Robust stability of delayed fuzzy Cohen-Grossberg neural networks," *Computers & Mathematics with Applications*, vol. 61, no. 8, pp. 2247–2250, 2011.

[21] T. Huang, C. Li, S. Duan, and J. A. Starzyk, "Robust exponential stability of uncertain delayed neural networks with stochastic perturbation and impulse effects," *IEEE Transactions on Neural Networks and Learning Systems*, vol. 23, no. 6, pp. 866–875, 2012.

[22] G. C. Adam, B. D. Hoskins, M. Prezioso, F. Merrikh-Bayat, B. Chakrabarti, and D. B. Strukov, "3-D memristor crossbars for analog and neuromorphic computing applications," *IEEE Transactions on Electron Devices*, vol. 64, no. 1, pp. 312–318, 2017.

[23] F.-X. Wu, "Delay-independent stability of genetic regulatory networks," *IEEE Transactions on Neural Networks*, vol. 22, no. 11, pp. 1685–1693, 2011.

[24] Z. Yi, "Foundations of implementing the competitive layer model by Lotka-Volterra recurrent neural networks," *IEEE Transactions on Neural Networks*, vol. 21, no. 3, pp. 494–507, 2010.

[25] Z. Yi, L. Zhang, J. Yu, and K. K. Tan, "Permitted and forbidden sets in discrete-time linear threshold recurrent neural networks," *IEEE Transactions on Neural Networks*, vol. 20, no. 6, pp. 952–963, 2009.

[26] J. Yu, C. Hu, and H. Jiang, "α-stability and α-synchronization for fractional-order neural networks," *Neural Networks*, vol. 35, pp. 82–87, 2012.

[27] J. Yu, C. Hu, H. J. Jiang, and X. L. Fan, "Projective synchronization for fractional neural networks," *Neural Networks*, vol. 49, pp. 87–95, 2014.

[28] H. Zhang, J. Liu, D. Ma, and Z. Wang, "Data-core-based fuzzy min-max neural network for pattern classification," *IEEE Transactions on Neural Networks*, vol. 22, no. 12, pp. 2339–2352, 2011.

[29] H. Zhang, Y. Luo, and D. Liu, "Neural-network-based near-optimal control for a class of discrete-time affine nonlinear systems with control constraints," *IEEE Transactions on Neural Networks*, vol. 20, no. 9, pp. 1490–1503, 2009.

[30] H. Zhang, T. Ma, G.-B. Huang, and Z. Wang, "Robust global exponential synchronization of uncertain chaotic delayed neural networks via dual-stage impulsive control," *IEEE Transactions on Systems, Man, and Cybernetics, Part B: Cybernetics*, vol. 40, no. 3, pp. 831–844, 2010.

[31] E. Devane and I. Lestas, "Delay-independent incremental stability in time-varying monotone systems satisfying a generalized condition of two-sided scalability," *Automatica*, vol. 76, pp. 1–9, 2017.

[32] Y. Wu, R. Lu, P. Shi, H. Su, and Z. Wu, "Adaptive output synchronization of heterogeneous network with an uncertain leader," *Automatica*, vol. 76, pp. 183–192, 2017.

[33] R. Naldi, M. Furci, R. G. Sanfelice, and L. Marconi, "Robust global trajectory tracking for underactuated VTOL aerial vehicles using inner-outer loop control paradigms," *IEEE Transactions on Automatic Control*, vol. 62, no. 1, pp. 97–112, 2017.

[34] A. Wu, L. Liu, T. Huang, and Z. Zeng, "Mittag-Leffler stability of fractional-order neural networks in the presence of generalized piecewise constant arguments," *Neural Networks*, vol. 85, pp. 118–127, 2017.

[35] C. P. Bechlioulis and G. A. Rovithakis, "Decentralized robust synchronization of unknown high order nonlinear multi-agent systems with prescribed transient and steady state performance," *IEEE Transactions on Automatic Control*, vol. 62, no. 1, pp. 123–134, 2017.

[36] I. E. Ebong and P. Mazumder, "CMOS and memristor-based neural network design for position detection," *Proceedings of the IEEE*, vol. 100, no. 6, pp. 2050–2060, 2012.

[37] K. C. Rahman, D. Hammerstrom, Y. Li, H. Castagnaro, and M. A. Perkowski, "Methodology and design of a massively parallel memristive stateful IMPLY logic-based reconfigurable architecture," *IEEE Transactions on Nanotechnology*, vol. 15, no. 4, pp. 675–686, 2016.

Hindawi Publishing Corporation
Advances in Mathematical Physics
Volume 2016, Article ID 4024836, 8 pages
http://dx.doi.org/10.1155/2016/4024836

Research Article

A Chaotic System with an Infinite Number of Equilibrium Points: Dynamics, Horseshoe, and Synchronization

Viet-Thanh Pham,[1] Christos Volos,[2] Sundarapandian Vaidyanathan,[3] and Xiong Wang[4]

[1] *School of Electronics and Telecommunications, Hanoi University of Science and Technology, 01 Dai Co Viet, Hanoi, Vietnam*
[2] *Department of Physics, Aristotle University of Thessaloniki, 54124 Thessaloniki, Greece*
[3] *Research and Development Centre, Vel Tech University, Avadi, Chennai 600062, India*
[4] *Institute for Advanced Study, Shenzhen University, Shenzhen, Guangdong 518060, China*

Correspondence should be addressed to Viet-Thanh Pham; pvt3010@gmail.com

Received 27 September 2016; Accepted 14 November 2016

Academic Editor: Zhi-Yuan Sun

Discovering systems with hidden attractors is a challenging topic which has received considerable interest of the scientific community recently. This work introduces a new chaotic system having hidden chaotic attractors with an infinite number of equilibrium points. We have studied dynamical properties of such special system via equilibrium analysis, bifurcation diagram, and maximal Lyapunov exponents. In order to confirm the system's chaotic behavior, the findings of topological horseshoes for the system are presented. In addition, the possibility of synchronization of two new chaotic systems with infinite equilibria is investigated by using adaptive control.

1. Introduction

Nonlinear systems with chaotic behavior have been exploited since the 1960s [1–4]. Their applications have been witnessed in numerous areas, for example, secure digital communication systems [5], multiple input multiple output radar [6], image encryption with random bit sequence [7], or optimization algorithms [8]. Although almost normal chaotic systems have a countable number of equilibrium points, few unusual systems with infinite number of equilibria have been investigated in the last five years [9]. Chaotic system with line equilibrium was reported in [9–11]. A new class of chaotic systems with circle and square equilibrium was discovered by using predefined general forms [12, 13]. In addition, hyperchaotic behavior was observed in a four-dimensional system with a curve of equilibria [14] or four-dimensional systems with a line of equilibria [15–17].

Remarkably, systems with an infinite number of equilibrium points are considered as systems with "hidden attractors" based on the view point of computation [18–21]. Hidden attractors cause unexpected effects for engineering systems [22–25]. However, the characteristics of hidden attractors are not well understood [26]. The community has raised some concerns about discovering hidden attractors in known systems [27, 28], finding new systems with hidden attractors [29, 30], studying synchronization schemes for systems with hidden attractors [31], or verifying chaotic dynamics in systems with hidden attractors with topological horseshoes [32, 33].

Motivated by special features of systems with hidden attractors, we introduce a new system with an open curve of equilibrium points in this work. In the next section, the model of the new system is described and its dynamics are discovered through different nonlinear tools. Chaotic dynamics of the proposed system are studied through topological horseshoes in Section 3. A possible synchronization of two new identical systems is discussed in Section 4. Finally, Section 5 concludes our work.

2. New System with an Infinite Number of Equilibrium Points and Its Properties

The new system proposed in the present work is a three-dimensional continuous system described as

$$\begin{aligned} \dot{x} &= -z, \\ \dot{y} &= xz^2, \\ \dot{z} &= x - y\tanh(y) + z\left(ay^2 - z^2\right), \end{aligned} \tag{1}$$

in which three state variables are x, y, and z. It is worth noting that there is only one positive parameter (a) in system (1).

It is straightforward to find the equilibrium points of the proposed system by setting the right hand side of (1) to equal zero, that is,

$$-z = 0, \tag{2}$$

$$xz^2 = 0, \tag{3}$$

$$x - y\tanh(y) + z\left(ay^2 - z^2\right) = 0. \tag{4}$$

Equation (2) reveals that $z = 0$. By substituting $z = 0$ into (3) and (4) we have

$$x - y\tanh(y) = 0. \tag{5}$$

In other words, system (1) has an infinite number of equilibrium points:

$$E = \left\{(x, y, z) \in R^3 \mid x = y^*\tanh(y^*),\ y = y^*,\ z = 0\right\}. \tag{6}$$

For the equilibrium E, the Jacobian matrix of system (1) is given by

$$\mathbf{J}_E = \begin{bmatrix} 0 & 0 & -1 \\ 0 & 0 & 0 \\ 1 & -\tanh(y^*) - y^*\left(1 - \tanh^2(y^*)\right) & a(y^*)^2 \end{bmatrix}. \tag{7}$$

On combining this result with $\det(\mathbf{J}_E - \lambda\mathbf{I}) = 0$, we obtain its characteristic equation

$$\lambda\left(\lambda^2 - a(y^*)^2\lambda + 1\right) = 0. \tag{8}$$

It is easy to verify that the characteristic equation (8) has one zero eigenvalue ($\lambda_1 = 0$) and two nonzero eigenvalues ($\lambda_{2,3}$) which depend on the sign of the discriminant:

$$\Delta = a^2(y^*)^4 - 4. \tag{9}$$

For $\Delta = 0$, we get positive eigenvalues $\lambda_{2,3} = a(y^*)^2/2$. Two nonzero eigenvalues are $\lambda_{2,3} = (a(y^*)^2 \pm \sqrt{\Delta})/2$ for the positive discriminant. When the discriminant (9) is negative, a pair of complex conjugate eigenvalues is $\lambda_{2,3} = (a(y^*)^2 \pm i\sqrt{\Delta})/2$. These eigenvalues state that the equilibrium point E is unstable for $a > 0$ and $y^* \neq 0$.

It is interesting that system (1) with uncountable equilibria is chaotic for $a = 2.9$ and the initial condition $(x(0), y(0), z(0)) = (0, 0.1, 0.2)$. Chaotic attractors of system (1) are presented in Figure 1. Its Lyapunov exponents and Kaplan–Yorke dimension are $L_1 = 0.0727$, $L_2 = 0$, $L_3 = -0.3122$, and $D_{\mathrm{KY}} = 2.2329$, respectively. The well-known Wolf's method [34] has been applied to calculate the Lyapunov exponents in our work. The time of computation is 10,000. It is worth noted that, in general, in numerical experiments one cannot expect to get the same values of the finite-time local Lyapunov exponents and the Lyapunov dimension for different points [35–37]. Therefore, the maximum of the finite-time local Lyapunov dimensions on the grid of points has to be considered [35–37].

The value of parameter a has been changed to get detailed dynamics of system (1) with infinite equilibria. By decreasing the value of the parameter a from 3.4 to 2.8, the bifurcation diagram and maximal Lyapunov exponents (MLEs) of system (1) are shown in Figures 2 and 3, respectively. It is possible to observe a route from period-doubling limit cycles to chaos when decreasing the value of the parameter a. When $a > 3.048$, system (1) remains at periodical states, for example, periodical states for $a = 3.35$ are illustrated in Figure 4. System (1) can generate chaotic attractors for $a \leq 3.048$.

3. Horseshoe in the Chaotic System with Infinite Equilibria

Topological horseshoe is a different effective approach to investigate chaos in dynamical systems [38–44]. There is significant attention about seeking topological horseshoe in chaotic systems with hidden attractors [32, 33]. Therefore, in this section we will discover topological horseshoes in the proposed system with infinite equilibria (1).

In order to support the verification of chaos in system with infinite equilibria (1), the most important results of topological horseshoe [45–47] are reviewed briefly. We define X and D as a metric space and a compact subset while f is a map $f : D \to X$. We assume that there are m mutually disjoint compact subsets of D (i.e., $D_1, D_2, \ldots, D_m$) and the restriction of f to each D_i is continuous. A compact subset d of D satisfies $d_i = d \cap D_i$ for $1 \leq i \leq m$. In this case, d is a connection with respect to m mutually disjoint compact subsets of D. We denote F as a family of connections with respect to m mutually disjoint compact subsets of D. The family F is an f-connected family with respect to m mutually disjoint compact subsets of D when

$$d \in F \Longrightarrow f(d_i) \in F. \tag{10}$$

Horseshoe Lemma (see [48]). *If there is an f-connected family F with respect to m mutually disjoint compact subsets of D, then there is the presence of a compact invariant set $K \subset D$ and semiconjugate to m-shift dynamics is $f \mid K$.*

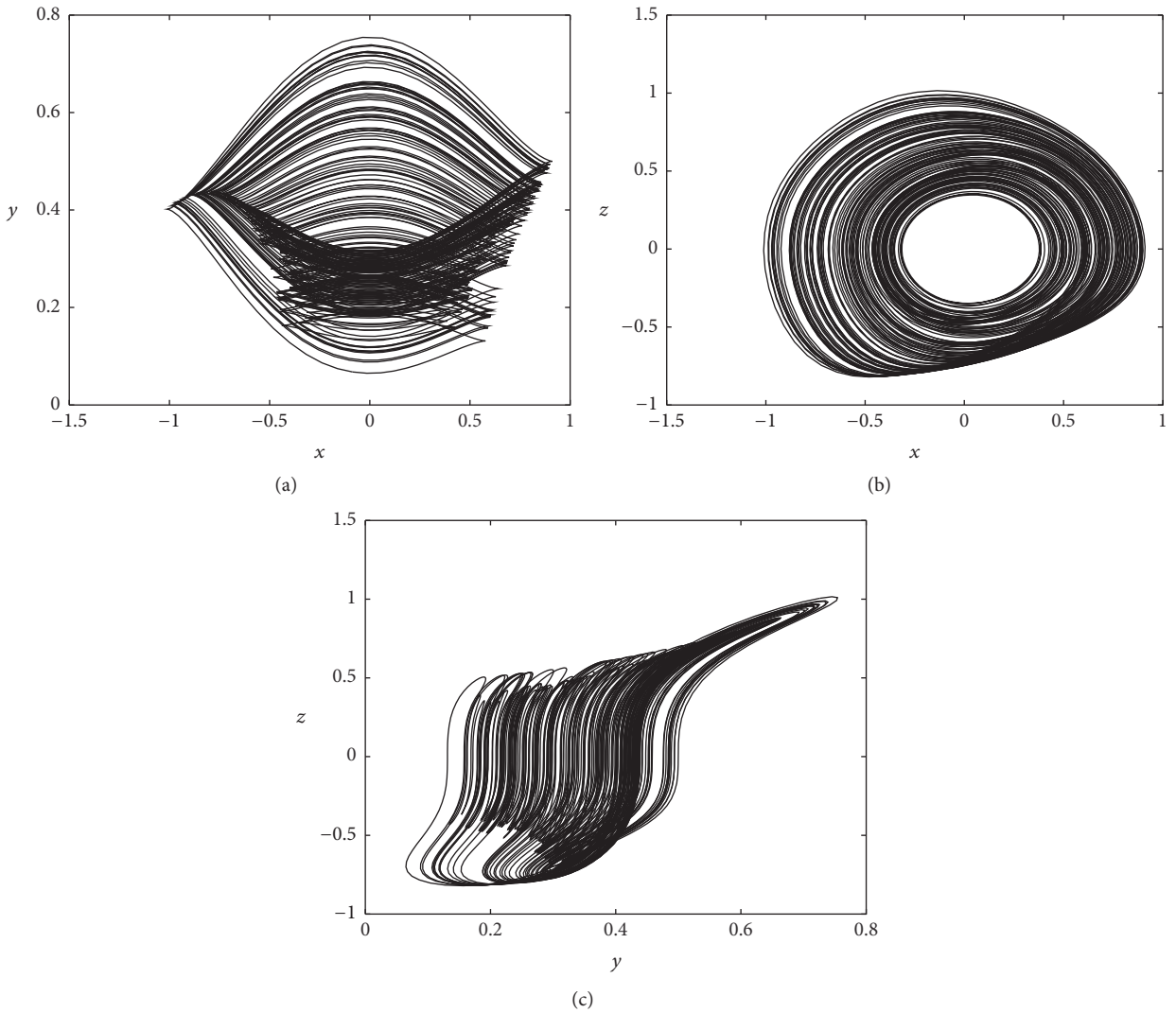

Figure 1: Chaotic attractor of the system with infinite equilibria (1) in (a) x-y plane, (b) x-z plane, and (c) y-z plane.

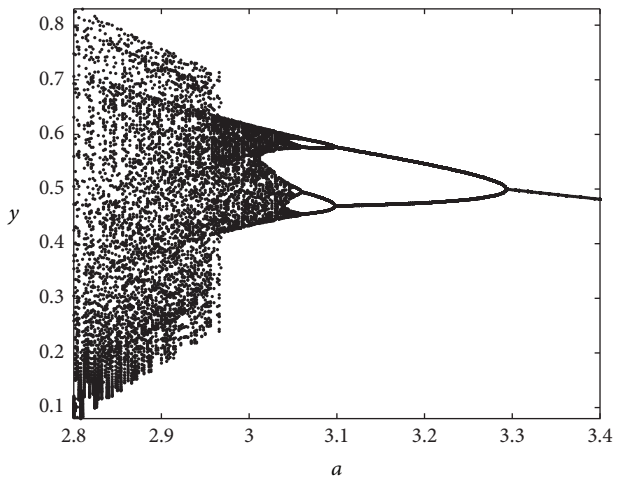

Figure 2: Bifurcation diagram of the system with infinite equilibria (1) when varying a.

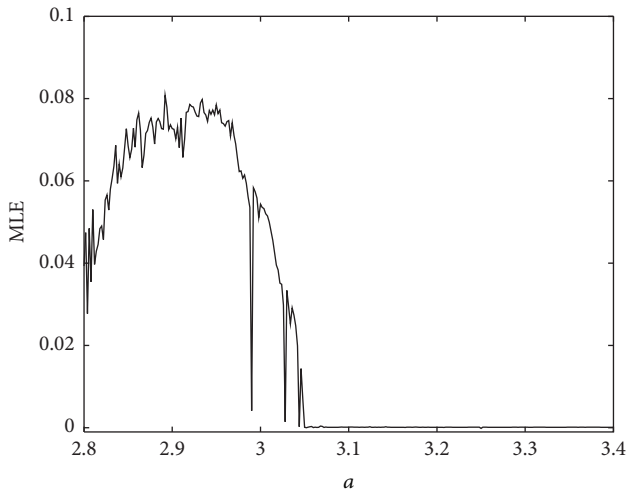

Figure 3: Maximal Lyapunov exponents of system (1) with respect to the bifurcation parameter a.

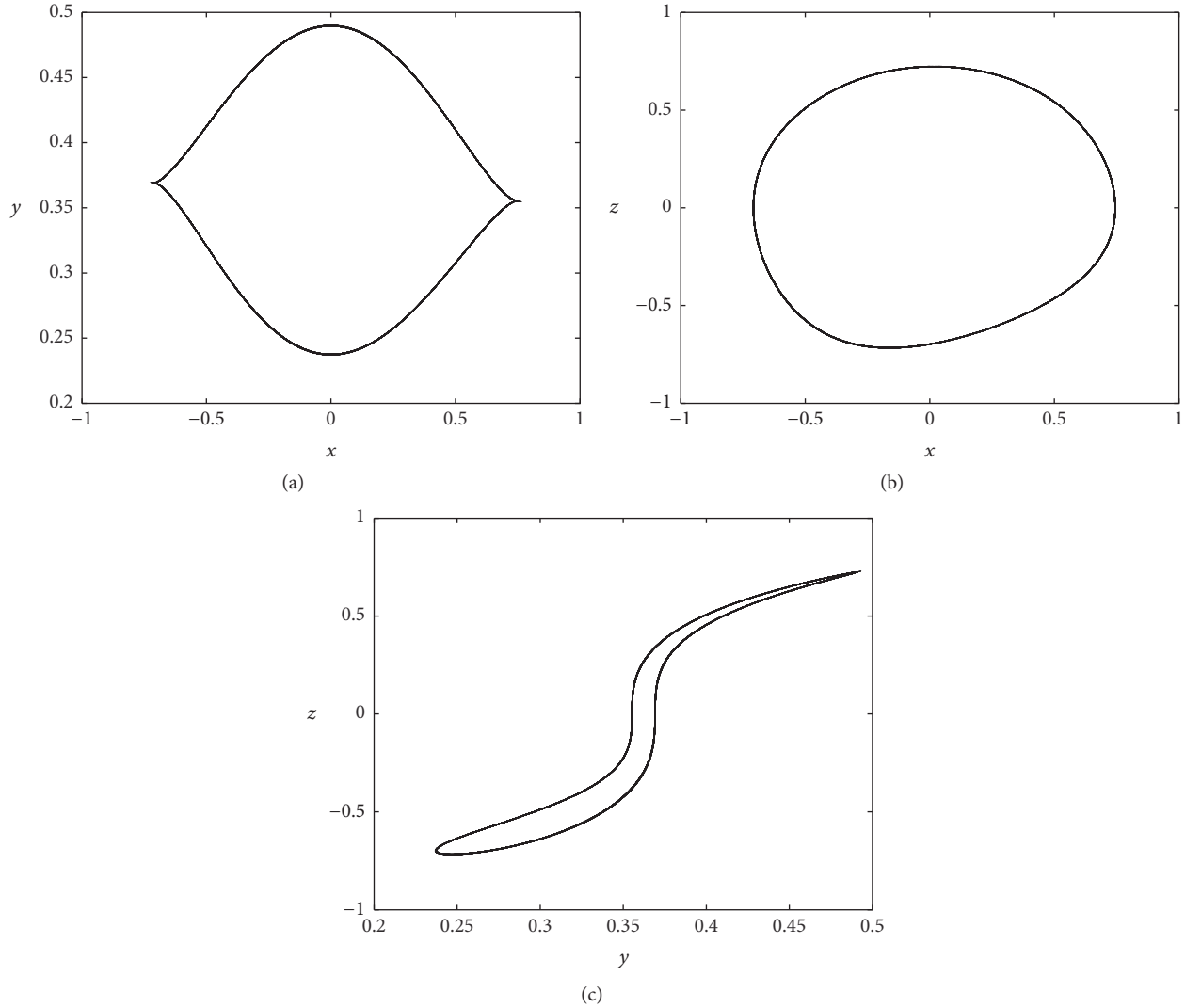

Figure 4: Limit cycle of the system with infinite equilibria (1) in (a) x-y plane, (b) x-z plane, and (c) y-z plane for $a = 3.35$.

In order to find the topology horseshoe, we select two polygon subsets D_1, D_2 in the Poincaré map Γ of the system with infinite equilibria (1):

$$\Gamma = \left\{(x, y, z) \in R^3 \mid z = 0\right\}. \tag{11}$$

The corresponding Poincaré map H is defined as

$$H : \Gamma \longrightarrow \Gamma. \tag{12}$$

Here $H(p)$ is the image of the initial p that returns back to Γ at the first time [48]. The same definition can be applied to the corresponding Poincaré map H^n. In this work, four vertices of the first polygon subset D_1 are selected as

$$\begin{aligned} &(0.822470322, 0.438565370), \\ &(0.823776275, 0.435278699), \\ &(0.815679371, 0.429691358), \\ &(0.813328658, 0.432978029), \end{aligned} \tag{13}$$

while four vertices of the second polygon subset D_2 are chosen as

$$\begin{aligned} &(0.796873661, 0.424104017), \\ &(0.798701994, 0.421146013), \\ &(0.794261757, 0.418188009), \\ &(0.792694615, 0.420160011). \end{aligned} \tag{14}$$

Two selected polygon subsets and their images are displayed in Figures 5 and 6. As shown in Figure 5, it is trivial to verify that $H^6(D_1)$ goes through both two polygon subsets D_1 and D_2. Similarly, $H^6(D_2)$ crosses two polygon subsets D_1 and D_2 as illustrated in Figure 6. According to the Horseshoe lemma, chaos of the system with infinite equilibria (1) is determined [45–47].

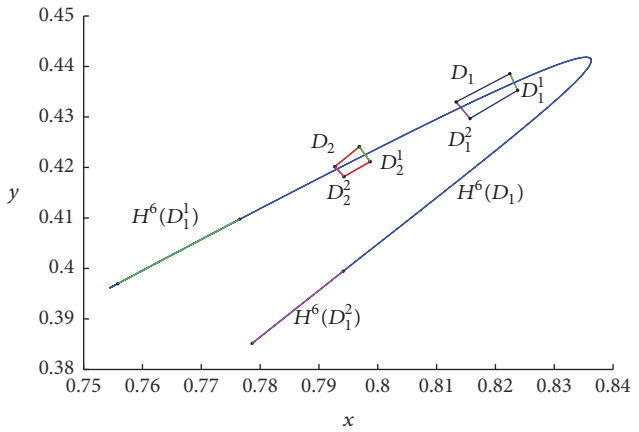

Figure 5: The quadrilateral subset D_1 and its image.

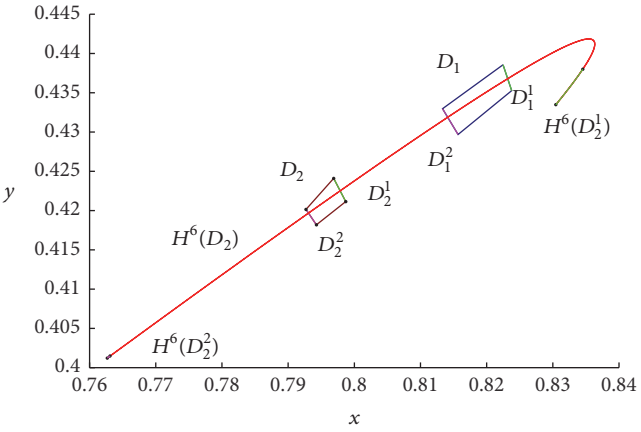

Figure 6: The quadrilateral subset D_2 and its image.

4. Synchronization of the Identical Systems with Infinite Equilibria

After the study of Pecora and Carroll about synchronization in chaotic systems [49], various synchronization techniques and related works were presented extensively [50–54]. Critically, the possibility of synchronization of two identical chaotic systems plays a vital role in practical applications [55–58]. In this section, we discover the synchronization of two new systems with infinite equilibria, called the master system and the slave system, by using an adaptive controller.

We consider the following master system with the unknown system parameter a:

$$\begin{aligned}\dot{x}_1 &= -z_1,\\ \dot{y}_1 &= x_1 z_1^2,\\ \dot{z}_1 &= x_1 - y_1 \tanh(y_1) + a y_1^2 z_1 - z_1^3.\end{aligned} \tag{15}$$

The slave system with adaptive control $\mathbf{u} = [u_x, u_y, u_z]^T$ is given as

$$\begin{aligned}\dot{x}_2 &= -z_2 + u_x,\\ \dot{y}_2 &= x_2 z_2^2 + u_y,\\ \dot{z}_2 &= x_2 - y_2 \tanh(y_2) + a y_2^2 z_2 - z_2^3 + u_z.\end{aligned} \tag{16}$$

The state errors between the slave system and the master system are calculated by

$$\begin{aligned}e_x &= x_2 - x_1,\\ e_y &= y_2 - y_1,\\ e_z &= z_2 - z_1.\end{aligned} \tag{17}$$

The parameter estimation error is defined as follows

$$e_a = a - \hat{a}, \tag{18}$$

in which $\hat{a}$ is the estimation of the unknown parameter a.

In order to synchronize the slave system and the master system, the adaptive control is constructed in the following form:

$$\begin{aligned}u_x &= e_z - k_x e_x,\\ u_y &= -x_2 z_2^2 + x_1 z_1^2 - k_y e_y,\\ u_z &= -e_x + y_2 \tanh(y_2) - y_1 \tanh(y_1)\\ &\quad - \hat{a}\left(y_2^2 z_2 - y_1^2 z_1\right) + z_2^3 - z_1^3 - k_z e_z,\end{aligned} \tag{19}$$

in which k_x, k_y, and k_z are three positive gain constants and the parameter update law is described by

$$\dot{\hat{a}} = e_z\left(y_2^2 z_2 - y_1^2 z_1\right). \tag{20}$$

By applying Lyapunov stability theory, we will prove that the master system (15) and the slave system (16) are synchronized when using the adaptive control (19).

In this work, the Lyapunov function is selected as

$$V\left(e_x, e_y, e_z, e_a\right) = \frac{1}{2}\left(e_x^2 + e_y^2 + e_z^2 + e_a^2\right). \tag{21}$$

Therefore, the differentiation of V is

$$\dot{V} = e_x \dot{e}_x + e_y \dot{e}_y + e_z \dot{e}_z + e_a \dot{e}_a. \tag{22}$$

From (17) and (18), we have

$$\begin{aligned}\dot{e}_x &= -k_x e_x,\\ \dot{e}_y &= -k_y e_y,\\ \dot{e}_z &= e_a\left(y_2^2 z_2 - y_1^2 z_1\right) - k_z e_z,\\ \dot{e}_a &= -\dot{\hat{a}}.\end{aligned} \tag{23}$$

By substituting (23) into (22), the differentiation of V can be expressed as

$$\dot{V} = -k_x e_x^2 - k_y e_y^2 - k_z e_z^2. \quad (24)$$

Because $\dot{V}$ is a negative semidefinite function, it is simply verified that $e_x \to 0$, $e_y \to 0$, and $e_z \to 0$ exponentially as $t \to \infty$ according to Barbalat's lemma [59]. In other words, we obtain the complete synchronization between the master system and the slave system.

We take an example to illustrate the calculation of the synchronization scheme. The parameter values of the master system and the slave system are fixed as

$$a = 2.9. \quad (25)$$

We assume that the initial states of the master system are

$$\begin{aligned} x_1(0) &= 0, \\ y_1(0) &= 0.1, \\ z_1(0) &= 0.2, \end{aligned} \quad (26)$$

while the initial states of the slave system are

$$\begin{aligned} x_2(0) &= -0.7, \\ y_2(0) &= 0.4, \\ z_2(0) &= -0.1. \end{aligned} \quad (27)$$

The positive gain constants are chosen as follows: $k_x = 4$, $k_y = 4$, and $k_z = 4$. We take the initial condition of the parameter estimate as

$$\widehat{a}(0) = 3. \quad (28)$$

The time-history of the synchronization errors e_x, e_y, e_z is shown in Figure 7. It is straightforward to verify that Figure 7 depicts the synchronization of the master and slave systems.

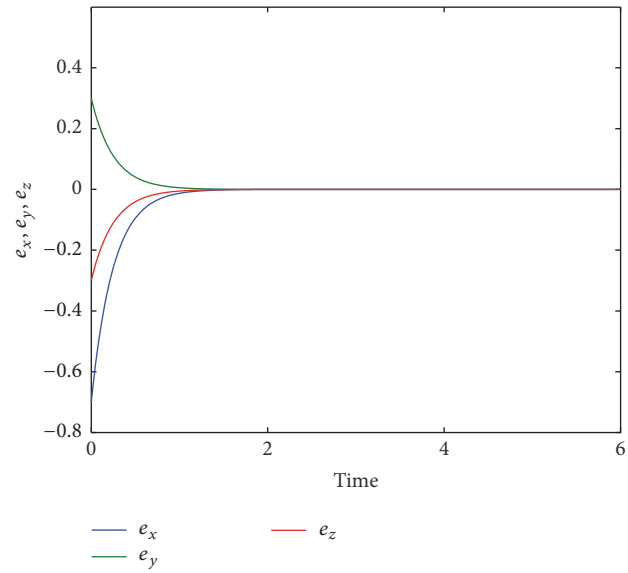

Figure 7: Time-history of the synchronization errors which indicates the synchronization between the master system and the slave system.

5. Conclusions

A new chaotic system with a curve of equilibria has been introduced in this work. Interestingly, because of having an infinite number of equilibrium points, the system is a special system with hidden attractors, which is rarely reported in the literature. Basic dynamical characters of the system with infinite equilibria are investigated via phase portraits, equilibrium analysis, Kaplan–Yorke dimension, maximal Lyapunov exponents, and bifurcation diagram. Although it is great challenge for researchers to find a topological horseshoe in systems with hidden attractor, horseshoe in such new system with infinite equilibria has been discovered in our work. After studying the possibility of synchronization of two novel chaotic systems, we believe that potential applications of such a system should be considered further in future works.

Competing Interests

The authors declare that there is no conflict of interests regarding the publication of this paper.

Acknowledgments

The authors are grateful to Professor Qingdu Li, Research Center of Analysis and Control for Complex Systems, Chongqing University of Post and Telecommunication, China, for his useful discussions and suggestions. The author Xiong Wang was supported by the National Natural Science Foundation of China (no. 61601306) and Shenzhen Overseas High Level Talent Peacock Project Fund (no. 20150215145C).

References

[1] E. N. Lorenz, "Deterministic nonperiodic flow," *Journal of the Atmospheric Sciences*, vol. 20, pp. 130–141, 1963.

[2] S. H. Strogatz, *Nonlinear Dynamics and Chaos: With Applications to Physics, Biology, Chemistry, and Engineering*, Perseus Books, Massachusetts, Mass, USA, 1994.

[3] S. Vaidyanathan and S. Rasappan, "Global Chaos Synchronization of n-Scroll Chua Circuit and Lur'e System using Backstepping Control Design with Recursive Feedback," *Arabian Journal for Science and Engineering*, vol. 39, no. 4, pp. 3351–3364, 2014.

[4] J. Sun, Y. Shen, and G. Cui, "Compound synchronization of four chaotic complex systems," *Advances in Mathematical Physics*, vol. 2015, Article ID 921515, 11 pages, 2015.

[5] Y.-Y. Hou, H.-C. Chen, J.-F. Chang, J.-J. Yan, and T.-L. Liao, "Design and implementation of the Sprott chaotic secure digital communication systems," *Applied Mathematics and Computation*, vol. 218, no. 24, pp. 11799–11805, 2012.

[6] M. Yang and G. Zhang, "An efficient method for anti-jamming in CS-MIMO chaotic radar direction finding," *Arabian Journal for Science and Engineering*, vol. 39, no. 12, pp. 8947–8955, 2014.

[7] H. Khanzadi, M. Eshghi, and S. E. Borujeni, "Image encryption using random bit sequence based on chaotic maps," *Arabian Journal for Science and Engineering*, vol. 39, no. 2, pp. 1039–1047, 2014.

[8] K. Tatsumi, T. Ibuki, and T. Tanino, "A chaotic particle swarm optimization exploiting a virtual quartic objective function based on the personal and global best solutions," *Applied Mathematics and Computation*, vol. 219, no. 17, pp. 8991–9011, 2013.

[9] S. Jafari and J. C. Sprott, "Simple chaotic flows with a line equilibrium," *Chaos, Solitons & Fractals*, vol. 57, pp. 79–84, 2013.

[10] C. Li and J. C. Sprott, "Chaotic flows with a single nonquadratic term," *Physics Letters. A*, vol. 378, no. 3, pp. 178–183, 2014.

[11] C. Li, J. C. Sprott, Z. Yuan, and H. Li, "Constructing chaotic systems with total amplitude control," *International Journal of Bifurcation and Chaos in Applied Sciences and Engineering*, vol. 25, no. 10, Article ID 1530025, 14 pages, 2015.

[12] T. Gotthans and J. Petržela, "New class of chaotic systems with circular equilibrium," *Nonlinear Dynamics*, vol. 81, no. 3, pp. 1143–1149, 2015.

[13] T. Gotthans, J. C. Sprott, and J. Petrzela, "Simple chaotic flow with circle and square equilibrium," *International Journal of Bifurcation and Chaos in Applied Sciences and Engineering*, vol. 26, no. 8, Article ID 1650137, 8 pages, 2016.

[14] Y. Chen and Q. Yang, "A new Lorenz-type hyperchaotic system with a curve of equilibria," *Mathematics and Computers in Simulation*, vol. 112, pp. 40–55, 2015.

[15] C. Li, J. C. Sprott, and W. Thio, "Bistability in a hyperchaotic system with a line equilibrium," *Journal of Experimental and Theoretical Physics*, vol. 118, no. 3, pp. 494–500, 2014.

[16] Q. Li, S. Tang, H. Zeng, and T. Zhou, "On hyperchaos in a small memristive neural network," *Nonlinear Dynamics*, vol. 78, no. 2, pp. 1087–1099, 2014.

[17] Q. Li, H. Zeng, and J. Li, "Hyperchaos in a 4D memristive circuit with infinitely many stable equilibria," *Nonlinear Dynamics*, vol. 79, no. 4, pp. 2295–2308, 2015.

[18] G. A. Leonov, N. V. Kuznetsov, O. A. Kuznetsova, S. M. Seledzhi, and V. I. Vagaitsev, "Hidden oscillations in dynamical systems," *Transactions on Systems and Control*, vol. 6, no. 2, pp. 54–67, 2011.

[19] G. A. Leonov, N. V. Kuznetsov, and V. I. Vagaitsev, "Localization of hidden Chua's attractors," *Physics Letters. A*, vol. 375, no. 23, pp. 2230–2233, 2011.

[20] G. A. Leonov, N. V. Kuznetsov, and V. I. Vagaitsev, "Hidden attractor in smooth Chua systems," *Physica D. Nonlinear Phenomena*, vol. 241, no. 18, pp. 1482–1486, 2012.

[21] G. A. Leonov and N. V. Kuznetsov, "Hidden attractors in dynamical systems. From hidden oscillations in Hilbert-Kolmogorov, Aizerman, and KALman problems to hidden chaotic attractor in Chua circuits," *International Journal of Bifurcation and Chaos in Applied Sciences and Engineering*, vol. 23, no. 1, Article ID 1330002, 69 pages, 2013.

[22] G. A. Leonov, N. V. Kuznetsov, M. A. Kiseleva, E. P. Solovyeva, and A. M. Zaretskiy, "Hidden oscillations in mathematical model of drilling system actuated by induction motor with a wound rotor," *Nonlinear Dynamics*, vol. 77, no. 1-2, pp. 277–288, 2014.

[23] A. Chudzik, P. Perlikowski, A. Stefanski, and T. Kapitaniak, "Multistability and rare attractors in van der Pol-duffing oscillator," *International Journal of Bifurcation and Chaos in Applied Sciences and Engineering*, vol. 21, no. 7, pp. 1907–1912, 2011.

[24] Z. T. Zhusubaliyev and E. Mosekilde, "Multistability and hidden attractors in a multilevel DC/DC converter," *Mathematics and Computers in Simulation*, vol. 109, pp. 32–45, 2015.

[25] G. A. Leonov, N. V. Kuznetsov, and T. N. Mokaev, "Hidden attractor and homoclinic orbit in Lorenz-like system describing convective fluid motion in rotating cavity," *Communications in Nonlinear Science and Numerical Simulation*, vol. 28, no. 1–3, pp. 166–174, 2015.

[26] D. Dudkowski, S. Jafari, T. Kapitaniak, N. V. Kuznetsov, G. A. Leonov, and A. Prasad, "Hidden attractors in dynamical systems," *Physics Reports. A Review Section of Physics Letters*, vol. 637, pp. 1–50, 2016.

[27] S. Brezetskyi, D. Dudkowski, and T. Kapitaniak, "Rare and hidden attractors in Van der Pol-Duffing oscillators," *European Physical Journal: Special Topics*, vol. 224, no. 8, pp. 1459–1467, 2015.

[28] Z. T. Zhusubaliyev, E. Mosekilde, V. G. Rubanov, and R. A. Nabokov, "Multistability and hidden attractors in a relay system with hysteresis," *Physica D. Nonlinear Phenomena*, vol. 306, pp. 6–15, 2015.

[29] Z. Wei, R. Wang, and A. Liu, "A new finding of the existence of hidden hyperchaotic attractors with no equilibria," *Mathematics and Computers in Simulation*, vol. 100, pp. 13–23, 2014.

[30] S. Jafari, J. C. Sprott, and F. Nazarimehr, "Recent new examples of hidden attractors," *European Physical Journal: Special Topics*, vol. 224, no. 8, pp. 1469–1476, 2015.

[31] Y. Feng, J. Pu, and Z. Wei, "Switched generalized function projective synchronization of two hyperchaotic systems with hidden attractors," *European Physical Journal: Special Topics*, vol. 224, no. 8, pp. 1593–1604, 2015.

[32] P. Zhou and F. Yang, "Hyperchaos, chaos, and horseshoe in a 4D nonlinear system with an infinite number of equilibrium points," *Nonlinear Dynamics*, vol. 76, no. 1, pp. 473–480, 2014.

[33] Q. Li, S. Hu, S. Tang, and G. Zeng, "Hyperchaos and horseshoe in a 4D memristive system with a line of equilibria and its implementation," *International Journal of Circuit Theory and Applications*, vol. 42, no. 11, pp. 1172–1188, 2014.

[34] A. Wolf, J. B. Swift, H. L. Swinney, and J. A. Vastano, "Determining Lyapunov exponents from a time series," *Physica D: Nonlinear Phenomena*, vol. 16, no. 3, pp. 285–317, 1985.

[35] N. V. Kuznetsov, "The Lyapunov dimension and its estimation via the Leonov method," *Physics Letters. A*, vol. 380, no. 25-26, pp. 2142–2149, 2016.

[36] N. V. Kuznetsov, T. A. Alexeeva, and G. A. Leonov, "Invariance of Lyapunov exponents and Lyapunov dimension for regular and irregular linearizations," *Nonlinear Dynamics. An International Journal of Nonlinear Dynamics and Chaos in Engineering Systems*, vol. 85, no. 1, pp. 195–201, 2016.

[37] G. A. Leonov, N. V. Kuznetsov, N. A. Korzhemanova, and D. V. Kusakin, "Lyapunov dimension formula for the global attractor of the Lorenz system," *Communications in Nonlinear Science and Numerical Simulation*, vol. 41, pp. 84–103, 2016.

[38] Q. Li, "A topological horseshoe in the hyperchaotic Rossler attractor," *Physics Letters. A*, vol. 372, no. 17, pp. 2989–2994, 2008.

[39] Q. Li and X.-S. Yang, "Two kinds of horseshoes in a hyperchaotic neural network," *International Journal of Bifurcation and Chaos*, vol. 22, no. 8, Article ID 1250200, 2012.

[40] K. Deng and S. Yu, "Estimating ultimate bound and finding topological horseshoe for a new chaotic system," *Optik*, vol. 125, no. 20, pp. 6044–6048, 2014.

[41] J. He, S. Yu, and J. Cai, "Topological horseshoe analysis for a three-dimensional anti-control system and its application," *Optik—International Journal for Light and Electron Optics*, vol. 127, no. 20, pp. 9444–9456, 2016.

[42] Z. Liao and Y. Huang, "Horseshoe and topological entropy estimate of a class of three-dimensional cellular neural networks," *Applied Mathematics and Computation*, vol. 197, no. 1, pp. 382–388, 2008.

[43] Q.-J. Fan, "Horseshoe in a modified Van der Pol-Duffing circuit," *Applied Mathematics and Computation*, vol. 210, no. 2, pp. 436–440, 2009.

[44] X.-S. Yang, Q. Li, and S. Cheng, "Horseshoe chaos and topological entropy estimate in a simple power system," *Applied Mathematics and Computation*, vol. 211, no. 2, pp. 467–473, 2009.

[45] X.-S. Yang, "Topological horseshoes in continuous maps," *Chaos, Solitons and Fractals*, vol. 33, no. 1, pp. 225–233, 2007.

[46] Q. Li and X.-S. Yang, "A simple method for finding topological horseshoes," *International Journal of Bifurcation and Chaos in Applied Sciences and Engineering*, vol. 20, no. 2, pp. 467–478, 2010.

[47] Q. Li, X.-S. Yang, and S. Chen, "Hyperchaos in a spacecraft power system," *International Journal of Bifurcation and Chaos*, vol. 21, no. 6, pp. 1719–1726, 2011.

[48] X.-S. Yang, "Topological horseshoes and computer assisted verification of chaotic dynamics," *International Journal of Bifurcation and Chaos*, vol. 19, no. 4, pp. 1127–1145, 2009.

[49] L. M. Pecora and T. L. Carroll, "Synchronization in chaotic systems," *Physical Review Letters*, vol. 64, no. 8, pp. 821–824, 1990.

[50] M.-C. Pai, "Global synchronization of uncertain chaotic systems via discrete-time sliding mode control," *Applied Mathematics and Computation*, vol. 227, pp. 663–671, 2014.

[51] V. Sundarapandian and I. Pehlivan, "Analysis, control, synchronization, and circuit design of a novel chaotic system," *Mathematical and Computer Modelling*, vol. 55, no. 7-8, pp. 1904–1915, 2012.

[52] X. Zhao, Z. Li, and S. Li, "Synchronization of a chaotic finance system," *Applied Mathematics and Computation*, vol. 217, no. 13, pp. 6031–6039, 2011.

[53] S. C. Jeong, D. H. Ji, J. H. Park, and S. C. Won, "Adaptive synchronization for uncertain chaotic neural networks with mixed time delays using fuzzy disturbance observer," *Applied Mathematics and Computation*, vol. 219, no. 11, pp. 5984–5995, 2013.

[54] R. Martínez-Guerra, D. M. Corona-Fortunio, and J. L. Mata-Machuca, "Synchronization of chaotic Liouvillian systems: an application to Chua's oscillator," *Applied Mathematics and Computation*, vol. 219, no. 23, pp. 10934–10944, 2013.

[55] S. Boccaletti, J. Kurths, G. Osipov, D. L. Valladares, and C. S. Zhou, "The synchronization of chaotic systems," *Physics Reports. A Review Section of Physics Letters*, vol. 366, no. 1-2, pp. 1–101, 2002.

[56] L. Fortuna and M. Frasca, "Experimental synchronization of single-transistor-based chaotic circuits," *Chaos*, vol. 17, no. 4, Article ID 043118, 2007.

[57] A. Abdullah, "Synchronization and secure communication of uncertain chaotic systems based on full-order and reduced-order output-affine observers," *Applied Mathematics and Computation*, vol. 219, no. 19, pp. 10000–10011, 2013.

[58] J. Sun, J. Guo, C. Yang, A. Zheng, and X. Zhang, "Adaptive generalized hybrid function projective dislocated synchronization of new four-dimensional uncertain chaotic systems," *Applied Mathematics and Computation*, vol. 252, pp. 304–314, 2015.

[59] H. K. Khalil, *Nonlinear Systems*, Prentice Hall, New Jersey, NJ, USA, 3rd edition, 2002.